

# MOUNTAIN-PLAINS CONSORTIUM

MPC 23-497 | J. Seo, E. Jeong and N. Wehbe

SUSTAINABLE  
ALTERNATIVE TO  
STRUCTURALLY  
DEFICIENT BRIDGES



A University Transportation Center sponsored by the U.S. Department of Transportation serving the Mountain-Plains Region. Consortium members:

Colorado State University  
North Dakota State University  
South Dakota State University

University of Colorado Denver  
University of Denver  
University of Utah

Utah State University  
University of Wyoming

**Technical Report Documentation Page**

1. Report No. MPC-576	2. Government Accession No.	3. Recipient's Catalog No.	
4. Title and Subtitle Sustainable Alternative to Structurally Deficient Bridges		5. Report Date March 2023	
		6. Performing Organization Code	
7. Author(s) Junwon Seo, Ph.D., P.E. Euiseok Jeong, GRA Nadim Wehbe, Ph.D., P.E.		8. Performing Organization Report No. MPC 23-497	
9. Performing Organization Name and Address Department of Civil and Environmental Engineering South Dakota State University 326 Crothers Engineering Hall Brookings, SD 57007		10. Work Unit No. (TRAIS)	
		11. Contract or Grant No.	
12. Sponsoring Agency Name and Address Mountain-Plains Consortium North Dakota State University PO Box 6050, Fargo, ND 58108		13. Type of Report and Period Covered Final Report	
		14. Sponsoring Agency Code	
15. Supplementary Notes Supported by a grant from the US DOT, University Transportation Centers Program			
16. Abstract <p>Structurally deficient bridges in the United States may be replaced with a viable alternative made with Cross Laminated Timber (CLT). The alternative promotes environmental sustainability, diversified wood production opportunities, and increased public safety and construction efficiency. CLT products' superior strength, durability and sustainability have led to commercialization for building applications, but CLT has never been applied to bridge systems. The ultimate goal of this project is to improve bridge sustainability and performance using CLT products. To achieve this goal, researchers will pursue the following research objectives: 1) conceptualize a new CLT girder bridge system; 2) design and manufacture the full-scale specimen; and 3) investigate structural performance of the bridge system. To succeed, one CLT fabricator, who serves as an industrial collaborator on this project, will provide practical input for the production of the specimen. Further, one graduate student will gain hands-on research experience and real-world solutions. The PI will integrate the findings into SDSU engineering courses, including CEE 792: Bridge Engineering, to introduce students to CLT bridge performance.</p>			
17. Key Word bridge construction, bridge design, girder bridges, laminated wood, prototypes, structural analysis, timber construction		18. Distribution Statement Public distribution	
19. Security Classif. (of this report) Unclassified	20. Security Classif. (of this page) Unclassified	21. No. of Pages 232	22. Price n/a

# **Sustainable Alternative to Structurally Deficient Bridges**

Junwon Seo, Ph.D., P.E.  
Euseok Jeong, GRA  
Nadim Wehbe, Ph.D., P.E.

Department of Civil and Environmental Engineering  
South Dakota State University  
Brookings, South Dakota

March 2023

## **Disclaimer**

The contents of this report reflect the views of the authors, who are responsible for the facts and the accuracy of the information presented. This document is disseminated under the sponsorship of the Department of Transportation, University Transportation Centers Program, in the interest of information exchange. The United States Government assumes no liability for the contents or use thereof.

NDSU does not discriminate in its programs and activities on the basis of age, color, gender expression/identity, genetic information, marital status, national origin, participation in lawful off-campus activity, physical or mental disability, pregnancy, public assistance status, race, religion, sex, sexual orientation, spousal relationship to current employee, or veteran status, as applicable. Direct inquiries to Vice Provost, Title IX/ADA Coordinator, Old Main 201, [\[701\] 231-7708](tel:7012317708), [ndsuoaa@ndsu.edu](mailto:ndsuoaa@ndsu.edu).

# TABLE OF CONTENTS

<b>1. PROJECT OBJECTIVES, OUTCOMES, AND IMPACTS.....</b>	<b>1</b>
<b>2. PROJECT ACTIVITIES.....</b>	<b>4</b>
2.1 CLT Bridge Conceptualization.....	4
2.1.1 Existing CLT Applications.....	4
2.1.1.1 Bridges.....	4
2.1.1.2 Other Structures.....	9
2.1.2 CLT Bridge Conceptualization.....	10
2.1.2.1 CLT Arch Bridge.....	11
2.1.2.2 CLT Double T-girder Bridge.....	11
2.1.2.3 CLT Girder Bridge.....	11
2.1.3 CLT Bridge Selection.....	12
2.1.4 Literature Search on CLT Structural Performance.....	12
2.1.4.1 CLT Component-level Testing.....	12
2.1.4.2 CLT System-level Testing.....	14
2.2 CLT Bridge Design According to Structural Engineering-based Standards.....	15
2.2.1 CLT Design Standards.....	15
2.2.2 CLT Bridge Design Details.....	16
2.2.2.1 CLT Girder Design.....	17
2.2.2.2 CLT Deck Design.....	22
2.2.2.3 CLT Connection Design.....	25
2.2.2.4 CLT Diaphragm.....	28
2.2.2.5 CLT Bridge Sketch and Details.....	31
2.3 CLT Bridge Component and System Production.....	32
2.3.1 CLT Component Manufacture.....	32
2.3.2 CLT Girder Fabrication.....	33
2.3.2.1 CLT Girder with Adhesive.....	33
2.3.2.2 CLT Girder with Adhesive and Fasteners.....	38
2.3.3 CLT Bridge System Production.....	42
2.3.3.1 Installation of CLT Diaphragm.....	43
2.3.3.2 Installation of CLT Deck.....	44
2.4 Ultimate Load Testing.....	46
2.4.1 Performance on CLT Girder with Adhesive.....	46
2.4.1.1 Instrumentation.....	46
2.4.1.2 Testing Procedure.....	53
2.4.1.3 Results and Discussion.....	55
2.4.2 Performance on CLT Girder with Adhesive and Fasteners.....	77
2.4.2.1 Instrumentation.....	77
2.4.2.2 Testing Procedure.....	83
2.4.2.3 Results and Discussion.....	84

2.4.3	Performance on CLT Bridge System.....	106
2.4.3.1	Instrumentation.....	106
2.4.3.2	Testing Procedure.....	114
2.4.3.3	Results and Discussion.....	115
2.5	Summary and Conclusions.....	138
2.5.1	CLT Bridge Conceptualization.....	138
2.5.2	CLT Bridge Design.....	138
2.5.3	CLT Bridge Production.....	138
2.5.4	Ultimate Load Testing.....	138
2.5.4.1	CLT Girder with Adhesive.....	139
2.5.4.2	CLT Girder with Adhesive and Fasteners.....	140
2.5.4.3	CLT Bridge System.....	141
<b>3.</b>	<b>REFERENCES.....</b>	<b>142</b>
	<b>APPENDIX A. CLT Properties.....</b>	<b>145</b>
	<b>APPENDIX B. CLT Quotation.....</b>	<b>151</b>
	<b>APPENDIX C. Polyurethane Adhesive Specification.....</b>	<b>153</b>
	<b>APPENDIX D. Fastener Specification.....</b>	<b>157</b>
	<b>APPENDIX E. Epoxy Glue Specification.....</b>	<b>172</b>
	<b>APPENDIX F. Epoxy-based Wood Filler Specification.....</b>	<b>194</b>
	<b>APPENDIX G. DJI Phantom 4 Specification.....</b>	<b>204</b>
	<b>APPENDIX H. iPhone 6s Plus's Image Sensor Specification.....</b>	<b>206</b>
	<b>APPENDIX I. DIC Sensor Specification.....</b>	<b>208</b>
	<b>APPENDIX J. DIC Lens Specification.....</b>	<b>210</b>
	<b>APPENDIX K. Solar Panel Specification.....</b>	<b>212</b>
	<b>APPENDIX L. AASHTO Strength I Limit Strength and Service I Limit Strength Calculation.....</b>	<b>214</b>

## LIST OF TABLES

Table 2.1	CLT bridge applications.....	4
Table 2.2	CLT building applications.....	9
Table 2.3	Details of identified propagated damage of CLT girder with adhesive. ....	74
Table 2.4	Details of identified propagated damage of CLT girder with adhesive and fasteners.....	104

## LIST OF FIGURES

Figure 2.1	Maicasagi Bridge (Egorov et al. 2018): (a) overall structure and (b) cross-section.....	5
Figure 2.2	Hundorp Bridge (Abrahamsen and Nyløkken 2010): (a) superstructure (b) cross-section .....	6
Figure 2.3	Ishikurazawa Bridge (Sasaki et al. 2017): (a) overall bridge and (b) cross-section.....	7
Figure 2.4	Arch bridge with CLT deck over River Mur, Austria (Behrens and Benner 2015).....	8
Figure 2.5	Mistassini Bridge (Lefebvre and Richard 2014): (a) picture and (b) sketch.....	8
Figure 2.6	Covered CLT bridge over River Mur, Austria (Behrens and Benner 2015): (a) outside of the brdge and (b) inside of the bridge .....	9
Figure 2.7	CLT arch bridge: (a) elevation view and (b) cross-section .....	11
Figure 2.8	CLT double T-girder applied bridge: (a) elevation view and (b) cross-section.....	11
Figure 2.9	Simple CLT girder bridge: (a) elevation view and (b) cross-section .....	12
Figure 2.10	CLT beam failures: (a) rolling shear; (b) rolling shear failure mechanism; and (c) flexural failure (Salokangas and Garnier 2013).....	13
Figure 2.11	CLT bridge design flowchart with design codes.....	16
Figure 2.12	Schematic of HS20-44 truck .....	16
Figure 2.13	Applied $wDL$ along the CLT girder.....	19
Figure 2.14	Location of the live load for maximum vertical shear .....	19
Figure 2.15	Wheel distribution width in the direction of the deck.....	22
Figure 2.16	Wheel load distribution width perpendicular to the deck.....	23
Figure 2.17	Applied wheel load for horizontal shear .....	24
Figure 2.18	Moment on overhang .....	24
Figure 2.19	Shear on overhang.....	25
Figure 2.20	Basic yield modes in dowel—type connection: (a) Mode <b>Im</b> ; (b) Mode <b>Is</b> ; (c) Mode <b>II</b> ; (d) Mode <b>III<sub>m</sub></b> ; (e) Mode <b>III<sub>s</sub></b> ; and (f) Mode <b>IV</b> .....	27
Figure 2.21	Effective deck width of CLT.....	28
Figure 2.22	CLT bridge design sketch: (a) cross-section; (b) plan view; and (c) elevation view .....	31
Figure 2.23	CLT shipment: (a) CLT move from the truck; (b) CLT move with the forklift crane; (c) the shipped CLT panels; and (d) dimension check.....	33



Figure 2.24	Schematic drawing of CLT bonded using adhesive: (a) beam moving and alignment; (b) adhesive spreading; and (c) clamping .....	34
Figure 2.25	CLT beams clamping cross-section .....	35
Figure 2.26	Adhesive CLT girder fabrication: (a) CLT beams shipping; (b) CLT bonding set-up; (c) spreading adhesive glue on CLT beam; (d) clamping two CLT beams; and (e) adhesive curing .....	36
Figure 2.27	CLT beam clamping sketch: (a) plan view; (b) elevation view; (c) detailed clamping with load cell; and (d) detailed clamping without load cell .....	37
Figure 2.28	Average clamping load for each load cell: (a) CLT girder 1; (b) CLT girder 2; (c) CLT girder 3; and (d) CLT girder 4.....	38
Figure 2.29	Schematic drawing of CLT bonded using adhesive: (a) girder moving and alignment; (b) adhesive spreading; (c) clamping; and (d) fastening screws .....	39
Figure 2.30	Drill guide fabrication using 3D printer: (a) 3D printer and (b) 3D sketch of drill guide....	40
Figure 2.31	CLT girder fabrication using fasteners: (a) marking hole locations on the girder; (b) making pre-drill holes; (c) tightening the fasteners; (d) cleaning girder surface; (e) filling the gap between the hole and fastener using epoxy glue; (f) curing epoxy glue; (g) filling the holes using the epoxy-based wood filler; and (h) curing epoxy-based wood filler .....	42
Figure 2.32	Installation of CLT diaphragm: (a) hole location mark; (b) drill holes on the girder; (c) drill holes on the diaphragm; (d) diaphragm installation using rods; (e) rod tightening; and (f) girder and diaphragm connection.....	44
Figure 2.33	Installation of CLT deck: (a) hole location mark; (b) drill holes on the deck; (c) deck moving on the girder; (d) adhesive application; (e) tightening the fasteners; (f) epoxy-based wood filler application; (g) epoxy-based wood filler curing; and (h) fabricated CLT bridge system.....	46
Figure 2.34	CLT girder test with adhesive bond: (a) test setup; (b) girder lam number designation; (c) data acquisition system; (d) control room; and (e) UAV-enabled inspection.....	48
Figure 2.35	Instrumentation plan for girder testing: (a) plan view; (b) elevation view (west side); (c) elevation view (east side); (d) string pot and strain gauges at mid-span; and (e) LVDTs at the south edge .....	49
Figure 2.36	Contact sensor installation: (a) strain gauges at mid-span; (b) strain gauges at distance $3d$ from north support; (c) strain gauges at distance $d$ from north support; (d) BDI strain sensors at distance $d$ from south support; (e) BDI strain sensors at distance $3d$ from south support; (f) LVDTs at south edge; (g) string pot; and (h) shear strain gauge mechanism .....	51
Figure 2.37	Non-contact sensor: (a) DIC system; (b) UAV and manipulator; and (c) solar panel .....	53
Figure 2.38	Testing and data collection procedure of CLT girder with adhesive .....	54

Figure 2.39	Load-displacement curve of CLT girder with adhesive.....	55
Figure 2.40	Representative CLT girder failure images: (a) slippage failure at south edge and (b) flexural failure at mid-span on west side.....	56
Figure 2.41	Slippage sign convention .....	57
Figure 2.42	Slippage between lams obtained by LVDTs.....	57
Figure 2.43	Strain gauges installed in mid-span of girder: (a) strain profile and (b) load-strain curves .....	59
Figure 2.44	Strain gauges installed at $3d$ from the north support: (a) strain profile and (b) load-strain curves .....	60
Figure 2.45	Strain gauges installed at $d$ from the north support: (a) strain profile (upper); (b) strain profile (lower); (c) load-strain curves (upper); and (d) load-strain curves (lower).....	61
Figure 2.46	Shear strain on $d$ from the north support: (a) strain profile and (b) load-strain curves .....	62
Figure 2.47	BDI strain sensors (upper) installed on $d$ from the south support: (a) strain profile (upper); (b) strain profile (lower); (c) load-strain curves (upper); and (d) load-strain curves (lower) .....	63
Figure 2.48	Shear strain on $d$ from the south support: (a) strain profile and (b) load-strain curves .....	64
Figure 2.49	BDI strain sensors installed on $3d$ from the south support: (a) strain profile and (b) load-strain curves.....	65
Figure 2.50	Non-contact sensor operation: (a) manipulator; (b) UAV; and (c) DIC system .....	66
Figure 2.51	Relative length measurement procedure on one side of the CLT girder.....	67
Figure 2.52	Deflection comparison between manipulator, UAV, and actuator .....	68
Figure 2.53	Inspection images captured by the manipulator and UAV: (a) 0 mm (manipulator); (b) 13.97 mm (manipulator); (c) 22.10 mm (manipulator); (d) 37.34 mm (manipulator); (e) 0 mm (UAV); (f) 37.34 mm (UAV); (g) Figure 2.53e adjusted with brightness 85% and contrast -10%; and (h) Figure 2.53f adjusted with brightness 85% and contrast -10% .....	69
Figure 2.54	Southeast sections of CLT girder before the testing captured by manipulator: (a) section 1; (b) section 2; (c) section 3; (d) section 4; (e) section 5; (f) section 6; (g) section 7; and (h) section 8.....	70
Figure 2.55	Southeast sections of CLT girder after the testing captured by manipulator: (a) section 1; (b) section 2; (c) section 3; (d) section 4; (e) section 5; (f) section 6; (g) section 7; and (h) section 8.....	71

Figure 2.56	Southeast sections of CLT girder before the testing captured by UAV: (a) Sections 1 through 4; (b) Figure 2.56a adjusted with brightness 70% and contrast -10%; (c) Sections 2 through 6; (d) Figure 2.56c adjusted with brightness 70% and contrast -10%; (e) Sections 4 through 8; and (f) Figure 2.56e adjusted with brightness 60% and contrast 10%.....	72
Figure 2.57	Damage map on the CLT girder with adhesive: (a) before the testing and (b) after the testing.....	73
Figure 2.58	DIC algorithm: (a) reference pattern and (b) deformed pattern.....	75
Figure 2.59	Strain profile calculated from DIC system applied to the CLT girder with adhesive.....	75
Figure 2.60	Relationship between voltage and displacement of CLT girder with adhesive.....	76
Figure 2.61	CLT girder test with adhesive and fastener bond: (a) test setup; (b) girder lam number designation; (c) data acquisition system; (d) control room; and (e) manipulator.....	78
Figure 2.62	Instrumentation plan for girder testing: (a) plan view; (b) elevation view (west side); (c) elevation view (east side); (d) string pot and strain gauges at mid-span; and (e) LVDTs at the south edge.....	79
Figure 2.63	Contact sensor installation: (a) strain gauges at mid-span; (b) SG-4 at distance $3d$ from north support; (c) strain gauges at distance $3d$ from north support; (d) strain gauges at distance $d$ from north support; (e) BDI strain sensors at distance $d$ from south support; (f) BDI strain sensors at distance $3d$ from south support; (g) LVDTs at south edge; and (h) string pot.....	82
Figure 2.64	Non-contact sensors: (a) DIC system; (b) UAV and manipulator; and (c) solar panel.....	83
Figure 2.65	Testing and data collection procedure of CLT girder with adhesive and fasteners.....	84
Figure 2.66	Load-displacement curve of CLT girder with adhesive and fasteners.....	85
Figure 2.67	Representative damage images: (a) flexural cracking on the east side of the girder at mid-span; (b) tilting of actuator; (c) damage due to tilting of actuator; (d) flexural failure on the west side of the girder at mid-span.....	86
Figure 2.68	Slippage sign convention.....	87
Figure 2.69	Slip between lams obtained by LVDTs.....	87
Figure 2.70	Strain gauges installed on mid-span of girder: (a) strain profile and (b) load-strain curves.....	89
Figure 2.71	Strain gauges installed on $3d$ from the north support: (a) strain profile and (b) load-strain curves.....	90
Figure 2.72	Strain gauges installed on $d$ from the north support: (a) strain profile (upper); (b) strain profile (lower); (c) load-strain curves (upper); and (d) load-strain curves (lower).....	91

Figure 2.73	Shear strain on <b>d</b> from the north support: (a) strain profile and (b) load-strain curves .....	92
Figure 2.74	BDI strain sensors (upper) installed on <b>d</b> from the south support: (a) strain profile (upper); (b) strain profile (lower); (c) load-strain curves (upper); and (d) load-strain curves (lower) .....	93
Figure 2.75	Shear strain on <b>d</b> from the south support: (a) strain profile and (b) load-strain curves .....	94
Figure 2.76	BDI strain sensors installed at <b>3d</b> from the south support: (a) strain profile and (b) load-strain curves.....	95
Figure 2.77	Non-contact sensor operation: (a) manipulator; (b) UAV; and (c) DIC system .....	96
Figure 2.78	Damage quantification procedure for adhesive and fastener CLT girder .....	97
Figure 2.79	Deflection comparison between manipulator, UAV, and actuator .....	98
Figure 2.80	Inspection images captured by the manipulator and UAV: (a) 0 mm (manipulator); (b) 13.97 mm (manipulator); (c) 22.10 mm (manipulator); (d) 37.34 mm (manipulator); (e) 0 mm (UAV); (f) 37.34 mm (UAV); (g) Figure 2.80e adjusted with brightness 85% and contrast -10%; and (h) Figure 2.80f adjusted with brightness 85% and contrast -10% .....	99
Figure 2.81	Southeast sections of CLT girder before the testing captured by manipulator: (a) section 1; (b) section 2; (c) section 3; (d) section 4; (e) section 5; (f) section 6; (g) section 7; and (h) section 8 .....	100
Figure 2.82	Southeast sections of CLT girder after the testing captured by manipulator: (a) section 1; (b) section 2; (c) section 3; (d) section 4; (e) section 5; (f) section 6; (g) section 7; and (h) section 8 .....	101
Figure 2.83	Southeast sections of CLT girder before the testing captured by UAV: (a) Sections 1 through 4; (b) Figure 2.83a adjusted with brightness 70% and contrast -10%; (c) Sections 2 through 6; (d) Figure 2.83c adjusted with brightness 70% and contrast -10%; (e) Sections 4 through 8; and (f) Figure 2.83e adjusted with brightness 60% and contrast 10%.....	102
Figure 2.84	Damage map on the CLT girder with adhesive and fasteners: (a) before the testing and (b) after the testing .....	103
Figure 2.85	Strain profile calculated from DIC system applied on the CLT girder with adhesive and fasteners.....	105
Figure 2.86	Relationship between voltage and displacement of CLT girder with adhesive and fasteners .....	106
Figure 2.87	Testing setup for CLT bridge system.....	107
Figure 2.88	Testing setup for CLT bridge system: (a) bridge lam number designation; (b) data acquisition system; (c) control room; and (d) DIC system .....	108

Figure 2.89	Instrumentation plan for bridge testing: (a) plan view; (b) elevation view (west); (c) elevation view (east); and (d) instrumentation at the south edge of the bridge .....	109
Figure 2.90	Contact sensor installation for CLT bridge system: (a) strain gauges at mid-span; (b) strain gauges at distance $3d$ from north support; (c) strain gauges at distance $d$ from north support; (d) strain gauge underneath west girder; (e) strain gauge underneath east girder; (f) strain gauges on north diaphragm; (g) strain gauges on south diaphragm; (h) BDI strain sensors at distance $d$ from south support; (i) LVDTs, string pot, and load cells at south edge; and (j) LVDTs at south edge .....	113
Figure 2.91	Non-contact sensor and solar panel for CLT bridge system: (a) DIC system; (b) UAV-enabled inspection; and (c) solar panel.....	114
Figure 2.92	Testing and data collection procedure of CLT bridge system.....	115
Figure 2.93	Load-displacement curve for tested CLT bridge system.....	116
Figure 2.94	Representative failure modes: (a) shear crack at south edge of the east girder, (b) slippage at south edge of the west girder, and (c) flexure failure on the east girder .....	117
Figure 2.95	Slippage sign convention .....	117
Figure 2.96	Slip between CLT lams obtained by LVDTs .....	118
Figure 2.97	Strain gauges installed on mid-span of bridge: (a) strain profile and (b) load-strain curves .....	119
Figure 2.98	Strain gauges installed on $3d$ from the north support: (a) strain profile and (b) load-strain curves.....	121
Figure 2.99	Strain gauges installed on $d$ from the north support: (a) strain profile (upper); (b) load-strain curves (upper); (c) strain profile (lower); and (d) load-strain curves (lower) .....	124
Figure 2.100	Shear strain on $d$ from the north support: (a) strain profile and (b) load-strain curves .....	125
Figure 2.101	Strain gauges installed underneath the girders at mid-span .....	126
Figure 2.102	Strain gauges installed on the diaphragms: (a) north diaphragm and (b) south diaphragm.....	127
Figure 2.103	BDI strain sensors installed on $d$ from the south support: (a) strain profile (upper); (b) load-strain curves (upper); (c) strain profile (lower); and (d) load-strain curves (lower).....	130
Figure 2.104	BDI strain sensors installed on $d$ from the south support: (a) strain profile and (b) load-strain curves .....	131
Figure 2.105	Non-contact sensor operation: (a) UAV and (c) DIC system .....	132
Figure 2.106	Deflection comparison using UAV and actuator .....	133

Figure 2.107	Inspection images captured depending on displacement of actuator: (a) 0 mm; (b) 51.21 mm; (c) Figure 2.107a adjusted with brightness 70% and contrast 20%; and (d) Figure 2.107b adjusted with brightness 70% and contrast 30%.....	134
Figure 2.108	Southeast sections of the east girder of the CLT bridge system before the testing captured by UAV: (a) Sections 1 through 4; (b) Figure 2.108a adjusted with brightness 70% and contrast -10%; (c) Sections 2 through 6; (d) Figure 2.108c adjusted with brightness 70% and contrast -10%; (e) Sections 4 through 8; and (f) Figure 2.108e adjusted with brightness 90% and contrast -20%.....	135
Figure 2.109	Strain profile calculated from DIC system applied on the CLT bridge system .....	136
Figure 2.110	Relationship between voltage and displacement of CLT bridge system .....	137

## EXECUTIVE SUMMARY

According to the 2017 ASCE Infrastructure Report Card (ASCE 2017), 9.1% of the U.S. bridges are structurally deficient. The majority of deficient bridges are in service on low-traffic volume roads, and these bridges should be replaced or repaired for public safety in a timely manner. As an alternative to the deficient bridges, a new bridge system made with cross-laminated timber (CLT), which exhibits desirable design strength and low environmental impacts, can replace them properly (APA 2016). CLT is the most advanced wood panel system comprising several sawn lumber layers oriented in alternating directions and bonded holistically with adhesive. The CLT bridge system can be a sustainable solution to expand the use of wood products and create new pertinent markets for rural economic development.

To implement CLT products into a bridge system, this project aimed to develop a novel CLT bridge system. The following research objective-oriented tasks were undertaken:

**Task 1:** A CLT bridge system was conceptualized through the analysis of findings from a literature review:

- a. To investigate the existing CLT applications in bridges and other structures
- b. To create several conceptualized CLT bridge options
- c. To select the most promising CLT bridge system
- d. To perform a literature search on the structural performance of CLT components

**Task 2:** The selected CLT bridge system was designed according to structural engineering-based standards:

- a. To understand the domestic and international CLT design standards
- b. To design the selected CLT bridge system in terms of strength and serviceability following available timber bridge design guidelines and CLT structure design specifications

**Task 3:** Multiple CLT bridge components were manufactured to be used for fabrication of the designed bridge system:

- a. To manufacture CLT bridge components at Smartlam, including CLT beams, CLT decking, and CLT diaphragms, and transport them to the South Dakota State University (SDSU) Structural Laboratory
- b. To fabricate CLT bridge girders using CLT beams with adhesive or adhesive and fasteners
- c. To fabricate the CLT bridge system using the CLT bridge girders and the CLT decking along with the CLT diaphragms

**Task 4:** The fabricated CLT bridge girders and CLT bridge system were tested to evaluate their performance:

- a. To determine ultimate strength of the CLT bridge girders through their testing
- b. To determine ultimate strength of the CLT bridge system under displacement-controlled loading until failure

**In Task 1**, three CLT bridge systems were conceptualized through the literature review on CLT bridge applications. Among the conceptualized systems, the most promising CLT bridge system selection was made. Specifically, the literature review was conducted with technical documentation pertaining to CLT applications to bridges and other structures along with structural performance of CLT components. It was found that the existing CLT bridges were able to be broadly categorized into three types: CLT girder bridge, CLT deck bridge, and covered CLT bridge. With the findings and the basic information on traditional timber bridges in the United States, the research team conceptualized and proposed three possible CLT bridge system options, including simply CLT girder bridge, CLT arch bridge, and CLT double T-girder bridge. Considering the efficient design, construction, and inspection, the simple CLT

girder bridge was selected as the most promising option. To examine CLT bridge performance, a supplementary literature review related to CLT load testing was also carried out. It was reported that the load testing for CLT components was performed for their individual CLT member strength determination (e.g., flexural strength), but as far as the team knew, no full-scale CLT bridge systems have been tested to date.

**In Task 2**, the simple CLT girder bridge system selected in Task 1 was designed with the traditional timber bridge design codes, the CLT building design standards, and the properties of CLT materials provided by a local CLT producer, Smartlam. All the following design references included: 1) Timber Bridges: Design, Construction, Inspection, and Maintenance (Ritter 1990), 2) National Design Specification (NDS) for Wood Construction (AWC 2015), 3) Standard for Performance-Rated Cross-Laminated Timber (ANSI/APA 2018), 4) American Association of State Highway and Transportation Officials (AASHTO) Standard Specifications for Highway Bridges (AASHTO 2002), 5) AASHTO Load Resistance Factored Design (LRFD) bridge design specifications (AASHTO 2012) and 6) Eurocode 5: Design of Timber Structures - Part 2: Bridges (CEN 2004). The final dimension of the designed CLT girder bridge system being composed of one CLT deck, two CLT girders, and two CLT diaphragms was 6.40m long and 1.22m wide.

**In Task 3**, the different CLT components required for the fabrication of the designed bridge system were manufactured at Smartlam, and they were transported to the SDSU Structural Laboratory. Included in the CLT components were one CLT decking (5-ply), eight CLT beams (each having 7-ply), and two CLT diaphragms (each having 7-ply). To support the CLT bridge deck and live loads, a higher strength CLT girder than the 7-ply beam was required; thus, a 14-ply CLT girder was proposed in two ways: 1) one 14-ply CLT girder fabricated by two 7-ply CLT beams with adhesive and 2) one 14-ply CLT girder fabricated by two 7-ply CLT beams with adhesive and fasteners. These 14-ply CLT girders were fabricated at the SDSU Structural Laboratory using an actuator (500 kN) and clamping system that was proposed for this project. The one CLT girder bonded with adhesive and one CLT bonded with adhesive and fasteners were used for ultimate strength testing to validate their structural performance. The remainder of the CLT girders with adhesive were utilized as the main flexural members by connecting them to the CLT bridge decking using adhesive and fasteners. Lastly, the CLT bridge system was built with 5-ply CLT decking, two 14-ply CLT girders, and 7-ply CLT diaphragms using connection parts. Note, each of the CLT diaphragms was linked to the CLT girders at the end supports using rods and nuts.

**In Task 4**, the structural performance of CLT girders and CLT bridge system that were fabricated in Task 3 was evaluated using a series of ultimate load tests, including 1) CLT girder bonded with only adhesive, 2) CLT girders bonded with adhesive and fasteners, and 3) CLT bridge system. The adhesively bonded CLT girder was first tested to explore its ultimate strength, and then the CLT girder bonded with adhesive and fasteners was tested using monotonic loads until failure. It turned out that the ultimate strength of the 14-ply CLT girder bonded with adhesive and fasteners was 21.47% higher than that with only adhesive. The CLT bridge system consisting of the CLT girders with adhesive and fasteners, CLT decking, and CLT diaphragms was tested with a concentric displacement-controlled loading at the mid-span until failure. It was found that the tested CLT bridge system was able to resist the concentric load up to 262.50 kN, which means the bridge system will safely withstand an HS20 design truck load equivalent to 177 kN. Based on the testing results, the research team has demonstrated the possibility of the CLT bridge system to be a sustainable and resilient alternative to the U.S. deficient bridges. Note, for all the tests, different contact and non-contact sensors were installed to record deformation and strain data along with inspection images. The contact sensors included linear variable differential transformers (LVDTs), load cells, strain gauges, Bridge Diagnostics, Inc. (BDI) strain sensor, and string pots, while the non-contact sensors encompassed digital image correlation (DIC), unmanned aerial vehicle (UAV) installed with a gimbal camera, and a manipulator mounted with a smartphone camera.



# 1. PROJECT OBJECTIVES, OUTCOMES, AND IMPACTS

## Task 1: CLT bridge system conceptualization

- a. To investigate the existing CLT applications in bridges and other structures
- b. To create several conceptualized CLT bridge options
- c. To select the most promising CLT bridge system
- e. To perform a literature search on the structural performance of CLT components

To achieve the four objectives of **Task 1**, CLT bridge system conceptualization was made based on the findings from a literature review focusing on existing CLT applications in different types of structures such as bridges and buildings. It was found that Canada, Japan, Austria, and Norway have started to apply CLT products to partial bridge components, while there have been no CLT bridge applications on the U.S. highways. For instance, Hundorp Bridge in Norway, a steel truss bridge, was first built with concrete decking that was replaced with a lightweight bridge plank. Significant damage on the plank deck was identified, and then it was substituted with a CLT decking system.

From the literature review, existing CLT bridges can be broken down into three main types: CLT girder bridge, CLT deck bridge, and covered CLT bridge. With these three types, our research team conceptualized three feasible CLT bridge options for roadways: 1) simple CLT girder bridge, 2) CLT arch bridge, and 3) double T-shaped CLT girder bridge. Among the three options, the simple CLT girder bridge was considered the most promising CLT bridge system due to its practical design and maintenance, especially easy-approaching inspection.

During the literature review, some studies that attempted to perform load testing for structural performance evaluation of CLT components were also investigated. It was reported that some load testings have been conducted for CLT component-level and CLT system-level strength determination. For instance, Salokangas and Garnier (2013) conducted the ultimate strength testing of CLT beams, and Masoudnia et al. (2018) performed the composite bridge made with a CLT panel and laminated veneer lumber (LVL) beams. Masoudnia et al. (2018) developed the equation for CLT panel's effective flange width prediction considering the CLT's dimensions and modulus of elasticity. As far as the research team's investigation of the literature review pertaining to load testing, a full-scale CLT bridge system has not yet been tested.

## Task 2: CLT bridge design according to structural engineering-based standards

- a. To understand the domestic and international CLT design standards
- b. To design the selected CLT bridge system in terms of strength and serviceability following available timber bridge design guidelines and CLT structure design specifications

The simple CLT girder bridge system that was selected in **Task 1** was designed under **Task 2** according to various domestic (e.g., AASHTO LRFD bridge design specifications [AASHTO 2012]) and international timber bridge design specifications (Eurocode 5: Design of timber structures - Part 2: Bridges [CEN 2004]) along with other structures design codes (e.g., NDS for Wood Construction [AWC 2015]) because the bridge system using CLT is in the early stage in U.S. bridge codes. The CLT bridge system made with CLT products available in a local CLT provider, Smartlam (2018a), consisted of one CLT decking, two CLT girders, and two CLT diaphragms along with connection parts. The CLT bridge system design was completed by designing four main CLT components: 1) CLT girders, 2) CLT decking, 3) connections between girders and decking, and 4) CLT diaphragms. In accordance with a handbook, "Timber Bridges" (Ritter 1990), the CLT girder design was done with respect to flexural and shear strength criteria, accounting for the reasonably assumed CLT deck size using engineering judgments. After the girder design, the deck size was checked to meet the required flexural and shear strength. Note that serviceability about the deflection was also evaluated during both girder and deck design. When the

girder and deck design satisfied all strength and serviceability requirements, the connections were designed using fasteners to connect the deck to the girders following the NDS requirements. Referring to “Standard Plans for Timber Bridge Superstructures” (Wacker and Smith 2001), the diaphragms’ size and location were directly determined using the CLT properties.

### **Task 3: CLT bridge component and system production**

- a. To manufacture CLT bridge components at Smartlam, including CLT beams, CLT decking and CLT diaphragms, and transport them to the SDSU Structural Laboratory
- b. To fabricate CLT bridge girders using CLT beams with adhesive or adhesive and fasteners
- c. To fabricate the CLT bridge system using the CLT bridge girders and the CLT decking along with the CLT diaphragms

To achieve the three objectives for **Task 3**, the research team contacted six CLT manufacturers, including Smartlam, DR Johnson, X-LAM USA, Structurlam, Sauter Timber, and Katerra. Considering the cost and feasibility of the designed CLT bridge system throughout each of these manufacturers, Smartlam CLT products were chosen as full-scale testing materials. In total, eight 7-ply CLT beams were fabricated, the CLT decking that was designed in **Task 2** was fabricated with one 5-ply CLT panel, and two 7-ply CLT diaphragms were manufactured at Smartlam. All the fabricated CLT components were delivered to the SDSU Structural Laboratory on April 24, 2019. It should be noted that the eight 7-ply CLT beams were used to fabricate four 14-ply CLT girders because individual 7-ply CLT beams made with SL-V4 available in Smartlam did not have sufficient load carrying capacity to meet the AASHTO strength requirements.

To fabricate the 14-ply CLT girder, two clamping methods were proposed using 1) two 7-ply CLT beams bonded with adhesive or 2) two 7-ply CLT beams bonded with adhesive and fasteners. In the 14-ply CLT girder fabrication, polyurethane glue used in Smartlam was applied. To bond two 7-ply CLT beams with adhesive, pressure ranging from 689 to 1034 kPa was applied along the top of the two girders. Steel plates, threaded rods, and nuts required for the beam clamping were designed and manufactured at a local steel fabricator in South Dakota. With the developed clamping apparatuses and the actuator (342 kN), the fabrication of all the 14-ply CLT girders was made at the SDSU Structural Laboratory. We tested the one CLT girder with adhesive and the one CLT with adhesive and fasteners for their ultimate strength determination. For the CLT bridge system fabrication, fasteners were used to connect the CLT decking with each of the remaining CLT girders with adhesives, while rods were fastened with nuts between the CLT girders and CLT diaphragms.

### **Task 4: Ultimate load testing**

- a. To determine ultimate strength of the CLT bridge girders through its testing
- b. To determine ultimate strength of the CLT bridge system under displacement-controlled loading until failure

**Task 4** aimed at performing ultimate load tests of 1) one 14-ply CLT girder bonded with adhesive, 2) one 14-ply CLT girder bonded with adhesive and fasteners, and 3) one CLT bridge system. It should be noted that for the ultimate strength tests, a network of contact sensors, including 13 LVDTs, four load cells, 26 strain gauges, 12 BDI strain sensors, and two string pots, were installed on the CLT girders and CLT bridge system to record their deformation and strain data from each test. Additionally, non-contact sensors comprising DIC sensors, UAV equipped with a gimbal camera, and a manipulator with a smartphone camera were used for efficient inspections of each specimen. The results obtained from the contact sensors were compared with those from the non-contact sensors.

The adhesively bonded CLT girder was loaded with monotonic loadings up to failure in an attempt to determine its ultimate strength. The CLT girder bonded with both adhesive and fasteners was then applied by increased loads until the girder failed. The results showed that the CLT girder bonded with adhesive and fasteners had 21.47% higher capacity against the CLT girder bonded with only adhesive. To determine the structural performance of the CLT bridge system, monotonic load testing was also conducted until the bridge failure occurred. The testing demonstrated that the CLT bridge system had 262.50 kN load capacity, which was higher than 177kN resulting from the standard design truck load (HS20 truck load). With the testing results, we have left open the possibility of replacing U.S. deficient bridges with the CLT bridge system as an environmentally sustainable and resilient alternative.

## 2. PROJECT ACTIVITIES

### 2.1 CLT Bridge Conceptualization

This section deals with the findings from the investigation of existing CLT applications, CLT bridge conceptualization, and CLT bridge selection along with the literature search on the structural performance of CLT components. The details for each are provided in the following subsections.

#### 2.1.1 Existing CLT Applications

Utilization of CLT products has been steadily increasing in bridges and other structures such as buildings. Past and current applications of CLT to bridges and other structures have been reviewed and summarized herein.

##### 2.1.1.1 Bridges

The applications of CLT to bridges have been completed with a focus on CLT bridge members combined with other traditional timber bridge materials such as glued-laminated timber (glulam), as listed in Table 2.1. From the literature review, six CLT bridges, including Maicasagi Bridge in Canada, Mistassini Bridge in Canada, Hundorp Bridge in Norway, Ishikurazawa Bridge in Japan, River Mur arch bridge in Austria, and River Mur covered bridge in Austria, were identified. Note, Hundorp Bridge's initial decking was replaced with a CLT panel during maintenance, while the other CLT bridges were designed and built with different elements made with CLT. It was also found that the CLT bridges can be broadly classified into three types: 1) CLT girder bridge, 2) CLT deck bridge, and 3) covered CLT bridge. Further details on each type are provided as indicated below.

**Table 2.1** CLT bridge applications

Bridge type	Bridge	Location	Built year	Bridge length (m)	Design live load (kN)
CLT girder	Maicasagi Bridge	Québec, Canada	2011	68	1800
CLT deck with truss	Hundorp Bridge	Gudbrandsdalen, Norway	1924 (2010)	200	590
CLT deck with girder	Ishikurazawa Bridge	Akita, Japan	2017	7	140
CLT deck with arch	River Mur Arch bridge	River Mur, Austria	NA	NA	NA
CLT deck with girder	Mistassini Bridge	Québec, Canada	2014	160	80
Covered CLT	River Mur Covered Bridge	River Mur Austria	NA	NA	NA

*Note: Hundorp Bridge was initially built in 1924, but the decking was replaced with CLT in 2010; NA indicates not available.*

### ***CLT Girder Bridge***

The Maicasagi Bridge is a girder bridge as shown in Figure 2.1a. The Maicasagi Bridge located in Québec in Canada is the longest single-span timber bridge in the world (Cecobois 2018). The components were assembled at a manufacturing plant and transported to the Maicasagi River bridge site. With the prefabricated bridge components, construction was completed in only five weeks from start to finish (Cecobois 2018). This bridge was capable of supporting an approximately 1800kN logging truck across a 68 m span length. To meet the design requirements, this bridge was designed using the combined CLT and glulam (Egorov et al. 2018). The bridge's details are provided in Figure 2.1b. In this figure, the glulam is used as two main box girders consisting of the upper and lower chords, while CLT is used for connecting the upper and lower chords and for the construction of diaphragms and decking.

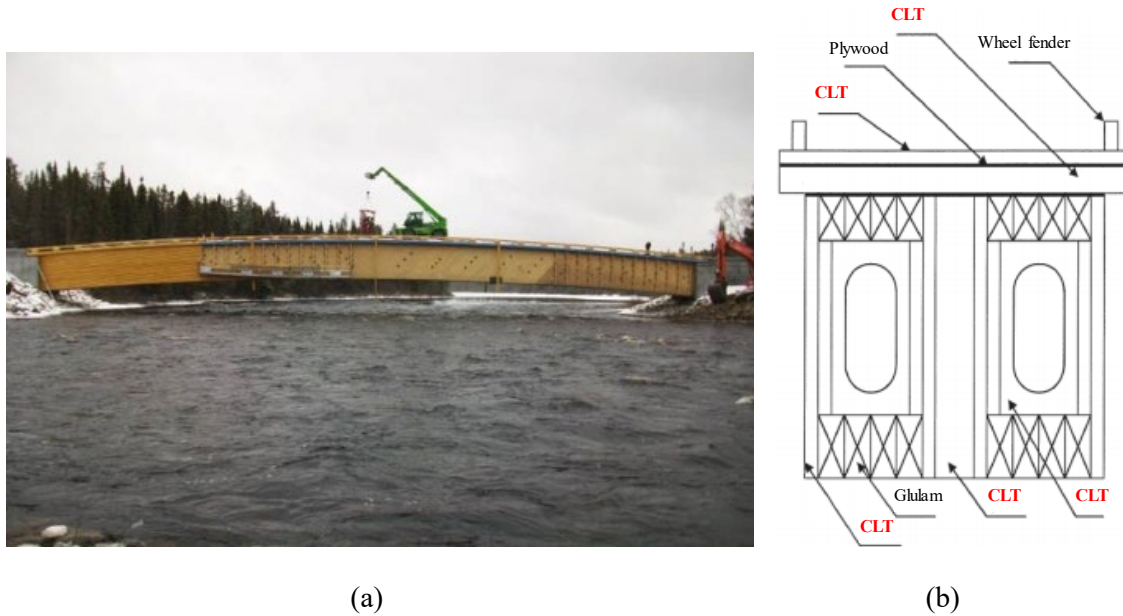


**Figure 2.1** Maicasagi Bridge (Egorov et al. 2018): (a) overall structure and (b) cross-section

### ***CLT Deck Bridge***

As shown in Table 2.1, Hundorp Bridge in Norway, Ishikurazawa Bridge in Japan, River Mur arch CLT deck bridge in Austria and Mistassini Bridge in Canada have utilized CLT as bridge decking. Each is detailed herein:

The Hundorp Bridge located in Gudbrandsdalen, Norway, was built in 1924. This bridge was a 200 m long steel truss bridge with concrete decking. In 1980, the concrete decking was replaced with a lightweight deck system consisting of corrugated steel plates with coating asphalt. In 2009, a hole in the deck was found, indicating the corrugated decking was no longer suitable for the Hundorp Bridge. Therefore, the corrugated decking was substituted with CLT decking due to its ease of maintenance (Abrahamsen and Nyløkken 2010) as shown in Figures 2.1a and 2.2b. The main purpose of the Norwegian Public Roads Administration for the deck replacement was to upgrade the bridge to endure higher traffic loads than current load demands.

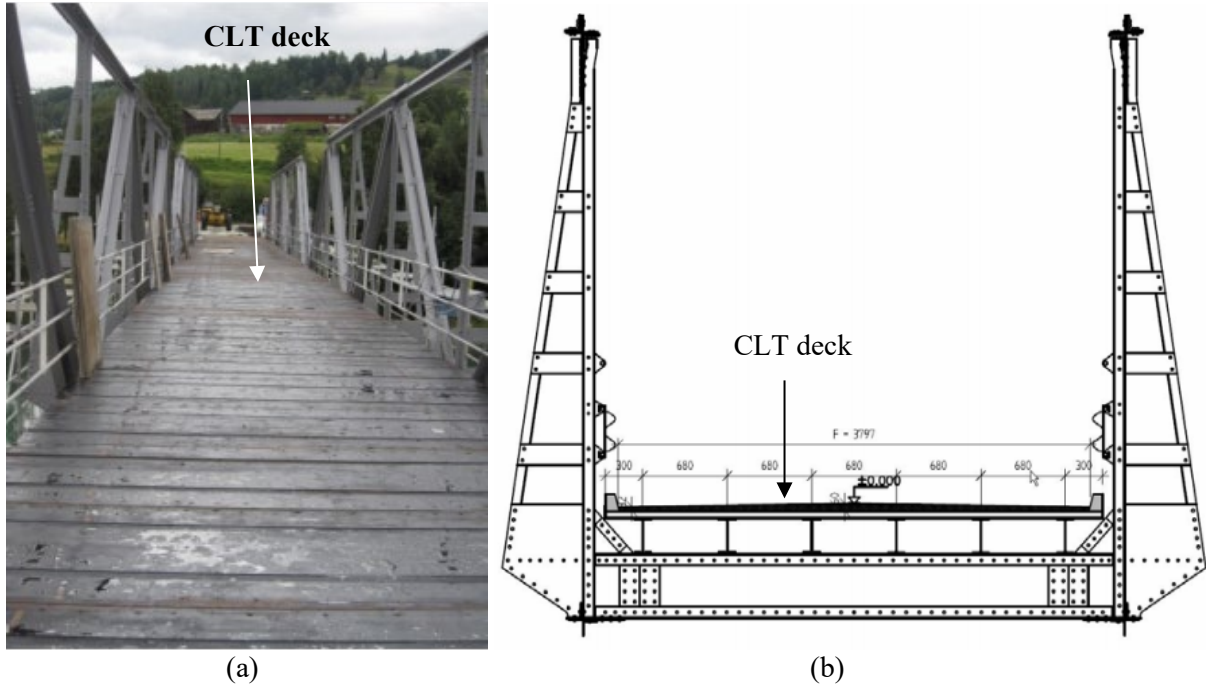


**Figure 2.2** Hundorp Bridge (Abrahamsen and Nyløkken 2010): (a) superstructure and (b) cross-section

The Ishikurazawa Bridge in Akita, Japan, is a forest road bridge, which used CLT for the deck as shown in Figures 2.3a and 2.3b. This bridge has a dimension of 7 m length and 3.5 m width, and the considered design load is 140 kN. Concrete abutments, steel girders, and CLT decking were applied to build the bridge system. It is well known that high moisture can cause visible damage on timbers. To improve water-resistance of CLT decking, fiber-reinforced plastic (FRP)-based waterproof treatments with spread type wood antiseptic, urethane painting, and polymer cement waterproofing were applied to the CLT bridge decking. To observe the treatment effects on the bridge, a load test was performed with trucks loaded with logs. In addition, Sasaki et al. (2017) carried out a study for practical use of CLT with the observation of its coating performance.

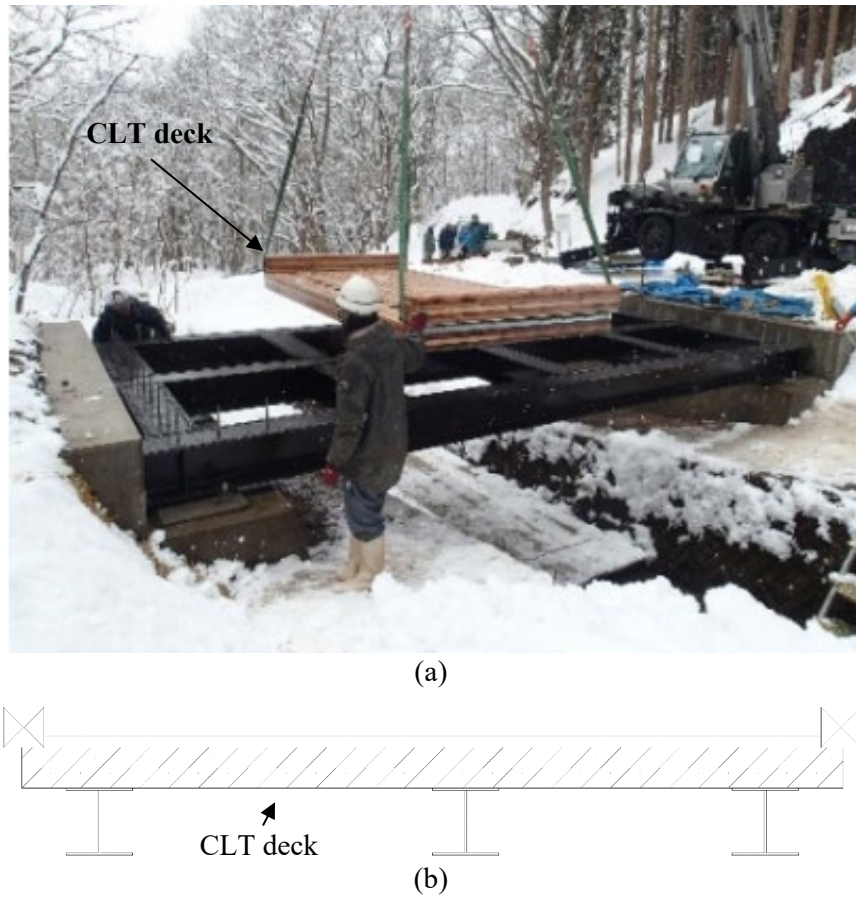


**Figure 2.3** Ishikurazawa Bridge (Sasaki et al. 2017): (a) overall bridge and (b) cross-section

Several timber bridges have been constructed over the river Mur in Austria. Among these, two bridges were constructed using CLT. For instance, Figure 2.4 shows an arch bridge with the ribbed CLT deck. This bridge was constructed for roadway use. Metal cladding was utilized to protect the CLT deck of this bridge.

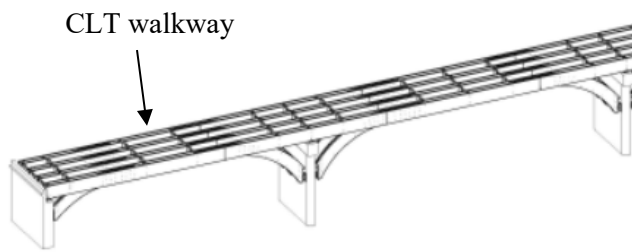


**Figure 2.4** Arch bridge with CLT deck over River Mur, Austria (Behrens and Benner 2015)

The Mistassini CLT Bridge (refer to Figures 2.5a and 2.5b) built in 2014 is located in Québec, Canada. This bridge used CLT as walkway decking (Lefebvre and Richard 2014). This bridge has a total 160m length. For the other components, glulams were applied to resist a design truck equivalent to 80 kN.



(a)



(b)

**Figure 2.5** Mistassini Bridge (Lefebvre and Richard 2014): (a) picture and (b) sketch

***Covered CLT Bridge***

A covered CLT bridge is located in River Mur, Austria, as shown in Figure 2.6a. This bridge consists of CLT deck, CLT walls, and CLT roof as depicted in Figure 2.6b. Metal claddings were employed to protect this bridge against environmental attacks (Behrens and Benner 2015).



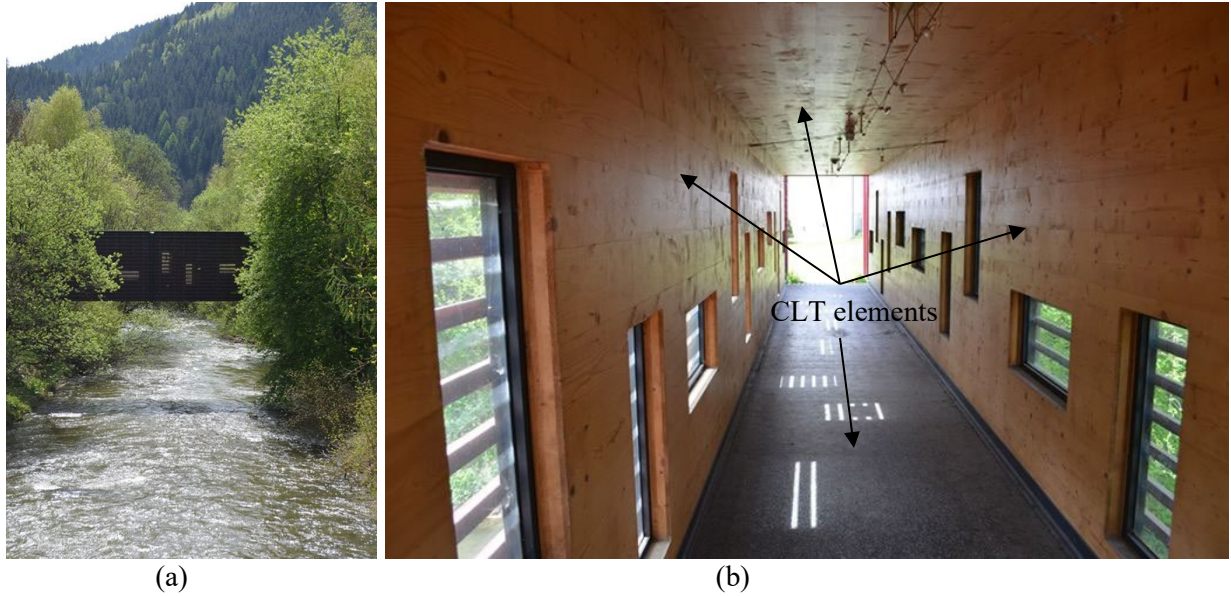


**Figure 2.6** Covered CLT bridge over River Mur, Austria (Behrens and Benner 2015): (a) outside of the bridge and (b) inside of the bridge.

### 2.1.1.2 Other Structures

The applications of CLT to other structures, especially buildings, have been observed as listed in Table 2.2. CLT has been in use from large commercial buildings, such as wholesale marts, to small commercial buildings, such as small restaurants and residential buildings. Further, the use of CLT products on residential buildings is prevalent in cities due to easy fabrication with prefabricated CLTs.

There have been many construction projects of buildings made with CLT in Europe, North America, and Japan. Among European countries, UK built the five-story CLT structure in 2005, which was the tallest residential building in the world at that time. The CLT building constructed under the Waterson Street project was a combination of a commercial and residential complex development at Waterson Street in London. At first, the CLT was applied to lift the shaft and stair core (Zumbrunnen 2013). Murray Grove, in which all the elements (walls, floor, and stairs) of the building were constructed with prefabricated CLT, is the first high rise building in London, UK (Table 2.2). Murray Grove showed the potential of CLT as an economical and eco-friendly building material. This building motivated the use of CLT in the UK and increased its use in the world (Waugh Thistleton Architects 2018).

**Table 2.2** CLT building applications

Building name	Location	Built year	CLT component	Story
Waterson St. project	London, UK	2005	All	5
Murray Grove	London, UK	2009	All	9
Bridport House	London, UK	2010	Wall, floor	8
Bristol project	Bristol, UK	2009	Wall, floor	3
Holz8 (H8)	Bad Aibling, Germany	2011	Wall, floor	8
Limnologen Project	Vaxjo, Sweden	2008	Wall, floor	8
Forte	Melbourne, Australia	2013	Wall, floor	10
Candlewood Suites	Alabama, U.S.	2016	NA	4
John W. Olver Design Building	Massachusetts, U.S.	2017	Wall	3
Ootoyo dormitory	Kochi, Japan	2014	Wall, floor	3

The Bridport House was rebuilt for London due to a problem in the planning step. Existing concrete frame structures were not allowed due to excessive weight. To simultaneously solve the problem of construction deadline and weight, the Bridport House was constructed using CLT. The framework, which is expected to take 20-24 weeks with the traditional material and method, was shortened to 10 weeks with the CLT. In addition, CLT was the best choice to solve the weight issue. This doubled the height of the original concrete building, while the load only increased by 10% compared with the load from the original building (Wood for Good 2018).

The Bristol project showed the possibility of expanding the CLT market through the economic feasibility of CLT. After the Waterson Street project, new mid-rise buildings were constructed. In Bristol, UK, a social housing project, known as the Bristol project, was built to three stories in 2009. In a price competition, the Bristol project proved that the CLT building materials were economically competitive to other conventional construction materials (Zumbrunnen 2013).

In addition to the UK's CLT buildings, Holz8 in Bad Aibling in Germany was constructed with CLT, as shown in Table 2.2. When designing the building with a height of 25 m, according to German building codes (Bauordnungsrecht 2016), high requirements for fire protection, statics, and sound insulation were considered to use the building for commercial purposes (Schrödter and Breuer 1998). Because of fire protection, the building stairs had to be built with reinforced concrete (Detail 2012).

For the Limnologen Project that was completed in Vaxjo, Sweden, CLT, was used for wall and floor construction. Note, the first floor was made with concrete to facilitate anchoring the floor above due to increasing self-weight, but all Limnologen exterior walls made of CLT were loadbearing. More than 40 rods were installed in every building to handle wind pressure uplift. These tension rods were fixed to the concrete on the first floor and extended from inside the inner CLT wall to the top (Serrano 2009). Meanwhile, Forte is a nine-story CLT building that was completed within 10 months in Melbourne, Australia. After the underground construction, including the foundation with concrete frame and pile, the upper part of the structure was constructed using CLT.

In the United States, building projects with CLT use have increased. For instance, the new Candlewood Suites at Redstone Arsenal opened in 2016 in Alabama is the first U.S. hotel that used CLT for construction. The John W. Olver Design Building, completed in 2017 at the University of Massachusetts Amherst, is the first university building in the U.S constructed with CLT (Athena Sustainable Materials Institute 2017; Gu and Bergman 2018).

Japan, an earthquake-prone country, has also increased an interest in the use of CLT. Japan announced a roadmap to pave the way to apply CLT in the Japanese construction market. The CLT system allows the opportunity to build taller wooden buildings than conventional timber buildings (CBI Ministry of Foreign Affairs 2017). The CLT material standard (JAS 3079, Japanese Agricultural Standard 3079) established in 2014 oversees CLT quality. In the same year, the first Japanese building constructed with CLT was completed and used as a dormitory structure in Ootoyo Town in Kochi Prefecture. CLT was used in the structure's flooring and shear walls (Fumoto 2014).

### **2.1.2 CLT Bridge Conceptualization**

This section presents the schematic design and shape of possible CLT bridges. Three CLT bridge options proposed based on the literature review findings include: 1) CLT arch bridge, 2) CLT double T-girder bridge, and 3) CLT girder bridge.

### 2.1.2.1 CLT Arch Bridge

Generally, an arch bridge is one in which the beam is supported at both ends and the end supports are restrained horizontally. The horizontal reaction force transmits the axial force together with bending moments to the main arch through columns. Because the bending moment generated by the horizontal reaction force acts to eliminate the bending moment generated by the axial force, only the axial force of the compression force occurs in the arch. The arch is more complex than a traditional simple girder bridge. The arch bridge has been popular for a while due to its structural efficiency and aesthetic values. However, it is believed that it is relatively difficult to maintain a CLT arch bridge in good condition economically over their life because of the difficulty of inspecting it in its complexity. Elevation and cross-section views of the CLT arch bridge are shown in Figures 2.7a and 2.7b, respectively.

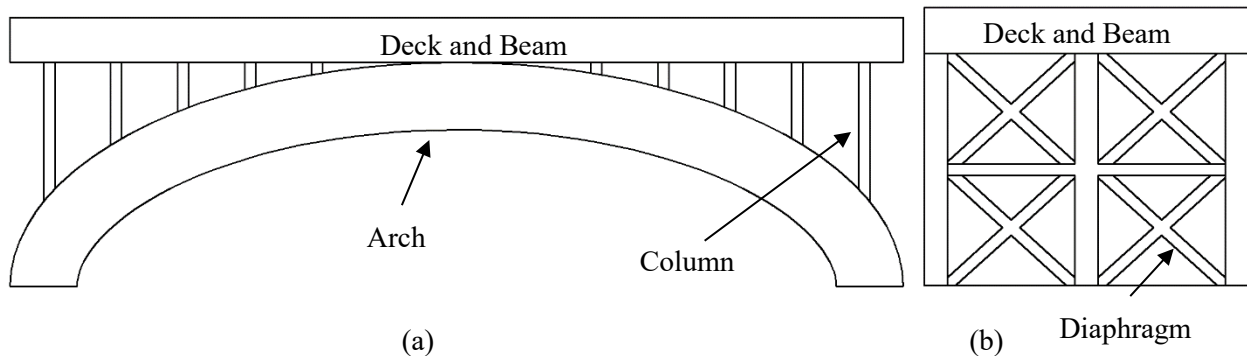


**Figure 2.7** CLT arch bridge: (a) elevation view and (b) cross-section

### 2.1.2.2 CLT Double T-girder Bridge

Figures 2.8a and 2.8b show elevation and cross-section views for a representative schematic of the CLT double T-girder bridge. This bridge option has similar advantages as the simple girder bridge. The simplicity of the bridge makes it more likely to be constructed and less affected by the terrain. For this reason, it is suitable for various construction sites. The bridge geometry can simplify the load and external conditions to consider in the design process. The strong coupling between the flange (upper horizontal part) and two stems (lower vertical part) can increase the capacity of the bridge as shown in Figure 8b. Because the double T-girder is known to have a higher load-resisting capacity than a conventional T-girder, the double T-girder construction using CLT is expected to be more resilient. It is expected that damage due to both external forces and moisture can be detected easily. However, the CLT double T-girder bridge may not have the strong coupling of the CLT flange and CLT stem due to minimal composite action between them.

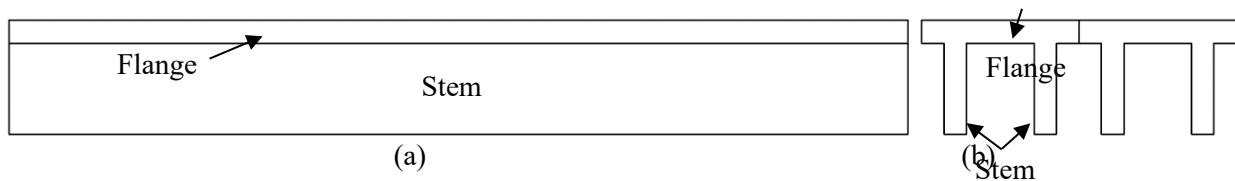


**Figure 2.8** CLT double T-girder applied bridge: (a) elevation view and (b) cross-section

### 2.1.2.3 CLT Girder Bridge

A simple CLT girder bridge (Figures 2.9a and 2.9b) consists of the CLT deck that is laid on CLT girder and simple rectangular-shape CLT girder. Vehicle wheel loads are transferred to the support points through bending, shear, or torsional resistance in the girder and deck members. The girder bridge is one of

the bridge types that has high constructability due to its simple shape. Because of its high adaptability, it can be used on a wide range of terrains. Since the shape is simple, the loads and external conditions to be considered for the design process are simplified. It is possible to minimize instability due to unknown external conditions. In addition, when the deck and girder is composited and constructed, the rigidity of the cross section is much increased. When compared with other types of bridges, such as concrete bridges, CLT bridges are highly vulnerable to moisture. For this reason, it is necessary to easily inspect the damage caused by external forces and damage caused by moisture.

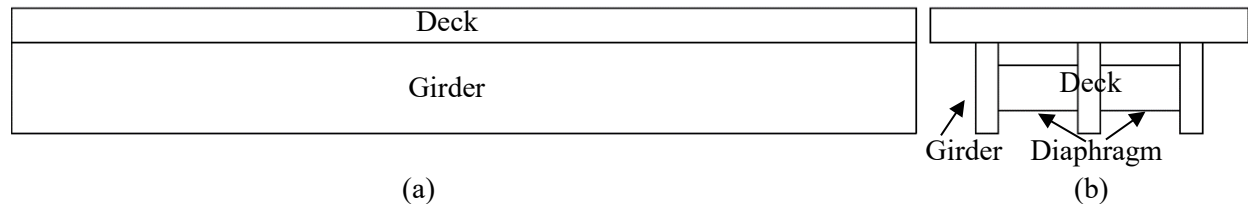


**Figure 2.9** Simple CLT girder bridge: (a) elevation view and (b) cross-section

### 2.1.3 CLT Bridge Selection

As presented in Section 2.1.2, the three possible CLT bridge options include CLT arch bridge, CLT double T-girder bridge, and CLT girder bridge. Among the three options, the CLT girder bridge with its simple geometry was selected as the most promising CLT bridge system for this project because of its feasible design and fabrication, practical maintenance, and easy-approaching inspection. In particular, the easy-approaching inspection is needed since high moisture can cause significant damage on traditional timber bridges like CLT bridges, compared with concrete and steel bridges.

### 2.1.4 Literature Search on CLT Structural Performance

To evaluate the structural performance of CLT components, the literature search on CLT load testing was conducted. Findings from the search on CLT component-level and CLT system-level tests are discussed in the following subsections.

#### 2.1.4.1 CLT Component-level Testing

Several previous studies have been performed on CLT components with a number of load tests by Salokangas and Garnier (2013), He et al. (2018), Buck et al. (2016), and Poulin et al. (2018). In general, there are two types of CLT component-level tests: a) CLT beam test and b) CLT panel test. In the CLT beam test, CLT has been used as a beam, while the CLT panel test refers to a load test performed on a wide plate type CLT, which can be possibly utilized as a bridge deck.

#### *Beam*

Salokangas and Garnier (2013) tested CLT beams at the longitudinal direction, which refers to flatwise bending testing, and then at 90° with respect to the longitudinal direction, which means edgewise bending testing. The flatwise CLT bending testing was to examine the local failure that may occur, while the edgewise CLT bending testing was to examine the overall failure of the beam rather than its local failure. Specifically, the flatwise bending test was performed with 1400 mm long x 150 mm wide x 149 mm deep beam, whereas the edgewise bending test was conducted with 5990 mm long x 159 mm wide x 300 mm deep beam. It was found that rolling shear failure, as shown in Figure 2.10a, was observed at 50 kN in the test with the flatwise bending beam. The rolling shear can be defined as shear stress occurring in the vertical direction perpendicular to the wood grain (Li 2014), as detailed in Figure 2.10b. The rolling shear is not considered as a basic characteristic property of the material in several studies; however, it could be

the substitutional smeared shear stiffness of wooden material (Aicher and Dill-Langer 2000). For concentrated loads on a short-span bridge, the low capacity of rolling shear stress is considered an important factor. Therefore, a sufficient capacity of rolling shear strength needs to be taken into account for the CLT beam design (Nie 2015). In addition to the flatwise bending testing, Salokangas and Garnier (2013) determined the ultimate strength of the edgewise CLT beam, which failed at 72 kN due to its flexural failure, as shown in Figure 2.10c. It was reported that the difference between the failure modes was caused by the orientation of the CLT beam, and that the ultimate strength of flatwise bending beam failed because the rolling shear was 30.56% lower than that of the edgewise beam.

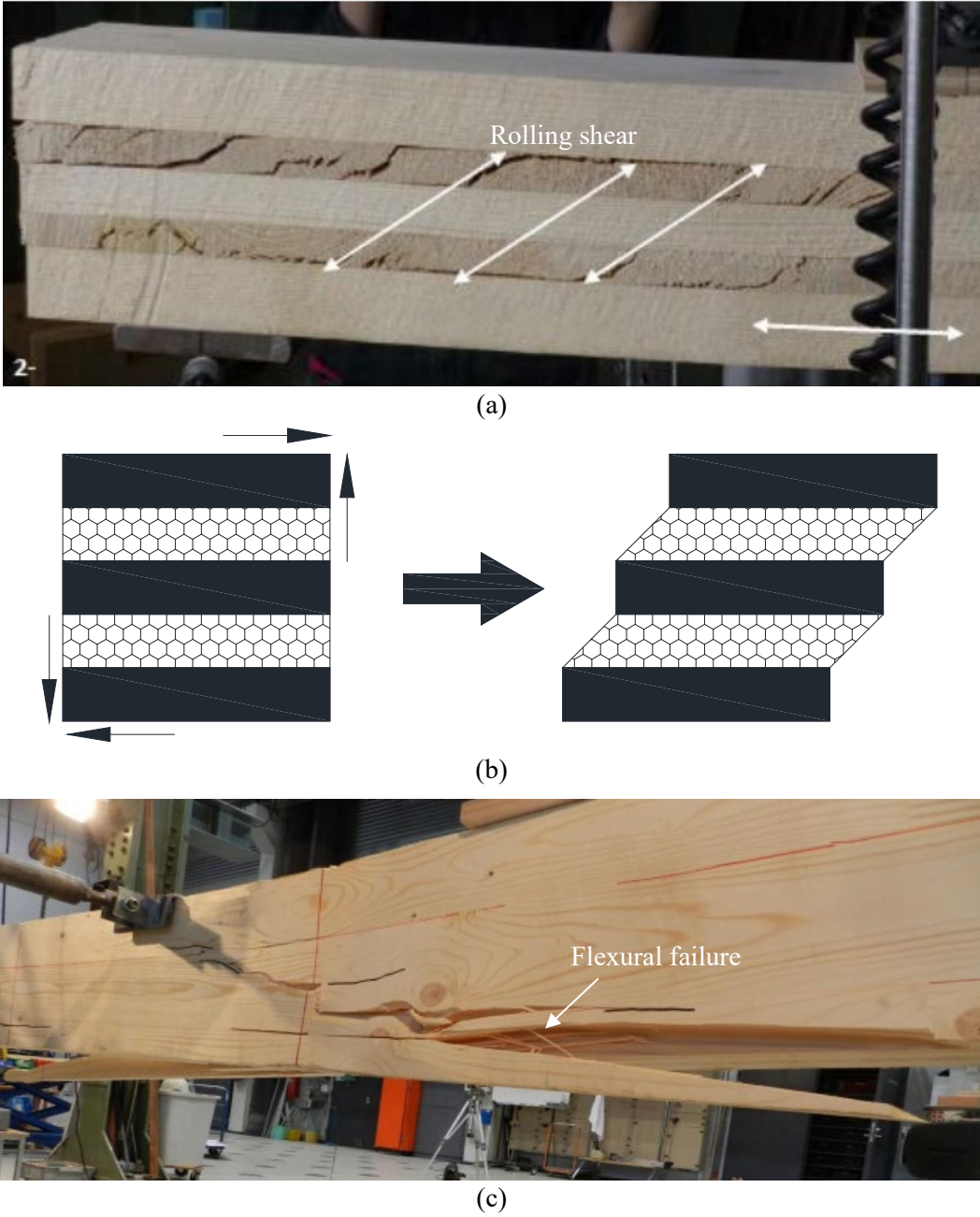


**Figure 2.10** CLT beam failures: (a) rolling shear; (b) rolling shear failure mechanism; and (c) flexural failure (Salokangas and Garnier 2013)

He et al. (2018) carried out the four-point bending tests on the CLT beams to evaluate their flexural strength on the longitudinal and transverse directions. It was concluded that the average flexural strength of the CLT beam in the longitudinal direction was 44 kN, whereas the strength of the CLT beam with respect to transverse axis was found to be 23 kN. Furthermore, the outer layer contributed less to the flexural strength when the outer wood particles extended perpendicular to the longitudinal direction. Also, it was found that the flexural failure was observed on the bottom layer of most CLT beams tested, and the rolling shear failure was identified in the inside layers of some CLT beams.

### ***Panel***

Buck et al. (2016) performed an experimental evaluation of a CLT panel laminated at an alternative angle. The size of the panel specimen consisting of five CLT layers was 95 mm deep × 590 mm wide × 2000 mm long. The tested CLT panel has two transverse layers arranged in +45° and -45°. The average ultimate load of the newly proposed CLT panel was found to be 148 kN, whereas the average ultimate load of the conventional CLT panel stacked crosswise at 90° was 110 kN. It was reported that the bond failure due to the initial rolling shear was observed in the conventional CLT panel, and the shear failure in the longitudinal direction was found in the alternative CLT panel.

Poulin et al. (2018) conducted load testing to investigate the out-of-plane behavior of CLT panels, including 3-ply and 5-ply panels under static loadings. The rolling shear was observed simultaneously with the initial fracture in both 3-ply and 5-ply panels. Additionally, Chen and Lam (2013) carried out a four-point flexural strength test to evaluate the stiffness of the CLT panel specimens with different layups, such as three-layer cross-laminated plates' panel and four-layer 45° laminated plates' panel. It was demonstrated that the 45° laminated panel had greater flexural stiffness values as compared with the other panels.

#### **2.1.4.2 CLT System-level Testing**

There are few studies regarding the CLT system-level testing (Chen and Lam 2013, Masoudnia et al. 2018). Chen and Lam (2013) attempted to determine the ultimate strength of box-shaped CLT systems subjected to out-of-plane loadings but failed to discover the load-carrying capacity for the majority of tested CLT systems. Masoudnia et al. (2018) tested a full-scale timber composite beam system comprising a CLT panel and LVL beams with variation in numbers of screws. They found that the amount in the monitored slip between the CLT panel and LVL beams decreased due to the reduction in the screw numbers, and the test data were used to help validate the numerical model to estimate the effective width of various timber composite beams.

## 2.2 CLT Bridge Design According to Structural Engineering-based Standards

The selected simple CLT girder bridge system was designed in compliance with the various domestic and international design specifications. The subsections below involve presenting the CLT design standards, which provide an overview of the CLT bridge design procedures, and the CLT design details for major CLT bridge components and their systems. Note, all design equations used herein were in accordance with U.S. customary units, and the dimensions and properties for the CLT girder bridge system were collected in U.S. customary units. Therefore, these equations in U.S. customary units were used, but all calculated values were converted in the International System of Units to make all units consistent through the report.

### 2.2.1 CLT Design Standards

An extensive literature review on the CLT design was completed for the design of the selected CLT girder bridge system. Through the literature review, different domestic design standards (e.g., the AASHTO and NDS specifications) and international design standards (e.g., Eurocode) were reviewed. It was found that the CLT bridge design has not been completed before in the U.S. and was in a rudimentary stage in other countries. Hence, the research team used the following conventional CLT design codes and timber bridge design specifications: 1) Timber Bridges: Design, Construction, Inspection, and Maintenance (Ritter 1990), 2) National Design Specification for Wood Construction (AWC 2015), 3) Standard for Performance-Rated Cross-Laminated Timber (ANSI/APA 2018), 4) Standard Specifications for Highway Bridges (AASHTO 2002), 5) AASHTO LRFD bridge design specifications (AASHTO 2012), 6) Wood Handbook (Forest Products Laboratory 2010), 7) CLT Handbook (Karacabeyli and Douglas 2013), and 8) Eurocode (EN 1995-2 2004).

Particularly, the CLT bridge was designed following the procedures provided in Timber Bridge (Ritter 1990) and some design procedures referenced other CLT design codes such as CLT Handbook, as shown in Figure 2.11. For instance, the research team referred to Wood Handbook (Forest Products Laboratory 2010) and CLT Handbook (Karacabeyli and Douglas 2013) for prediction of deflections of CLT beams and decks rather than Timber Bridge (Ritter 1990). This was because the deflection check in Timber Bridges (Ritter 1990) was based on the conventional timbers such as glulam and sawn lumber. To check deflection in conventional timbers, bending stiffness,  $EI$ , was required, while the CLT bridge needed apparent modulus of elasticity,  $EI_{app}$ , that can be calculated by the effective bending stiffness,  $EI_{eff}$ , and the shear deformation adjustment factor. Wood Handbook (Forest Products Laboratory 2010) and CLT Handbook (Karacabeyli and Douglas 2013) were referred to obtain the CLT effective bending stiffness and shear adjustment factor. Details on how to design the CLT bridge are provided in the next sections.

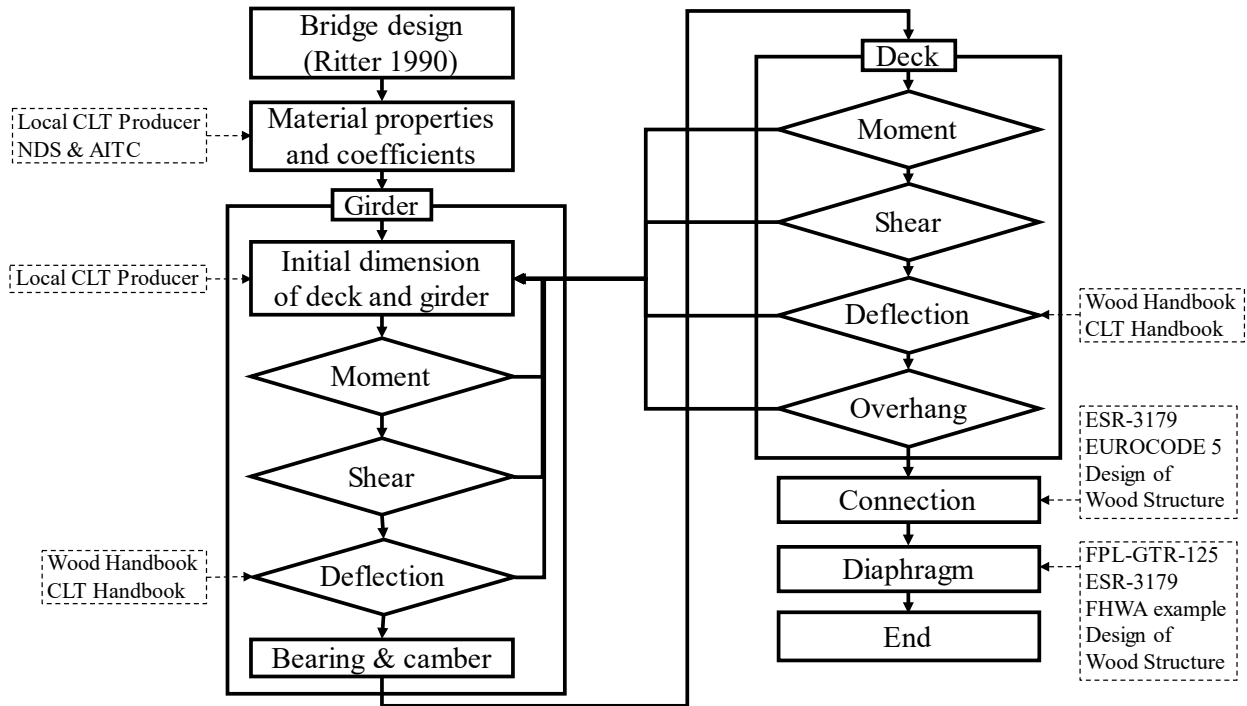


Figure 2.11 CLT bridge design flowchart with design codes

2.2.2 CLT Bridge Design Details

The CLT girder bridge that was selected in Section 3.1.3 is designed herein. The dimensions of the bridge in the initial design process were 1.22 m x 0.66 m x 6.40 m (width x depth x length). Note that width, depth, and length indicate the roadway width, the depth of the bridge system from the bottom of the girder to the top of the deck, and the span length of the center-to-center bearing, respectively. The thickness of the initially chosen deck was 0.17 m. The bridge was designed for one-lane traffic and the AASHTO Load Group I loading with a HS 20-44 vehicle (Figure 2.12) according to Timber Bridge (Ritter 1990). Referring to the flowchart shown in Figure 2.11, the design of a CLT girder required the initial dimensions of the deck. If an unsolvable design error in the deck and/or girder is found, the deck dimensions need to be changed, and then other bridge components should be redesigned.

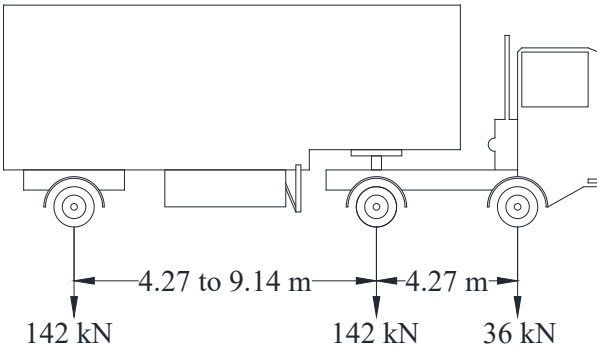


Figure 2.12 Schematic of HS20-44 truck



### 2.2.2.1 CLT Girder Design

According to the aforementioned bridge design guidelines, particularly Timber Bridge (Ritter 1990) and Wood Handbook (Forest Products Laboratory 2010), the design of a CLT bridge girder with the initially assumed deck dimensions was completed. Details on the CLT girder design are presented as follows:

#### *Strength Criteria*

With the deck dimensions determined in Section 3.2.2, two CLT girders with a spacing of 0.61 m and 0.3 m overhang length was chosen following the design recommendations from Timber Bridge (Ritter 1990). Each girder was designed with CLT V4 products available from the local CLT producer Smartlam (Smartlam 2018b), having compression strength perpendicular to grain design value ( $F_{c\perp}$ ) = 2.31 MPa and shear design values ( $F_{v,0}$ ) = 0.93 MPa.

CLT girders 0.24 m wide x 0.48 m deep x 6.40 m long were selected at an initial phase. The total dead load was calculated considering the weight and thickness of the CLT deck and CLT girder with the girder spacing of 0.61 m. Note that the exterior girder was calculated without consideration of vehicular railing in this design. The dead load,  $w_{DL}$ , was calculated from the dimension of deck and CLT weight (387.65 kg/m<sup>3</sup>). The maximum moment due to the dead load,  $M_{DL}$ , was then calculated in Equation 1.

$$M_{DL} = \frac{w_{DL}L^2}{8} \quad (1)$$

where  $M_{DL}$  = the maximum moment due to dead load, kip.

$w_{DL}$  = the uniformly distributed dead load, kip.

$L$  = the span length, ft.

*Note: 1 kip = 4.45 kN and 1 ft = 0.3048 m*

The moment resulting from live loads was calculated from Equation 2. There are no requirements on how to distribute live loads over the CLT girders in the AASHTO Standard AASHTO Standard (2002) and the AASHTO LRFD (2012). It was assumed that live load distribution factors (LLDFs) necessary for the determination of live load effects on each CLT girder, which is similar to a glued laminated girder, were calculated with  $s_g/10$  for the glued laminated panels on glued laminated stringers given in Table 4.6.2.2a-1 of AASHTO LRFD (2012), and the resulting moment was determined given in Table 16-8 of Timber Bridges (Ritter 1990). Note,  $s_g$  indicates the spacing between the girders.

$$M_{LLDF} = M_{LL}(LLDF) \quad (2)$$

where  $M_{LLDF}$  = the maximum moment due to live load with consideration of DF, kip.

$M_{LL}$  = the maximum moment due to live load without consideration of DF, kip.

$LLDF$  = the live load distribution factor,  $s_g/10$ , for glulam deck on glulam beam.

The initial section modulus,  $S_x$ , of the CLT girder was calculated based on the moments created by dead and live loads from the deck. The initial load distribution factor ( $C_D$ ), wet service factor ( $C_M$ ), temperature factor ( $C_t$ ), and beam stability factor ( $C_L$ ) were assumed to be 1.0. Lateral stability factor of the girder  $C_L$  is 1.0 due to consideration of a diaphragm designed in National Design Specification for Wood Construction (AWC 2015). Note,  $F_b'S_{eff}$  can be obtained from the CLT product report ( $F_b'S_{eff}$  of 7-lam V4 CLT = 32.58 kN-m/m) provided by the local CLT producer Smartlam (2018a).

$$F'_b S_{\text{eff}} = F_b S_{\text{eff}} C_D C_M C_t C_L \quad (3)$$

where  $F'_b$  = the adjusted bending design value, psi.

$S_{\text{eff}}$  = the effective section modulus, in<sup>3</sup>.

$F_b$  = the reference bending design value, psi.

$C_D$  = the load distribution factor.

$C_M$  = the wet service factor.

$C_t$  = the temperature factor.

$C_L$  = the beam stability factor.

Note: 1 psi = 6.89 kPa and 1 in<sup>3</sup> = 16387.1 mm<sup>3</sup>

The total moment of the CLT girder subjected to the considered loads is equal to the sum of the moments generated by dead and live loads, as shown in Equation 4.

$$M = M_{DL} + M_{LLDF} \quad (4)$$

$S_x$  can be obtained using the maximum total moment, as shown in Equation 5. The CLT girder size was determined using  $S_x$  obtained from Equation 5. Adjusted bending design value,  $F'_b$ , can be calculated with  $F'_b = F_b C_D C_M C_t C_L$ .

$$S_x = \frac{M}{F'_b} \quad (5)$$

where  $S_x$  = the section modulus, in<sup>3</sup>.

$F'_b$  = the adjusted bending design value, psi.

Since  $S_x$  from the initial CLT dimensions satisfied the required value of  $S_x$  calculated by Equation 5, the dimensions with the calculated  $S_x$  can be used for the further design. The calculated section properties of the CLT girder with 0.24 m wide and 0.48 m deep are as follows:  $A = 0.1180 \text{ m}^2$ ,  $S_x = 0.0096 \text{ m}^3$ ,  $I_x = 0.0024 \text{ m}^4$ , and weight = 45.74 kg/m. Note, the depth of the CLT girder was the same as the thickness of 14-ply CLT that can be fabricated with two 7-ply CLT beams producible in Smartlam.  $F'_b$  was calculated based on the section properties of the 14-ply CLT girder, as shown in Equation 6. The girder is adequate in terms of flexural strength if  $F'_b$  is greater than  $f_b$ .

$$f_b = \frac{M}{S_x} \quad (6)$$

where  $f_b$  = actual bending stress, psi.

The maximum shear of the CLT girder can be calculated from Equation 7. The uniformly distributed loads ( $w_{DL}$ ) in the equation were applied to the total dead load obtained from the moment calculation. The  $w_{DL}$  at a distance  $d$  from support shall be neglected when wooden members are supported by the bearing given in the AASHTO Standard 13.6.5.2 (AASHTO 2002). Figure 2.13 shows the position of  $w_{DL}$  neglecting the loads under the depth of girder ( $d$ ).

$$V_{DL} = w_{DL} \left( \frac{L}{2} - d \right) \quad (7)$$

where  $V_{DL}$  = the maximum shear due to dead load at a distance of  $d$  from the support, kip.  
 $d$  = the depth of girder, ft.

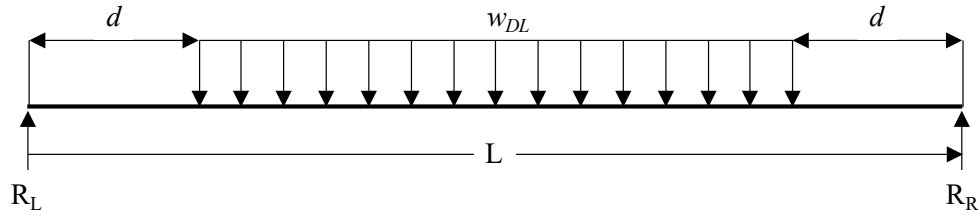


**Figure 2.13** Applied  $w_{DL}$  along the CLT girder.

The AASHTO Standard (2002) suggested that the maximum shear force due to undistributed live load ( $V_{LU}$ ) occurs at the minimum distance of  $3d$  or  $L/4$  from the point (Figure 2.14). Shear LLDF was calculated from the Table 4.6.2.2.2a-1 of AASHTO LRFD Bridge (2012).

$$V_{LD} = V_{LU}(LLDF) \tag{8}$$

where  $V_{LD}$  = the maximum vertical shear at  $3d$  or  $L/4$  due to wheel loads distributed laterally as specified for a moment, kip.

$V_{LU}$  = the maximum vertical shear at  $3d$  or  $L/4$  due to undistributed wheel loads, kip.

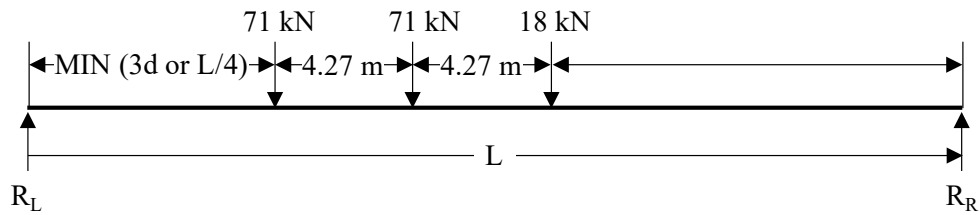


**Figure 2.14** Location of the live load for maximum vertical shear

$V_{LL}$  was obtained through Equation 9 that was obtained from the AASHTO Standard 13.6.5.2 (2002) and AASHTO LRFD 4.6.2.2a (2012) to determine the maximum shear considering the considered HS 20-44 vehicle.

$$V_{LL} = 0.5[(0.6V_{LU}) + V_{LD}] \tag{9}$$

where  $V_{LL}$  = the distributed live load vertical shear, kip.

Shear stress can be calculated from Equation 10, where  $A$  is the cross-sectional area of the selected CLT girder. The required shear stress (Equation 10) is compared with the reference shear stress, which can be determined in Equation 11. The total shear force ( $V$ ) is the sum of the values obtained from Equations 7 ( $V_{DL}$ ) and 9 ( $V_{LL}$ ).

$$f_v = \frac{1.5V}{A} \tag{10}$$

where  $f_v$  = the actual shear stress, psi.

$$V = V_{DL} + V_{LL}, \text{ kips.}$$

The shear stress  $F_v'$  is calculated based on the values of shear LLDF and the assumed wet service and temperature on the material properties of the considered CLT girder, as shown in Equation 11. The girder is considered adequate in shear if  $F_v'$  is larger than  $f_v$ .

$$F_v' = F_v C_D C_M C_t \quad (11)$$

where  $F_v'$  = the adjusted shear design value, psi.

$F_v$  = the reference shear design value, psi.

Area of the bearing can be calculated from Equation 12. The bearing in the girder design was considered for dry service condition since the CLT girder bridge was set up for the test inside the laboratory. Considering the conditions, wet service factor ( $C_M$ ) and temperature factor ( $C_t$ ) were selected as 1.0 and bearing area factor,  $C_b$ , was calculated using Equation 13 from NDS (2015).

$$F_{C\perp}' = F_{C\perp} C_M C_t C_b \quad (12)$$

where  $F_{C\perp}'$  = the adjusted compression design value perpendicular to grain, psi.

$F_{C\perp}$  = the reference compression design value perpendicular to grain, psi.

$$C_b = \frac{\ell_b + 0.375}{\ell_b} \quad (13)$$

where  $\ell_b$  = the bearing length measured parallel to grain, ft.

$R_{DL}$  and  $R_{LL}$  need to be calculated to obtain the required bearing length, as shown in Equation 14.  $R_{DL}$  is the reaction force generated by the dead load, and  $R_{LL}$  is the reaction force generated by the live load considering the LLDF. For conservative design considerations and ease of construction, the bearing length longer than required was selected. Note, the final girder length (out-to-out) was the sum of initial girder length and selected bearing length.

$$\text{Required bearing length} = \frac{R_{DL} + R_{LL}}{b(F_{C\perp}')} \quad (14)$$

where  $R_{DL}$  = the reaction force due to dead load, kip.

$R_{LL}$  = the reaction force due to live load, kip.

$b$  = the width of girder, ft.

$F_{C\perp}'$  (Equation 12) and  $f_{C\perp}$  (Equation 15) are compared to confirm the stability of the girder with the new length.

$$f_{C\perp} = \frac{R_{DL} + R_{LL}}{A} \quad (15)$$

## Deflection Criteria

The deflection criteria for the CLT girder bridge are not provided in the AASHTO LRFD (2012) and Timber Bridge (Ritter 1990). According to the AASHTO LRFD C2.5.2.6.2 (2012), however, deflection for timber bridges is recommended to follow the recommendations of Chapters 7, 8, and 9 in Timber Bridge (Ritter 1990). Ritter (1990) recommended the maximum deflection for timber bridge design as follows:

1. For live loads, the limitation of maximum deflection is  $L/360$ .
2. For the combination of live load and dead load, limitation of maximum deflection is  $L/240$ .

These recommendations were used for the CLT girder bridge design. To determine deflection of the girder on dead load, Equation 16 was utilized. The value of constants  $k_s$  and  $k_b$  are obtained from Table 9-1 of Wood Handbook (2010). These values of constants were determined according to loading conditions, girder ends, and position of deflection.

$$\Delta_{DL} = \frac{k_b w L^3}{EI_{eff}} + \frac{k_s w L}{GA'} \quad (16)$$

$$EI_{eff} = \sum_{i=1}^n E_i \cdot b_i \cdot \frac{h_i^3}{12} + \sum_{i=1}^n E_i \cdot A_i \cdot z_i^2 \quad (17)$$

where  $\Delta_{DL}$  = the deflection of the beam due to dead load, in.

$w$  = the self-weight of CLT, lb.

$EI_{eff}$  = the effective bending stiffness, kip-ft<sup>2</sup>.

$E_i$  = the modulus of elasticity of each laminated layer, psi.

$b_i$  = the width of each laminated layer, in.

$h_i$  = the height of each laminated layer, in.

$A_i$  = the cross-sectional area of each laminated layer, in<sup>2</sup>.

$z_i$  = the distance of each laminated layer from the neutral axis, in.

Note: 1 lb = 0.45 kg, 1 kip-ft<sup>2</sup> = 2.87 N-m<sup>2</sup>, 1 in = 25.4 mm, and 1 in<sup>2</sup> = 645.16 mm<sup>2</sup>

The deflection of the CLT for live loads was based on the deflection formula of the structural analysis method using the effective bending stiffness ( $EI_{eff}$ ) value. The  $EI_{eff}$  was calculated from Equation 17, where this equation can be found in the CLT Handbook (Karacabeyli and Douglas 2013). The live load-induced deflection ( $\Delta_{LL}$ ) calculated using Equation 18 is considered satisfactory if the deflection is smaller than  $L/360$ . In addition, the girder is considered safe if the total deflection, which is the sum of deflection due to live load ( $\Delta_{LL}$ ) and dead load ( $\Delta_{DL}$ ), is smaller than  $L/240$ .

$$\Delta_{LL} = \frac{M}{EI_{eff}} \quad (18)$$

where  $\Delta_{LL}$  = the deflection of the girder due to live loads, in.

### 2.2.2.2 CLT Deck Design

#### *Strength Criteria*

The dimensions of the CLT girders determined from Section 2.2.2.1 were used to design the CLT deck. It should be noted that the CLT bridge design should be redesigned from the CLT girder design phase to meet its overall requirements if the applied strength is larger than the allowable strength in deck design. In the AASHTO Standard 3.25.1.2 (2002), the effective deck span ( $s_e$ ) was defined as the clear distance between the girders plus half of the girder width. It is, however, unacceptable if  $s_e$  exceeds the clear span distance plus deck thickness.

Effective section properties of the deck can be calculated with wheel load distribution width in the direction of the deck span ( $b_t$ ) and wheel load distribution width perpendicular to the deck span ( $b_d$ ) following the AASHTO Standard 3.25.1 (2000).  $b_t$  is shown in Figure 2.15 and can be calculated from Equation 19.

$$b_t = 20 \text{ in} \quad (19)$$

where  $b_t$  = the wheel load distribution width in the direction of the deck span, in.

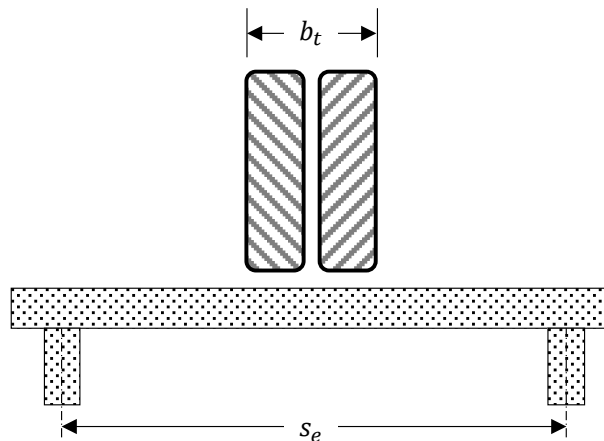


**Figure 2.15** Wheel distribution width in the direction of the deck

The wheel load distribution width perpendicular to the deck span,  $b_d$ , can be calculated from Equation 20. Figure 2.16 shows the load distribution width due to wheel load perpendicular to the deck span.

$$b_d = t + 15 \leq \text{panel width} \quad (20)$$

where  $b_d$  = the wheel load distribution width perpendicular to the deck span, in.

$t$  = the thickness of the deck, in.

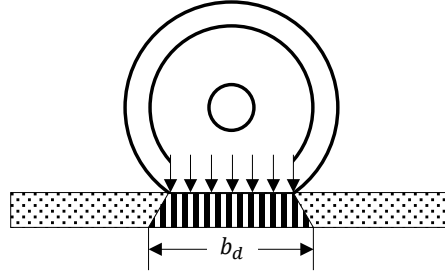


**Figure 2.16** Wheel load distribution width perpendicular to the deck

The effective area, the effective section modulus, and the effective moment of inertia of deck sections can be calculated using Equations 21 through 23.

$$A_{eff} = b_d t \quad (21)$$

$$S_y = \frac{b_d t^2}{6} \quad (22)$$

$$I_y = \frac{b_d t^3}{12} \quad (23)$$

where  $A$  = the effective deck area, in<sup>2</sup>.

$S_y$  = the effective deck section modulus, in<sup>3</sup>.

$I_y$  = the effective deck moment of inertia, in<sup>4</sup>.

*Note:*  $1 \text{ in}^4 = 416231.43 \text{ mm}^4$ .

The maximum moment caused by the live loads can be calculated according to the effective deck span from Equation 24. These equations were developed for a maximum moment considering wheel loads at the center of the span by Ritter (1990).

$$M_{LL} = \begin{cases} 3,000s_e - 25,983 & \text{for } 17.32'' < s_e \leq 122'' \\ 6,000s_e + \frac{7,776,000}{s_e} - 457,983 & \text{for } 122'' < s_e \end{cases} \quad (24)$$

where  $s_e$  = the effective deck span, in.

Similar to the CLT girder design in Section 3.2.2.1.a, the total bending moment for the deck subjected to dead and live loads can be calculated from Equation 3. The bending moment capacity with the CLT material's properties provided by Smartlam can be calculated from Equation 3. The CLT properties were  $F_{b,90} = 5.34 \text{ MPa}$ ,  $F_{v,90} = 0.93 \text{ MPa}$ , and  $E_{90} = 7.58 \text{ GPa}$ , while the load distribution factor ( $C_D$ ), wet service factor ( $C_M$ ), temperature factor ( $C_t$ ), and stability factor ( $C_L$ ) were assumed to be 1.0 in accordance with NDS (2015).

As determined in Section 2.2.2.1a, the maximum shear force due to dead loads for the deck can be calculated using Equation 7. The shear force due to live loads was calculated along the wheel load distribution width ( $b_i$ ) at the distance ( $d$ ) from the support, where  $d$  is equal to the deck thickness, as

shown in Figure 2.17. As described in Section 2.2.2.1a, the shear stress was calculated from Equation 25. The AITC (1987) recommended employing  $A_v$  with conservative  $b_t$  for timber bridges such as glulam. Note, the AITC does not provide an equation for  $A_v$  specific for CLT. For this design,  $A_v$  was calculated with the recommendation of AITC (1987). The reference shear stress  $F_v'$  was calculated by taking the  $C_D$ ,  $C_M$  and  $C_t$  values into account for the material properties, as shown in Equation 11.

$$f_v = \frac{1.5V}{A_v} \quad (25)$$

where  $A_v = t(15 + 2t)$ , in.

$t$  = the thickness of the deck, in.

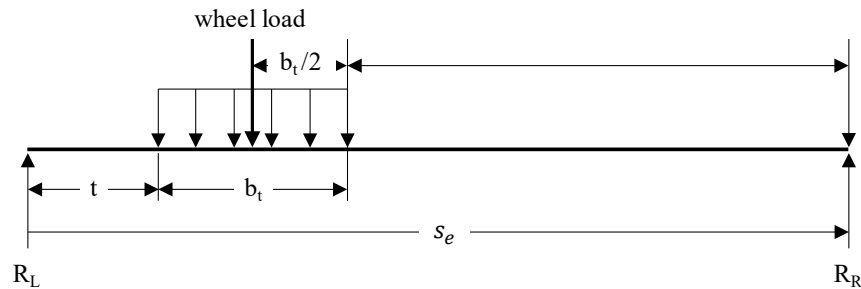


**Figure 2.17** Applied wheel load for horizontal shear

The design evaluation of the deck overhang for the bending moment and shear force was done by applying wheel load 0.3048 m away from the face of the rail, as shown in Figure 2.18. The moment was calculated based on the position shifted from the outer edge of the girder by 1/4 of the girder thickness toward the center of the girder.

$$f_b = \frac{M}{S_y} \quad (26)$$

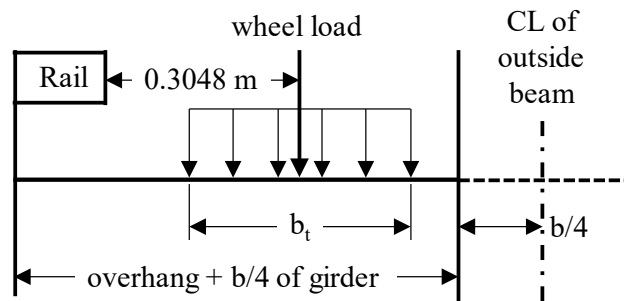


**Figure 2.18** Moment on overhang

The shear of the deck overhang was also considered to occur at a distance of deck thickness plus one-fourth of the girder width ( $t + b/4$ ) from the center of the girder (Figure 2.19). The external forces within this distance were not taken into consideration based on the recommendation by Ritter (1990). Since the load was superimposed on the distance, a distributed load that was the total load size of 71.17 kN divided by the wheel load width was applied to avoid the load in the overlapping distance. The shear force was calculated considering both the dead and live loads.



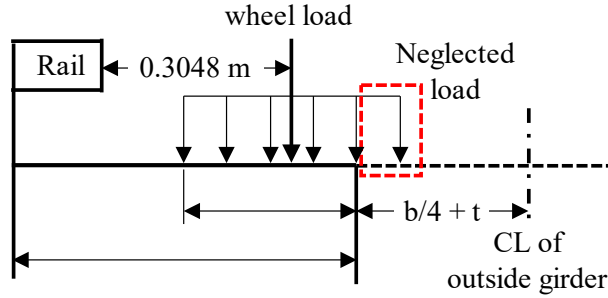


**Figure 2.19** Shear on overhang

### **Deflection Criteria**

The maximum deflection of the designed CLT deck under the dead load provided in the CLT Handbook (Karacabeyli and Douglas 2013) can be determined, as shown in Equation 27. The shear coefficient form factor ( $k$ ) is assumed to be 1.2. The effective bending stiffness of composite section ( $EI_{eff}$ ) and effective shear stiffness of composite section ( $GA_{eff}$ ) are calculated by Equation 17 and 28, respectively. The calculation of deflection for the CLT deck considering the live loads was completed with Equation 18.

$$\Delta_{DL} = \frac{5}{384} \cdot \frac{wL^4}{EI_{eff}} + \frac{1}{8} \cdot \frac{wL^2k}{GA_{eff}} \quad (27)$$

$$GA_{eff} = \frac{a^2}{\left[ \left( \frac{h_1}{2 \cdot G_1 \cdot b} \right) + \left( \sum_{i=2}^{n-1} \frac{h_i}{G_i \cdot b_i} \right) + \left( \frac{h_n}{2 \cdot G_n \cdot b} \right) \right]} \quad (28)$$

where  $\Delta_{DL}$  = the deflection of the deck due to dead load, kip.

$L$  = the span length of deck, ft.

$k$  = the shear coefficient form factor.

$EI_{eff}$  = the effective bending stiffness, kip-ft<sup>2</sup>.

$GA_{eff}$  = the effective shear stiffness, kip-ft<sup>2</sup>.

It was assumed that the CLT deck is considered satisfactory if the maximum deck deflection due to live loads is less than  $L/360$  and the deflection due to total dead and live loads is less than  $L/240$ .

### **2.2.2.3 CLT Connection Design**

There are many ways to connect the CLT girders and CLT decking. For example, there are dowel-type fasteners such as screws, rivets, spike grids, split rings, epoxy and so on. For this project, the fastener connection was used and designed following the design process of Design of Wood Structures—ASD/LRFD (Breyer et al. 2007) by referencing the properties of the screw from ESR-3179 (2018). To select a reference lateral design value ( $Z$ ), all  $Z$  values were calculated from Equations 29 through 34 considering all possible yield failure modes of the connection, as shown in Figure 2.20 and compared with each other. The design value was then selected as the smallest value among the calculated  $Z$  values. *Mode I<sub>m</sub>* indicates the yield mode of crushing in the main member. *Mode I<sub>s</sub>* stands for the yield mode of crushing in the side member. *Mode II* means the yield mode of rotation of the fastener. *Mode III<sub>m</sub>* denotes yield mode of the plastic hinge and crushing in the main member. *Mode III<sub>s</sub>* specifies the yield

mode of plastic hinge and crushing inside member, whereas, *Mode IV* indicates the yield mode of two plastic hinges per shear plane.

$$Z = \frac{Dl_m F_{em}}{K_D} \text{ for Mode I}_m \quad (29)$$

$$Z = \frac{Dl_s F_{es}}{K_D} \text{ for Mode I}_s \quad (30)$$

$$Z = \frac{k_1 D l_s F_{es}}{K_D} \text{ for Mode II} \quad (31)$$

$$Z = \frac{k_2 D l_s F_{em}}{(1 + 2R_e) K_D} \text{ for Mode III}_m \quad (32)$$

$$Z = \frac{k_3 D l_s F_{em}}{(2 + R_e) K_D} \text{ for Mode III}_s \quad (33)$$

$$Z = \frac{D^2}{K_D} \sqrt{\frac{2F_{em} F_{yb}}{3(1 + R_e)}} \text{ for Mode IV} \quad (34)$$

where  $Z$  = the reference lateral design value, psi.

$l_m$  = the dowel bearing length of connector in main member, in.

$l_s$  = the length of connector, in.

$F_{es}$  = the dowel bearing strength of side member, psi.

$F_{em}$  = the dowel bearing strength of main member, psi.

$F_{yb}$  = the bending yield strength of connector, psi.

$D$  = the diameter of connector, in.

$K_D$  = the reduction coefficient for connector.

$$= \frac{\sqrt{R_e + 2R_e^2(1 + R_t + R_t^2) + R_t^2 R_e^3 - R_e(1 + R_t)}}{1 + R_e}$$

$$k_2 = -1 + \sqrt{2(1 + R_e) + \frac{2F_{yb}(1 + 2R_e)D^2}{3F_{em}l_m^2}}$$

$$k_3 = -1 + \sqrt{\frac{2(1 + R_e)}{R_e} + \frac{2F_{yb}(2 + R_e)D^2}{3F_{em}l_s^2}}$$

where  $R_e = \frac{F_{em}}{F_{es}}$  and  $R_t = \frac{l_m}{l_s}$

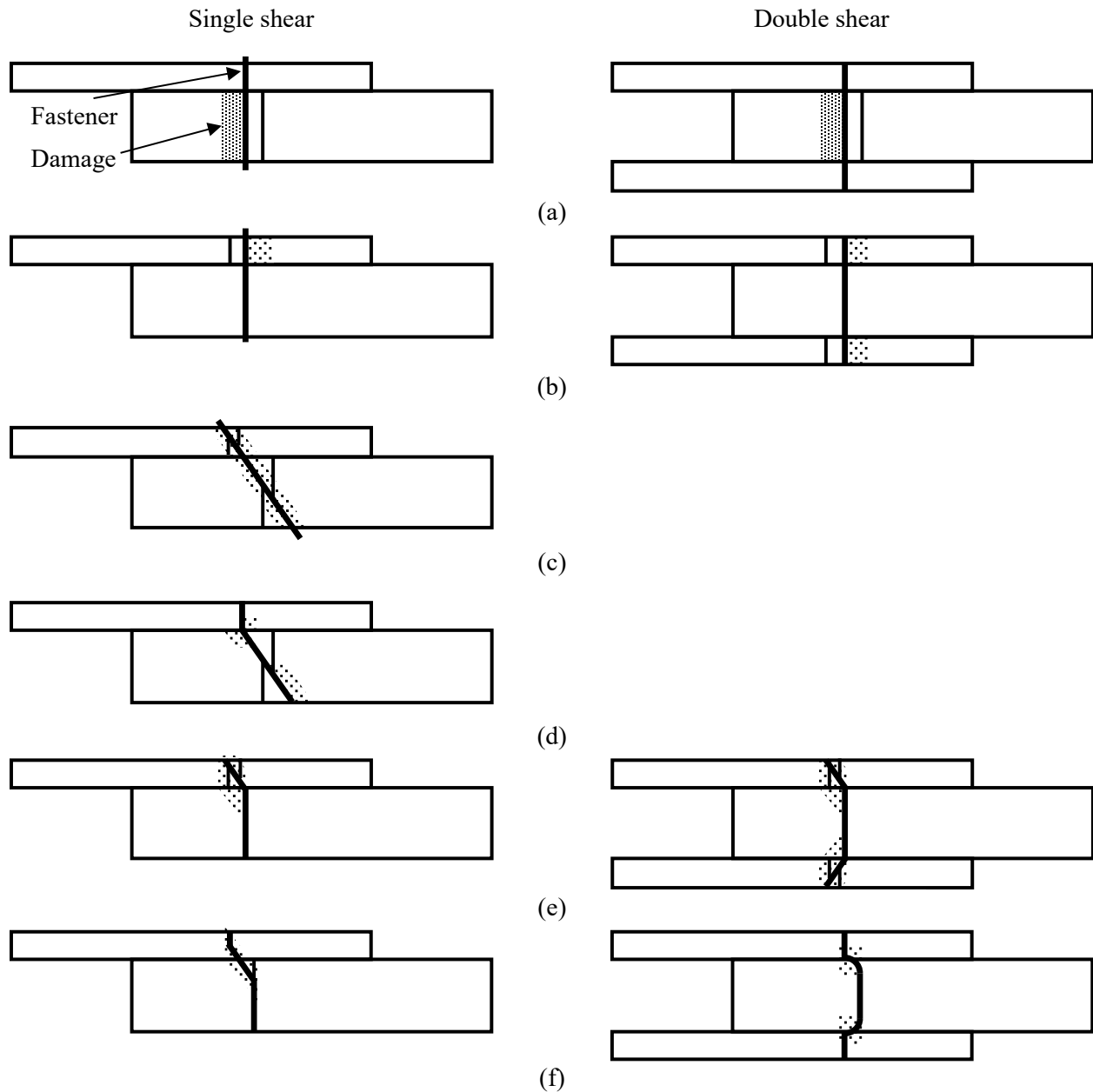


**Figure 2.20** Basic yield modes in dowel—type connection: (a) Mode  $I_m$ ; (b) Mode  $I_s$ ; (c) Mode  $II$ ; (d) Mode  $III_m$ ; (e) Mode  $III_s$ ; and (f) Mode  $IV$ .

The reference shear strength ( $V$ ) was deemed as the smaller value of shear strength of the CLT decking and girders. The area of the girder was the actual design area of the girder, and the effective width of the deck was calculated as shown in Equation 35 specified by Eurocode 5 (2004). There is no guidance for determination of the CLT effective deck width in the AASHTO Standard (2002), AASHTO LRFD (2012), Ritter’s Timber Bridge (1990), or NDS (2015). Therefore, Eurocode (2004) is referenced to calculate the effective width of the CLT deck. As illustrated in Figure 2.21, the width of the loaded area at the reference plane in the middle of the deck plate ( $b_{w,middle}$ ) was expanded by applying a dispersion angle  $\beta$  ( $45^\circ$  for CLT) from the top of the deck to the center of the deck. An initial width of the load area was 0.5 m, which is the tire contact area of HS 20-44 from the AASHTO Standard (2002).

$$b_{eff} = b_{w,middle} + a \quad (35)$$

where  $b_w$  = the width of the loaded area on the contact surface of the deck, in.

$b_{w,middle}$  = the width of the loaded area at the reference plane in the middle of the deck plate, in.

$\beta$  = the angle of dispersion, 45° for CLT.

$a$  = 0.5 m for CLT (Eurocode).

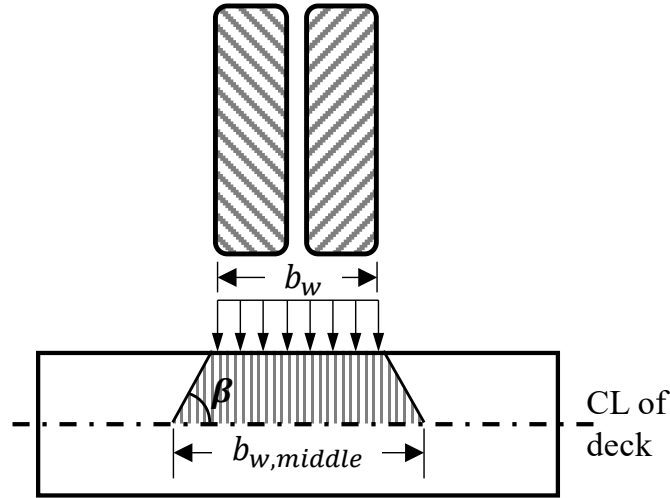


**Figure 2.21** Effective deck width of CLT

The number of connectors ( $N$ ) was determined by the formula  $V/Z'$ , where  $Z'$  was calculated from Equation 36 (AWC 2015). For the  $Z'$  calculation, the following factors considered were load distribution, wet service, temperature, end grain, diaphragm, and toe-nail. For a conservative design with ease of construction, the fastener interval (rounded-down) was calculated by dividing span length with determined  $N$ . Then, the  $N$  (rounded-up) was obtained using a fastener interval.

$$Z' = Z C_D C_M C_t C_{eg} C_{di} C_{tn} \quad (36)$$

where  $Z'$  = the adjusted lateral design value, kip.

$C_{eg}$  = the end grain factor.

$C_{di}$  = the diaphragm factor.

$C_{tn}$  = the toe-nail factor.

#### 2.2.2.4 CLT Diaphragm

This section focuses on the design of CLT diaphragm enabling the horizontal stability of the CLT girders. According to Timber Bridge (Ritter 1990), the diaphragm was designed separately to design the lateral support in detail.

Assuming a maximum distance of 7.62 m between a lateral support to an end support, a transverse bracing or diaphragm should be installed at the end and center of the CLT girders (Ritter 1990). Ritter (1990) classified the short ( $0 < C_s \leq 10$ ), intermediate ( $10 < C_s \leq C_k$ ), and long girders ( $C_k < C_s \leq 50$ ) based on the value of  $C_s$  (see Equation 37).

$$C_s = \sqrt{\frac{\ell_e d}{b^2}} \quad (37)$$

where  $C_s$  = the slenderness factor for bending member.

$\ell_e$  = the effective span length of the bending member, in.

The unsupported distance ( $\ell_u$ ) of the designed CLT girder, which is the distance between two lateral supports, is 7.62 m for the CLT bridge. Equation 38 for determining the effective span length ( $\ell_e$ ) followed the formulas in Table 3.3.3 of NDS (AWC 2015). The value of  $\ell_e$  depends on the size of  $\ell_u/d$ , as shown in this equation.

$$\ell_e = \begin{cases} 2.06 \times \ell_u & \text{for } \ell_u < 7 \\ 1.63 \times \ell_u + 3d & \text{for } \ell_u \geq 7 \end{cases} \quad (38)$$

where  $\ell_e$  = the effective span length of the bending member, in.

$\ell_u$  = the laterally unsupported span length of bending member, in.

The CLT girder slenderness factor ( $C_s$ ) can be calculated using the value of  $\ell_e$ . The calculated  $C_s$  was less than 10; thus, the designed CLT girder was classified as a short girder. The value of  $C_k$  for the CLT diaphragm is not given but can be determined in Equation 39 available in Timber Bridges (Ritter 1990). The use of modified,  $C_k$ , is a designer choice, although it is recommended to apply in bridge design (Ritter 1990).

$$C_k = 0.956 \sqrt{\frac{E'}{F_b''}} \quad (39)$$

where  $C_k$  = the slenderness factor defined later for intermediate beams.

$$E' = EC_M$$

$$F_b'' = F_b C_M$$

In the USDA FS report (Wacker and Smith 2001), timber diaphragms were suggested for 7.62 m or longer timber bridges like glulam bridges. For this project, the CLT diaphragms were designed conservatively, similar to the glulam bridge diaphragm design with the CLT bridge properties and dimensions.

The CLT diaphragm design was divided into the design of the CLT diaphragm and design of the tie rod connecting the CLT girder and CLT diaphragm. First, the CLT diaphragm was designed to effectively resist live loads. The diaphragm design was similar to the CLT girder design and CLT deck in Section 2.2.2.1 and 2.2.2.2 using the moment and shear strength, respectively. Reference design values of moment strength in Equation 3 and shear strength in Equation 11 were compared with the maximum moment strength acquired from Equation 6 and shear strength obtained in Equation 10 after determining the initial geometry of the CLT diaphragm. The CLT diaphragm geometry can be finalized if the reference moment and shear design values are greater than the respective applied strengths.

The design of CLT diaphragm connection was analogous to the connection design between the CLT girder and CLT deck shown in Section 2.2.2.3. However, the diaphragm design differs from the connection design using the tie rod, which means double shear. Equations 40 through 43 for the different failure modes of the connector considered in this design are as follows.

$$Z = \frac{Dl_m F_{em}}{4K_\theta} \text{ for Mode I}_m \quad (40)$$

$$Z = \frac{2Dl_s F_{es}}{4K_\theta} \text{ for Mode I}_s \quad (41)$$

$$Z = \frac{2k_3 D l_s F_{em}}{3.2(2 + R_e)K_\theta} \text{ for Mode III}_s \quad (42)$$

$$Z = \frac{2D^2}{3.2K_\theta} \sqrt{\frac{2F_{em}F_{yb}}{3(1 + R_e)}} \text{ for Mode IV} \quad (43)$$

where  $Z$  = the reference lateral design value, kip.

$l_m$  = the dowel bearing length of connector in main member, in.

$F_{es}$  = the dowel bearing strength of side member, psi.

$l_s$  = the length of connector, in.

$F_{em}$  = the dowel bearing strength of main member, psi.

$F_{yb}$  = the bending yield strength of connector, psi.

$D$  = the diameter of connector, in.

$$k_3 = -1 + \sqrt{\frac{2(1+R_e)}{R_e} + \frac{2F_{yb}(2+R_e)D^2}{3F_{em}l_s^2}}$$

$$K_\theta = 1 + \frac{\theta}{360}$$

$\theta$  = the maximum angle of load to grain for any member in connection.

where  $R_e = \frac{F_{em}}{F_{es}}$

$$R_t = \frac{l_m}{l_s}$$

The smallest value of  $Z$  was selected from Equations 40 to 43.  $Z'$  was calculated from Equation 36. The shear force due to live loads was considered for determining the diaphragm geometry, as suggested by Ritter (1990). The shear force due to live loads was considered the maximum shear force and the number of the tie rod ( $N$ ) was calculated from  $V/Z'$ . For this design, one tie rod in the center of the diaphragm met the required strength, but two threaded rods were applied to the diaphragm following the recommendation by the report (Wacker and Smith 2001).

### 2.2.2.5 CLT Bridge Sketch and Details

The CLT girder bridge system designed through Sections 2.2.2.1 and 2.2.2.4 is illustrated in Figure 2.22. The CLT bridge system is a simply supported structure with a span length of 6.4 m. The bridge has two CLT girders (0.24 m wide x 0.48 m deep) with 0.61 m girder spacing center-to-center to support the CLT decking (0.17 m thick and 1.22 m width) with an overhang length of 0.30 m and two CLT diaphragms (0.37 m long x 0.13 wide x 0.24 m deep). Figure 2.22a shows a cross-section of the CLT bridge system consisting of one CLT deck, two CLT girders, and two CLT diaphragms. In Figure 2.22b, a plan view of the bridge system showing the designed fasteners (12.7 mm diameter and 582.4 mm long with 165.1 mm spacing) with adhesives that was used to enhance connectivity between the CLT deck and CLT girders is provided. Figure 2.22c displays an elevation view of the bridge system.

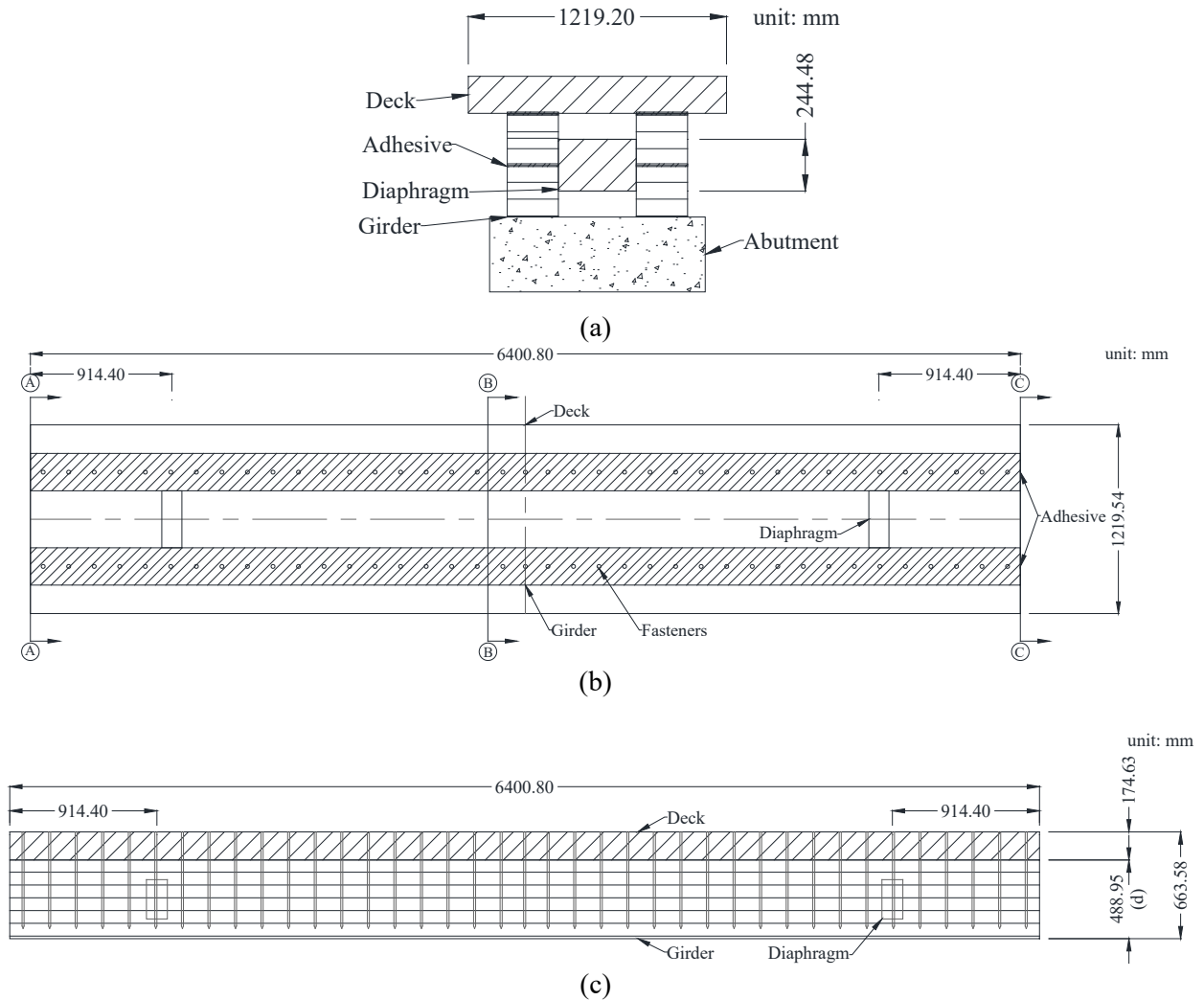


**Figure 2.22** CLT bridge design sketch: (a) cross-section; (b) plan view; and (c) elevation view

## 2.3 CLT Bridge Component and System Production

After the design of the CLT bridge system in Section 2.2, a local CLT producer was selected to manufacture the CLT components required for the CLT bridge system production as mentioned before. This section presents CLT component manufacture, CLT girder fabrication, and CLT bridge system production.

### 2.3.1 CLT Component Manufacture

With the designed CLT bridge system, the research team contacted several CLT manufacturers in the U.S. and Canada for the fabrication of CLT, including Smartlam, DR Johnson, X-LAM USA, Structurlam, Sauter Timber, and Katterra. Smartlam was considered the most ideal CLT manufacturer for this project because it has many years of experience in CLT production and is located in Montana, which is more cost-saving than the other manufacturers for delivery and CLT production.

Along with Smartlam's producible CLT V4 made with visually graded No. 2 SPF-S (spruce-pine-fir south), the CLT bridge system design was completed as described in Section 2.2. Specifically, the CLT material properties provided by Smartlam were incorporated into the entire design process of the CLT girder bridge. Again, the two 7-ply CLT beams were utilized to create a new 14-ply CLT girder because a 7-ply beam had insufficient strength to support the dead and live loads that were considered. The CLT material properties required for the CLT bridge design are detailed in Appendix A.

All the CLT components with the complete dimensions, including eight 7-ply CLT beams, one 5-ply CLT panel, and two 7-ply CLT diaphragms, were manufactured in Smartlam, and they were delivered to the SDSU Structural Laboratory on April 24, 2019. The CLT components were then stacked in the SDSU Structural Lab with a forklift crane vehicle (Figures 2.23a, 2.23b, and 2.23c). After the CLT components were delivered, all the dimensions of each CLT component were measured to ensure the manufactured and measured dimensions were identical, as shown in Figure 2.23d. The quotation of all the delivered CLT components is shown in Appendix B.



(a)



(b)



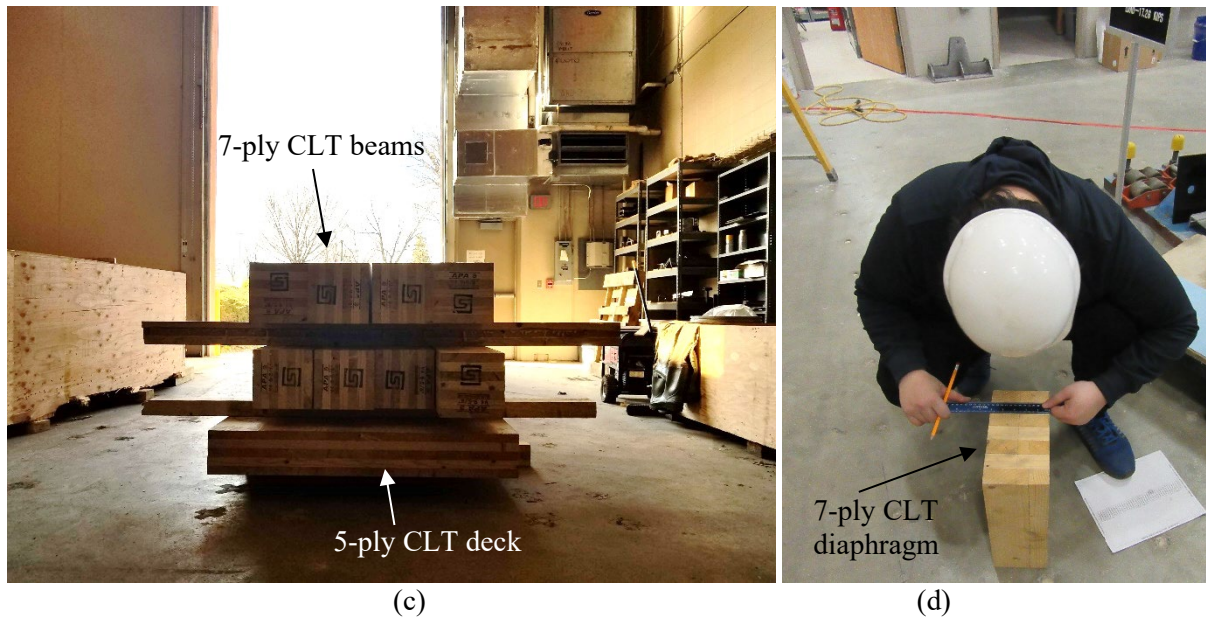


**Figure 2.23** CLT shipment: (a) CLT move from the truck; (b) CLT move with the forklift crane; (c) the shipped CLT panels; and (d) dimension check.

## 2.3.2 CLT Girder Fabrication

The eight 7-ply CLT beams manufactured by Smartlam were utilized to assemble four 14-ply CLT girders. The CLT girders were fabricated using two methods: 1) a CLT girder with adhesive, which means adhesive was only applied across connected surfaces between two 7-ply beams to be bonded, and 2) a CLT girder with adhesive and fasteners, where both adhesive and fasteners were used to bond two 7-ply beams. Each is detailed in the subsections.

### 2.3.2.1 CLT Girder with Adhesive

According to polyurethane adhesive's specification (see Appendix C), pressure ranging between 689 to 1034 kPa is required to appropriately bond two 7-ply CLT beams for one 14-ply CLT girder. The process of fabricating CLT girders with adhesive is illustrated in Figure 2.24 with schematic drawings. The CLT beams were first placed in alignment, as displayed in Figure 2.24a. The polyurethane adhesive was spread on top of the bottom CLT girder with a roller (Figure 2.24b) and clamped with steel plates to apply consistent pressure of 689 kPa to both CLT beams (Figure 2.24c). Floor anchor bolts, nuts, steel plates, and load cells were used for effective loadings during clamping, as shown in Figure 2.25. During the clamping, floor anchor bolts were fastened into the floor holes. Note, the load cells were installed between the steel plates tightened with nuts to the anchor bolts after the application of adhesive and placing both CLT beams in alignment. The required pressure on the CLT beams was controlled by monitoring the load recorded by load cells. In total, four 14-ply CLT girders with adhesive were built through the fabrication process.

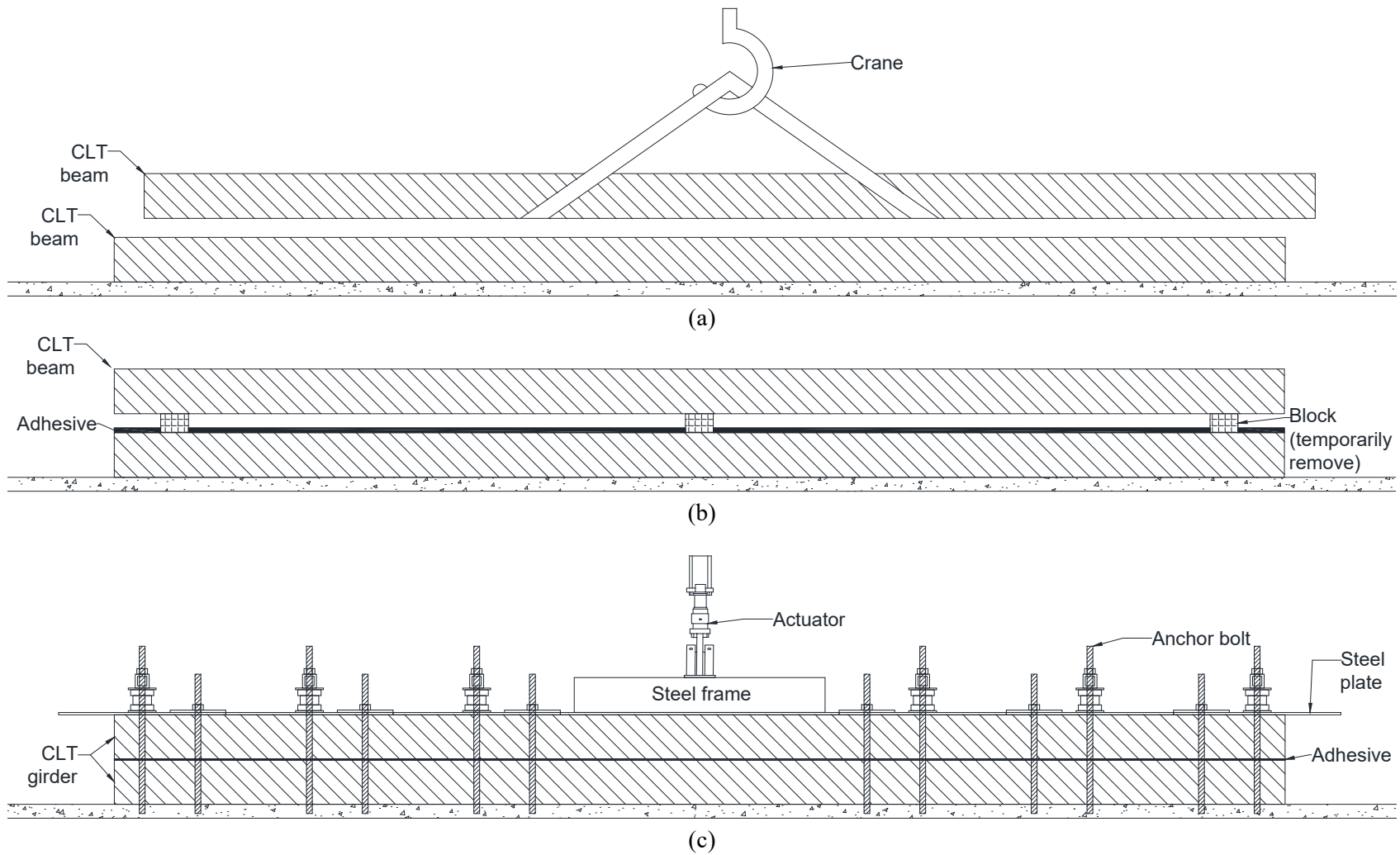


**Figure 2.24** Schematic drawing of CLT bonded using adhesive: (a) beam moving and alignment; (b) adhesive spreading; and (c) clamping

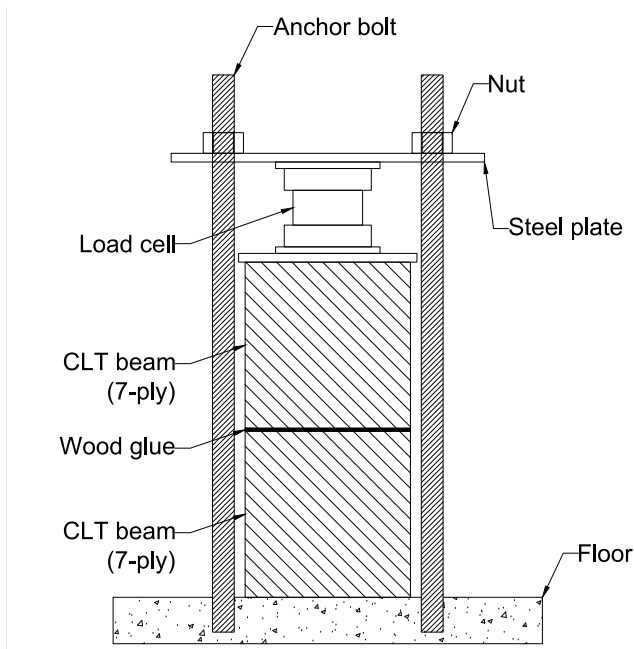


**Figure 2.25** CLT beams clamping cross-section

As shown in Figure 2.26, fabrication of CLT girders with bonding of the CLT beams was conducted in five steps based on the aforementioned clamping processes: 1) CLT beam shipping; 2) CLT bonding set-up; 3) spreading adhesive on CLT beam; 4) clamping two CLT beams; and 5) adhesive curing.



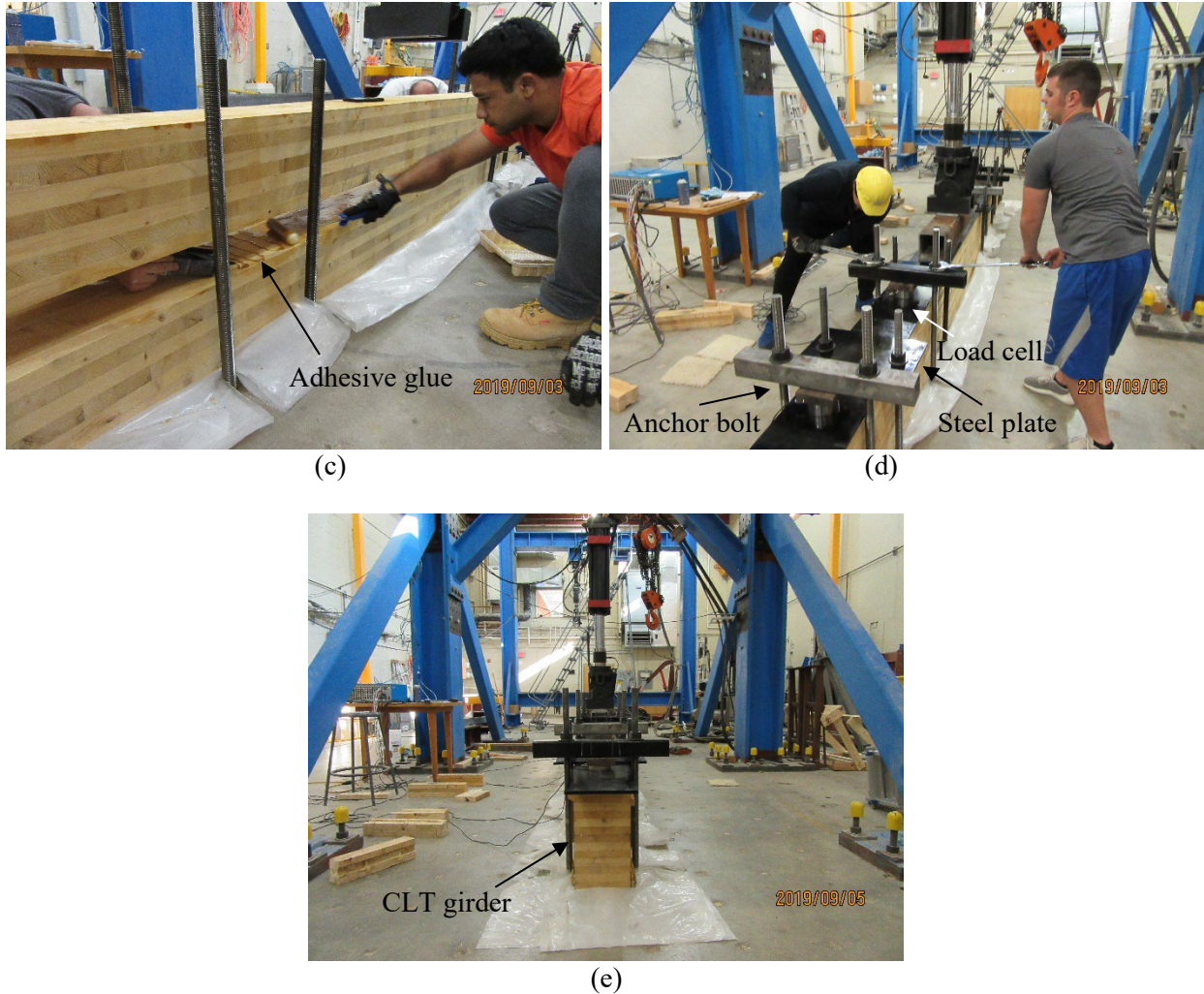


**Figure 2.26** Adhesive CLT girder fabrication: (a) CLT beams shipping; (b) CLT bonding set-up; (c) spreading adhesive glue on CLT beam; (d) clamping two CLT beams; and (e) adhesive curing.

All the CLT beams were moved using a crane in the SDSU Structural Lab, as shown in Figure 2.26a. For safety, all members wore steel toe shoes and hard hats while working in the lab during fabrication of girders. All items necessary for clamping, including steel plates, anchor bolts, nuts, and load cells, were placed on the side of the CLT beams after moving the CLT beam, as shown in Figure 2.26b. Spreading adhesive (Figure 2.26c) and clamping two CLT beams (Figure 2.26d) were accomplished within 45 minutes following the guidelines of polyurethane adhesive specification (Appendix C). According to the adhesive guidelines, the CLT girders were clamped with the loads for four hours and left to cure for additional two hours (Figure 2.26e).

With all dimensions, the process of clamping the CLT beams for the CLT girder fabrication is further depicted in Figure 2.27. The steel plates were placed on CLT beams (Figure 2.27a), and 75.93 kN was evenly applied to the CLT beams by tightening the anchor bolts, as shown in Figure 2.27b. Note, the center portion of the CLT beams was loaded with 253.15 kN through the actuator during clamping. The detailed elevation views for clamping are displayed in Figures 2.27c and 2.27d.

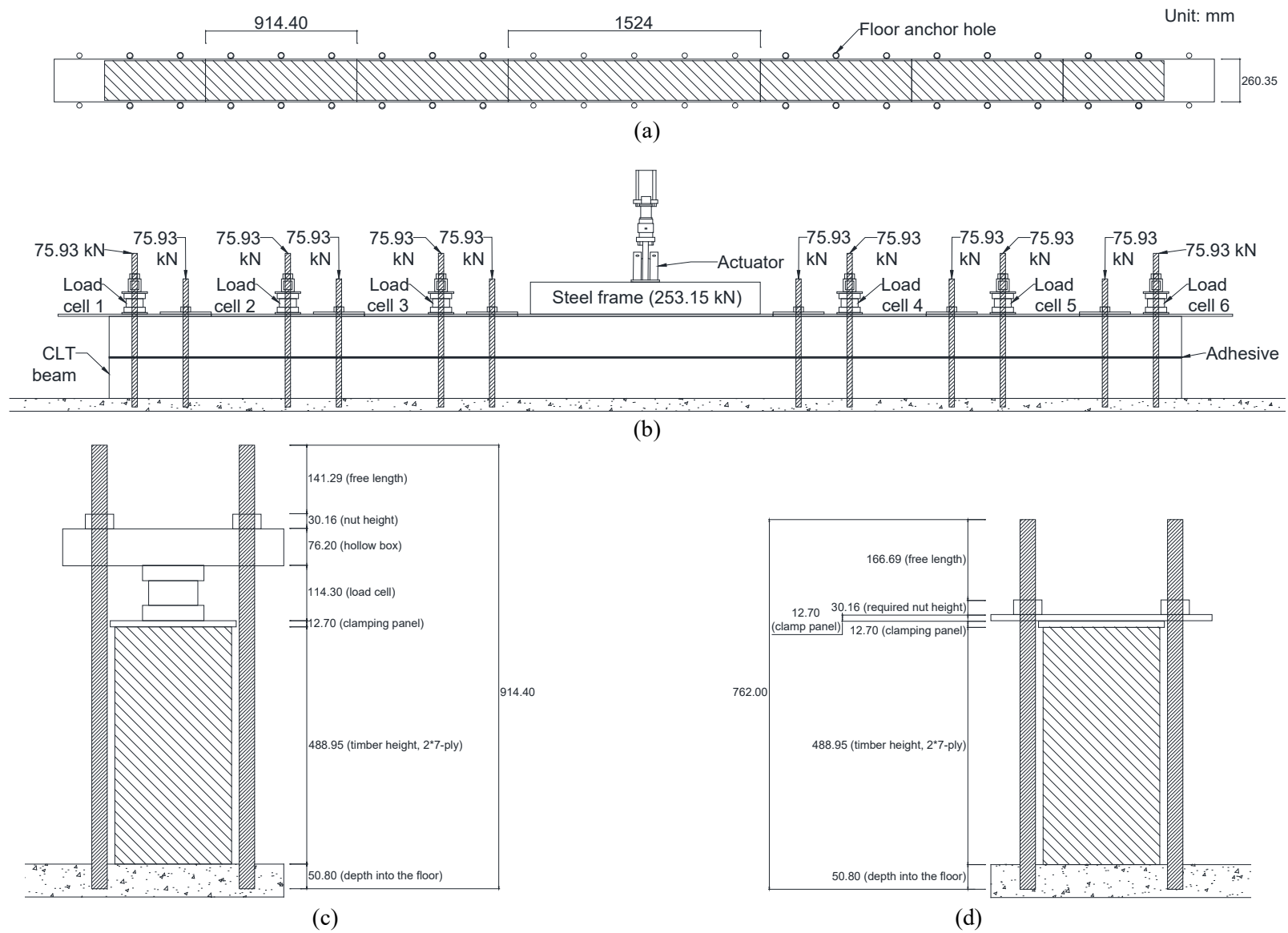


**Figure 2.27** CLT beam clamping sketch: (a) plan view; (b) elevation view; (c) detailed clamping with load cell; and (d) detailed clamping without load cell

The research team monitored the clamping loads from six load cells marked with numbers in order (Figure 2.27b) for the entire period of curing for each of the 14-ply CLT girders. Figure 2.28 shows the average clamping loads measured from each load cell in bar charts. It appears that all the average clamping loads measured from each, per CLT girder, reach or slightly exceed the required load of 75.93 kN (gray dashed line).

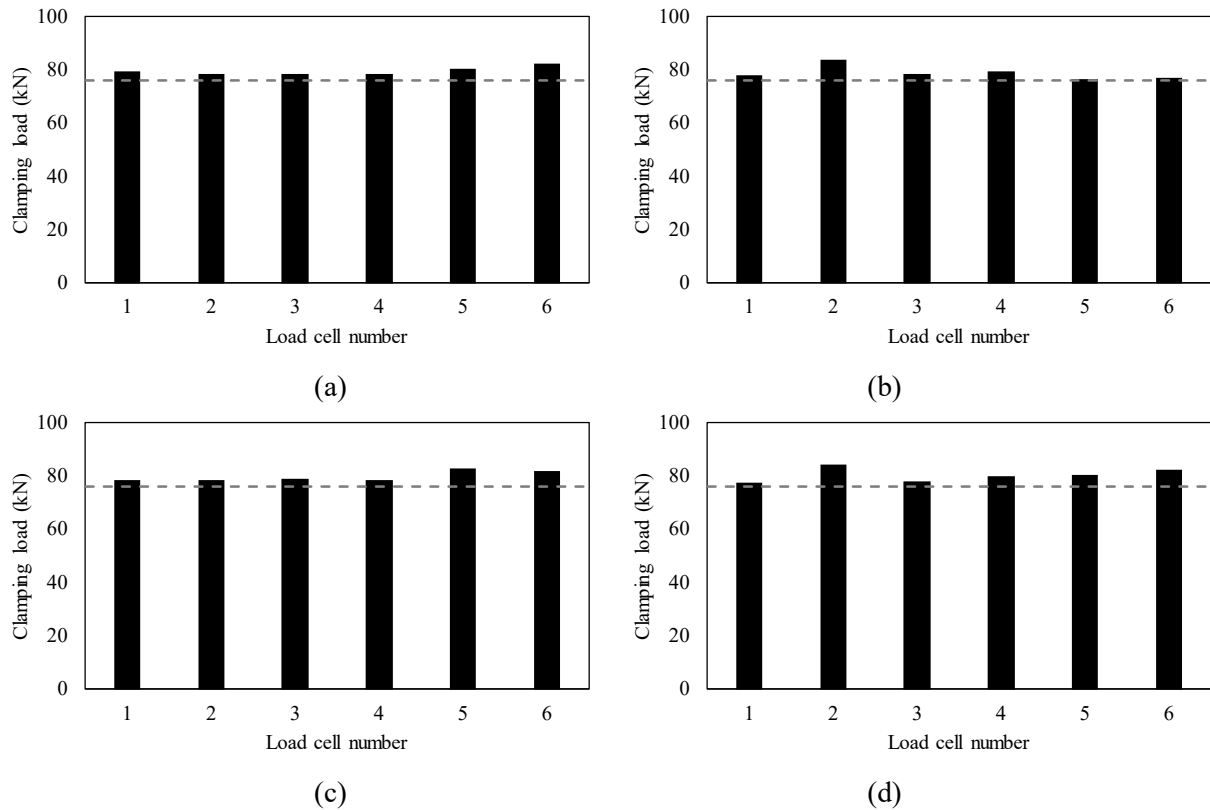


**Figure 2.28** Average clamping load for each load cell: (a) CLT girder 1; (b) CLT girder 2; (c) CLT girder 3; and (d) CLT girder 4.

### 2.3.2.2 CLT Girder with Adhesive and Fasteners

To improve the bond strength of the CLT girders, one demonstration CLT girder with adhesive was further built using carbon steel fasteners (Appendix D). Figure 2.29 shows an entire procedure on how to fabricate the CLT girder with adhesive and fasteners. As shown in Figures 2.29a through 2.29c, the procedure is the same as that of the adhesively bonded CLT girder. After fabrication of the adhesively bonded CLT girder, the fasteners 12.7 mm in diameter and 381 mm in length, as selected in Section 2.2.2.3, were screwed into the CLT girder, as shown in Figure 2.29d. Note, maintaining 90° between the girder and screw is of utmost importance while screwing.

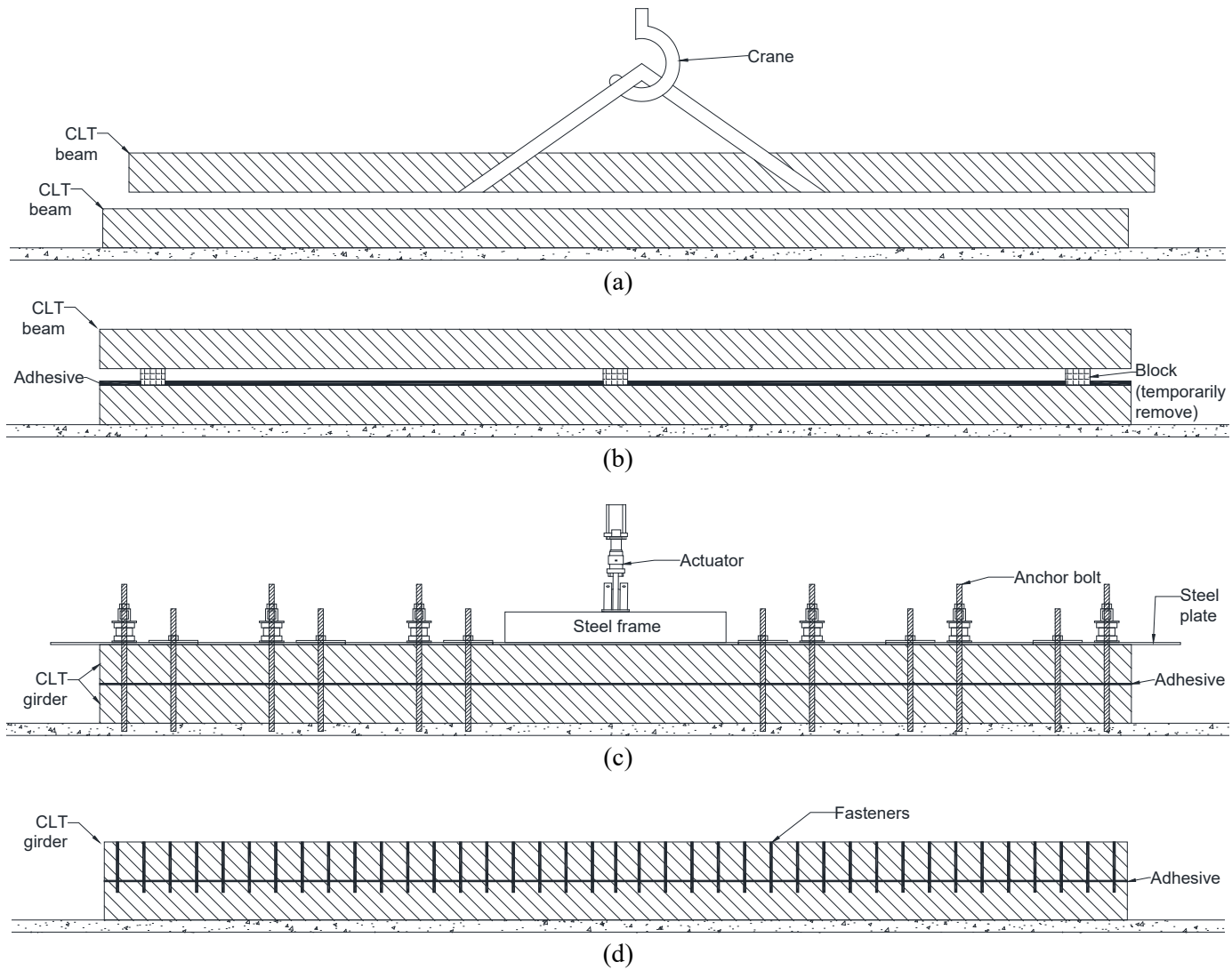


**Figure 2.29** Schematic drawing of CLT bonded using adhesive: (a) girder moving and alignment; (b) adhesive spreading; (c) clamping; and (d) fastening screws

To screw fasteners perpendicularly into the CLT girder, a drill guide was built using a 3D printer, as shown in Figure 2.30a. A sketch of the drill guide is provided in Figure 2.30b. The research team aligned the center of the drill guide using four outside holes and marks on the girder, and then put the drill bit into the center hole of the drill guide.

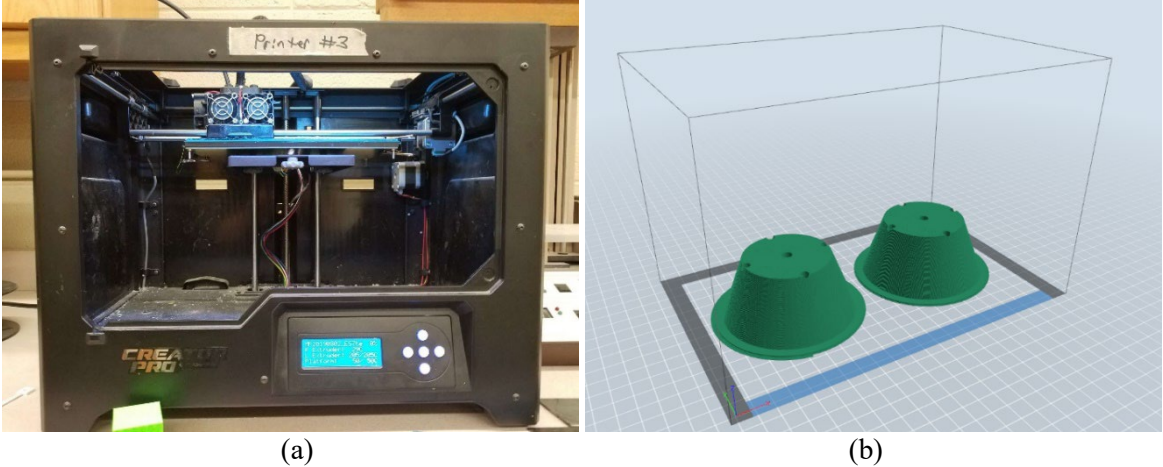
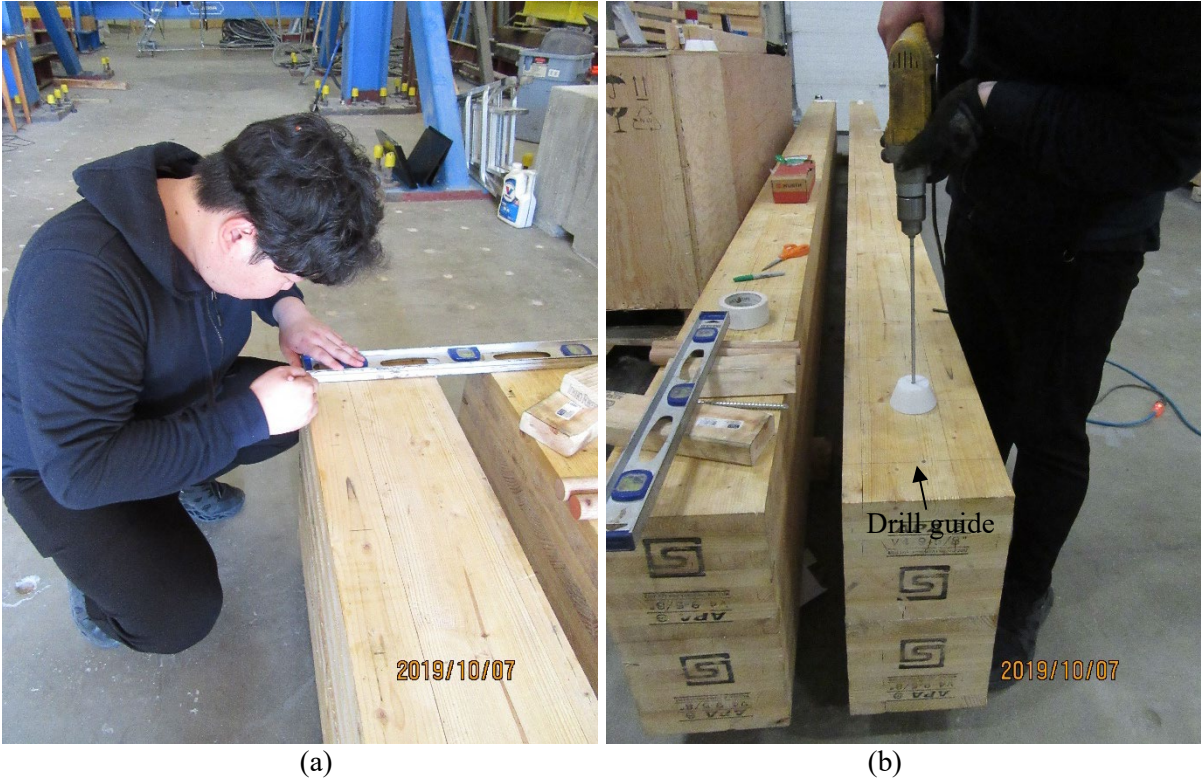


**Figure 2.30** Drill guide fabrication using 3D printer: (a) 3D printer and (b) 3D sketch of drill guide

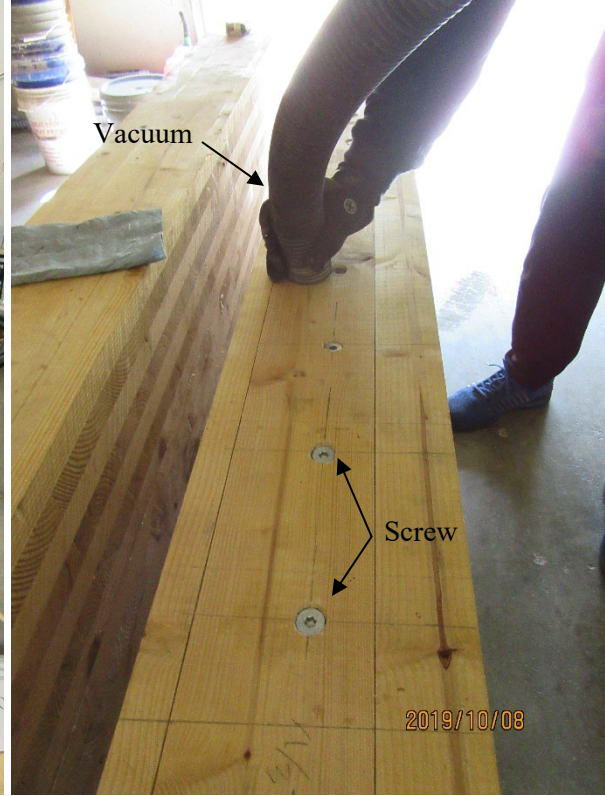
Fabrication of the adhesive CLT girders with fasteners has eight steps (Figure 2.31): 1) marking hole locations on the girder; 2) making pre-drill holes; 3) tightening the fasteners; 4) cleaning girder surface; 5) filling the gap between the hole and fastener using epoxy glue; 6) curing epoxy glue; 7) filling the holes using the epoxy-based wood filler; and 8) curing epoxy-based wood filler.







(c)



(d)



(e)



(f)

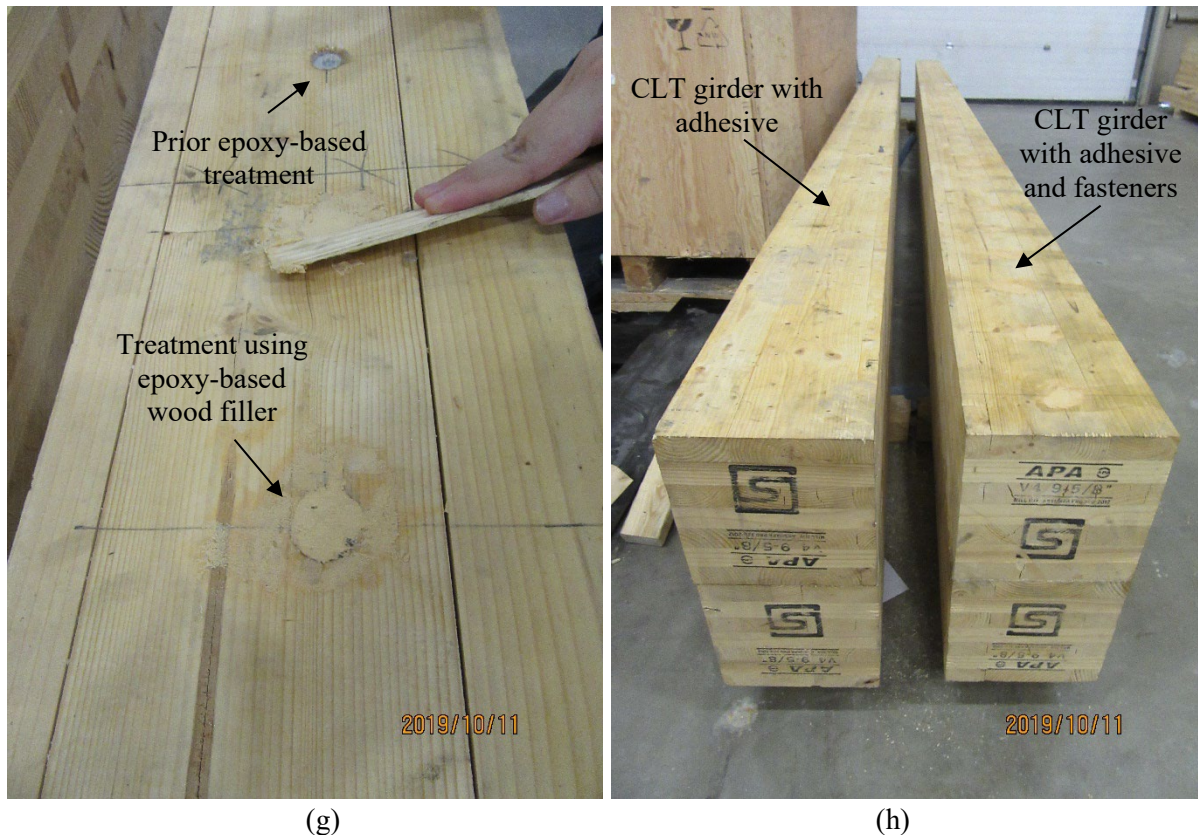


**Figure 2.31** CLT girder fabrication using fasteners: (a) marking hole locations on the girder; (b) making pre-drill holes; (c) tightening the fasteners; (d) cleaning girder surface; (e) filling the gap between the hole and fastener using epoxy glue; (f) curing epoxy glue; (g) filling the holes using the epoxy-based wood filler; and (h) curing epoxy-based wood filler.

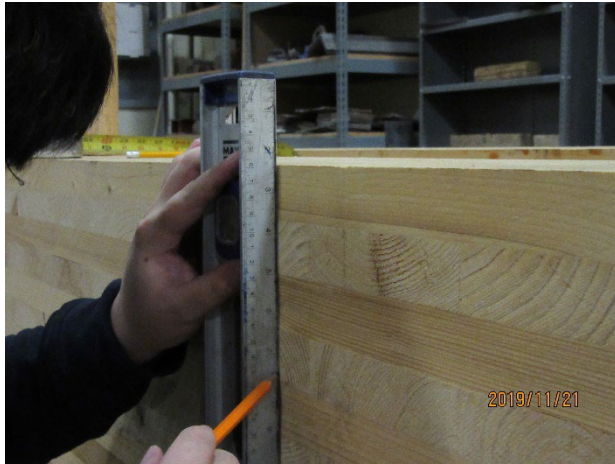
As described above, the research team first marked the hole locations on the CLT girder, as shown in Figure 2.31a. The team made pre-drill holes using the 3D printed drill guide, as shown in Figure 2.31b. A drill bit 6.35 mm in diameter and 457.2 mm in length was used to make pre-drill holes (Figure 2.31c). The fasteners 12.7 mm diameter and 381 mm length were screwed into the CLT girder after pre-drilling (Figure 2.31c). Because drill holes in the timber can, in general, cause decay, the team used two different epoxy-based products, including epoxy glue (Appendix E) and epoxy-based wood filler (Appendix F), to fill the holes. This application of epoxy products to the drill holds was based on the finding by Avent (1985), recommending that sealing the hole gaps with epoxy helped prevent timber decay. The surface of the girder was cleaned up (Figure 2.31d) to pour the epoxy glue in the gaps between holes and fasteners, as displayed in Figure 2.31e. The epoxy was applied first since it can penetrate the small gaps due to low viscosity. The surface was left for one hour for effective epoxy curing, as exhibited in Figure 2.31f. The holes were further filled with epoxy-based wood filler (Figure 2.31g) and cured for an additional six hours, as illustrated in Figure 2.31h.

### 2.3.3 CLT Bridge System Production

The CLT bridge system was produced with two adhesive-bonded 14-ply CLT girders, two 7-ply CLT diaphragms, and a 5-ply CLT deck. The fabrication of a CLT bridge system is explained in two major subsections described below.

### 2.3.3.1 Installation of CLT Diaphragm

Two 14-ply CLT girders were aligned on the floor first. Two 7-ply diaphragms were installed at a distance of 0.91 m from both ends of the CLT girder. The size of CLT diaphragm that was designed in Section 2.2.2.4 is 0.12 m width, 0.23 m depth, and 0.36 m length. The CLT diaphragms and CLT girders were marked at appropriate locations for making the holes (Figure 2.32a). Two sets of holes were drilled in the CLT girders at a distance of 914.4 mm from both ends of the girders (Figure 2.32b), and two sets of holes were also drilled in each diaphragm at designated locations (Figure 2.32c). Note, a drill bit of 15.88 mm in diameter was used for making the holes. The CLT diaphragms were positioned between the two CLT girders, as illustrated in Figure 2.32d. Two rods 12.7 mm in diameter were inserted through the girders and diaphragms and tightened with nuts and adjustable wrenches (Figure 2.32e). Figure 2.32f shows the installed CLT diaphragm between the two CLT girders.



(a)



(b)



(c)



(d)

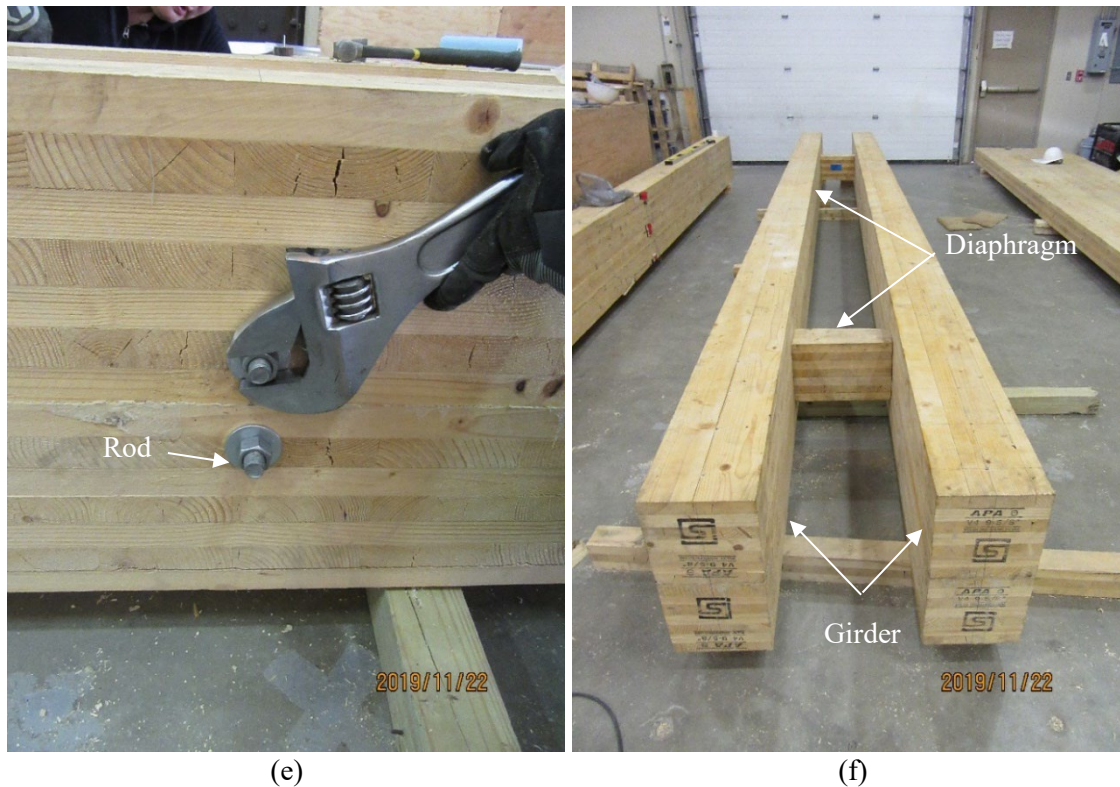


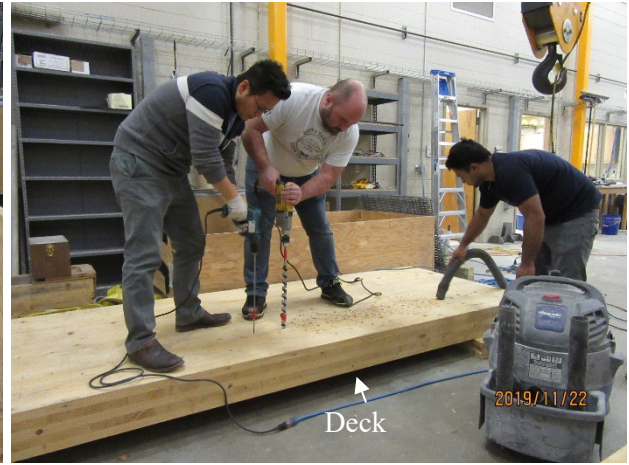
**Figure 2.32** Installation of CLT diaphragm: (a) hole location mark; (b) drill holes on the girder; (c) drill holes on the diaphragm; (d) diaphragm installation using rods; (e) rod tightening; and (f) girder and diaphragm connection.

### 2.3.3.2 Installation of CLT Deck

The 5-ply CLT deck 6400.8 mm long, 1219.2 mm wide, and 174.63 mm deep was used to fabricate the entire CLT girder bridge system. Both polyurethane glue, adhesive (Appendix C), and carbon steel fasteners (Appendix D) for wood connection purposes were used to make a connection between the CLT girders and CLT deck. The 14-ply CLT girders were fabricated with the adhesive, as referred to in Section 2.3.2. The CLT girders and CLT deck were marked at specific locations where the carbon steel fasteners 12.7 mm in diameter and 584.2 mm in length needed to be screwed (Figure 2.33a). Each marked location on the girders and deck was pre-drilled with 9.53 mm holes for effective screwing of the fasteners (Figure 2.33b). The deck was moved on top of the girders and wood blocks were placed between the deck and girder temporarily (Figure 2.33c). The adhesive was spread on top of the girder and wood blocks were removed (Figure 2.33d). The carbon steel fasteners 12.7 mm in diameter and 584.2 mm in length were screwed through the deck and girder (Figure 2.33e). In total, 39 fasteners were screwed for each of the CLT girders for fabrication of the CLT bridge system. The research team further applied epoxy glue to the gaps in the holes to prevent any decay in the timber (Figure 2.33f). Figures 2.33g and 2.33h show the epoxy filler curing on the CLT girder and the fabricated CLT bridge system, respectively.



(a)



(b)



(c)



(d)



(e)



(f)

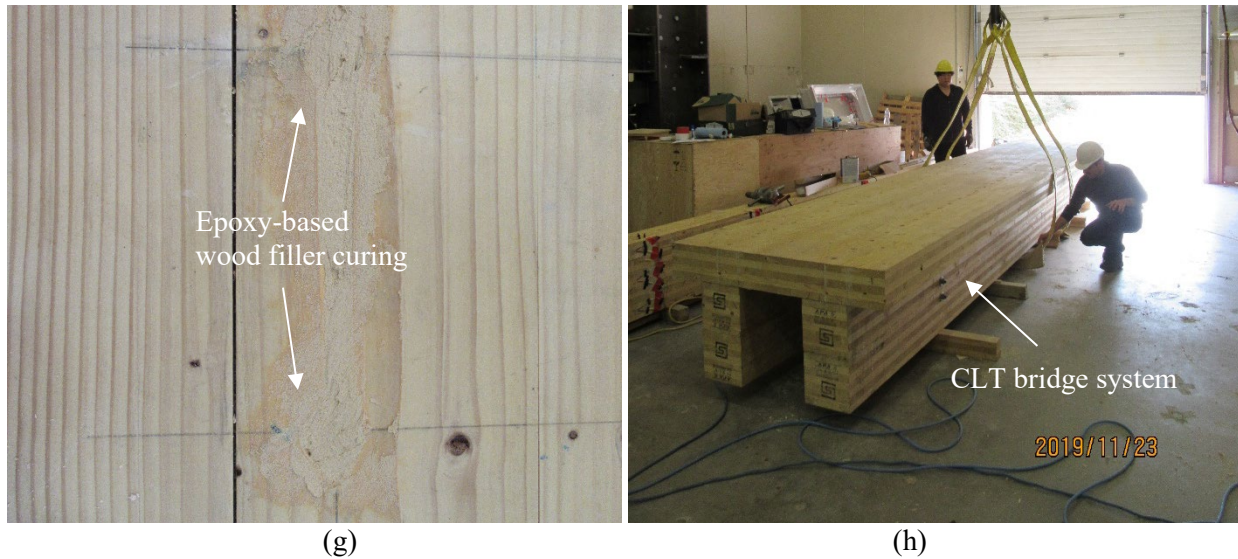


**Figure 2.33** Installation of CLT deck: (a) hole location mark; (b) drill holes on the deck; (c) deck moving on the girder; (d) adhesive application; (e) tightening the fasteners; (f) epoxy-based wood filler application; (g) epoxy-based wood filler curing; and (h) fabricated CLT bridge system

## 2.4 Ultimate Load Testing

Both the CLT girders and CLT bridge system designed in Section 2.2 and fabricated in Section 2.3 were tested to determine their ultimate strength. In detail, the ultimate strength testing was performed on 1) the CLT girder bonded with adhesive; 2) the CLT girder bonded with adhesive and fasteners; and 3) the CLT bridge system. Details on each testing are provided as indicated below:

### 2.4.1 Performance on CLT Girder with Adhesive

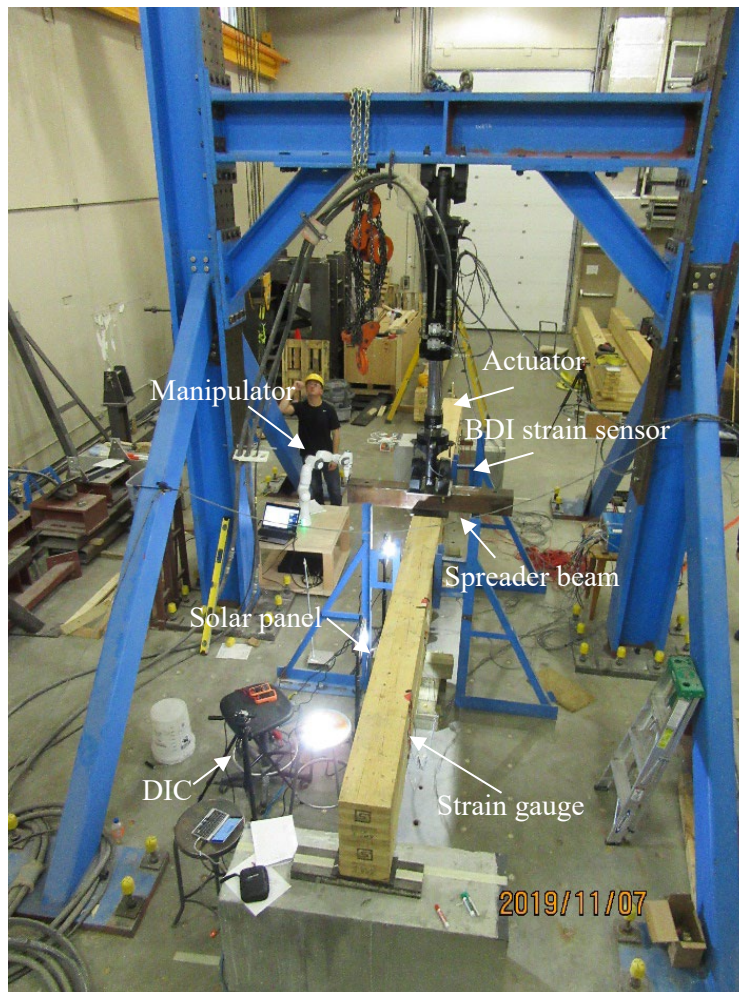
This section covers instrumentation for ultimate strength testing for the CLT girder bonded with adhesive, testing procedure, and results and discussion.

#### 2.4.1.1 Instrumentation

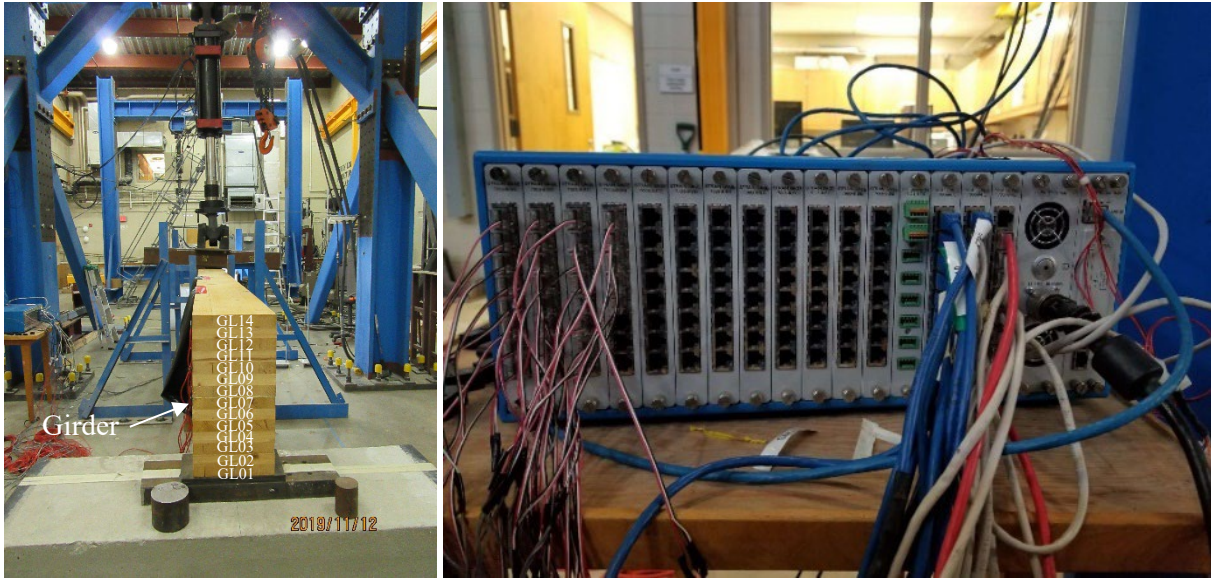
The full-scale laboratory testing of the adhesively bonded 14-ply CLT girder, which has 14 lams, is shown in Figure 2.34a. The CLT girder's dimensions are 6.40 m length, 0.48 m depth, and 0.24 m width. The 14 lams in the girder were designated as GL01 through GL14 from the bottom lam, as shown in Figure 2.34b. To measure testing data, such as deflection, strain, and slippage, and capture inspection images, both contact and non-contact sensors were installed on the CLT girder. The contact sensors included strain gauges (PFL-30-115LJC), BDI strain sensors (ST350), string pot, and LVDTs, while the non-contact sensors encompassed UAV DJI Phantom 4 (Appendix G) installed with a gimbal camera (12.4 mega pixels), a manipulator mounted with a smartphone camera (iPhone 6s Plus) (Appendix H), a digital camera, and DIC (Digital Image Correlation) camera (Basler acA1600-20um camera [Appendix I] and Computar M5028-MPW2 lens [Appendix J]).

A data acquisition system named “7000-128-SM” (Figure 2.34c) was used to record the data from the contact sensors during the ultimate strength test of the CLT girder. The actuator and data logger system connected with the contact sensors were controlled through computers in the testing control room, as shown in Figure 2.34d. Imagery from the non-contact sensors such as the UAV camera (Figure 2.34e) were captured from the cameras mounted in each robot during the test. The overall instrumentation is

shown in Figure 2.35. Figure 2.35a shows the plan view of this testing setup. Figure 2.35b displays the location of the strain gauges and BDI strain sensors installed on the west side of the CLT girder. The DIC system and solar panels mounted on the east side of the CLT girder are shown in Figure 2.35c. In this figure, the CLT girder was inspected with the UAV and manipulator on the southeast side. Figure 2.35d shows the string pot installed underneath the CLT girder and strain gages attached to the CLT girder, and the schematic of LVDTs to measure horizontal displacements marked “ $H$ ” is provided in Figure 2.35e.



(a)



(b)

(c)



(d)

(e)

**Figure 2.34** CLT girder test with adhesive bond: (a) test setup; (b) girder lam number designation; (c) data acquisition system; (d) control room; and (e) UAV-enabled inspection.



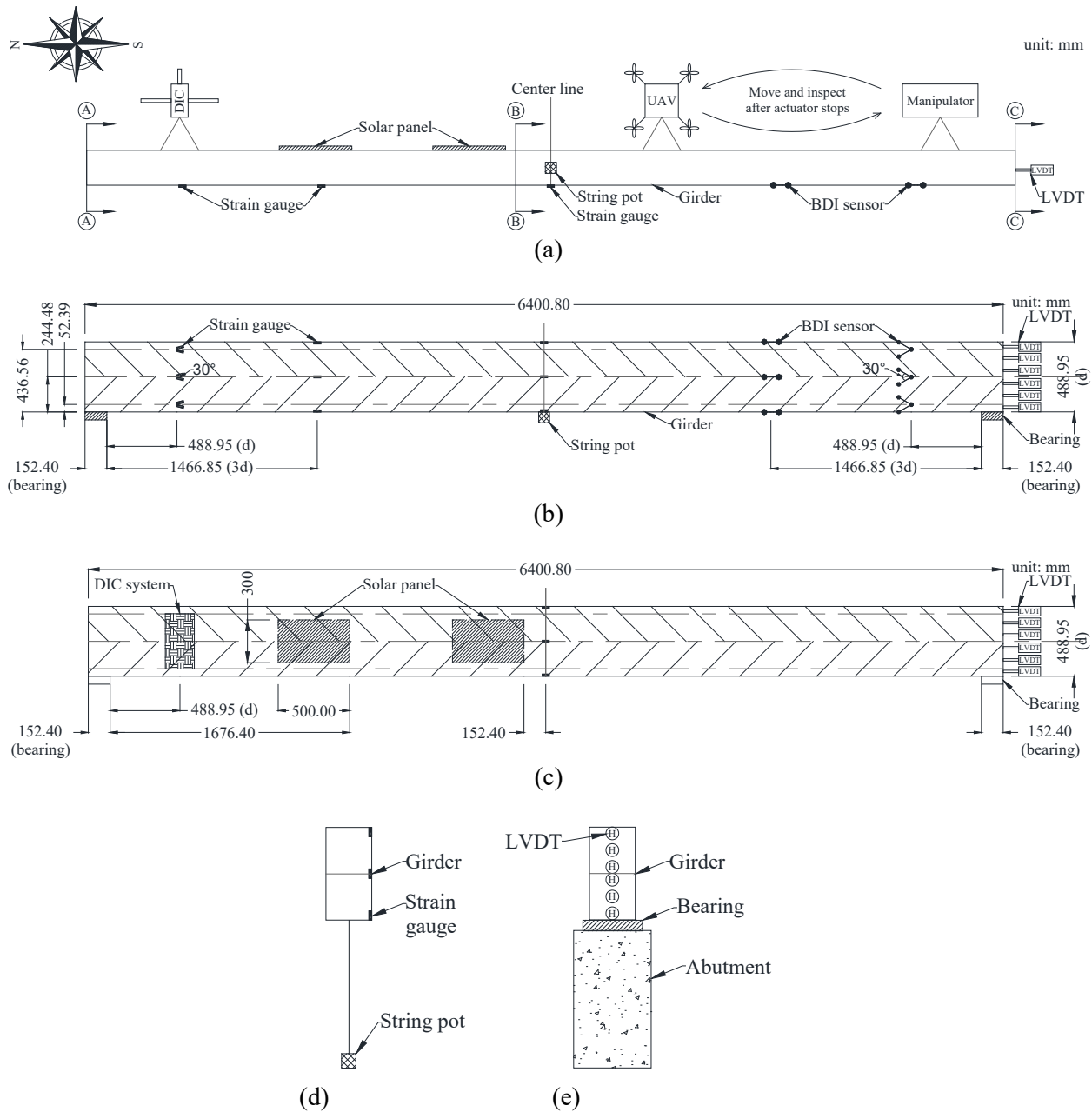


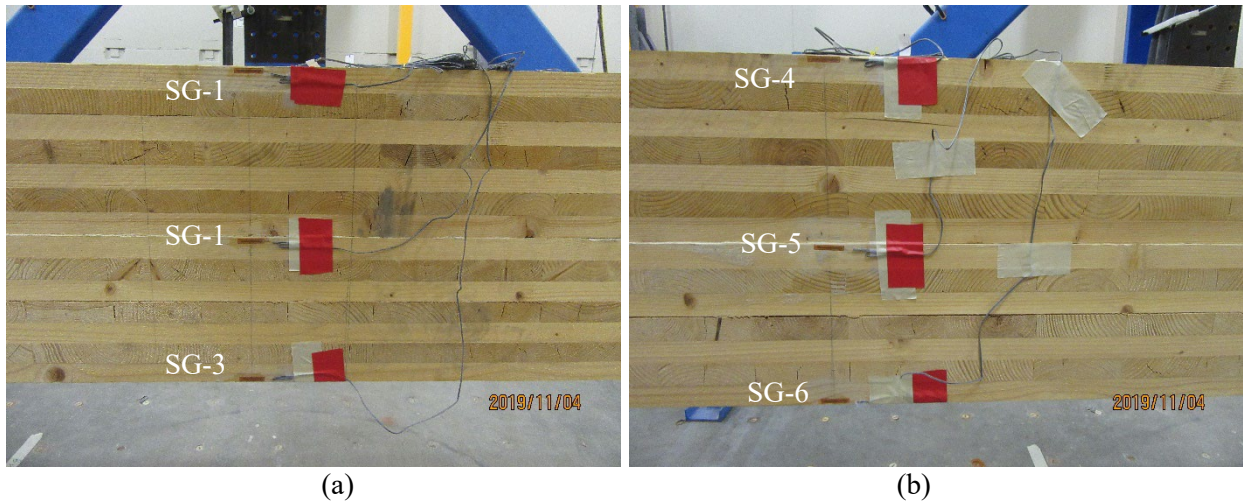
**Figure 2.35** Instrumentation plan for girder testing: (a) plan view; (b) elevation view (west side); (c) elevation view (east side); (d) string pot and strain gauges at mid-span; and (e) LVDTs at the south edge.

Regarding the contact sensor installation, the 12 strain gauges and 9 BDI strain sensors were attached to the west side of the CLT girder (Figure 2.35b). The six strain gauges were installed at a distance of  $d$  from the support at the north end of the CLT girder and the three strain gauges were installed at a distance of  $3d$  from the support at the north end of the CLT girder. It should be noted that  $d$  indicates the design depth of the CLT girder. The remainder of the strain gauges were attached to the mid-span of the CLT girder. Similarly, the six BDI strain sensors were mounted at a distance of  $d$  from the support at the south end of the girder, and the remaining three sensors were installed at  $3d$  from the south support end. The strain gauges and BDI strain sensors were installed at a distance  $d$  and  $3d$  from the support to analyze the

shear strain in the CLT girder where the maximum shear is expected (AASHTO, 2012). The strain gauges and BDI strain sensors were also installed at  $3d$  from the support of the girder where the critical shear may occur (AASHTO 2012). In Figure 2.35b, the string pot was installed in the center at the bottom of the CLT girder to collect deflection, and six LVDTs were instrumented at the south edge of the CLT girder to measure slippage between CLT lam. Specifically, two LVDTs installed on the upper side (GL13 and GL14) and two LVDTs installed on the lower side (GL01 and GL02) recorded local slip between lam, while two LVDTs located in the middle of the CLT girder (GL07 and GL08) recorded slip between two 7-ply CLT beams to evaluate its bonding performance.

Figure 2.36 illustrates the installed strain sensors and LVDTs in the CLT girder on the west side. Figures 2.36a, 2.36b, and 2.36c show strain gauges SG-1 through SG-3 installed at the mid-span, SG-4 through SG-6 at  $3d$  from the north support, and SG-7 through SG-12 at  $d$  from the north support. Figures 2.36d and 2.36e display BDI strain sensors BDI-1 through BDI-6 at  $d$  from the south support and BDI-7 through BDI-9 at  $3d$  from the south support. Figures 2.36f and 2.36g present six LVDTs on the south face and one string pot installed at the center, respectively. Note, two strain gauges were mounted at a  $30^\circ$  angle between gauges to precisely record shear strain, as shown in Figures 2.36c and 2.36d, respectively. According to the strain gauge installation manual (micro-measurement, 2010), shear strain is calculated from Equation 44. The schematic for the installation of strain gauges to determine shear strain is shown in Figure 2.36h.

$$\gamma_{xy} = \frac{\epsilon_1 - \epsilon_2}{\sin 2a} \quad (44)$$



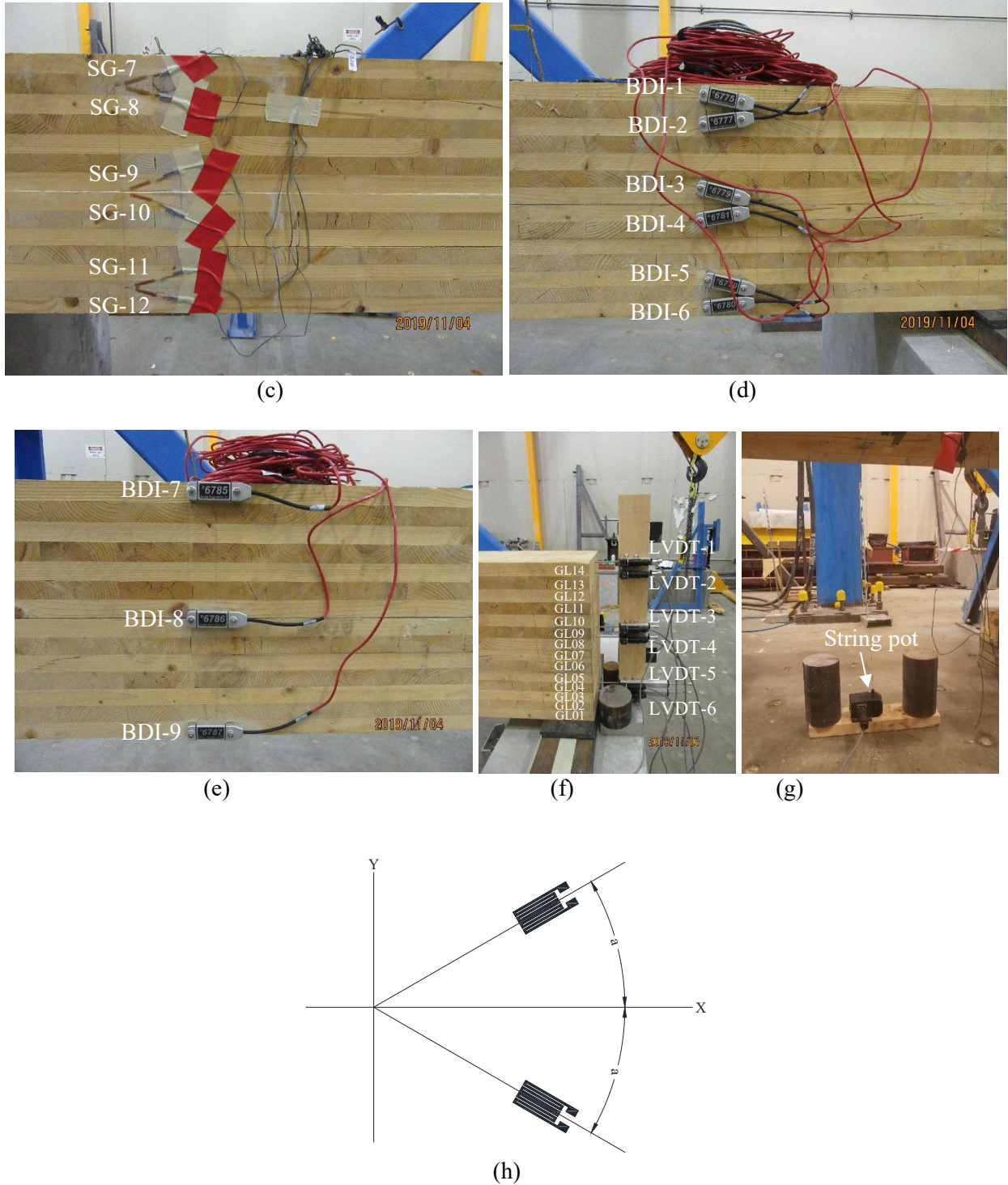


**Figure 2.36** Contact sensor installation: (a) strain gauges at mid-span; (b) strain gauges at distance  $3d$  from north support; (c) strain gauges at distance  $d$  from north support; (d) BDI strain sensors at distance  $d$  from south support; (e) BDI strain sensors at distance  $3d$  from south support; (f) LVDTs at south edge; (g) string pot; and (h) shear strain gauge mechanism.

The non-contact sensors, which contained the UAV Phantom 4 equipped with the gimbal camera, the manipulator with the smart phone camera, and the DIC camera, were installed on the east side of the CLT girder, as shown in Figure 2.35c. In this figure, the UAV and manipulator collected numerous images on the southeast surface of the CLT girder during individual inspections, while the DIC system was installed on the northeast side of the CLT girder at a distance  $d$  from the north support. It should be noted that the images from the UAV and manipulator were used to identify damage and estimate deflections at the mid-span of the girder in a new fashion. On the other hand, images to estimate corresponding strain values were collected from the DIC system. Note that the image-based strain values were compared with those from the contact sensors installed on northwest side of the CLT girder at the same distance from the north support. The installation of the non-contact sensors is shown in Figures 37a for the DIC system and 37b for the UAV and manipulator.

In addition to the contact and non-contact sensor installation, two solar panels (Nuzamas portable 20W, Appendix K) were installed on the east side of the CLT girder to examine the correlation between solar energy harvesting and girder behavior resulting from the testing, as seen in Figure 2.35c. In Figure 2.37c, one solar panel, “solar panel 1,” was located at a distance of 2.55 m to collect the solar energy at the most critical damage location, while the other solar panel, “solar panel 2,” was mounted 1.33 m from the north edge of the girder. To explore an amount of solar energy harvested during the testing, two lights were installed, where each was capable of harvesting the maximum voltage of 16.91 V.



**Figure 2.37** Non-contact sensor: (a) DIC system; (b) UAV and manipulator; and (c) solar panel

### 2.4.1.2 Testing Procedure

A flowchart presenting the procedure of the test is shown in Figure 2.38. The test was performed in three major steps: 1) loading, 2) measurement, and 3) inspection. As the first step, the CLT girder was loaded until failure. The actuator with a capacity of 500 kN was used to apply a monotonic load on the top of the girder at mid-span with displacement control.

As the second step, data from all the contact sensors, such as strain gauges and LVDTs, were recorded during loadings; whereas, the non-contact sensors, including DIC system, UAV camera, and camera mounted on the manipulator, were employed to capture images at each inspection phase. Note, the DIC system was used to capture strain quantities through multiple images from the testing. Voltage data from

each of the solar panels were recorded manually from a multimeter at each loading step. All of the contact sensors were networked to the data acquisition system with 128 channels. This data acquisition system can record 10 sets of data per second for each channel. All data, including load, deflection, and strain responses, were recorded for each test run. Voltage and current data from each solar panel were also manually recorded through the multimeter for each test run.

As the final step, the CLT girder was inspected at regular loading intervals. When it was necessary to identify damage and/or to capture associated images at a certain test run, visual inspection was conducted. For example, when a cracking sound was heard, the inspection was carried out. The visual inspection was performed on all sides of the girders using the UAV, manipulator, and digital cameras. During this test, the girder was tested with 185 test runs and 14 inspections, including the initial inspection before the testing was conducted.

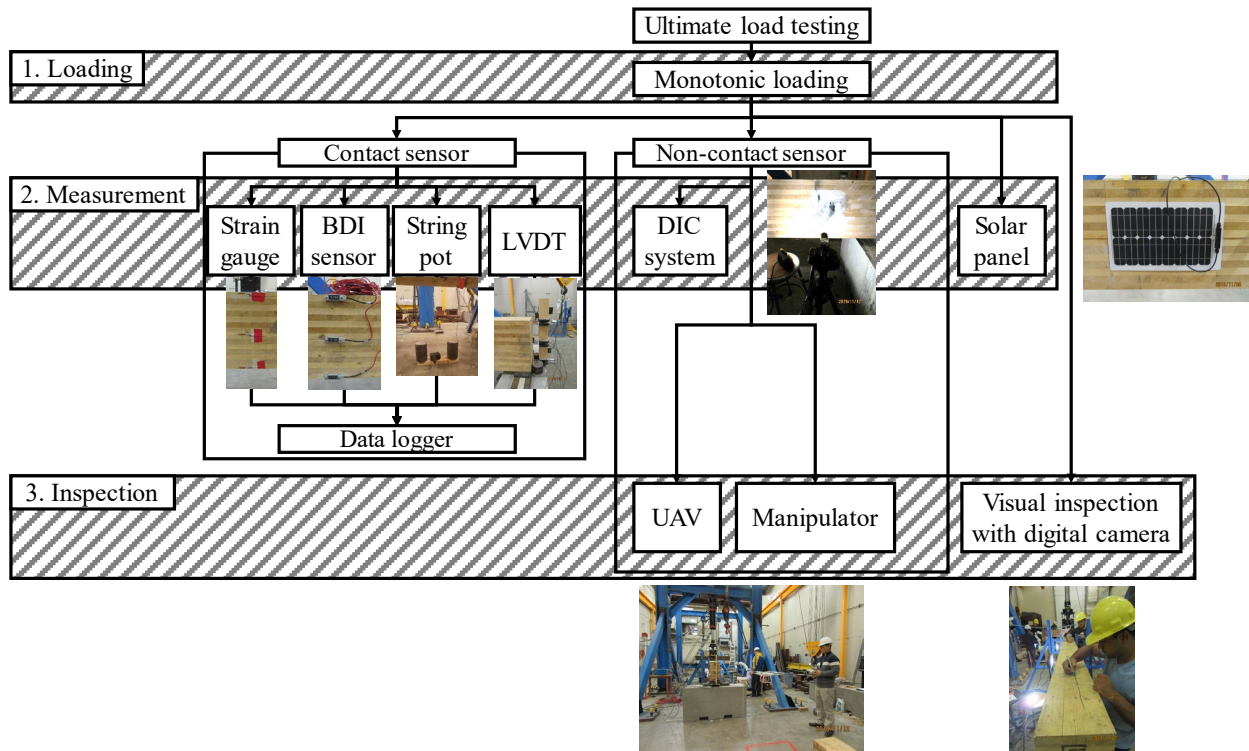


**Figure 2.38** Testing and data collection procedure of CLT girder with adhesive

### 2.4.1.3 Results and Discussion

This section describes data obtained from the ultimate strength testing for the CLT girder bonded with adhesive. All the data obtained from the contact and non-contact sensors, including strain, slippage, deflection, voltage, and imagery, have been analyzed in-depth to evaluate structural performance of the tested CLT girder

#### *Data from Contact Sensors*

A load-displacement curve is presented in Figure 2.39, where two different failures, slippage failure at 49.53 mm resulting from 62.74 kN and flexural failure at 73.66 mm corresponding to 52.32 kN, can be observed.

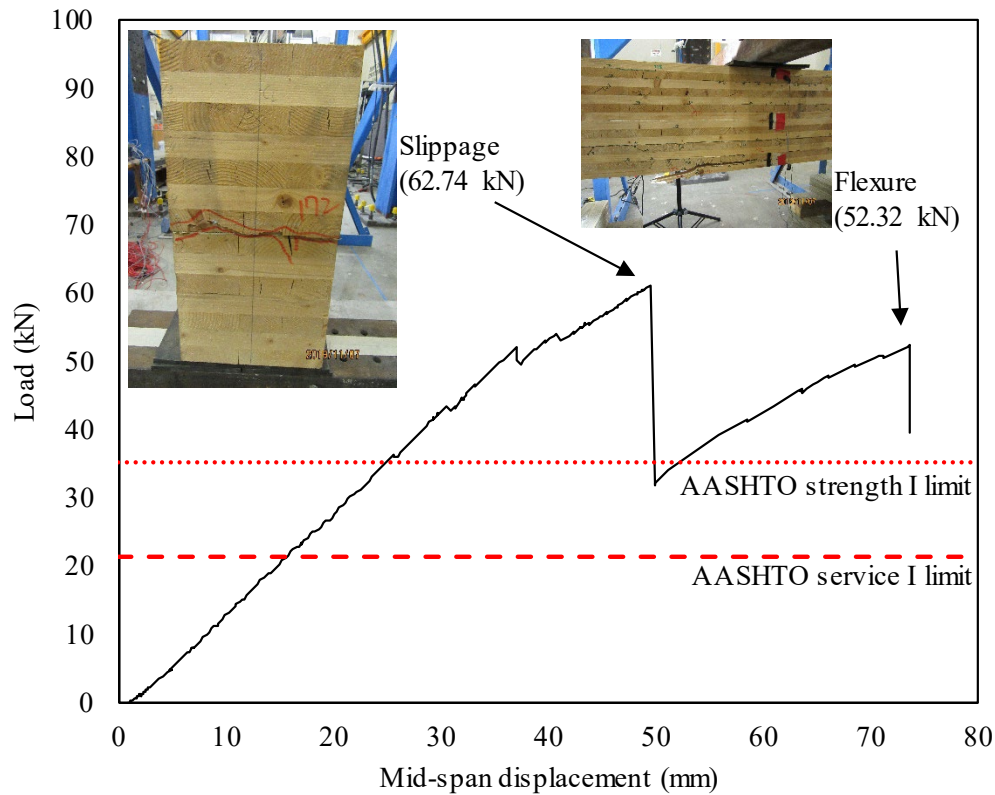


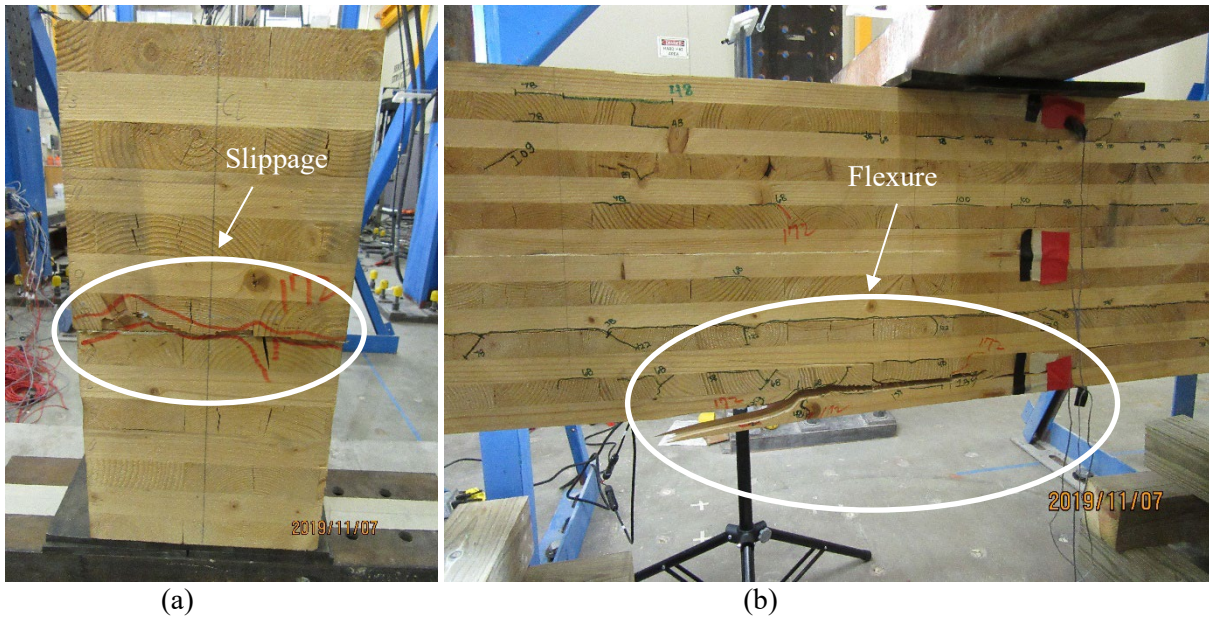
**Figure 2.39** Load-displacement curve of CLT girder with adhesive

As illustrated in Figure 2.40a, the first failure was spotted with the slippage between the top and bottom of 7-ply CLT beams. The second flexure failure was observed at the bottom of the girder at mid-span, as shown in Figure 2.40b. Based on the results, the ultimate strength of the CLT girder bonded with adhesive was found to be 62.74 kN at slippage failure. The strength of the tested CLT girder is 43.74% higher than AASHTO's strength I limit and 65.73% higher than AASHTO's service I limit strength, respectively. The AASHTO strengths are also included in Figure 2.39. Note, the AASHTO strength I limit strength and service I limit strength were calculated using Equations 45 and 46 (Appendix L).

$$\text{AASHTO Strength I limit} = 1.25 DC + 1.75 LL \quad (45)$$

$$\text{AASHTO Service I limit} = 1.0 DC + 1.0 LL + 0.3 WS \quad (46)$$

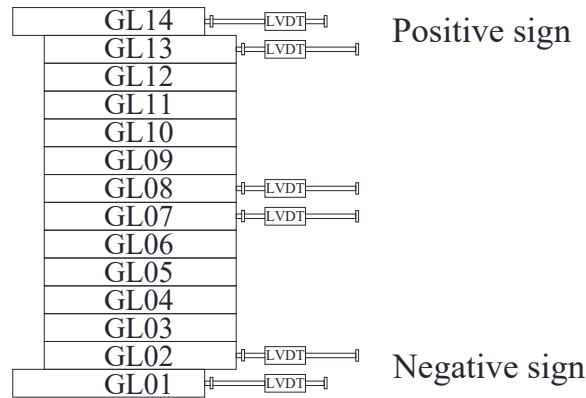
where DC = component self-weight  
 LL = vehicle live load  
 WS = wind load on structure



**Figure 2.40** Representative CLT girder failure images: (a) slippage failure at south edge and (b) flexural failure at mid-span on west side

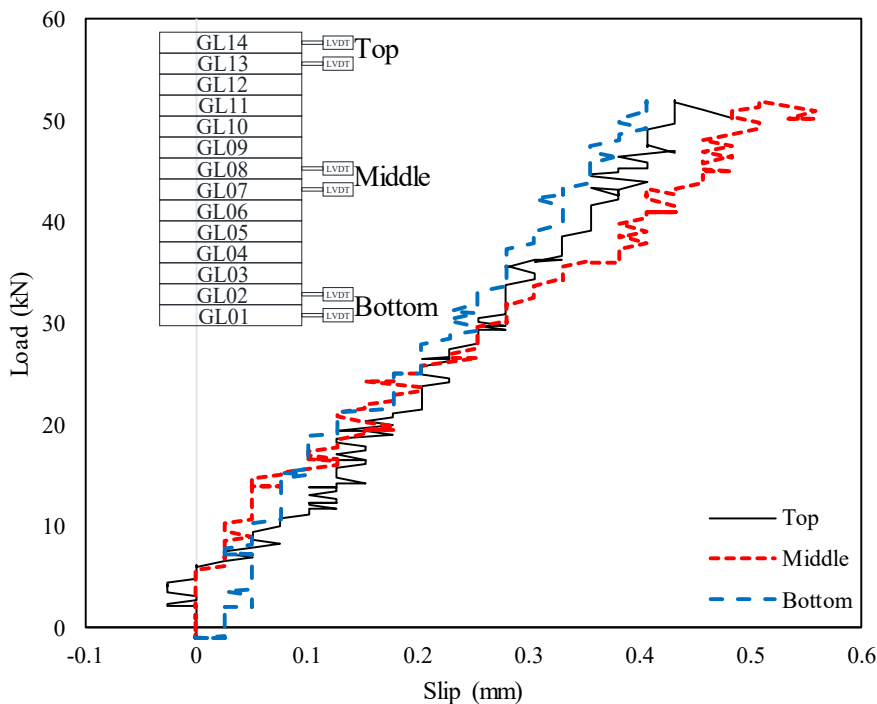
As mentioned previously, six LVDTs were installed to collect lateral displacements of six lam. The LVDTs were located at GL01, GL02, GL07, GL08, GL13, and GL14 (Figure 2.41), where GL indicates “Girder Lam.” For example, GL01 means the first lam in the girder from the bottom. Again, three sets of LVDTs were installed at the top of the girder (GL13 and GL14), in the middle of the girder (GL08 and GL07), and at the lowest two lam (GL02 and GL01). These LVDTs recorded local slippage defined as the difference in two lam’s lateral displacements, as shown in Figure 2.41. In Figure 2.41, the slippage was expressed in terms of positive and negative signs. One set of LVDTs observed slippage between the lam, as shown in Figure 2.41. If the displacement in the upper lam is greater than the displacement in the lower lam, the value is considered as a positive slippage, while negative slippage is considered when the lower lam’s displacement is larger.





**Figure 2.41** Slippage sign convention

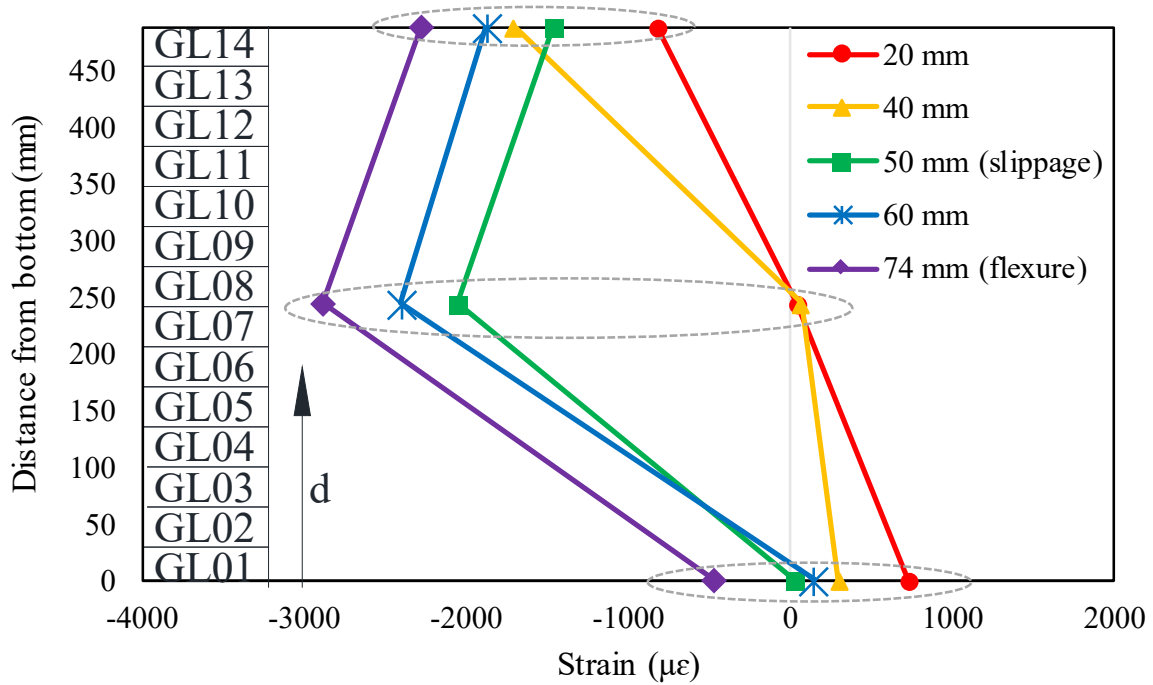
In Figure 2.41, the LVDT sets showed positive values of slippage except for the initial negative slippage at the top of the girder during the test. As expected, as the load increased, the slippages increased at the top, middle, and bottom of the CLT girder, as shown in this figure. Note, the LVDTs were removed before the first failure due to slippage to avoid any damage to the instruments. The maximum slippages at the top, middle, and bottom of the girder were 0.48 mm, 0.56 mm, and 0.41 mm, respectively, before the first failure. With these results, it was concluded that the maximum value was reached before the slippage failure between the two 7-ply beams (GL07 and GL08).



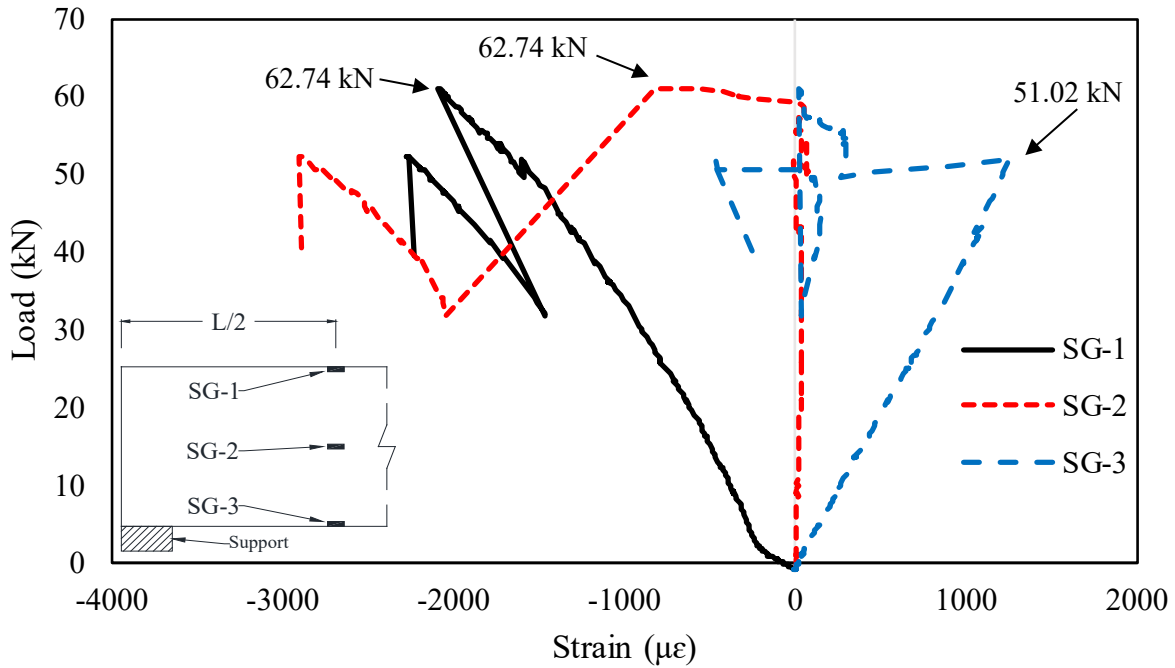
**Figure 2.42** Slippage between lams obtained by LVDTs

Figure 2.43a shows the strain profile along the distance from the bottom of the CLT girder to evaluate the neutral axis of the CLT girder at mid-span. Three strain gauges collected strain data on the west side at mid-span of the CLT girder. As stated before, the strain gauges were installed at the top of the girder (SG-1), in the middle of the girder (SG-2), and at the bottom of the girder (SG-3). Before the slippage failure,

strain values at 20 mm and 40 mm deflections indicated that the neutral axes were located at 235.41 mm and 233.11 mm from the bottom of the CLT girder, respectively. It was proved that the neutral axes were near the center of the CLT girder depth before the slippage failure; however, the neutral axis moved down to the bottom of the CLT girder after the slippage failure at deflections of 50 mm, 60 mm, and 74 mm. In Figure 2.43b, SG-1 and SG-2 showed significant change in the strain at 62.74 kN due to the slippage failure, whereas SG-3 showed change in the strain at 51.02 kN corresponding to 36.93 mm. Based on these observations, loss of section properties in the CLT girder was found to be initiated from 36.93 mm deflection, and additional significant section properties losses were found after slippage failure.



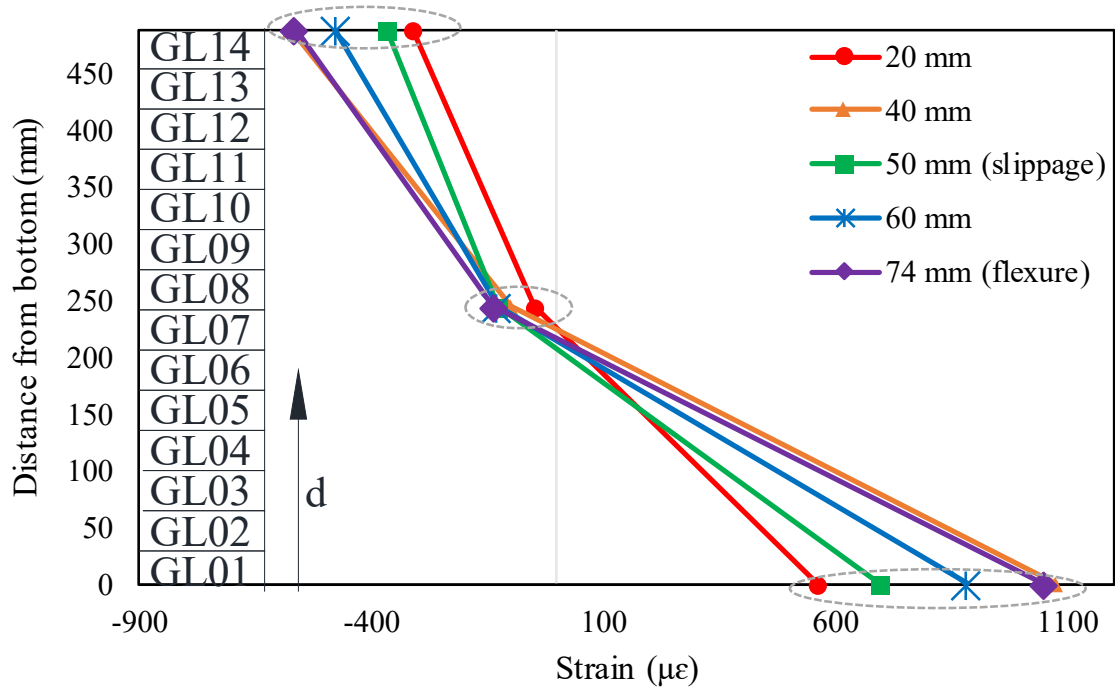
(a)



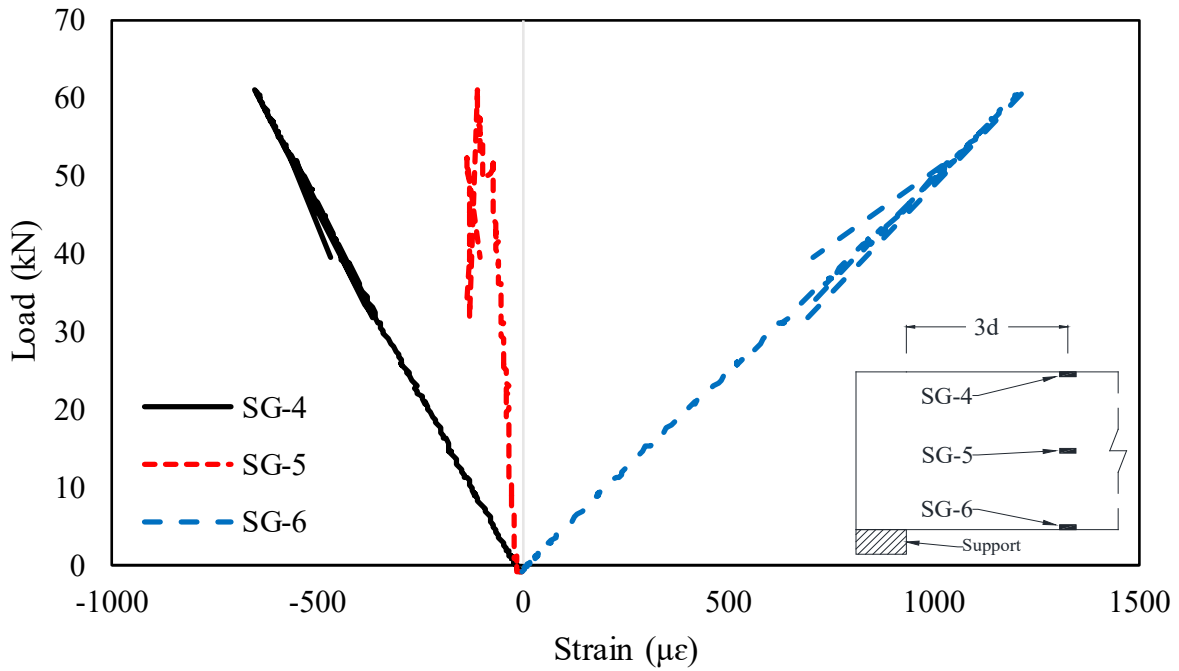
(b)

**Figure 2.43** Strain gauges installed in mid-span of girder: (a) strain profile and (b) load-strain curves

Figure 2.44a shows the strain values based on the distance from the bottom of the CLT girder to evaluate its neutral axis at  $3d$  from the north support. Three strain gauges installed at the top (SG-4), in the middle (SG-5), and at the bottom (SG-6) of the CLT girder collected strain data on the west side of the girder at  $3d$  from the north support. The average neutral axis at the deflections of 20 mm through 74 mm was located at 236.44 mm from the bottom of the CLT girder, where all the neutral axes were located near the center of the girder depth, which indicated it did not move significantly during the testing. It has been demonstrated that the slippage failure has insignificantly affected the neutral axis of the CLT girder at  $3d$  from the north support. In Figure 2.44b, negative strain in compression can be seen, as anticipated, at the SG-4 and SG-5 location, whereas positive strain in tension was found at the SG-6 location. A significant change in the strain was observed in all strain gauge locations due to slippage failure after the load reached 62.74 kN. From the results, substantial section property loss of the CLT girder at the bottom and remarkable strain value changes were observed at slippage failure.



(a)



(b)

**Figure 2.44** Strain gauges installed at  $3d$  from the north support: (a) strain profile and (b) load-strain curves.

As shown in Figure 2.45, strain profiles were plotted from the data measured from the strain gauges installed at  $d$  from the north support. The strain gauges were installed at the top (SG-7 and SG-8), in the middle (SG-9 and SG-10), and at the bottom (SG-11 and SG-12) of the CLT girder. Note, SG-7, SG-9, and SG-11 in Figures 2.45a and 2.45c indicate upper gauges installed at a  $15^\circ$  up angle with respect to a reference horizontal line of the CLT girder, whereas SG-8, SG-10, and SG-12 in Figures 2.45b and 2.45d indicate lower gauges mounted on a  $15^\circ$  down angle from the reference line.

In Figures 2.45a, the average neutral axis at the deflections of 50 mm through 74 mm was located at 419.24 mm from the bottom of the CLT girder. The neutral axes corresponding to 50 mm, 60 mm, and 74 mm were positioned near the top of girder depth. In Figure 2.45c, negative strain values in compression are observed in all strain gauges after the slippage failure (62.74 kN) except at SG-7. As shown in Figure 2.45b, at the deflections of 20 mm through 74 mm, the neutral axis was out of boundary of the CLT girder depth. No significant change in the position of neutral axes was found during the test. All strain gauges observed positive strain values in tension, as shown in Figure 2.45d. Figures 2.45c and 2.45d show that the strain values change abruptly after the slippage failure at 62.74 kN load.

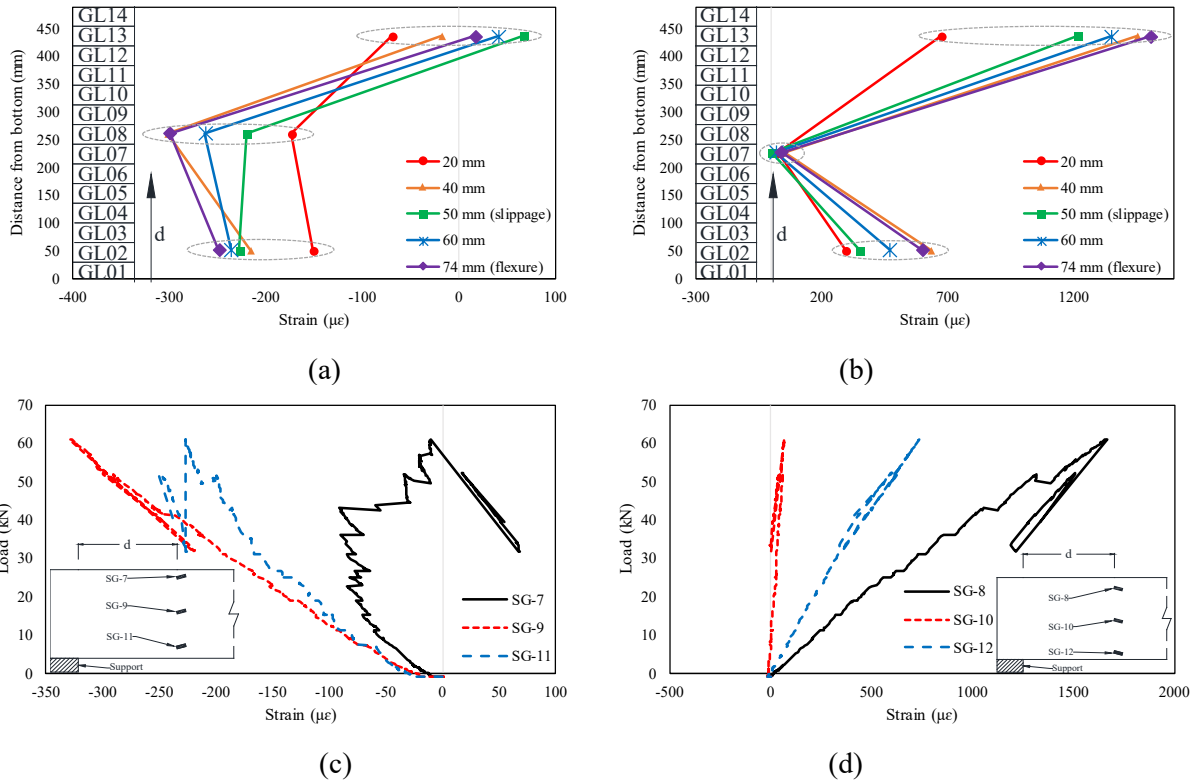
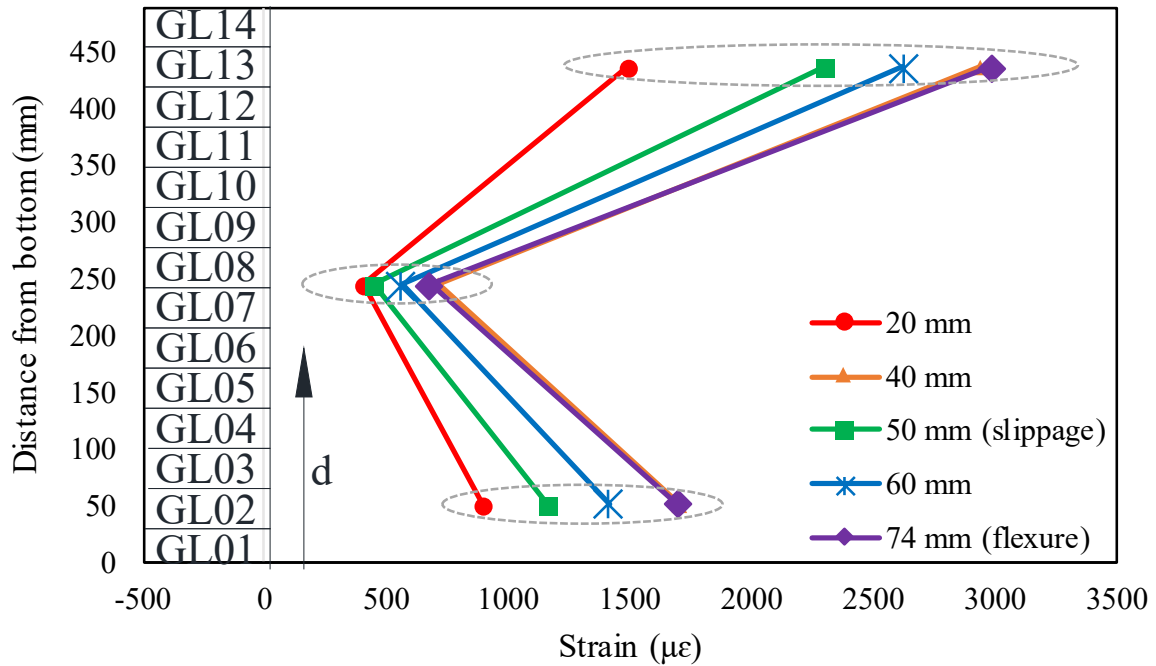
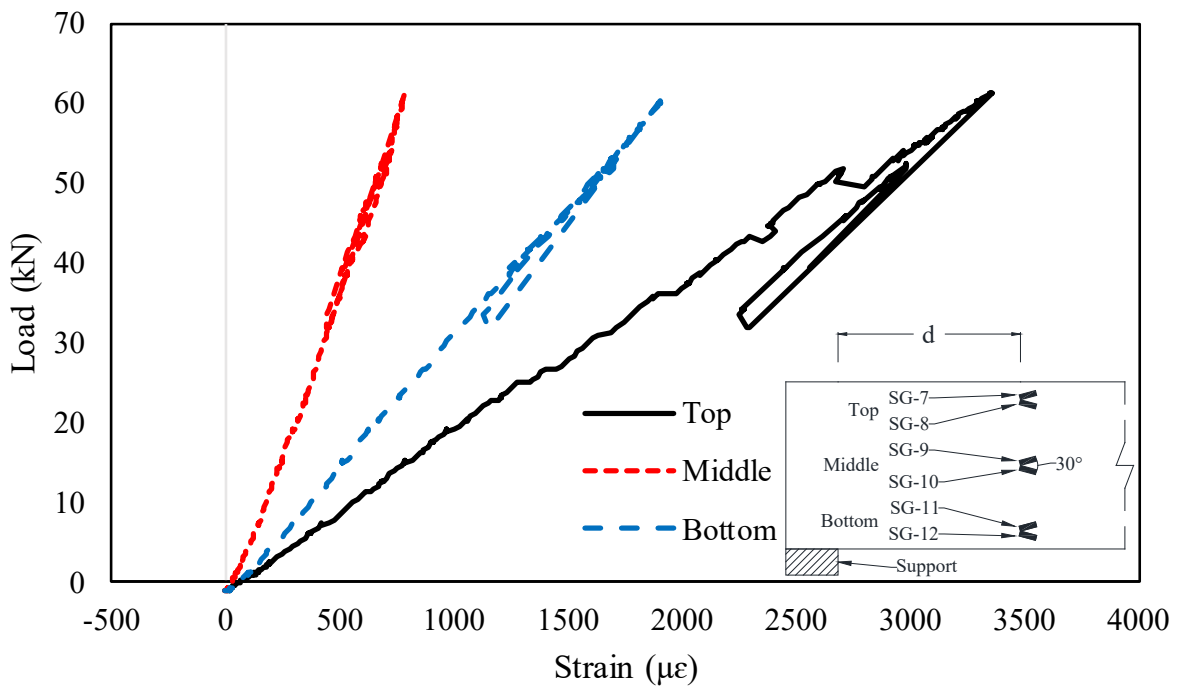


**Figure 2.45** Strain gauges installed at  $d$  from the north support: (a) strain profile (upper); (b) strain profile (lower); (c) load-strain curves (upper); and (d) load-strain curves (lower)

The shear strains calculated using the data from a pair of two strain gauges installed at  $30^\circ$  (e.g., SG-7 and SG-8) through Equation 44 are plotted in Figure 2.46a for the strain profile and Figure 2.46b for the load-strain curve. At the deflections of 20 mm through 74 mm, the neutral axis was not able to be found within the girder depth in Figure 2.46a. As shown in Figure 2.46b, the maximum shear strain appears at the top of the girder because of the slippage failure between GL07 and GL08. This trend is not consistent with the fact that maximum shear strain occurs at the center of normal girders that do not tend to have any slippage failure.



(a)



(b)

**Figure 2.46** Shear strain on  $d$  from the north support: (a) strain profile and (b) load-strain curves

Figures 2.47 and 2.48 display the strain profile and load-strain curves recorded from BDI strain sensors at  $d$  from the south support of the CLT girder. The strain sensors were installed at the top (BDI-1 and BDI-2), in the middle (BDI-3 and BDI-4), and at the bottom (BDI-5 and BDI-6) of the girder. Note, BDI-1, BDI-3, and BDI-5 in Figures 2.47a and 2.47c indicate upper gauges installed at a 15° up angle with

respect to the reference line, whereas BDI-2, BDI-4, and BDI-6 in Figures 2.47b and 2.47d stand for lower gauges mounted at a 15° down angle from the reference line at  $d$  from the south edge. In Figure 2.47a, the average neutral axis was situated at 171.23 mm from the bottom of the CLT girder at the deflections of 20 mm through 74 mm. The results demonstrated no significant movement of the neutral axis. In Figure 2.47c, negative strain in compression can be observed at the BDI-1 and BDI-3 location, whereas positive strain in tension can be found at the BDI-5 position. As illustrated in Figure 2.47b, the neutral axes were positioned at 364.50 mm and 431.24 mm from the bottom of the CLT girder at the deflections of 20 mm to 40 mm, respectively. As seen in Figure 2.47d, BDI-2 appears to be in compression with the negative strain, whereas BDI-4 and BDI-6 are found to be in tension with the positive strain until the slippage failure at 62.74 kN. BDI-4 showed a significant change of strain from tension to compression after the slippage failure.

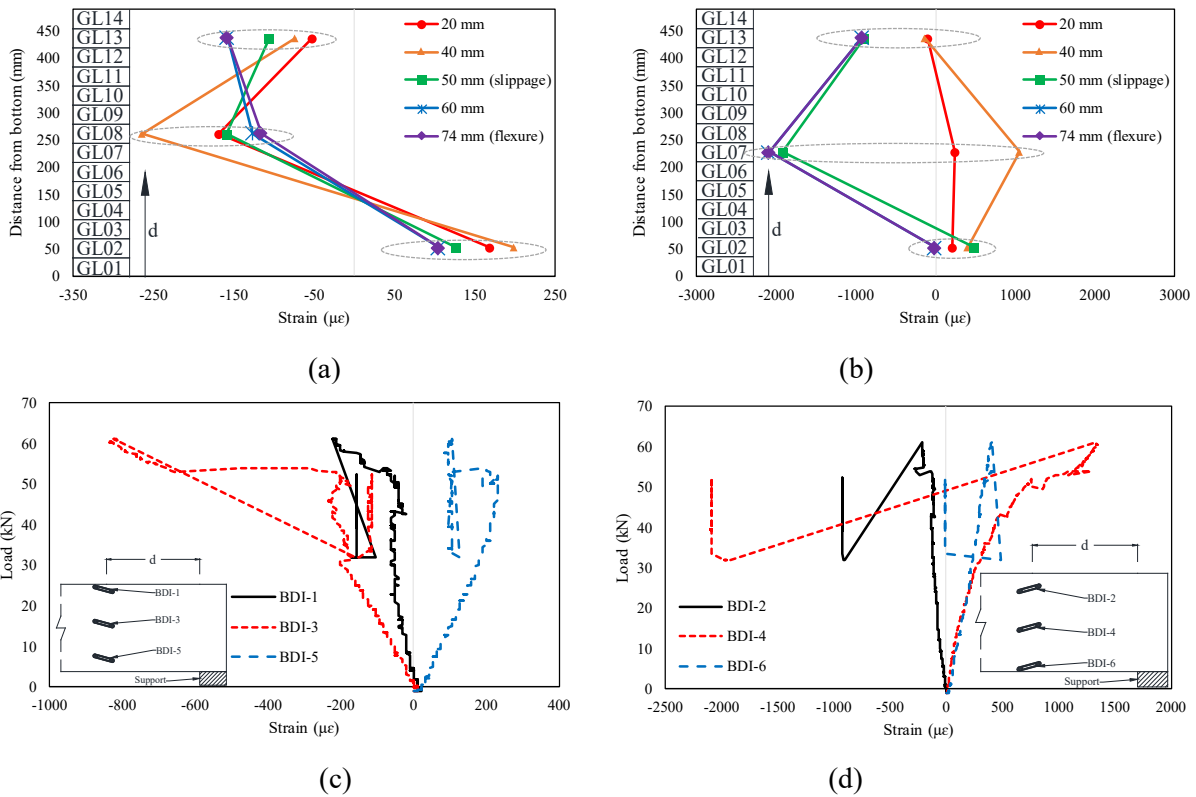


**Figure 2.47** BDI strain sensors (upper) installed on  $d$  from the south support: (a) strain profile (upper); (b) strain profile (lower); (c) load-strain curves (upper); and (d) load-strain curves (lower)

Figure 2.48 shows the shear strain values calculated using the data from a pair of two strain gauges mounted at 30° through Equation 44. As shown in Figure 2.48a, the neutral axes were positioned at 436.21 mm, 430.25 mm, and 82.24 mm corresponding to the deflections of 20 mm, 40 mm, and 50 mm. The maximum shear strain is found to be at the middle of the CLT girder before the slippage failure, as shown in Figure 2.48b. This follows the evidence, where maximum shear strain occurs at the center of conventional girders such as concrete girders (Hearn 1997).

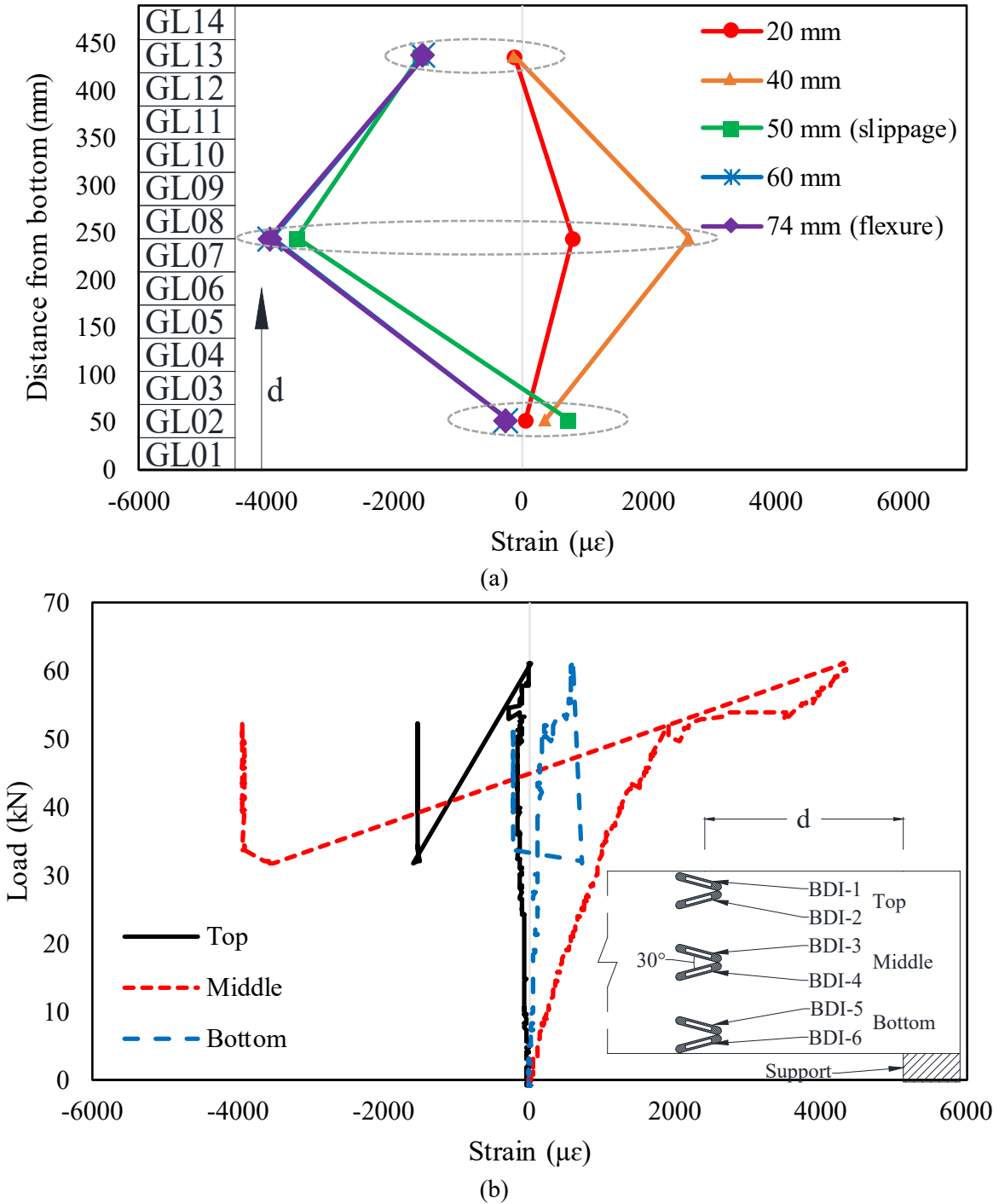
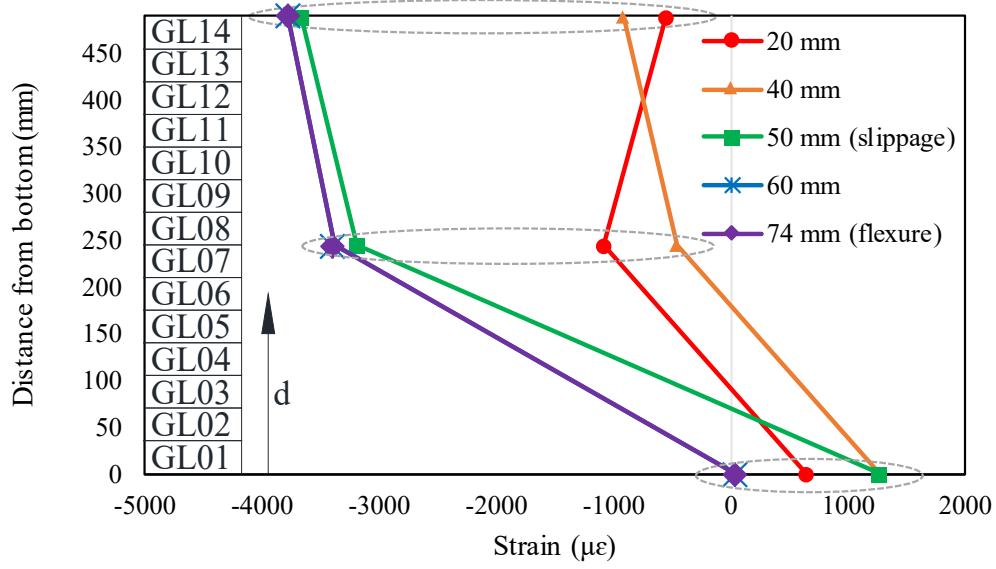


**Figure 2.48** Shear strain on  $d$  from the south support: (a) strain profile and (b) load-strain curves

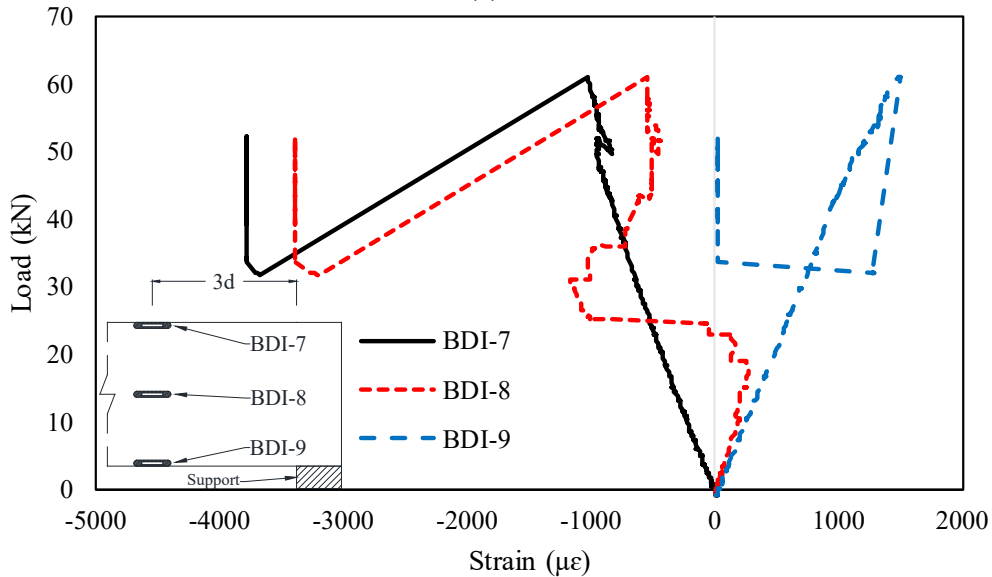
Strain values recorded from the BDI sensors installed at  $3d$  from the south support are shown in Figure 2.49. Figure 2.49a shows the average neutral axis for the deflections of 60 mm and 74 mm, indicating that the post slippage failure is located 3.13 mm from the bottom of the CLT girder. BDI-7 showed negative strain on compression, while BDI-9 showed positive strain in tension during the test, as shown in Figure 49b. BDI-8, however, changed the sign of strain from positive (tension) to negative (compression) during



the test. A significant change in the strain values was found in all BDI strain sensors after the slippage failure at 62.74 kN.



(a)



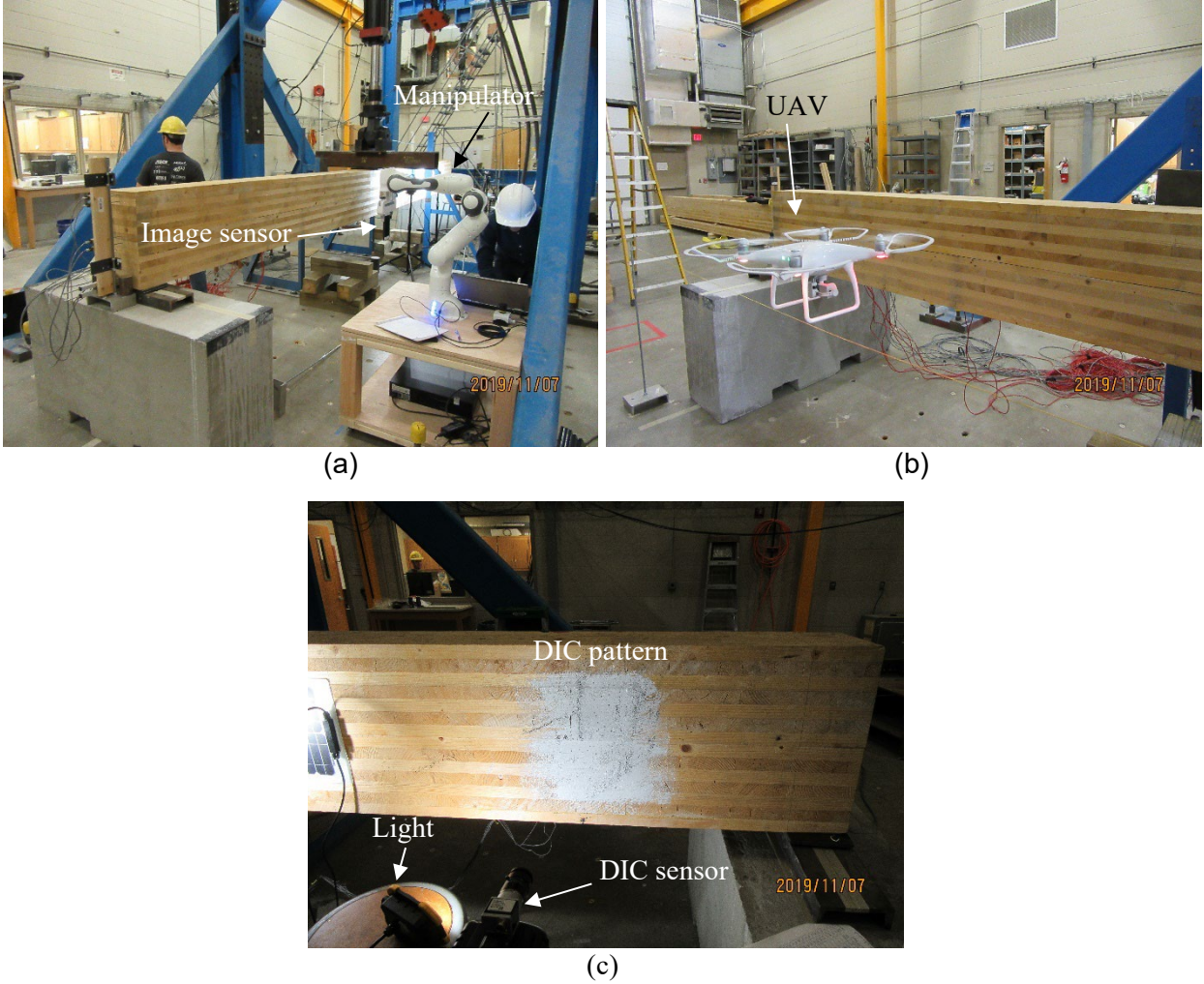
(b)

**Figure 2.49** BDI strain sensors installed on  $3d$  from the south support: (a) strain profile and (b) load-strain curves

### Data from Non-contact Sensors

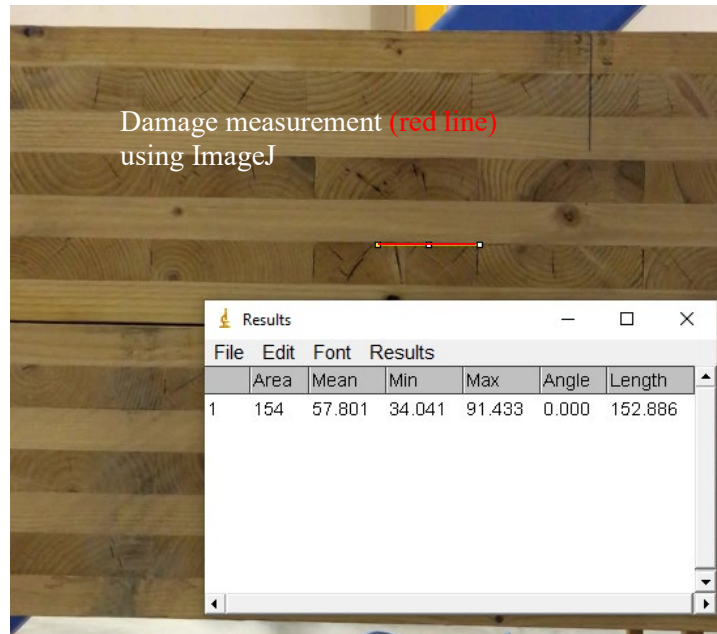
During the testing, the CLT girder was inspected at regular intervals with the non-contact sensors, as shown in Figure 2.50. The manipulator (Figure 2.50a), UAV Phantom 4 (Figure 2.50b), and DIC system (Figure 2.50c) along with the digital camera were used during the individual inspections. As stated earlier, 14 inspections, encompassing the initial inspection prior to the testing, were performed on all sides of the CLT girder. Numerous images were taken with the iPhone 6s Plus mounted on the manipulator and the gimbal camera installed on the UAV to not only measure the deflections, but also quantify damage from

image analysis at each interval. For the image analysis, image analysis software, ImageJ, which is capable of measuring a relative length between two points based on the number of pixels in an image, was employed. To obtain an actual length, a reference length such as depth of the girder and lam thickness was needed. The actual length of the target measurements such as deflection was calculated from a ratio of the pixel number of the reference length to the pixel number of the target length.



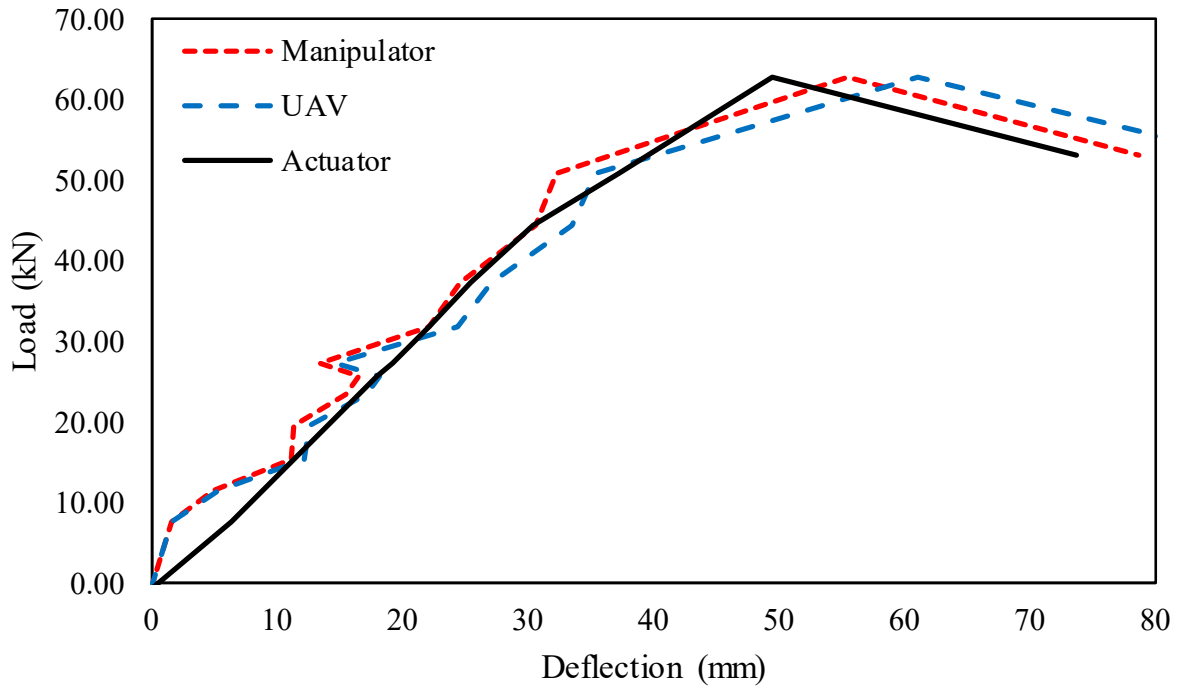
**Figure 2.50** Non-contact sensor operation: (a) manipulator; (b) UAV; and (c) DIC system

Figure 2.51 shows an example to measure a relative length in red within ImageJ. When measuring deflection from the image analysis with the inspection images from the manipulator and UAV, a lam thickness of 34.93 mm was taken as a reference length.



**Figure 2.51** Relative length measurement procedure on one side of the CLT girder

A comparison of the mid-span deflections of the girder calculated from the image analysis of the inspection images from the manipulator and UAV and those recorded from the actuator was made, as shown in Figure 2.52. Overall, the deflections acquired from the manipulator and UAV agree with those recorded from the actuator. The average difference between the deflections measured from the manipulator and UAV and the directly measured deflections through the actuator over the testing was found to be 2.09 mm and 2.01 mm, respectively, and corresponding average percentage errors were 17.49% and 16.72%. The maximum difference in the deflection between the manipulator and UAV and the actuator were found to be only 5.23 mm and 4.89 mm, correspondingly. Therefore, the results demonstrated that the level of precision the image analysis with the inspection images from the manipulator and UAV was capable of acquiring, along with the average percentage errors for the deflection.



**Figure 2.52** Deflection comparison between manipulator, UAV, and actuator

The inspection images selected for the mid-span deflection measurement are shown in Figure 2.53. Figures 2.53a through 2.53d show the clear inspection images at the mid-span of the CLT girder were captured by the manipulator. Along with the inspection, images used as input images were necessary for the image analysis to be capable of producing mid-span deflections. As shown in Figures 2.53e and 2.53f, original inspection images captured by the UAV have a lack of brightness. These low-quality images did not enable the clear identification of the position of the actuator and the accurate measurement of the mid-span deflections. Therefore, these images were adjusted with the brightness of 85% and contrast of -10%, as shown in Figures 2.53g and 2.53h. With the adjusted images, the CLT girder and other structural components were identified visibly and then the mid-span deflections were also calculated through the image analysis.

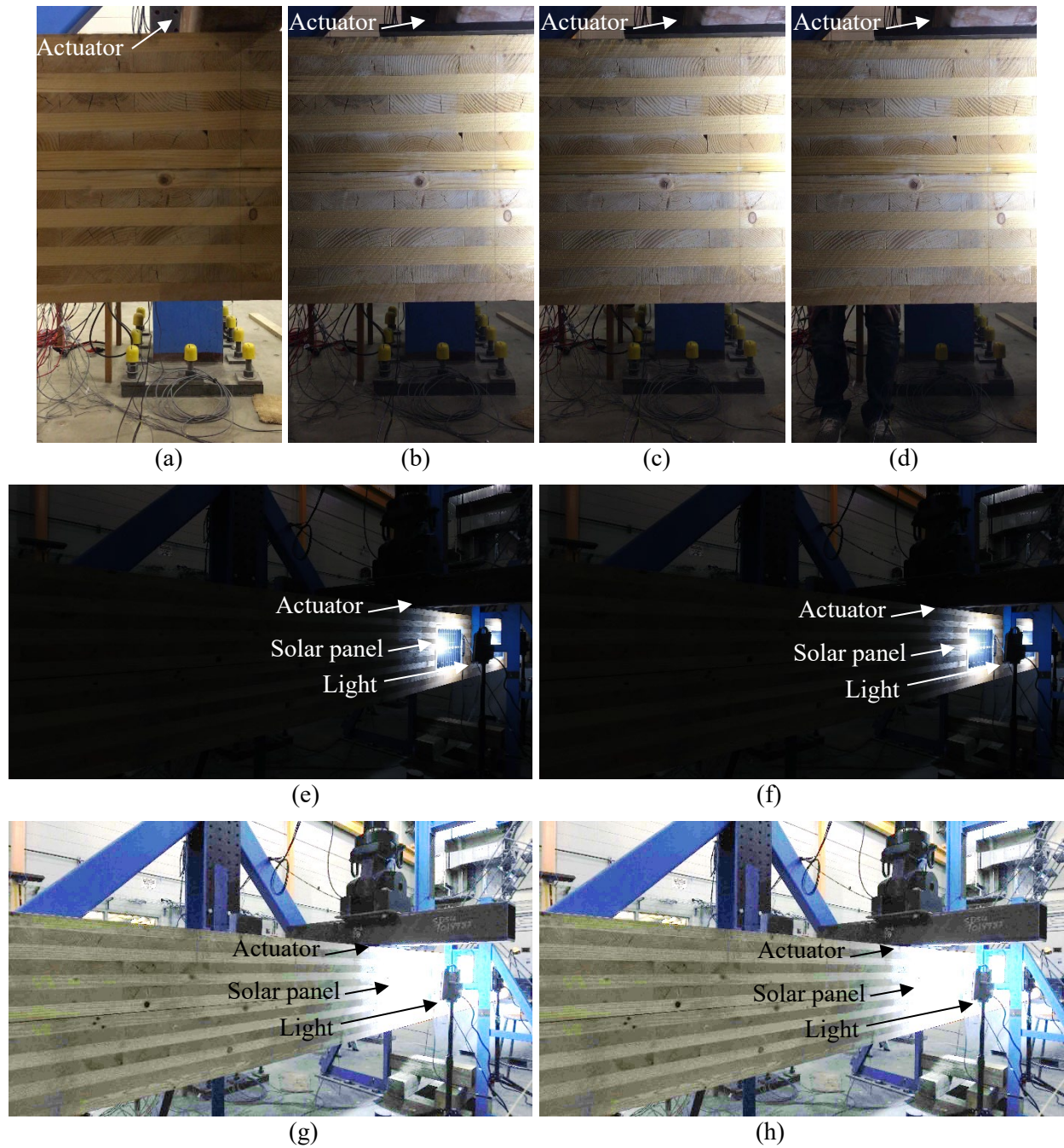


**Figure 2.53** Inspection images captured by the manipulator and UAV: (a) 0 mm (manipulator); (b) 13.97 mm (manipulator); (c) 22.10 mm (manipulator); (d) 37.34 mm (manipulator); (e) 0 mm (UAV); (f) 37.34 mm (UAV); (g) Figure 53e adjusted with brightness 85% and contrast -10%; and (h) Figure 53f adjusted with brightness 85% and contrast -10%.

Damage on the CLT girder was also identified from the inspection images obtained from the manipulator, as shown in Figures 2.54 and 2.55. For the damage identification, the CLT girder imaged by the manipulator was divided into eight sections from the south support. Figure 2.54 shows the inspection images of the girder side view before the testing, while Figure 2.55 displays corresponding images after the testing. During the testing, some damage was found to be propagated significantly in sections 4 and 5. Note that white lines in these figures indicate the existing damage on the CLT girder.

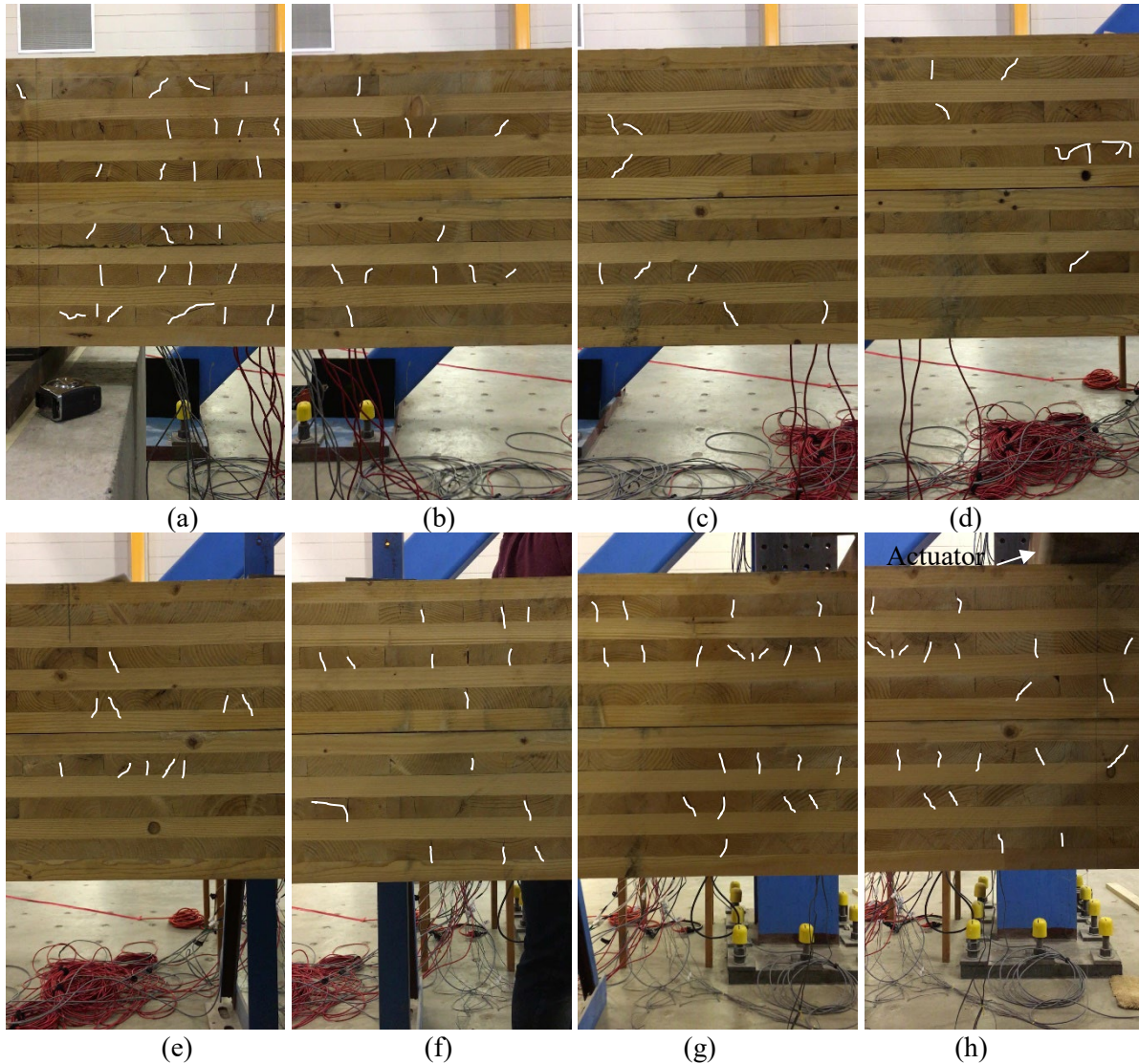


**Figure 2.54** Southeast sections of CLT girder before the testing was captured by manipulator: (a) section 1; (b) section 2; (c) section 3; (d) section 4; (e) section 5; (f) section 6; (g) section 7; and (h) section 8.

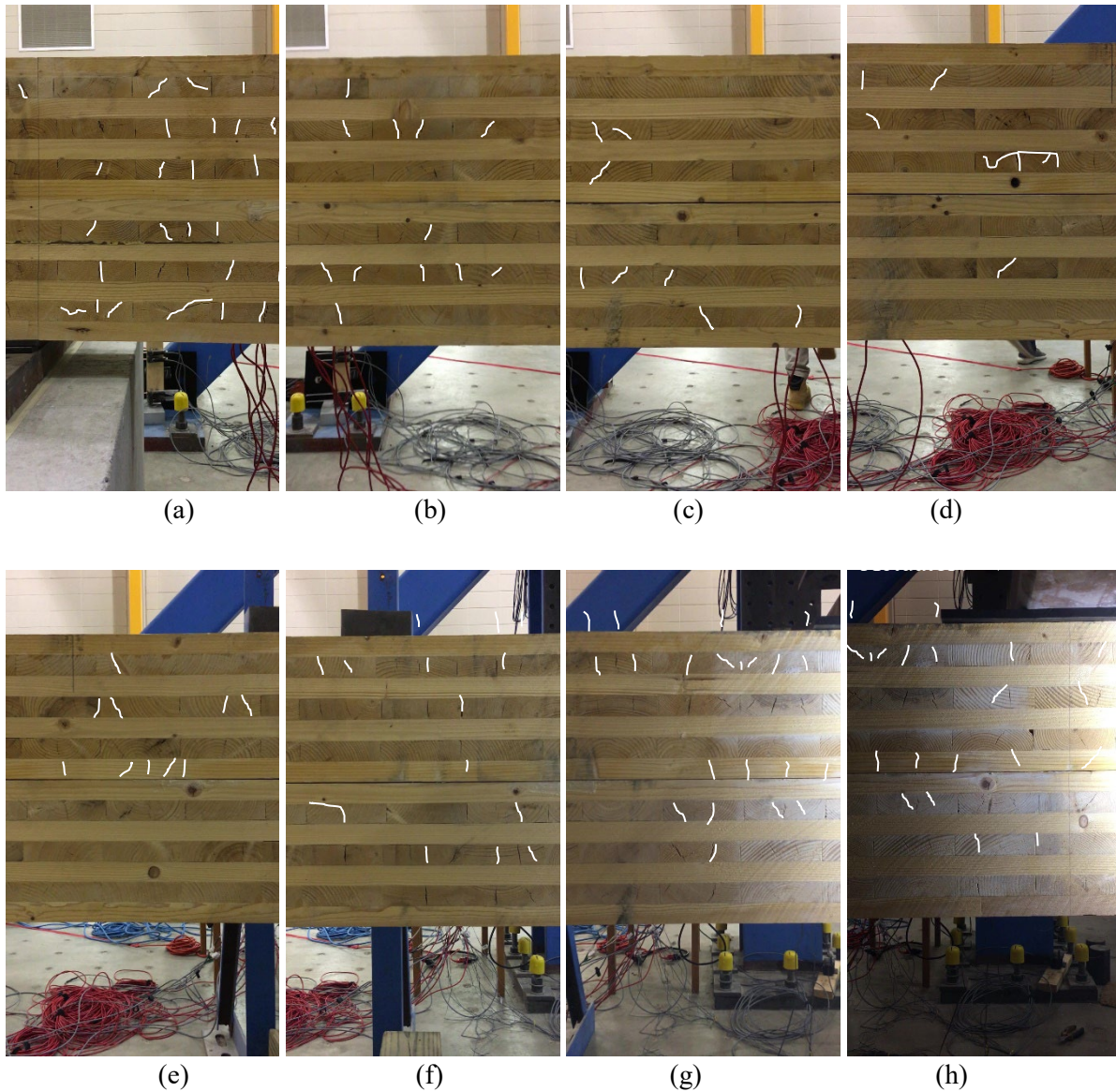


**Figure 2.55** Southeast sections of CLT girder after the testing was captured by manipulator:  
 (a) section 1; (b) section 2; (c) section 3; (d) section 4; (e) section 5; (f) section 6;  
 (g) section 7; and (h) section 8

The damage identified by the manipulator was also identified from the inspection images obtained from UAV. Figure 2.56 shows the detailed inspection images. Due to the low brightness of original UAV inspection images (Figures 2.56a, 2.56c, and 2.56e), the brightness and contrast of the original images were adjusted, as displayed in Figures 2.56b, 2.56d, and 2.56f. Figures 2.56a and 2.56c were adjusted with the brightness of 70% and contrast of -10%, as shown in Figures 2.56b and 2.56d, respectively, whereas Figure 2.56e was adjusted by increasing 60% brightness and 10% contrast, as depicted in Figure 2.56f. The damage was identified from the adjusted images of the CLT girder.

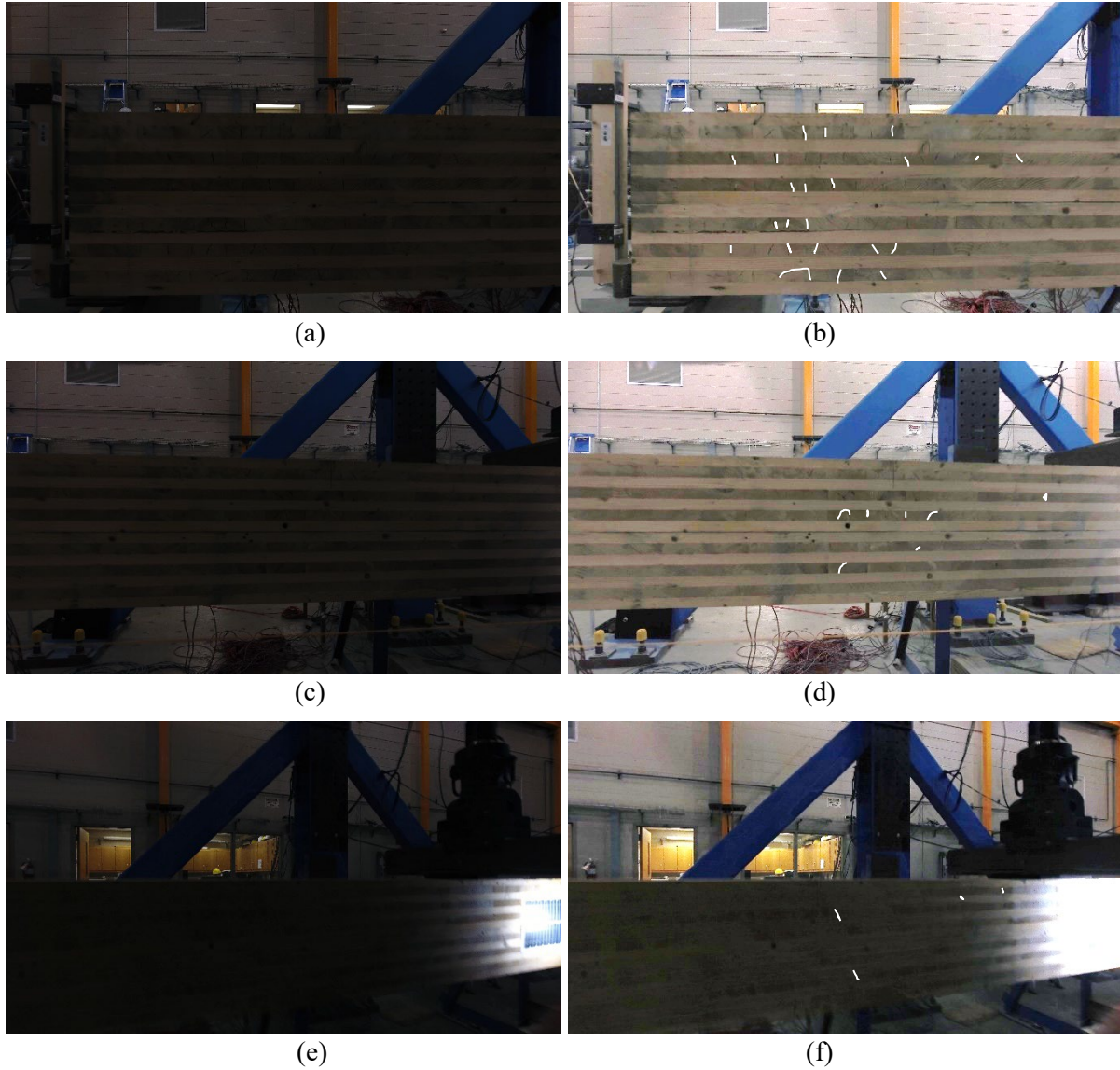
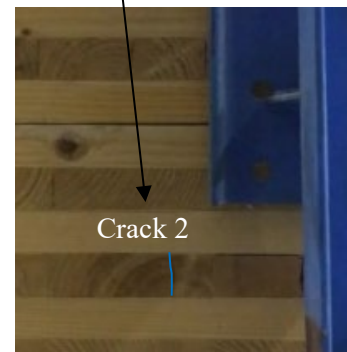
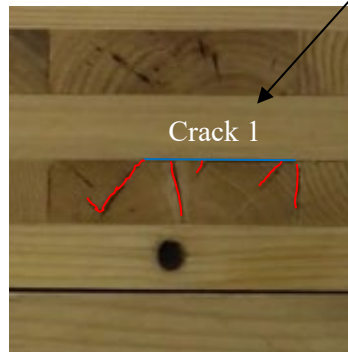
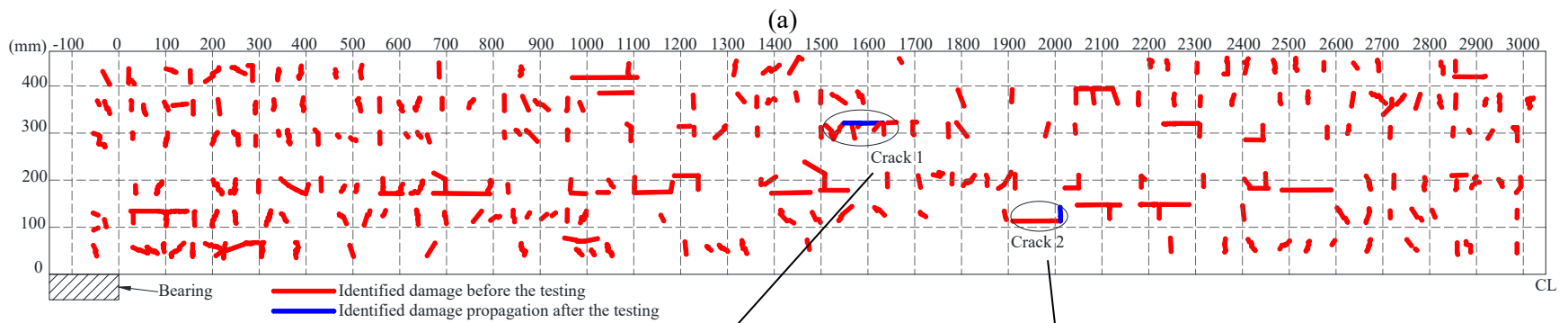
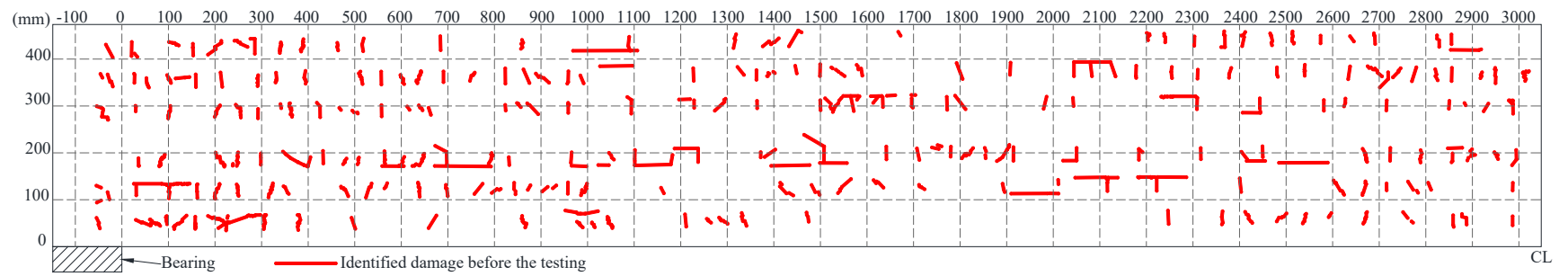


**Figure 2.56** Southeast sections of CLT girder before the testing was captured by UAV: (a) Sections 1 through 4; (b) Figure 2.56a adjusted with brightness 70% and contrast -10%; (c) Sections 2 through 6; (d) Figure 2.56c adjusted with brightness 70% and contrast -10%; (e) Sections 4 through 8; and (f) Figure 2.56e adjusted with brightness 60% and contrast 10%.

A comprehensive damage map was developed using the damage identified from the inspection images from the manipulator, as shown in Figure 2.57. It appears that locations and sizes of the identified damage can be observed in the image-based drawing. Figure 2.57a shows the existing damage on the girder before the testing, whereas Figure 2.57b displays the extended damage in the girder after the testing. In these figures, red lines indicate the existing damage, whereas blue lines indicate the propagated damage from the initial inspection. Damage propagations marked “crack 1” and “crack 2” were observed, as shown in Figure 2.57b.





(b)

**Figure 2.57** Damage map on the CLT girder with adhesive: (a) before the testing and (b) after the testing

Along with the identified propagated damage (i.e., cracks 1 and 2) on the southeast side of the girder, these cracks were quantified using the inspection images from the manipulator and UAV. The details of the propagated damage are tabulated in Table 2.3. For example, the propagated lengths of cracks 1 and 2 obtained from the manipulator are 60.23 mm and 34.93mm, and those from the UAV are 61.13 mm and 33.52 mm after the testing. As shown in Figure 2.57a, the existing crack 1 consisting of two horizontal, small cracks (12.37 mm and 43.85 mm measured by the manipulator and 12.32 mm and 43.81mm measured by the UAV), which have a total of length of 56.22 mm from the manipulator and 56.13 mm gained from the UAV, were not connected before the testing. As shown in Figure 2.57b, the two horizontal, small cracks were connected to the extended crack 1 after the testing; thus, the propagated length of crack 1,  $\Delta l$ , ends up becoming 4.01 mm from the manipulator and 5.00 mm from the UAV. Similarly, the propagated length of crack 2,  $\Delta l$ , is 8.06 mm and 7.61 mm resulting from the manipulator and UAV, respectively.

**Table 2.3** Details of identified propagated damage of CLT girder with adhesive

Damage	Initial length (mm)	Propagated length (mm)	$\Delta l$ (mm)	Initial thickness (mm)	Propagated thickness (mm)	$\Delta t$ (mm)
Crack 1 (manipulator)	12.37 and 43.85	60.23	4.01	1.03	1.10	0.07
Crack 2 (manipulator)	26.87	34.93	8.06	0.79	0.85	0.06
Crack 1 (UAV)	12.32 and 43.81	61.13	5.00	1.45	1.51	0.06
Crack 2 (UAV)	25.91	33.52	7.61	0.92	1.00	0.08

During the testing, the DIC system was also applied to collect images on the east side of the CLT girder at a distance of  $d$  from the north support. The DIC system was programmed to record two images per second, irrespective of the displacement of the actuator. The collected images were used to calculate the deformation and strain at  $d$  from the north support based on a DIC algorithm. The DIC algorithm was designed to measure the movement of the target section based on the changes in the surface. For instance, a distance between  $P_1$  and  $P_2$  in a reference pattern of the section (Figure 2.58a) was initially measured with a separate distance of  $u$  and  $v$ . Note that the distances  $u$  and  $v$  indicate the relative distance in the horizontal and vertical directions, respectively. After any deformation on the surface of the section, the distance between  $P_1'$  and  $P_2'$  in a deformed pattern (Figure 2.58b) was measured using the deformed distances  $u'$  and  $v'$ . The relative deformation (or strain) between the two points was measured by calculating the difference between the initial and deformed distances.

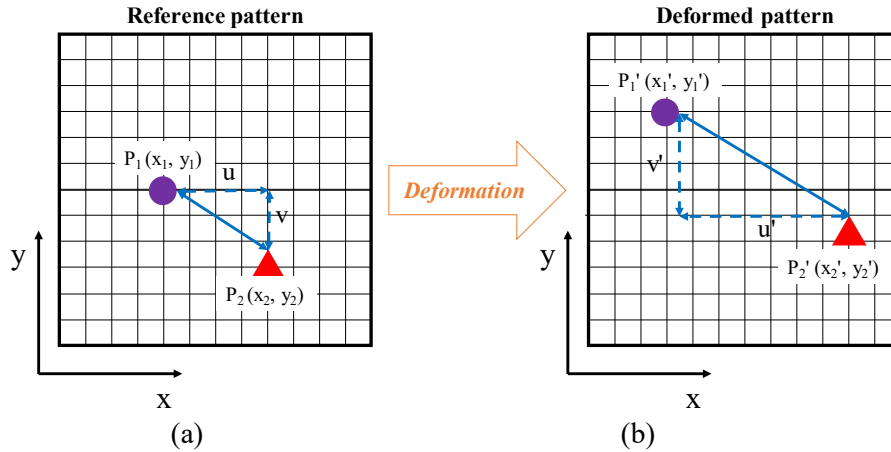


**Figure 2.58** DIC algorithm: (a) reference pattern and (b) deformed pattern

Through the integrated DIC system and algorithm, the strain corresponding to the images was determined and plotted in Figure 2.59. It appears that the change in the strain direction is observed at the 1,184<sup>th</sup>, 4,208<sup>th</sup>, and 8,663<sup>rd</sup> images. The slippage failure was found at the 4208<sup>th</sup> image, which means that it alters the strain direction in the section. Note that the DIC strain profile was not able to be plotted against the actuator load; thus, the profile could not be compared with the strain profile obtained from the contact sensors, strain gages (SG-9 and SG-10).

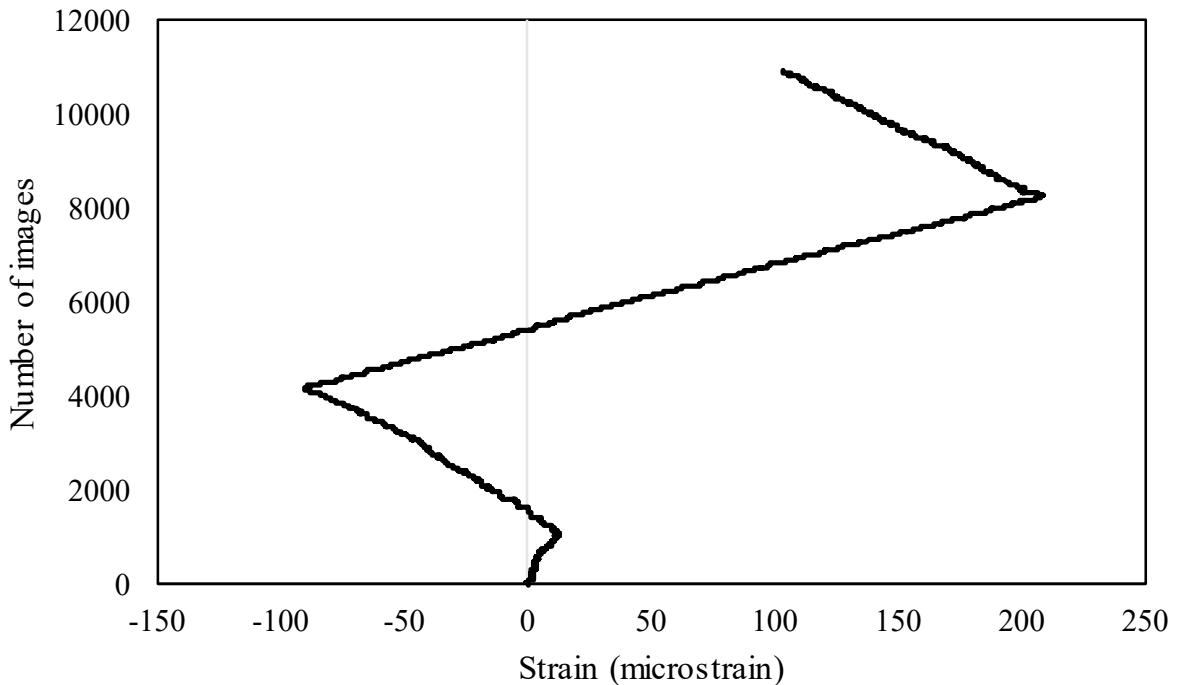


**Figure 2.59** Strain profile calculated from DIC system applied to the CLT girder with adhesive

### Data from Solar Panels

As mentioned before, the two solar panels, including solar panels 1 and 2, were installed on the east side of the CLT girder to evaluate the efficiency of energy harvesting during the ultimate load test. Voltages from the solar panels were recorded manually for every test run. Note that there were 185 test runs. Figure 2.60 shows a relationship between voltages from each solar panel and the mid-span displacements measured from the actuator. In this figure, the voltages in both the solar panels are observed to be decreased with an increase in the mid-span displacement of the girder. This trend was attributed to the fact that both solar panels were shifted downward from the light source as the tested girder was deflected with the increased load. The amount of voltage generated between solar panels 1 and 2 are found to be slightly different. Specifically, the voltage of solar panel 1 appears to have decreased significantly at 49.53 mm after the slippage failure, whereas the voltage of solar panel 2 is found to have increased abruptly at 49.53 mm deflection due to its upward movement after the slippage failure. Note that both solar panels were not damaged during the test. Based upon the voltage-displacement relationship, it can be concluded that the efficiency of energy harvesting was dependent on the location of solar panels from the applied load under the same conditions as the light source.

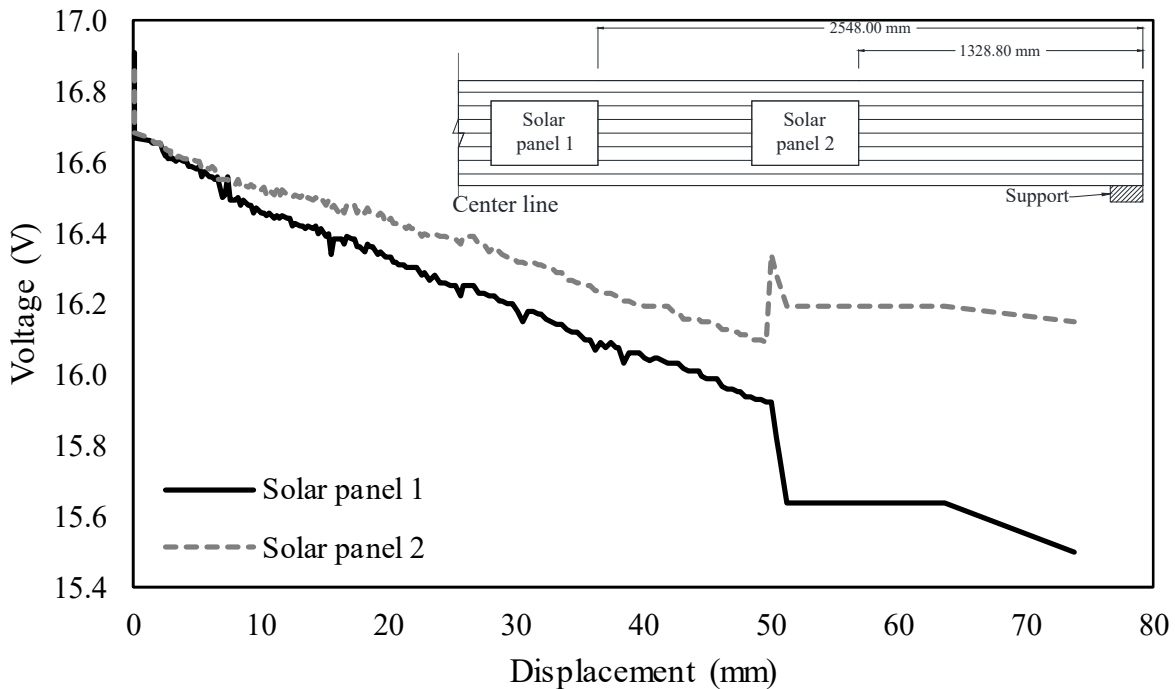


**Figure 2.60** Relationship between voltage and displacement of CLT girder with adhesive

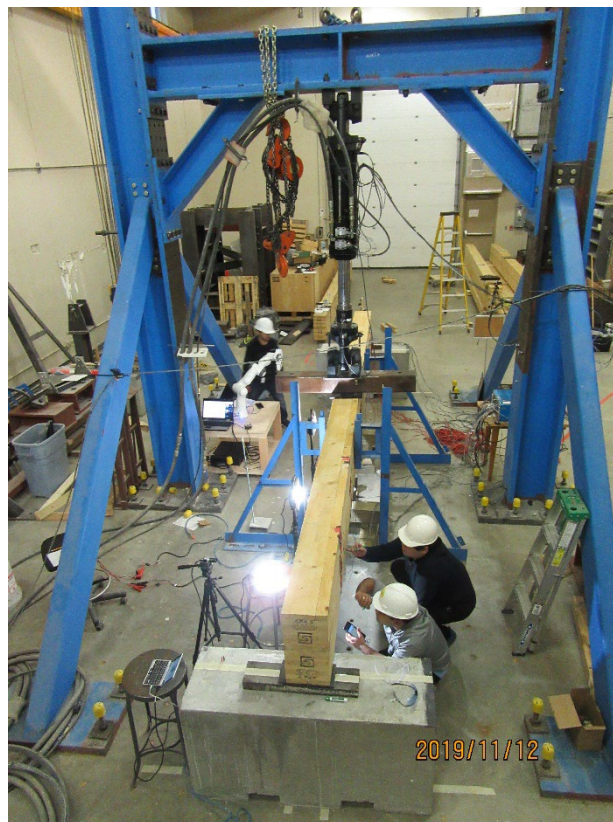
## 2.4.2 Performance on CLT Girder with Adhesive and Fasteners

This section deals with instrumentation for ultimate strength testing, testing procedure, and results and discussion for the CLT girder bonded with adhesive and fasteners.

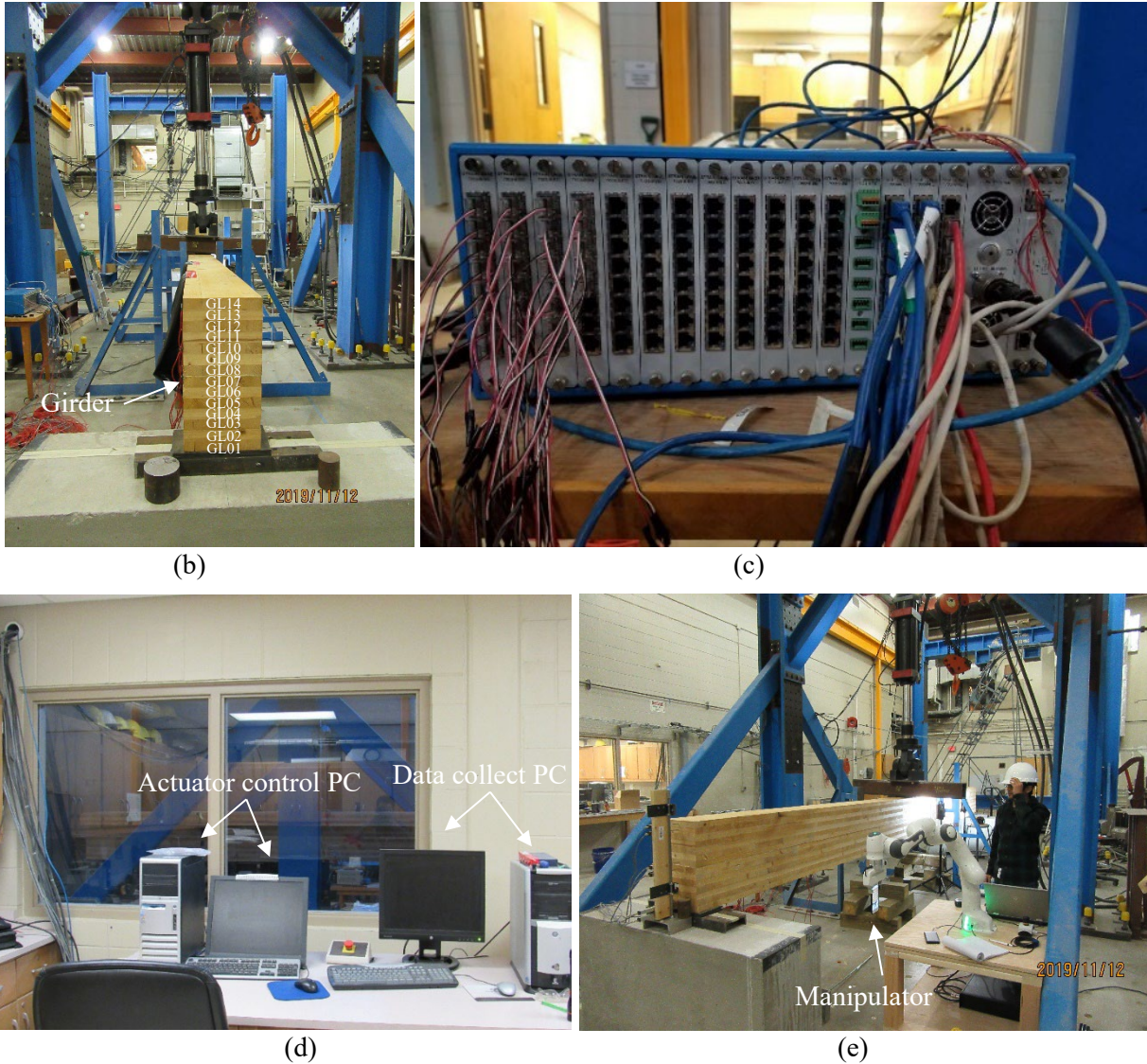
### 2.4.2.1 Instrumentation

The full-sized laboratory testing of the bonded CLT girder comprising 14 lams with adhesive and fasteners is shown in Figure 2.61a. The CLT girder with fasteners has dimensions of 6.40 m length, 0.48 m depth, and 0.24 m width, and the applied fasteners have dimensions of 12.7 mm diameter and 381 mm length. As described in the previous section for the adhesive CLT girder testing, the 14 lams in the girder were also designated as GL01 through GL14 from the bottom lam, as shown in Figure 2.61b. To take measurements of deflection, strain, and slippage, as well as pictures, both contact and non-contact sensors used in the adhesively bonded CLT girder testing were installed on the tested CLT girder with adhesive and fasteners.

The 7000-128-SM data acquisition system (Figure 2.61c) was used to collect the data from the contact sensors during the ultimate strength test of the CLT girder. The actuator and data logger system linked to the contact sensors were controlled through the computers in the control room, as shown in Figure 2.61d. Images from the non-contact sensors, such as the manipulator camera, (Figure 2.61e) were captured from the cameras installed on each robot during the test.

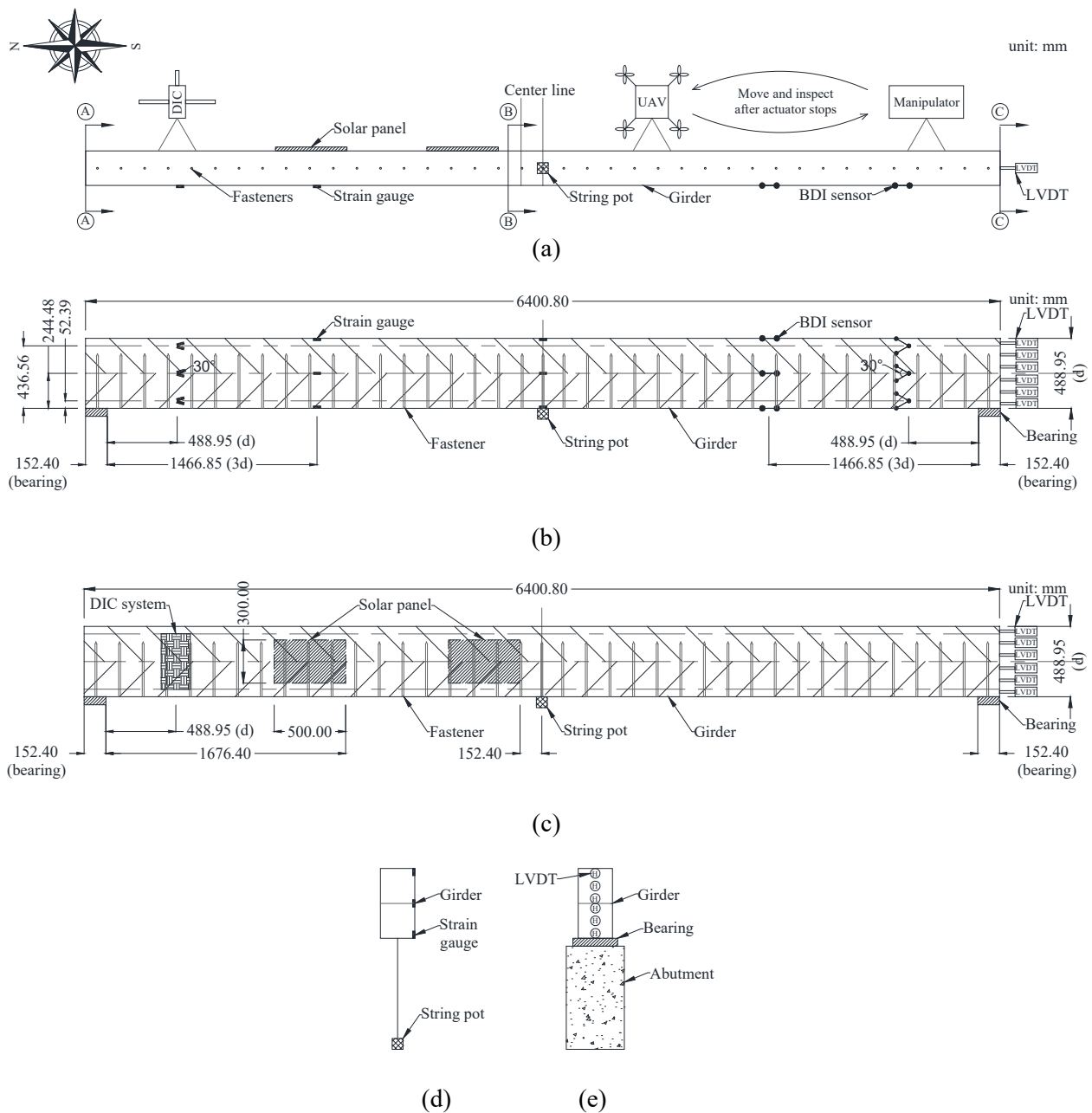


(a)



**Figure 2.61** CLT girder test with adhesive and fastener bond: (a) test setup; (b) girder lam number designation; (c) data acquisition system; (d) control room; and (e) manipulator

The overall instrumentation is shown in Figure 2.62. Figure 2.62a shows the plan view of the fastener CLT testing setup. Figure 2.62b presents the location of the strain gauges and BDI strain sensors installed on the west side of the CLT girder. The DIC system and solar panels mounted on the east side of the CLT girder are shown in Figure 2.62c. In this figure, the CLT girder was inspected with UAV and manipulator on the southeast side. Figure 2.62d shows the string pot installed underneath the CLT girder and strain gages attached to the CLT girder, and the schematic of LVDTs is provided in Figure 2.62e.



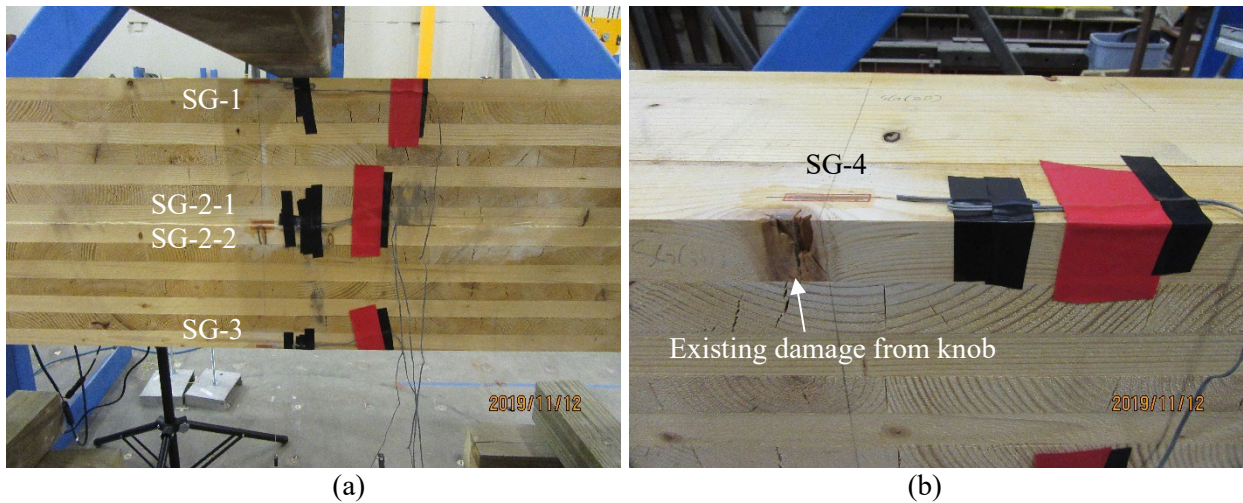
**Figure 2.62** Instrumentation plan for girder testing: (a) plan view; (b) elevation view (west side); (c) elevation view (east side); (d) string pot and strain gauges at mid-span; and (e) LVDTs at the south edge.

Figure 2.63 shows the location of the strain and BDI sensors along with string pot in the CLT fastener girder on the west side. The 13 strain gauges (e.g., SG-1) and nine BDI (e.g., BDI-1) strain sensors were attached to the west side of the CLT girder (Figure 2.63b). The strain gauges SG-1, SG-2-1, SG-2-2, and SG-3 were installed at the mid-span (Figure 2.63a), SG-4 through SG-6 were installed at  $3d$  from the north support (Figures 2.63b and 2.63c), and SG-7 through SG-12 were installed at  $d$  from the north support (Figure 2.63d). Again,  $d$  indicates the design depth of the CLT girder. Note, there was a knot on

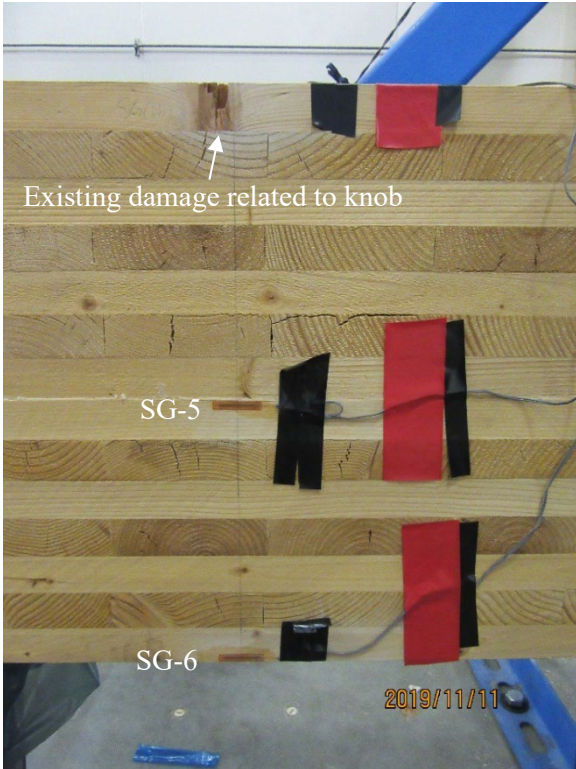
the bottom of the girder centerline, but not a knot on the top of it; thus, both SG-2-1 and SG-2-2 were mounted on both the bottom and top of the CLT girder. Also, SG-4 was installed on the girder's top surface in lieu of (or "in the event of") its top side having existing damage to avoid the possibility of noisy data caused by the damage, as shown in Figure 2.63b.

Similarly, the BDI strain sensors BDI-1 through BDI-6 were mounted at  $d$  from the south support (Figure 2.63e), and BDI-7 through BDI-9 were installed at  $3d$  from the south support (Figure 2.63f). As mentioned before, the strain gauges and BDI sensors were installed at  $d$  and  $3d$  from the support to analyze the shear strain in the CLT girder where the maximum shear is expected (AASHTO, 2012). To reiterate, two strain gauges were mounted at a  $30^\circ$  angle between gauges at  $d$  to take records of shear strain, as shown in Figures 2.63d and 2.63e, respectively. According to the strain gauge installation manual (micro-measurement, 2010), shear strain can be calculated from Equation 44.

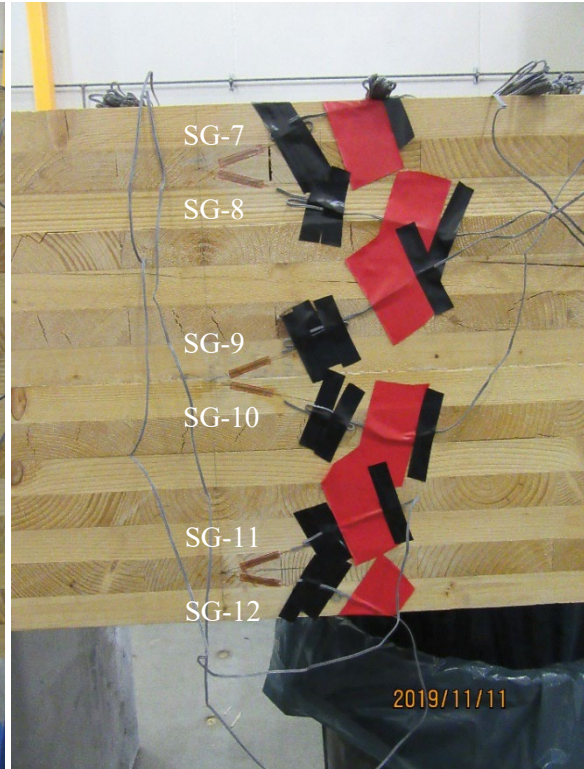
Six LVDTs were attached on the south face of the CLT girder, as displayed in Figure 2.63g. Strictly speaking, two LVDTs installed on the upper side (GL13 and GL14) and two LVDTs installed on the lower side (GL01 and GL02) recorded local slip between lams, while two LVDTs located in the middle of girder (GL07 and GL08) recorded slip between two 7-ply CLT beams to evaluate its bonding performance. As shown in Figure 63h, the string pot was mounted in the center at the bottom of the CLT girder to measure deflection data.



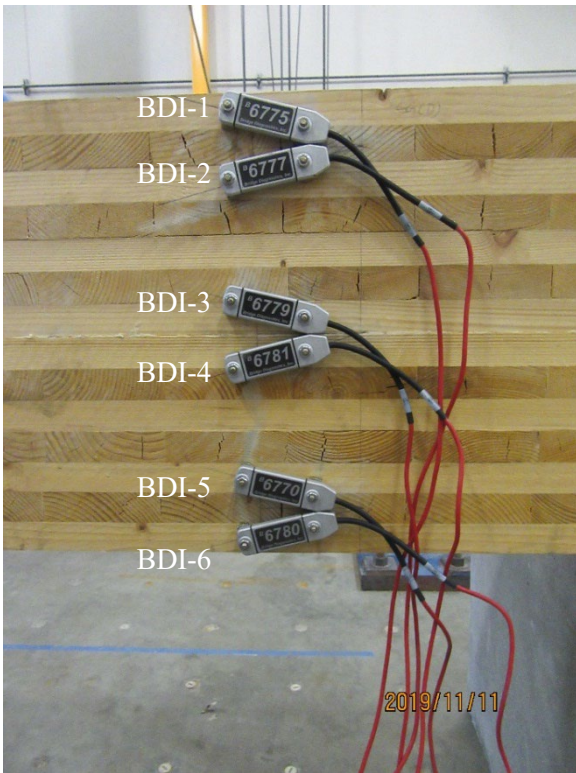




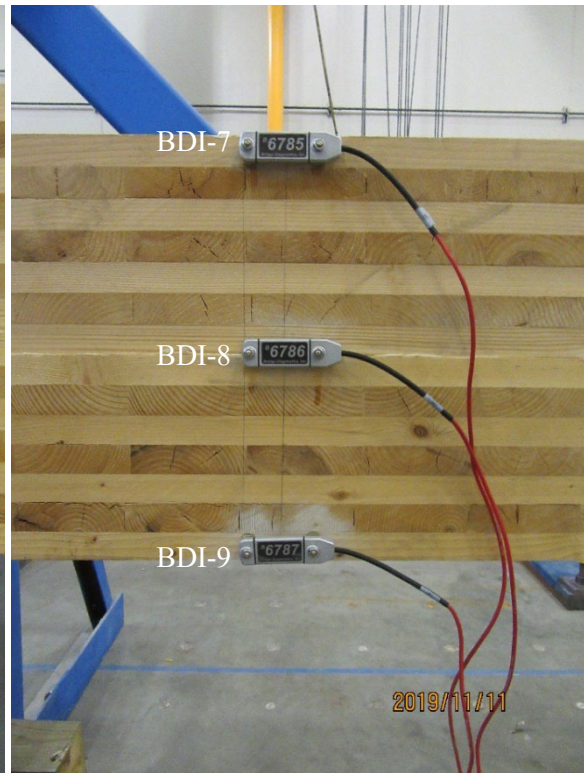
(c)



(d)



(e)



(f)

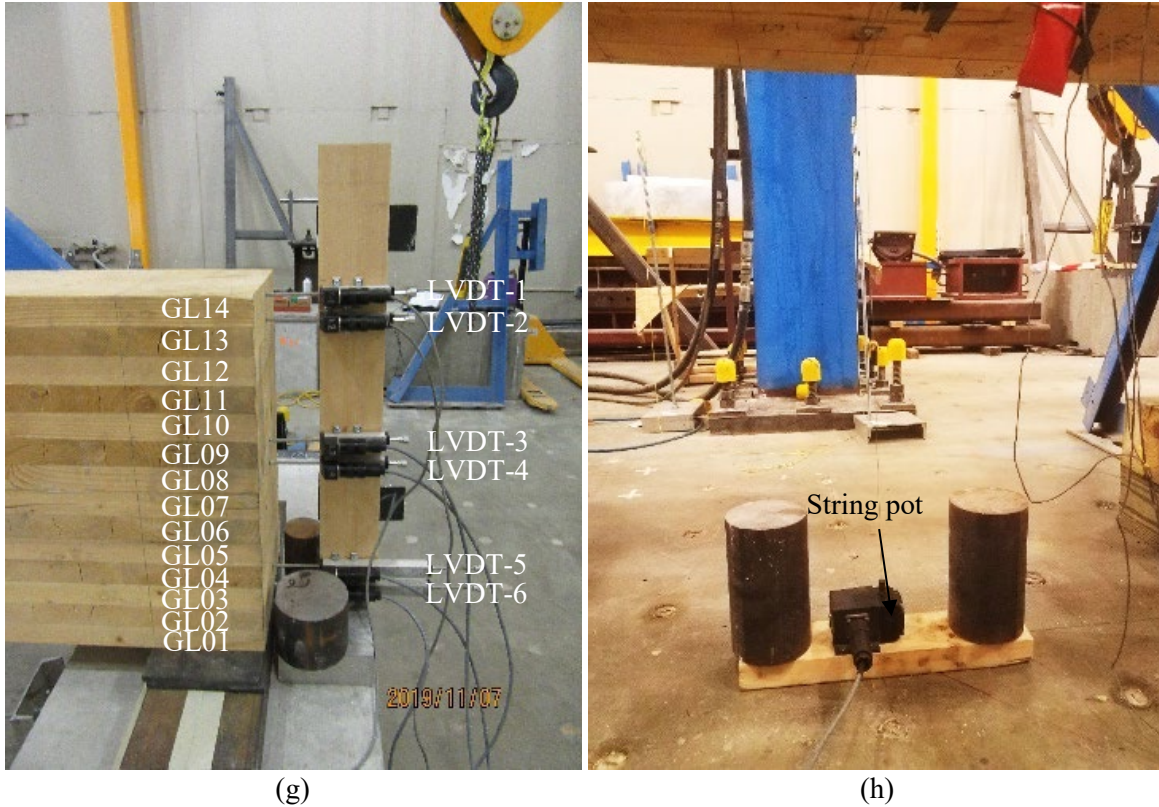


**Figure 2.63** Contact sensor installation: (a) strain gauges at mid-span; (b) SG-4 at distance  $3d$  from north support; (c) strain gauges at distance  $3d$  from north support; (d) strain gauges at distance  $d$  from north support; (e) BDI strain sensors at distance  $d$  from south support; (f) BDI strain sensors at distance  $3d$  from south support; (g) LVDTs at south edge; and (h) string pot

As shown in Figure 2.64, the non-contact sensors (i.e., the UAV Phantom 4, the manipulator, and the DIC camera) were set up on the east side of the fastener CLT girder. The installation of the DIC system and the UAV and manipulator are shown in Figures 2.64a and 2.64b, correspondingly. The UAV and manipulator equipped with the mini digital cameras collected a number of images on the southeast surface of the girder for each inspection phase, while the DIC system was installed on the northeast side of the girder at  $d$  from the north support. Again, the images from UAV and manipulator were used to identify damage and estimate deflections at the mid-span of the girder in another way. The DIC system was employed to capture images for the strain estimate. The DIC-aided strain values were compared with those from the contact sensors.

Two solar panels (Nuzamas portable 20W, Appendix K) were mounted on the east side of the CLT girder to explore the relationship between solar energy harvesting and CLT girder behavior, as seen in Figure 2.62c. In Figure 2.64c, one solar panel marked “solar panel 1” was located 2.55 m from the north support of the girder to collect solar energy at the most critical damage location, while the other solar panel marked “solar panel 2” was attached 1.33 m away from the north support of the girder. To collect an amount of solar energy harvested during the test, a light was installed at a 0.15 m distance from each solar panel, where each was capable of harvesting the maximum voltage of 16.64 V.

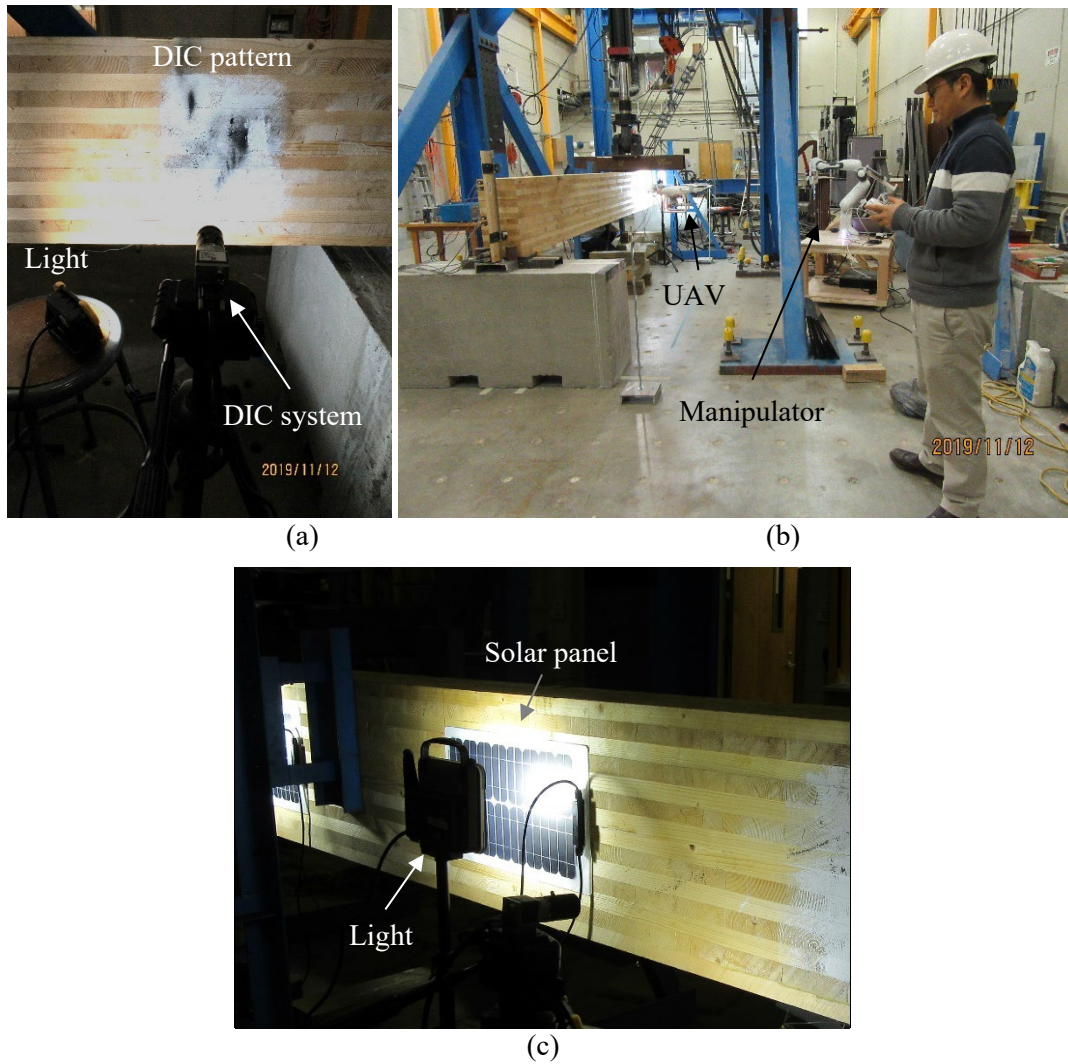


**Figure 2.64** Non-contact sensors: (a) DIC system; (b) UAV and manipulator; and (c) solar panel

### 2.4.2.2 Testing Procedure

A flowchart showing the test procedure of the CLT girder with fasteners is shown in Figure 2.65. The test was performed in three major steps: 1) loading, 2) measurement, and 3) inspection. The first step was to load the girder until failure. The actuator with a capacity of 500 kN applied a monotonic load on the top of the CLT girder at mid-span with displacement control.

The second step was to record data from all the contact sensors (e.g., strain gauges and LVDTs) during loading, whereas the non-contact sensors (e.g., DIC system and UAV camera) were used to capture images at each inspection phase. As mentioned in the testing of the adhesively bonded CLT girder, the DIC system was also utilized to determine strain quantities through images from the testing, and voltage data from each solar panel were simultaneously recorded manually from a multimeter at each loading step. All of the contact sensors were connected to the data acquisition system. The acquisition system was able to record 10 sets of data per second for each channel. All loads, deflections, and strain responses were recorded for each test run, and voltage and current data from each solar panel were also collected by hand for each test run.

The fastener CLT girder was inspected at regular intervals of the test run and when a cracking sound was heard. Manual inspections and robotic-aided inspections using the UAV and manipulator were performed on all sides of the girder. The CLT girder was tested with a total of 170 test runs and nine inspections, including initial inspection performed prior to the testing.

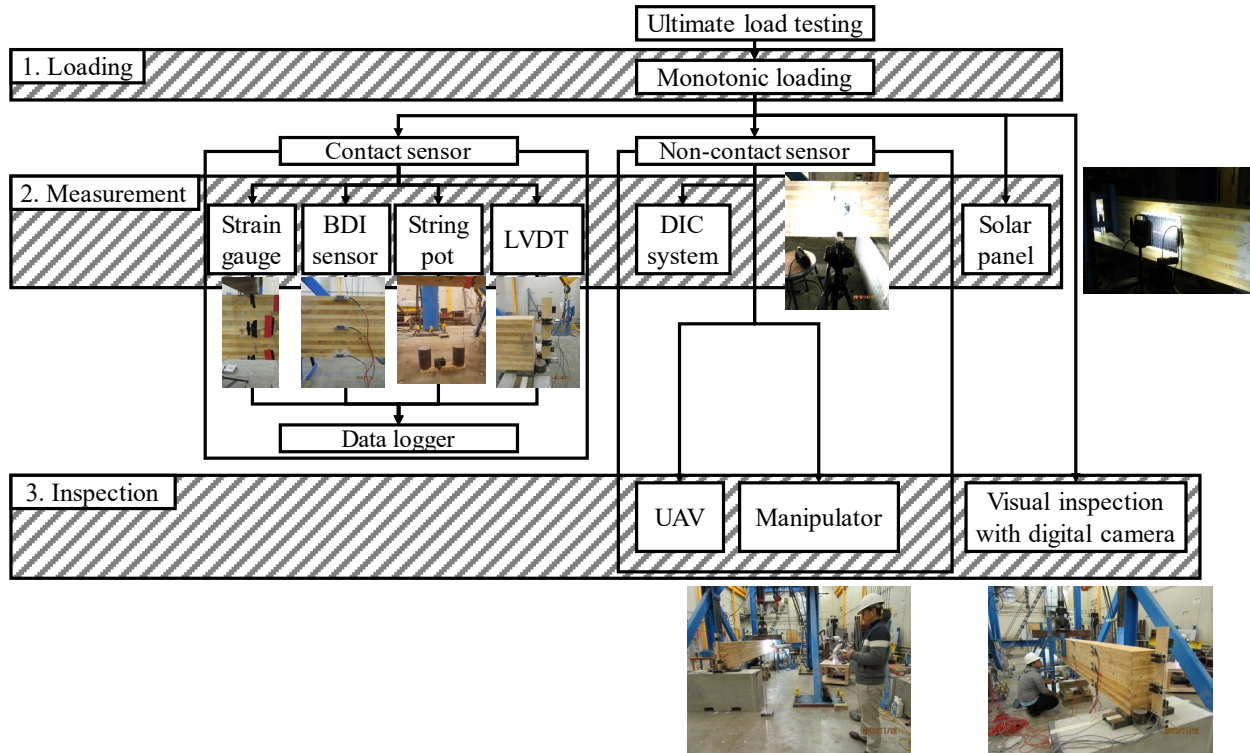


**Figure 2.65** Testing and data collection procedure of CLT girder with adhesive and fasteners

### 2.4.2.3 Results and Discussion

This section describes data obtained from the ultimate strength testing for the CLT girder bonded with adhesive and fasteners. All the data, including strain, slippage, deflection, and voltage, along with imagery, obtained from the contact and non-contact sensors have been analyzed to evaluate performance of the fastener CLT girder.

### Data from Contact Sensors

A load-displacement curve is presented in Figure 2.66, where significant flexural cracking at 45.34 mm resulting from 74.77 kN and complete flexural failure at 58.45 mm corresponding to 79.89 kN, are observed at the bottom of the CLT girder in the mid-span.

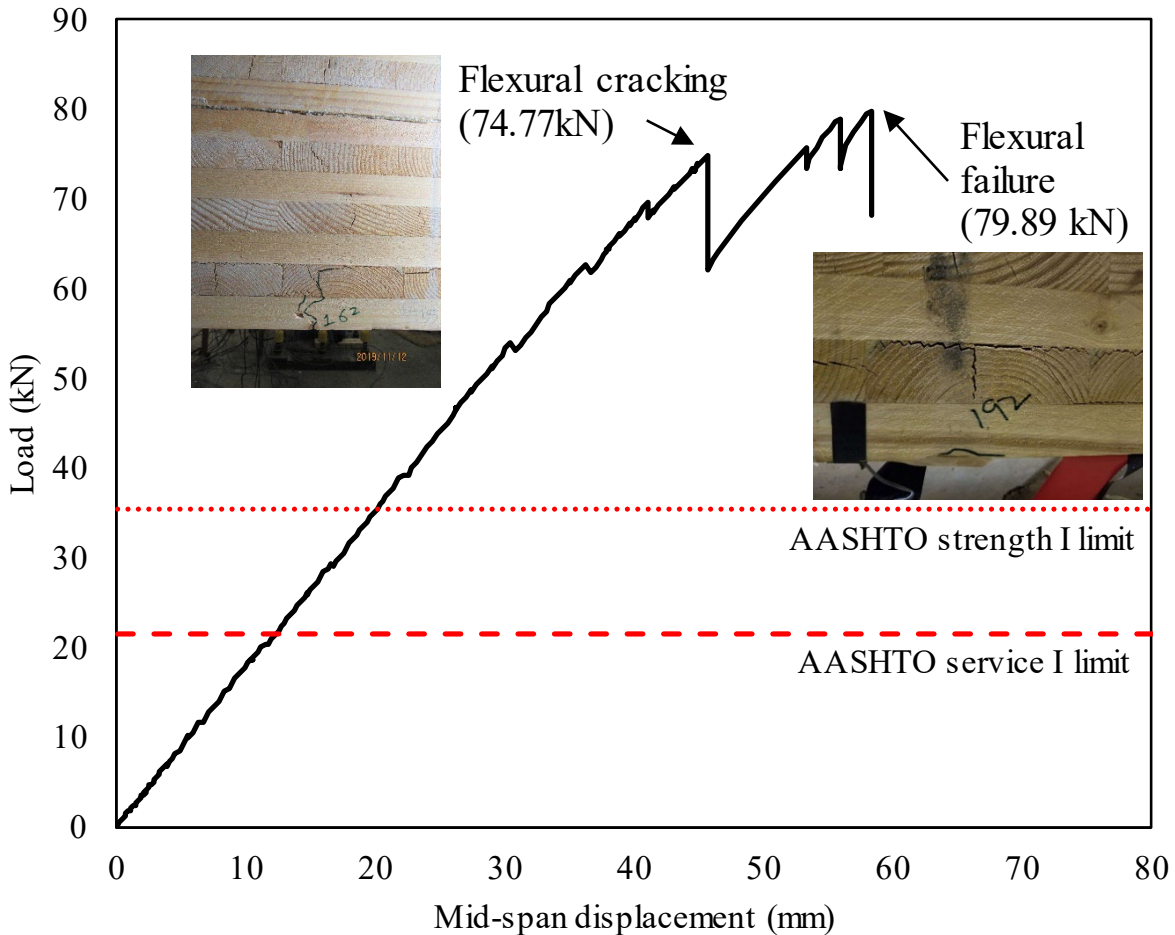


**Figure 2.66** Load-displacement curve of CLT girder with adhesive and fasteners

As illustrated in Figure 2.67a, flexural cracking was observed at the bottom of the CLT girder at mid-span. As seen in Figure 2.67b, the actuator was tilted due to the damage in compression on the top of the girder at mid-span. The damage can be seen in Figure 2.67c. The actuator was adjusted in place, and testing was continued until the girder failure. The significant flexural cracking was propagated from the bottom lam to the bottom surface at mid-span, as shown in Figure 2.67d. Along with analysis of the results, the ultimate strength of the CLT girder bonded with adhesive and fasteners was found to be 79.89 kN at the flexural failure. The strength of the tested CLT girder is 55.81% higher than the AASHTO strength I limit strength and 73.09% higher than the AASHTO service I limit strength, respectively. The AASHTO strength values are also incorporated into Figure 2.66. Note, the AASHTO strength I limit strength and service I limit strength were calculated using Equations 47 and 48 (see the detailed calculation of strength in Appendix L).

$$\text{AASHTO Strength I limit} = 1.25 DC + 1.75 LL \quad (47)$$

$$\text{AASHTO Service I limit} = 1.0 DC + 1.0 LL + 0.3 WS \quad (48)$$

where DC = component self-weight  
 LL = vehicle live load  
 WS = wind load on structure



**Figure 2.67** Representative damage images: (a) flexural cracking on the east side of the girder at mid-span; (b) tilting of actuator; (c) damage due to tilting of actuator; (d) flexural failure on the west side of the girder at mid-span

As shown in Figure 2.68, three sets of LVDTs were installed at the top of the girder (GL13 and GL14), in the middle of the girder (GL08 and GL07), and at the lowest two lams (GL02 and GL01). This figure also includes the slippage sign convention for the tested girder with adhesive and fasteners.

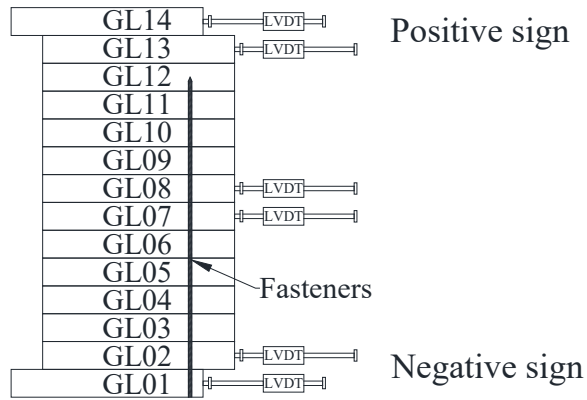


**Figure 2.68** Slippage sign convention

Figure 2.69 illustrates the slippage between the considered lams, where all the LVDT sets show positive values of slippage, excluding the initial negative slippage at the top of the girder during the test. As previously demonstrated, as the load increases, the slippages increase at the top, middle, and bottom of the girder. Note, the LVDTs were removed prior to the significant flexure cracking to prevent the LVDTs slippage. The maximum slippage values at the top, middle, and bottom of the girder were 0.84 mm, 0.43 mm, and 0.41 mm, respectively. The largest maximum slippage at the top of the girder occurred due to the lower bonding strength between the unscrewed two top lams (GL13 and GL14) compared with the screwed lams.

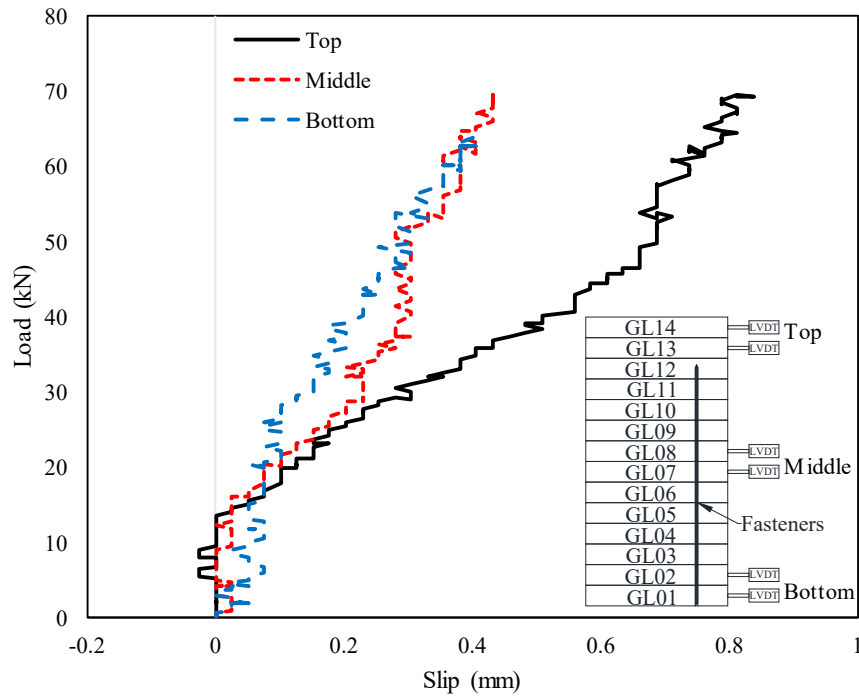
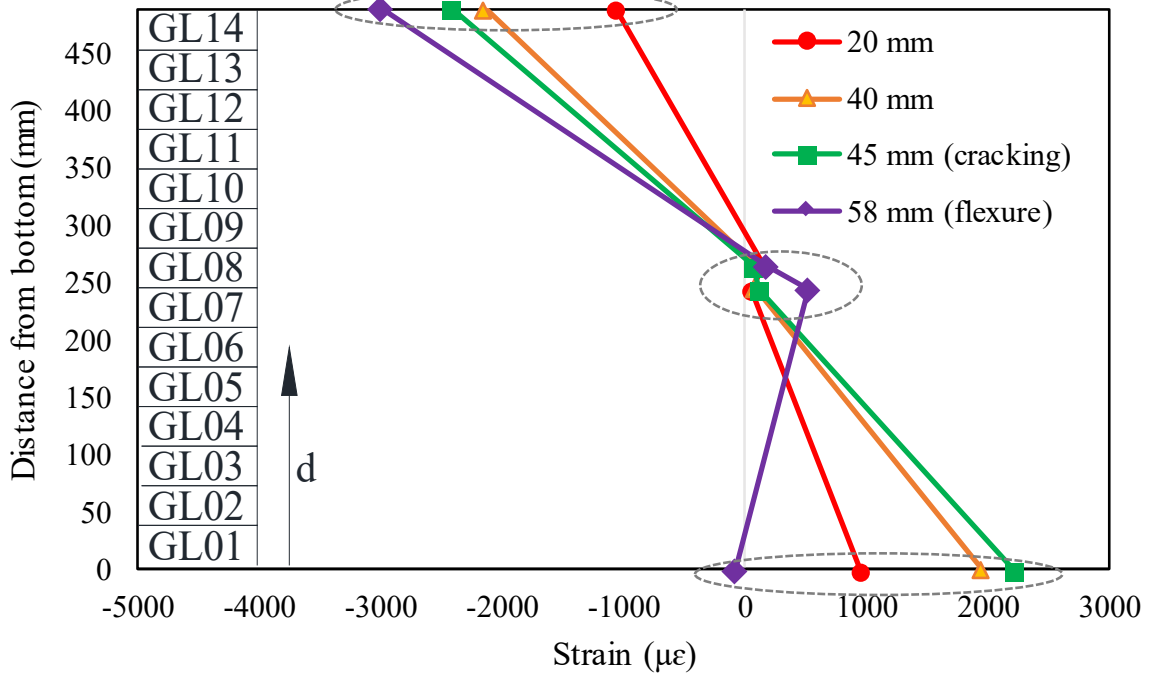


**Figure 2.69** Slip between lams obtained by LVDTs

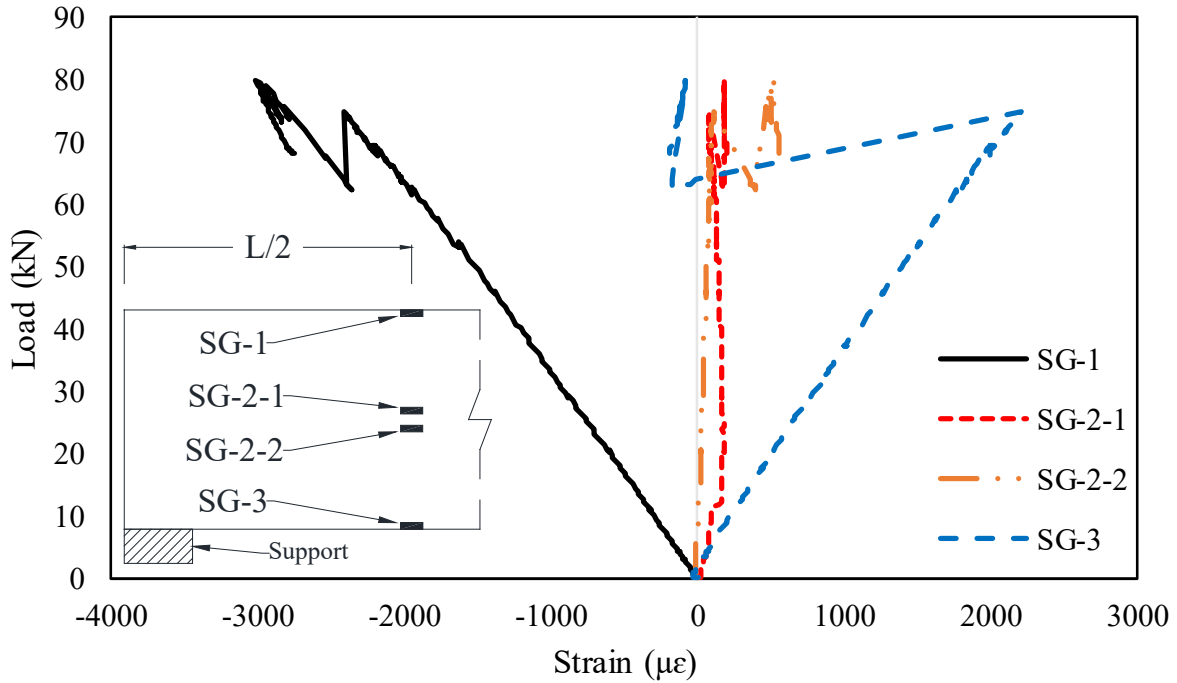
Figure 2.70a shows the strain profile along the depth from the bottom of the girder to evaluate the neutral axis of the girder at mid-span. Three strain gauges collected strain data on the west side at mid-span of the girder. As stated before, the gauges were installed at the top of the girder (SG-1), in the middle of the girder (SG-2-1 and SG-2-2), and at the bottom of the girder (SG-3). Before the flexural failure, the strain values at 20 mm, 40 mm, and 45 mm deflections indicated that the neutral axes were located at 293.29

mm, 273.79 mm, and 270.88 mm from the bottom of the girder, respectively. It was demonstrated that the neutral axes were near the center of the girder depth before the flexural failure; however, the neutral axis shifted down to the bottom of the girder at 58 mm deflection after the flexural failure. In Figure 2.70b, all strain gauges show significant change in the strain at 74.77kN due to the flexural cracking and at 79.89 kN due to the flexural failure. The strain values observed in SG-3 were changed meaningfully from positive to negative due to the flexural cracking and failure.



(a)

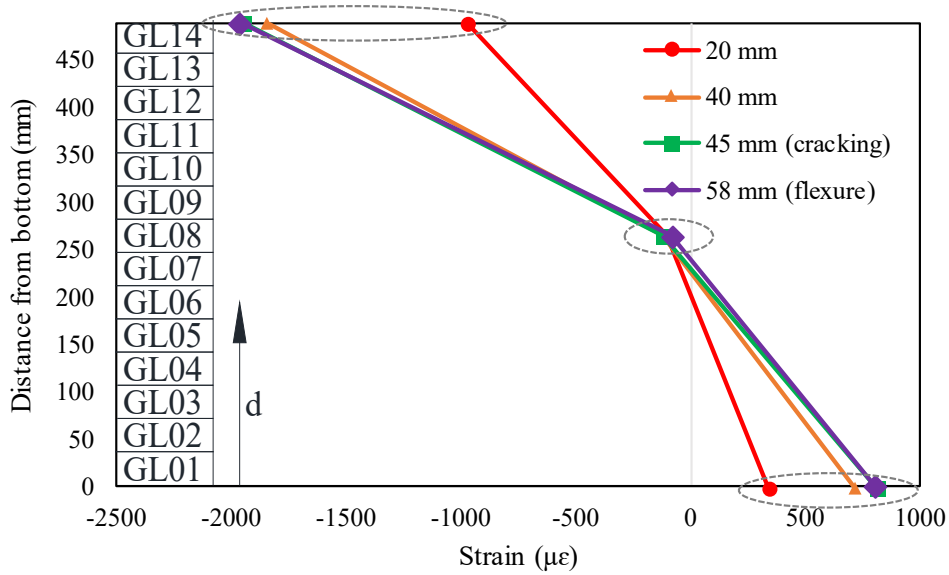




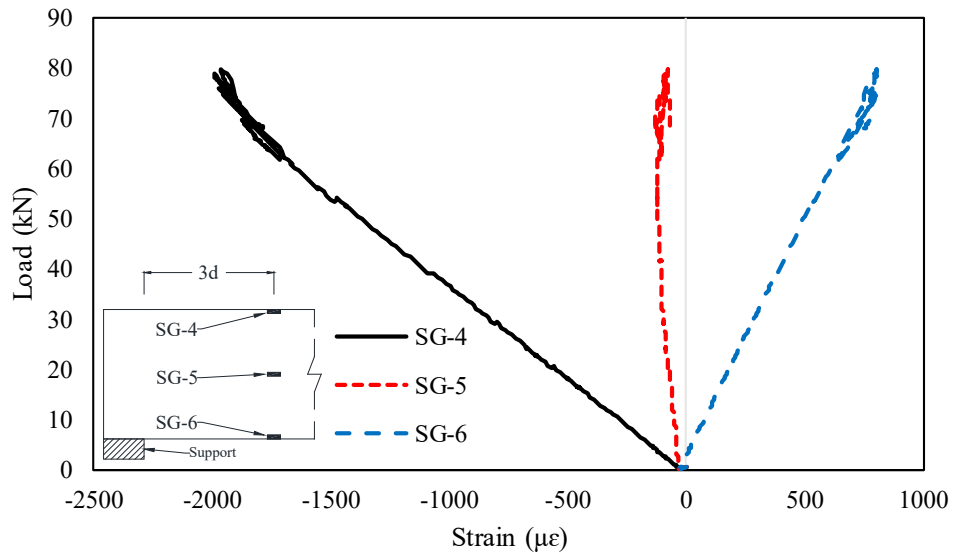
(b)

**Figure 2.70** Strain gauges installed on mid-span of girder: (a) strain profile and (b) load-strain curves

Figure 2.71a shows the strain values based on the distance from the bottom of the girder to determine the neutral axis of the girder at  $3d$  from the north support. As stated earlier, the strain gauges were installed at the top of the girder (SG-4), in the middle of the girder (SG-5), and at the bottom of the girder (SG-6). The average neutral axis at the deflections of 20 mm through 58 mm was located at 224.20 mm from the bottom of the girder, where all the neutral axes were located near the center of the girder depth, which indicated it did not move significantly during the testing. It was demonstrated that the flexural failure has insignificantly affected the neutral axis of the girder at  $3d$  from the north support. In Figure 2.71b, negative strain in compression can be seen at the location of SG-4 and SG-5, whereas positive strain in tension was found at the location of SG-6. A significant change in the strain was observed in all strain gauge locations due to flexural cracking and failure.



(a)

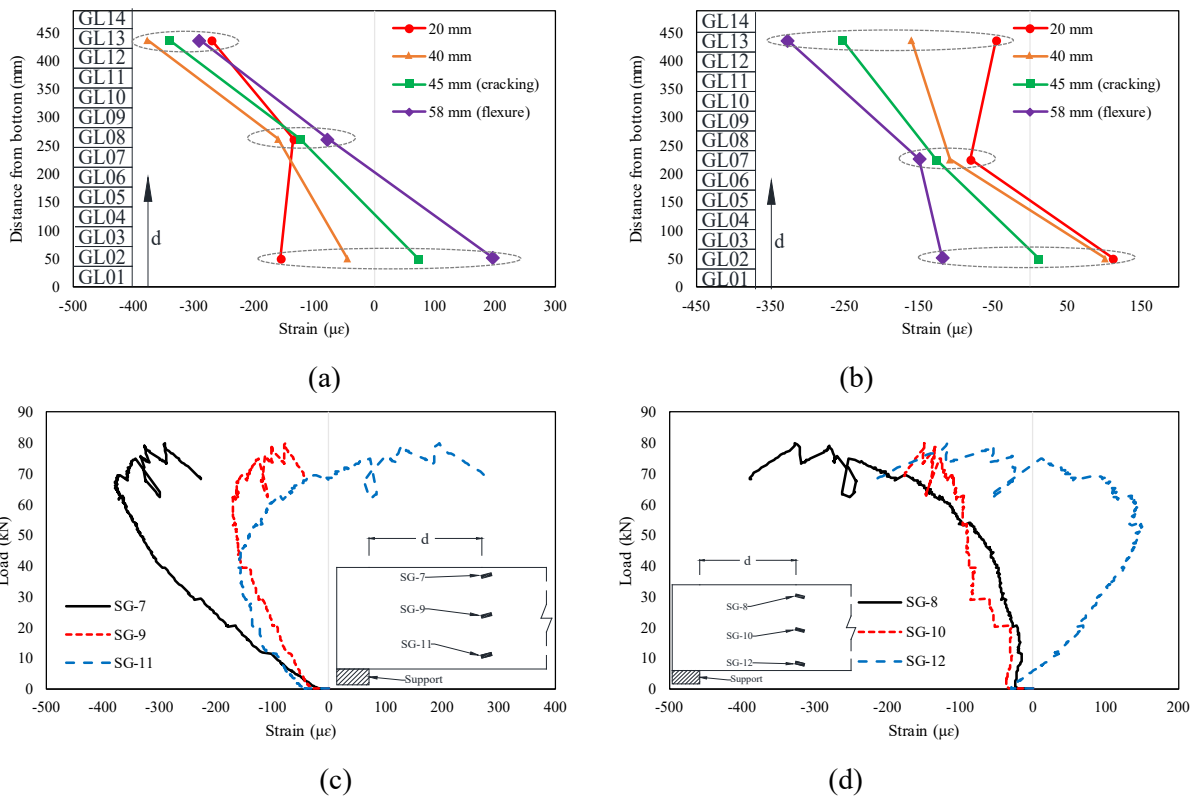


(b)

**Figure 2.71** Strain gauges installed on  $3d$  from the north support: (a) strain profile and (b) load-strain curves

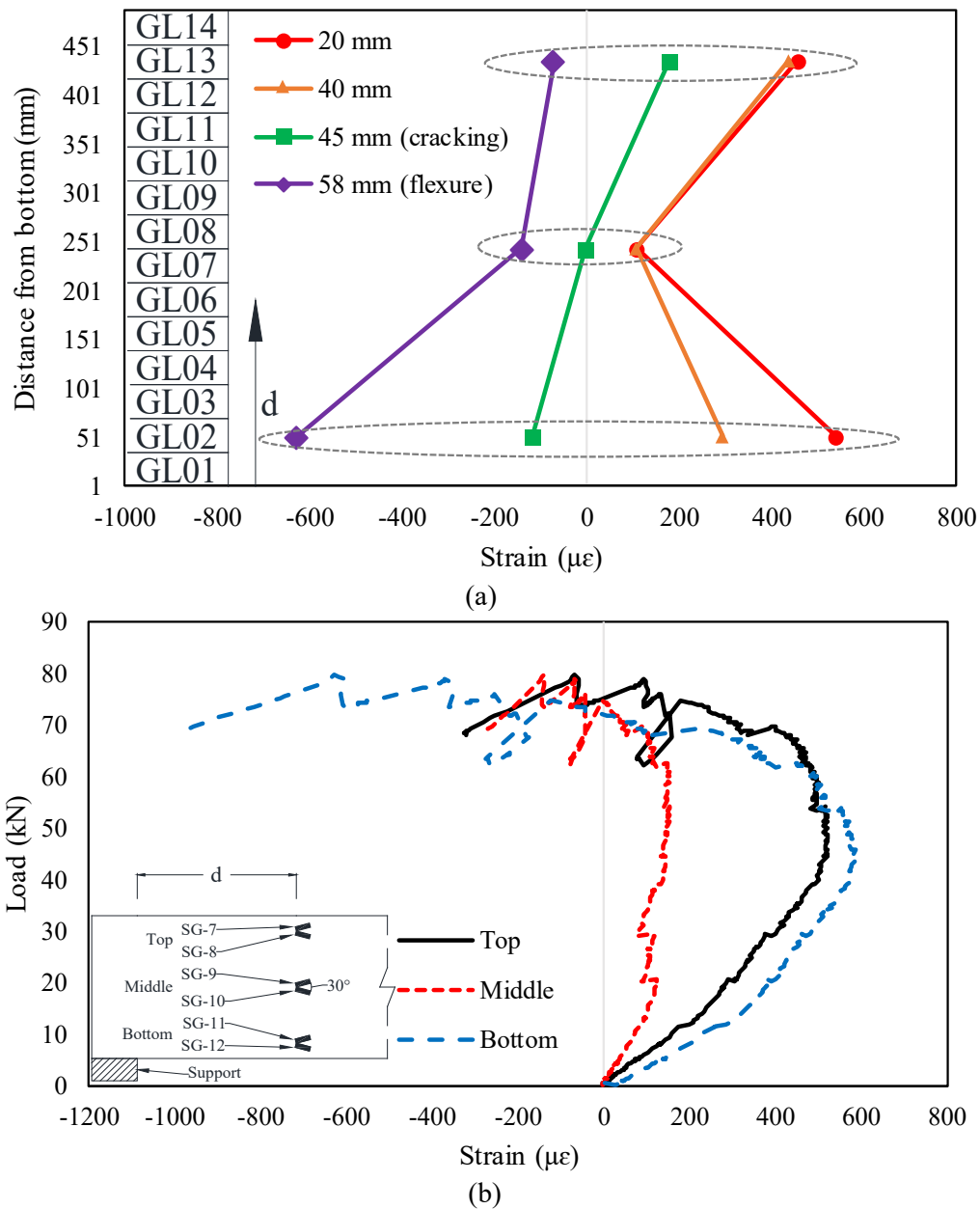
Figure 2.72 displays strain profiles plotted from data measured from the strain gauges attached to  $d$  from the north support of the girder. Figures 2.72a through 2.72d present strain patterns specific to each gauge. The strain gauges were installed at the top of girder (SG-7 and SG-8), in the middle of the girder (SG-9 and SG-10), and at the bottom of the girder (SG-11 and SG-12). SG-7, SG-9, and SG-11 in Figures 2.72a and 2.72c indicate the upper gauges installed at a  $15^\circ$  up angle with respect to a reference horizontal line, whereas SG-8, SG-10, and SG-12 in Figures 2.72b and 2.72d denote the lower gauges mounted on a  $15^\circ$  down angle from the reference line.

In Figure 2.72a, the neutral axes at the deflections of 45 mm and 58 mm were individually located at 128.97 mm and 202.28 mm from the bottom of the girder. No neutral axis was observed at the deflections of 20 mm and 40 mm. In Figure 2.72c, negative strain in compression is observed in all strain gauges except at SG-11. As shown in Figure 2.72b, at the deflection of 58 mm (flexural failure), the neutral axis was out of boundary of the girder depth. All the gauges observed negative strain in compression except at SG-12, as shown in Figures 2.72d. Figures 2.72c and 2.72d show that the strain values changed abruptly after the flexural cracking at 74.77kN and flexural failure at 79.89 kN.



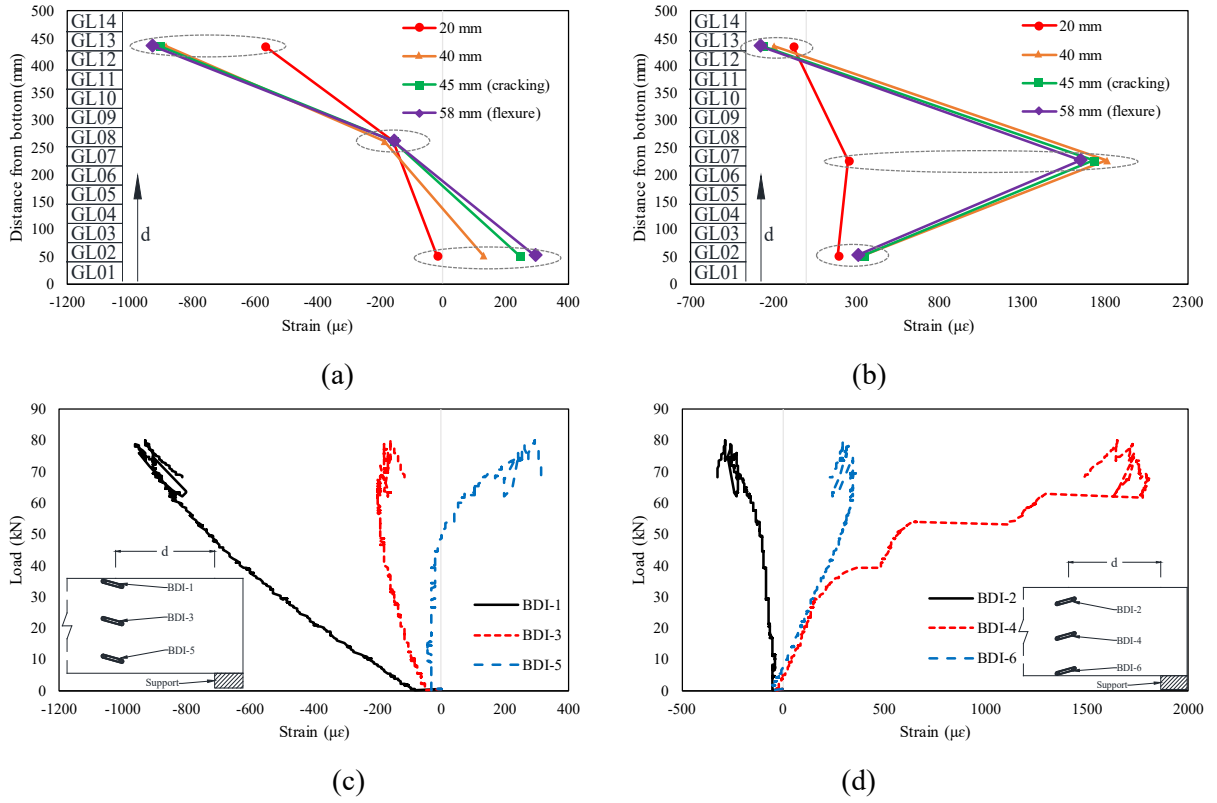
**Figure 2.72** Strain gauges installed on  $d$  from the north support: (a) strain profile (upper); (b) strain profile (lower); (c) load-strain curves (upper); and (d) load-strain curves (lower)

The shear strain calculated using the strain values gained from a pair of two strain gauges installed at  $30^\circ$  (e.g., SG-7 and SG-8) through Equation 44 are created in Figure 2.73a for the strain profile and Figure 73b for the load-strain curve. In Figure 2.73a, it appears that the neutral axes are not found within the girder depth at the deflections of 20 mm, 40 mm, and 58 mm. As shown in Figure 2.73b, the maximum shear strain is found at the bottom of the girder.



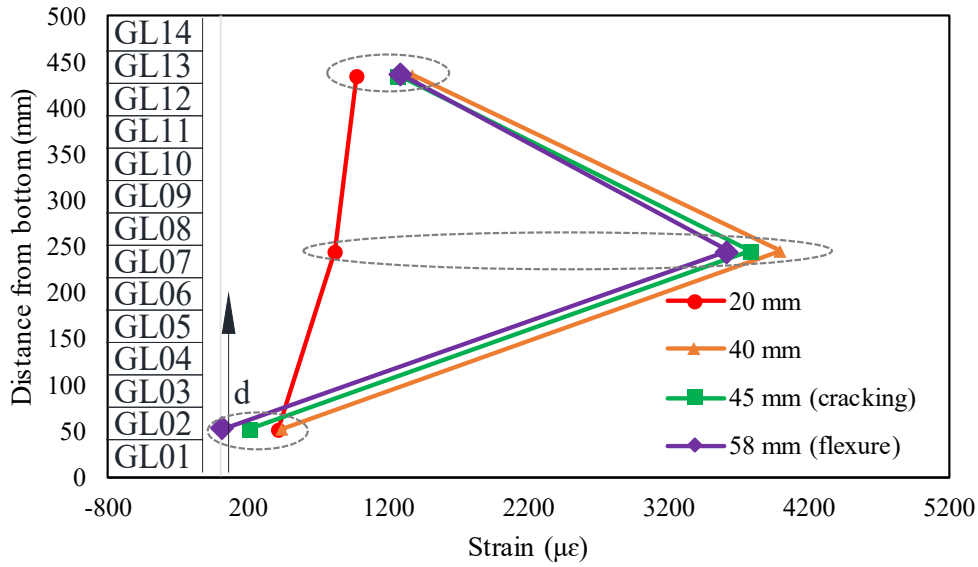
**Figure 2.73** Shear strain on  $d$  from the north support: (a) strain profile and (b) load-strain curves

Figure 2.74 displays the strain profiles and load-strain curves recorded from BDI strain sensors at  $d$  from the south support of the girder. Figures 2.74a and 2.74b show the strain profiles along the girder depth, while Figures 2.74c and 2.74d present the load-strain curves. In Figure 2.74a, the average neutral axis was situated at 214.94 mm from the bottom of the girder at the deflections of 45 mm through 58 mm. The results demonstrated no significant movement of the neutral axis. In Figure 2.74c, negative strain in compression can be observed at the location of BDI-1 and BDI-3, whereas negative and positive strain (i.e., compression and tension) can be found at the position of BDI-5. As illustrated in Figure 2.74b, the average neutral axis was positioned at 403.39 mm from the bottom of the girder at the deflections of 20 mm through 58 mm. As seen in Figure 2.74d, BDI-2 appears to be in compression with the negative strain, whereas BDI-4 and BDI-6 are found to be in tension with the positive strain.

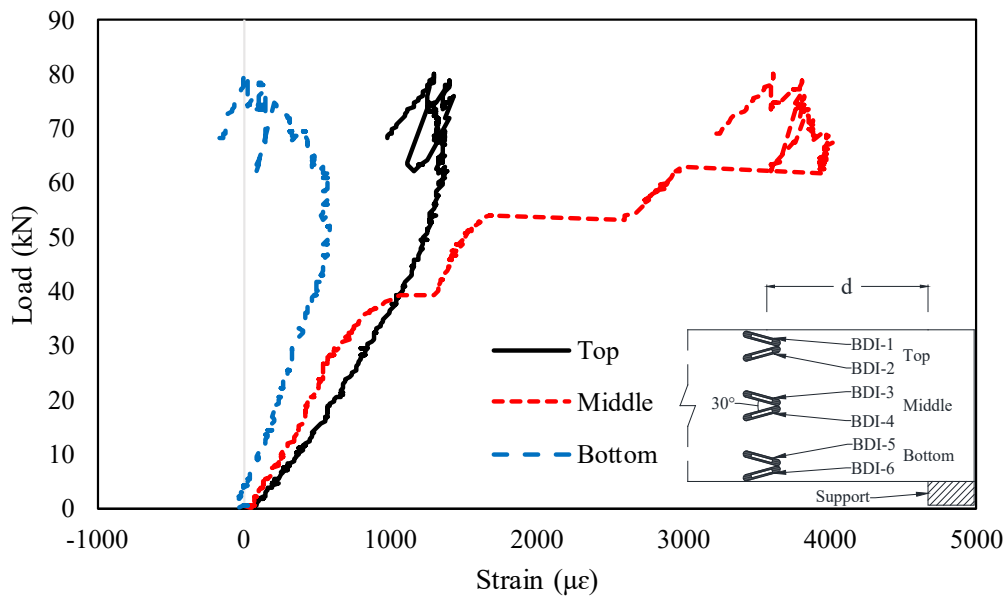


**Figure 2.74** BDI strain sensors (upper) installed on *d* from the south support: (a) strain profile (upper); (b) strain profile (lower); (c) load-strain curves (upper); and (d) load-strain curves (lower)

Figure 2.75 presents the shear strain values calculated from Equation 44 using the data from each pair of the up and down angle gauges. Figure 2.74a shows the relation between the distance from the bottom of the girder and all the shear strains. In this figure, the neutral axes were not positioned within the girder depth at all the deflections of 20 mm through 58 mm. As displayed in Figure 2.75b, the maximum shear strain is found at the center of the girder before the flexural cracking and failure. This follows the evidence, where maximum shear strain occurs at the center of conventional girders (Hearn 1997).



(a)



(b)

**Figure 2.75** Shear strain on  $d$  from the south support: (a) strain profile and (b) load-strain curves

Figure 2.76 graphically describes strain recorded from the BDI strain sensors installed at  $3d$  from the south support. Figure 2.76a shows the average neutral axis for the deflections of 20 mm and 58 mm is located at 218.16 mm from the bottom of the girder. As exhibited in Figure 2.76b, BDI-7 and BDI-8 present negative strain in compression, while BDI-9 showed positive strain in tension up to the flexural failure. A large change in the strain was found in all BDI strain sensors after the flexural cracking and failure. These results suggest that the substantial section property loss of the girder, especially for the bottom of the girder, occurred due to both the flexural cracking and failure.

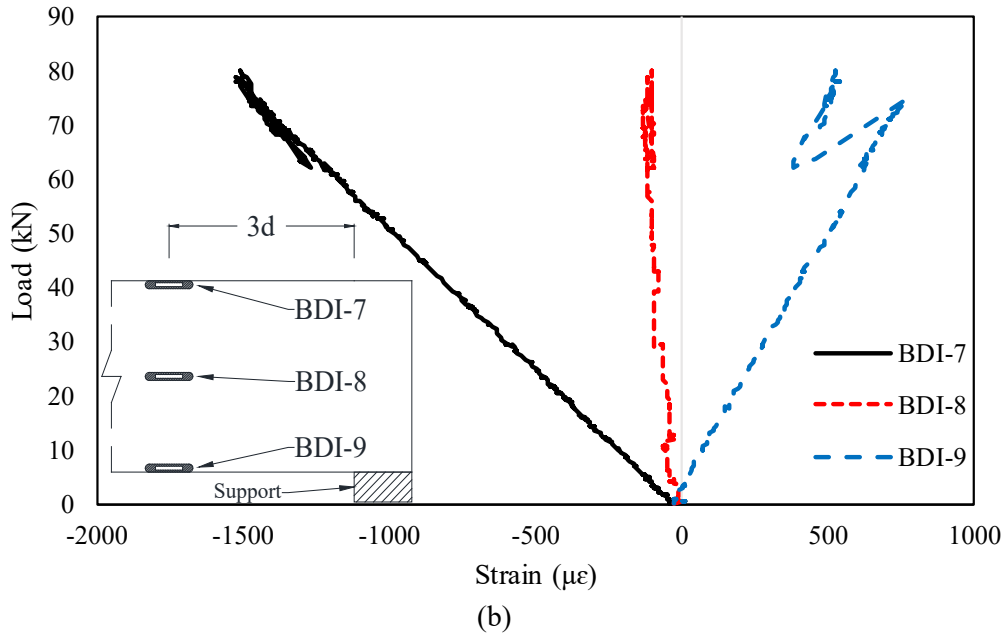
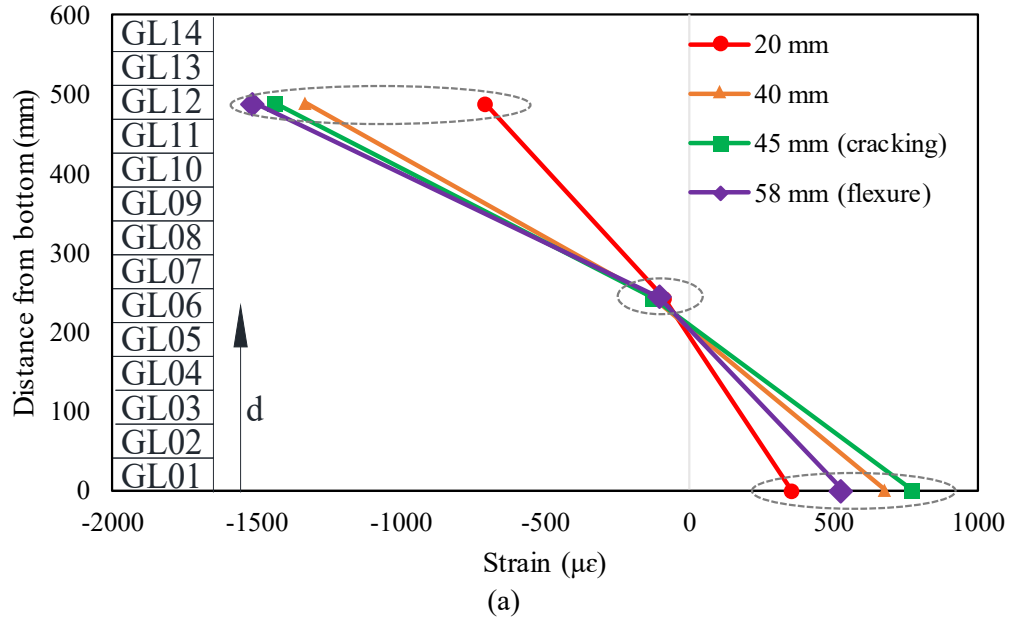


**Figure 2.76** BDI strain sensors installed at  $3d$  from the south support: (a) strain profile and (b) load-strain curves

### Data from Non-contact Sensors

During the testing, the CLT girder with adhesive and fasteners was regularly inspected with the non-contact sensors, as shown in Figure 2.77.

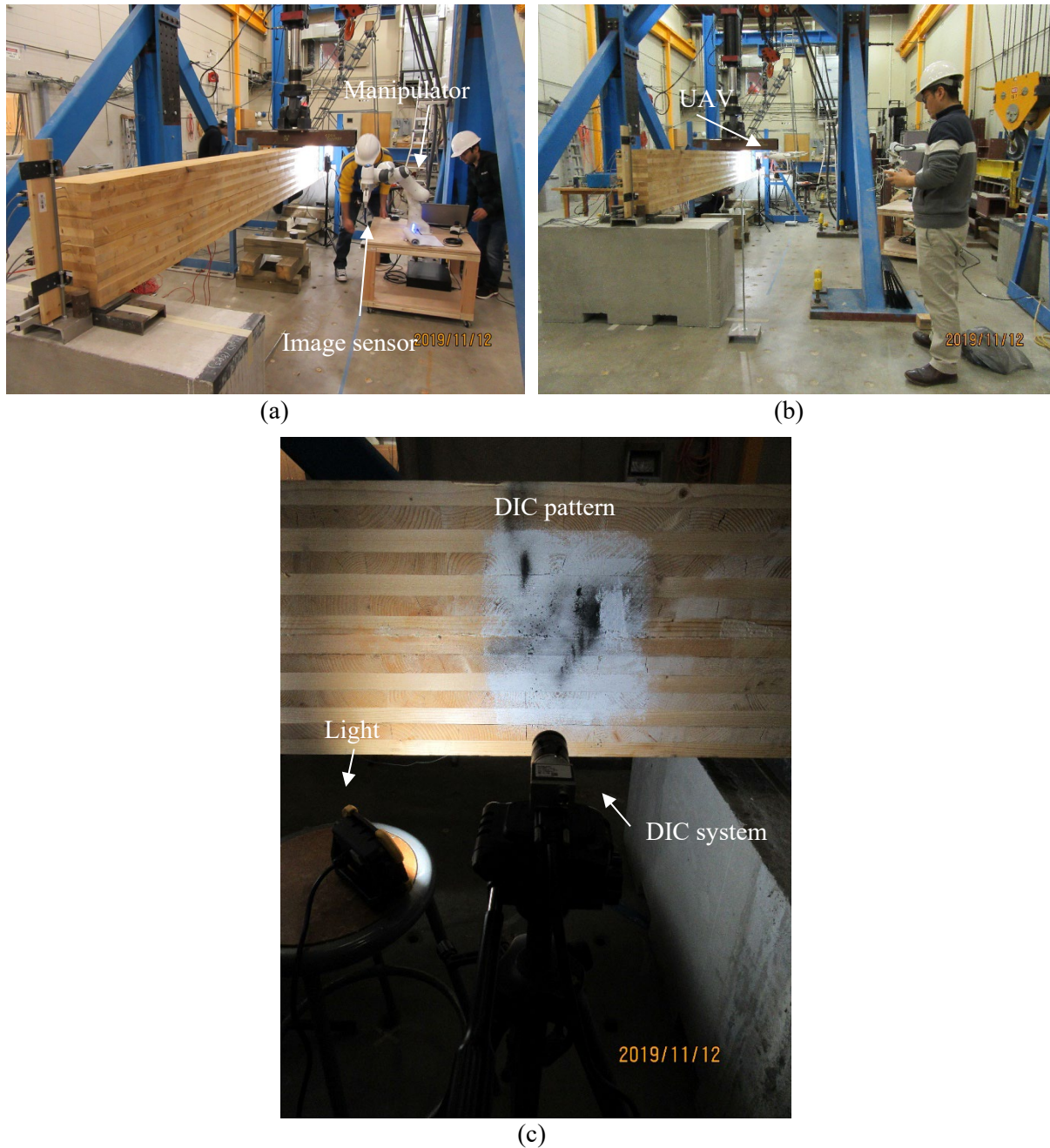


**Figure 2.77** Non-contact sensor operation: (a) manipulator; (b) UAV; and (c) DIC system

In this testing, the manipulator (Figure 2.77a), UAV (Figure 2.77b), and DIC system (Figure 2.77c), as well as the digital camera, were applied for the regular inspections. Nine inspections were performed on the tested adhesive and fastener CLT girder. A number of images were captured from the iPhone 6s Plus installed on the manipulator and the gimbal camera attached to UAV Phantom 4 to measure the deflection and quantify damage from rigorous image analysis. ImageJ coupled with the same algorithm was used as



in the previous adhesive CLT girder testing to measure the deflection and damage in the adhesive and fastener girder. A sample picture of the damage quantification for the tested girder using ImageJ can be seen in Figure 2.78.

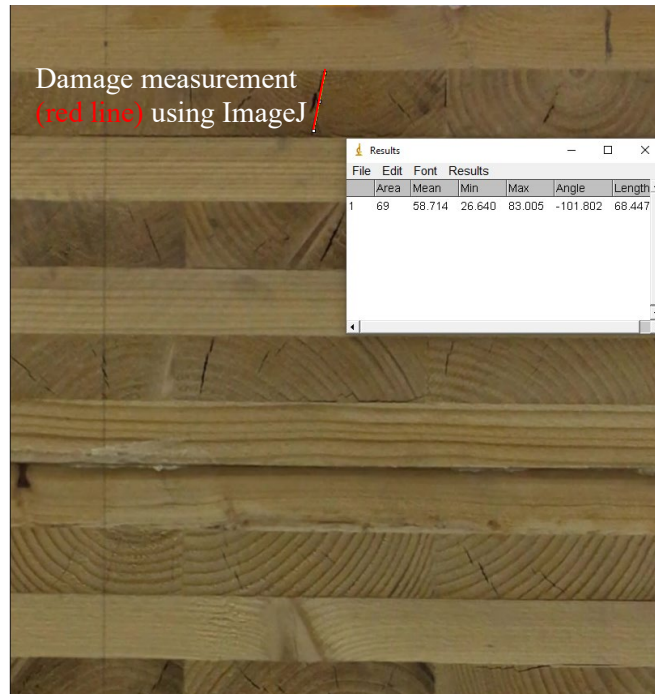


**Figure 2.78** Damage quantification procedure for adhesive and fastener CLT girder

A graphical comparison of the deflections in the mid-span recorded from the manipulator, UAV, and actuator is shown in Figure 2.79. The average differences between the deflections measured individually through image analysis of the inspection images captured from the manipulator and UAV and the actuator's deflection were 5.45 mm and 6.60 mm, and respective average percentage errors of 18.46% and 18.66% were observed. The maximum difference in the deflections obtained from the manipulator and actuator against the actuator's deflection was found to be 13.31 mm and 13.48 mm, respectively. The results indicated that the image analysis, coupled with the manipulator-based and UAV-based inspection images, was able to estimate the mid-span deflections of the CLT girder with a reasonable level of accuracy.

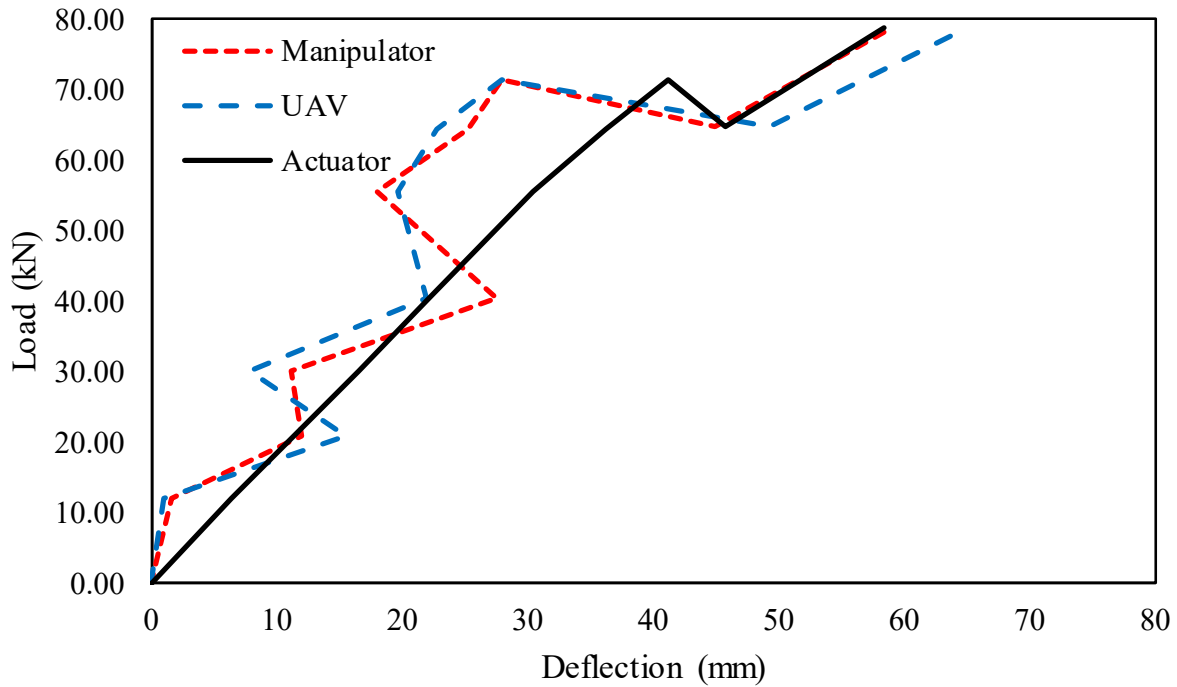


**Figure 2.79** Deflection comparison between manipulator, UAV, and actuator

Figure 2.80 depicts the inspection images obtained from the manipulator and UAV, which were used for the deflection measurement. Figures 2.80a through 2.80d show the inspection images at the mid-span of the girder captured by the manipulator at different deflections of the actuator. As shown in Figures 2.80e and 2.80f, original inspection images taken by the UAV at 0 mm and 37.34 mm deflection lack brightness. As delineated earlier, these low-quality images were not able to efficiently identify the position of the actuator and accurately determine the mid-span deflections. Hence, these images were amended with the brightness of 85% and contrast of -10%, as shown in Figures 2.80g and 2.80h. Along with the amended images, all the testing items and the adhesive and fastener CLT girder were identified in an efficient manner, and then the mid-span deflections were determined through the image analysis.

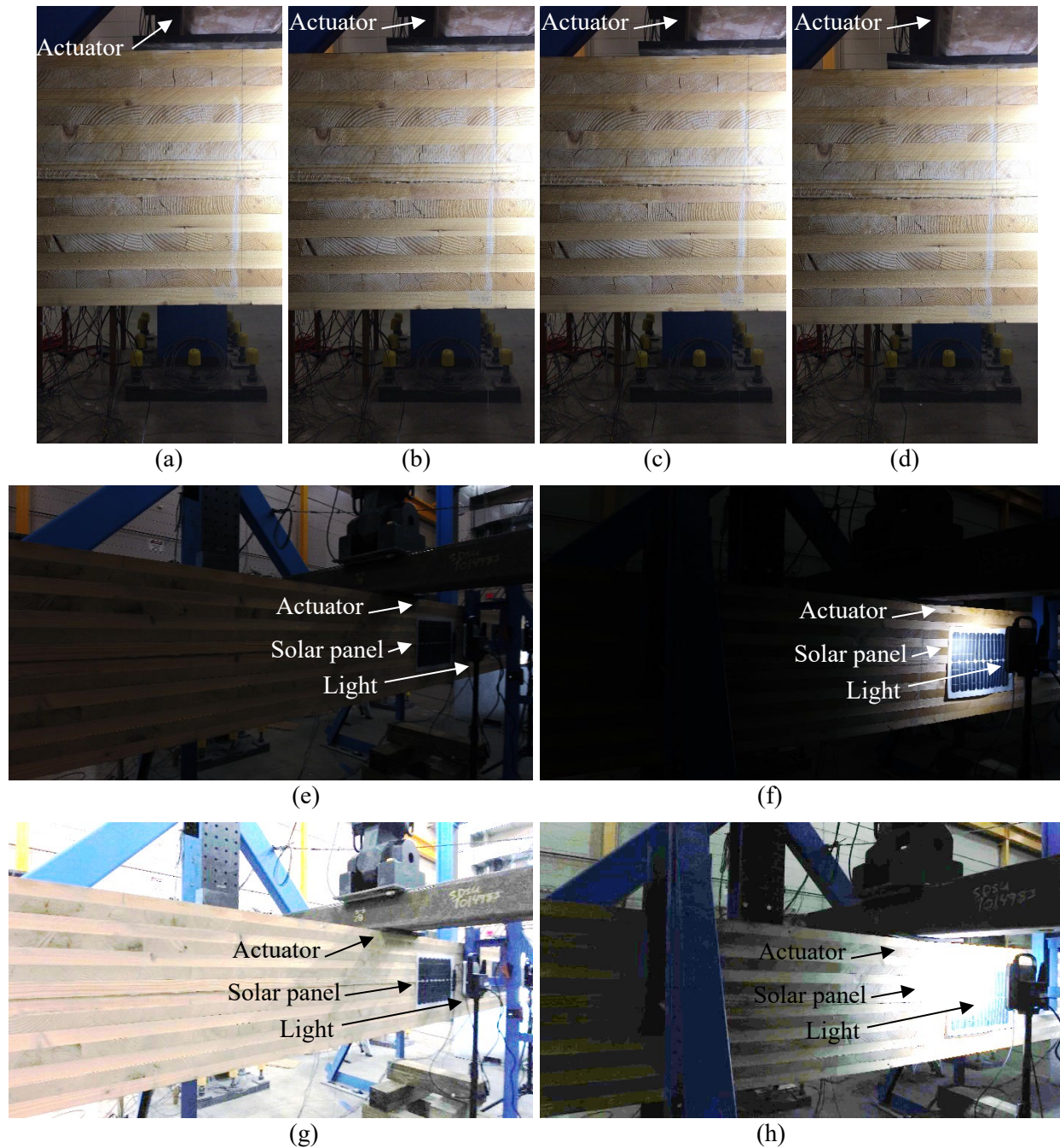


**Figure 2.80** Inspection images captured by the manipulator and UAV: (a) 0 mm (manipulator); (b) 13.97 mm (manipulator); (c) 22.10 mm (manipulator); (d) 37.34 mm (manipulator); (e) 0 mm (UAV); (f) 37.34 mm (UAV); (g) Figure 2.80e adjusted with brightness 85% and contrast -10%; and (h) Figure 2.80f adjusted with brightness 85% and contrast -10%

With the inspection images obtained from manipulator, all visible cracks on the CLT girder with adhesive and fasteners are observed, as shown in Figures 2.81 and 2.82. The CLT girder was divided into eight sections between the south support and mid-span. Figures 2.81 and 2.82 show the inspection images before the testing and after the testing, respectively. During the testing, significant damage propagation was detected on sections 4 and 5. Note, the white lines in both figures indicate cracks on the tested CLT girder.



**Figure 2.81** Southeast sections of CLT girder before the testing captured by manipulator: (a) section 1; (b) section 2; (c) section 3; (d) section 4; (e) section 5; (f) section 6; (g) section 7; and (h) section 8



**Figure 2.82** Southeast sections of CLT girder after the testing captured by manipulator: (a) section 1; (b) section 2; (c) section 3; (d) section 4; (e) section 5; (f) section 6; (g) section 7; and (h) section 8.

The cracks detected by the manipulator were also identified through the inspection images taken by the UAV. Figure 2.83 depicts the inspection images from the UAV. Due to low brightness in the original inspection images (Figures 2.83a, 2.83c, and 2.83e), brightness and contrast of the images were modified, as shown in Figures 2.83b, 2.83d, and 2.83f. Figures 2.83a and 2.83c were modified with brightness of 70% and contrast of -10%, as shown in Figures 2.83b and 2.83d, respectively. Figure 2.83e was modified with increments of 60% brightness and 10% contrast, as shown in Figure 2.83f.

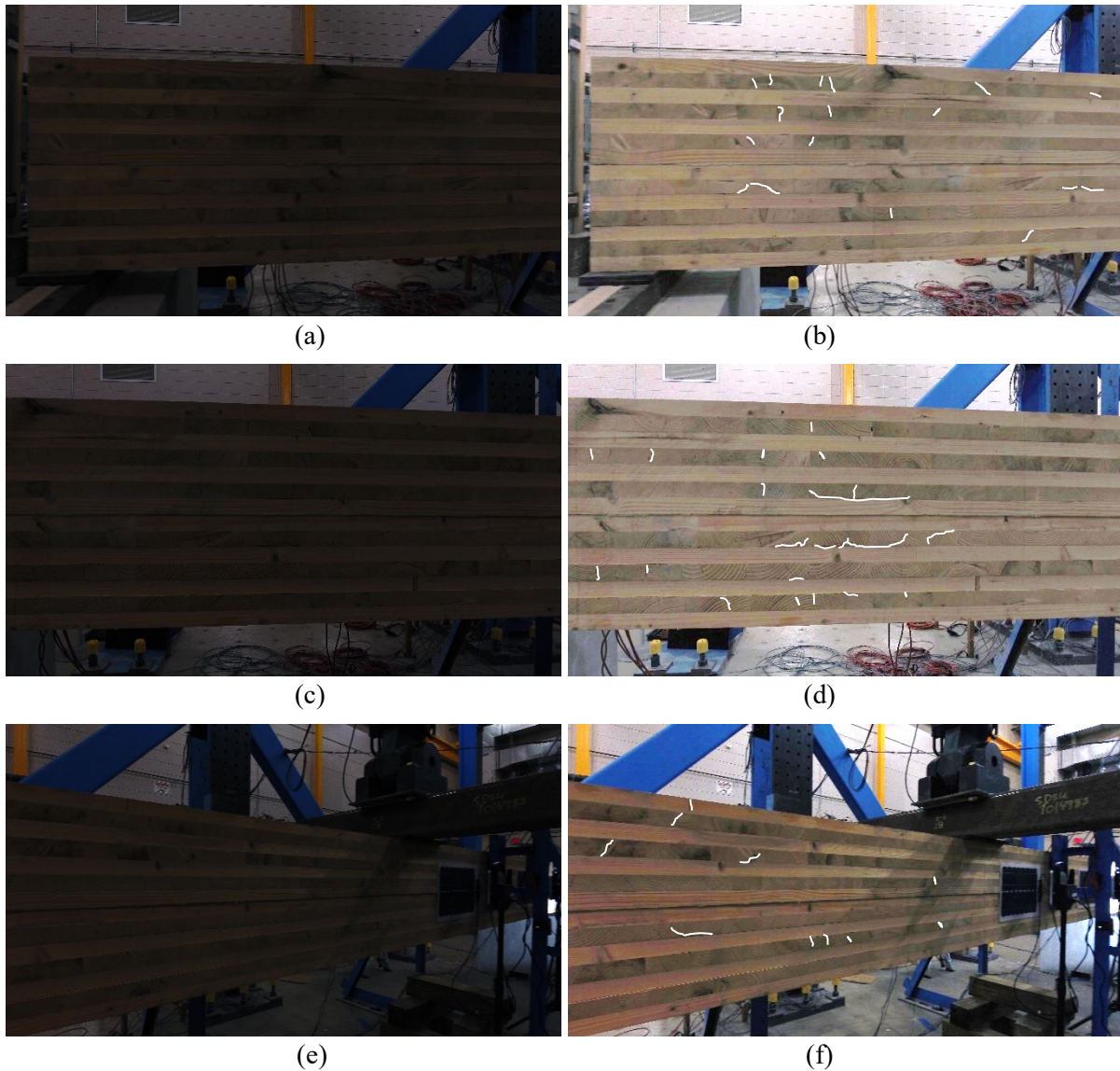


**Figure 2.83** Southeast sections of CLT girder before the testing captured by UAV: (a) Sections 1 through 4; (b) Figure 2.83a adjusted with brightness 70% and contrast -10%; (c) Sections 2 through 6; (d) Figure 2.83c adjusted with brightness 70% and contrast -10%; (e) Sections 4 through 8; and (f) Figure 2.83e adjusted with brightness 60% and contrast 10%.

A detailed damage map (including all cracks) created using the cracks detected from the inspection images from the manipulator can be seen in Figure 2.84a for prior testing and 2.84b for the post testing. These figures show the locations and sizes of the identified cracks. Figure 2.84a and 2.84b show the existing cracks and the existing and propagated cracks on the southeast sections of the CLT girder, respectively. Note that red lines signify the existing cracks, whereas blue lines denote the propagated cracks from the initial cracks. The propagated cracks marked “crack 1,” “crack 2,” and “crack 3” and corresponding pictures are seen in Figure 2.84b.

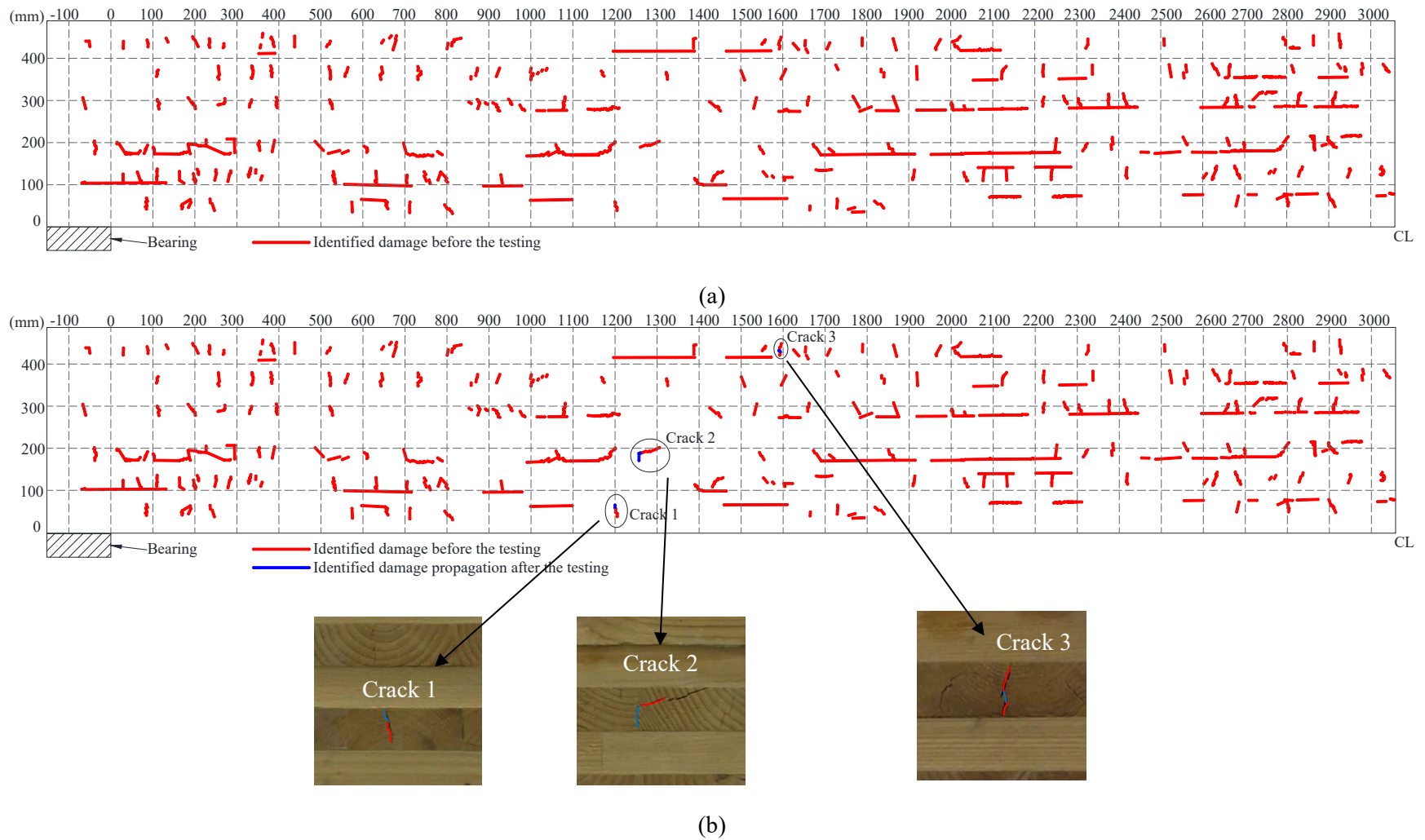


**Figure 2.84** Damage map on the CLT girder with adhesive and fasteners: (a) before the testing and (b) after the testing

As stated before, the damage was identified on the south east side of the girder. During this damage identification and quantification, crack propagation was found and measured. As shown in Figure 2.84, the marked Cracks 1 and 2 (22.45 mm and 14.32 mm, respectively) on Section 3 were propagated to 30.22 mm and 35.31 mm, respectively. Another crack propagation on Section 4 was observed as shown in Figure 2.84. Initial length of the marked cracks (11.23 mm and 20.87 mm) were not connected before the test, but the marked cracks, 36.23 mm, was propagated and connected during the testing which can be seen in the image of the girder after the test as displayed in Figure 2.84. The details related to damage propagation is provided in Table 2.4.

Based on the identified propagated cracks (i.e., cracks 1, 2, and 3) on the south east side of the girder, these cracks were quantified using the inspection images from the manipulator and UAV. The details of the propagated damage are listed in Table 2.4. For instance, the propagated lengths of cracks 1, 2, and 3 obtained from the manipulator are 30.22 mm, 35.31 mm, and 40.13 mm, and those from the UAV are 31.42 mm, 37.22 mm, and 39.25 mm after the testing. As shown in Figure 2.84a, the existing crack 1 has a total of length of 22.45 mm from the manipulator and 24.27 mm gained from the UAV before the testing. As shown in Figure 2.84b, the propagated length of crack 1,  $\Delta l$ , become 7.77 mm from the manipulator and 7.15 mm from the UAV. Likewise, the propagated length of crack 2,  $\Delta l$ , is 20.99 mm and 20.98 mm resulting from the manipulator and UAV, respectively. The existing crack 3 comprising two horizontal, small cracks (11.23 mm and 20.87 mm measured by the manipulator and 10.87 mm and 19.97 mm measured by the UAV), which has a total of length of 32.10 mm from the manipulator and 30.84 mm acquired from the UAV, were not connected before the testing. The two horizontal, small cracks were connected to the extended crack 3 after the testing; thus, the propagated length of crack 3,  $\Delta l$ , results in 8.03 mm from the manipulator and 8.41 mm from the UAV.

**Table 2.4** Details of identified propagated damage of CLT girder with adhesive and fasteners

Damage	Initial length (mm)	Propagated length (mm)	$\Delta l$ (mm)	Initial thickness (mm)	Propagated thickness (mm)	$\Delta t$ (mm)
Crack 1 (manipulator)	22.45	30.22	7.77	0.87	0.99	0.12
Crack 2 (manipulator)	14.32	35.31	20.99	1.00	1.10	0.10
Crack 3 (manipulator)	11.23 and 20.87	40.13	8.03	2.45	2.60	0.15
Crack 1 (UAV)	24.27	31.42	7.15	0.91	1.04	0.13
Crack 2 (UAV)	16.24	37.22	20.98	1.07	1.20	0.13
Crack 3 (UAV)	10.87 and 19.97	39.25	8.41	2.34	2.55	0.16

The DIC system was applied to the CLT girder, in an attempt to measure the strain on the east side of the girder. Again, the DIC system was designed to record two images per second regardless of the displacement controlled by the actuator during the testing. A plot of strain versus number of images collected by the DIC system is presented in Figure 2.85. It is apparent that significant changes in the strain are found at 6001<sup>st</sup> and 8001<sup>st</sup> image. In detail, the cause of significant change in the direction of the strain at 6001<sup>st</sup> was found to be the flexural cracking that occurred during the testing. It is learned that the flexural cracking altered the strain in the tested CLT girder. It should be noted that the strain acquired from the DIC system could not be plotted against the actuator load. Therefore, the DIC-based strain



profile was not be able to be compared with the strain profile obtained from the contact sensors, strain gages (SG-9 and SG-10) in particular.

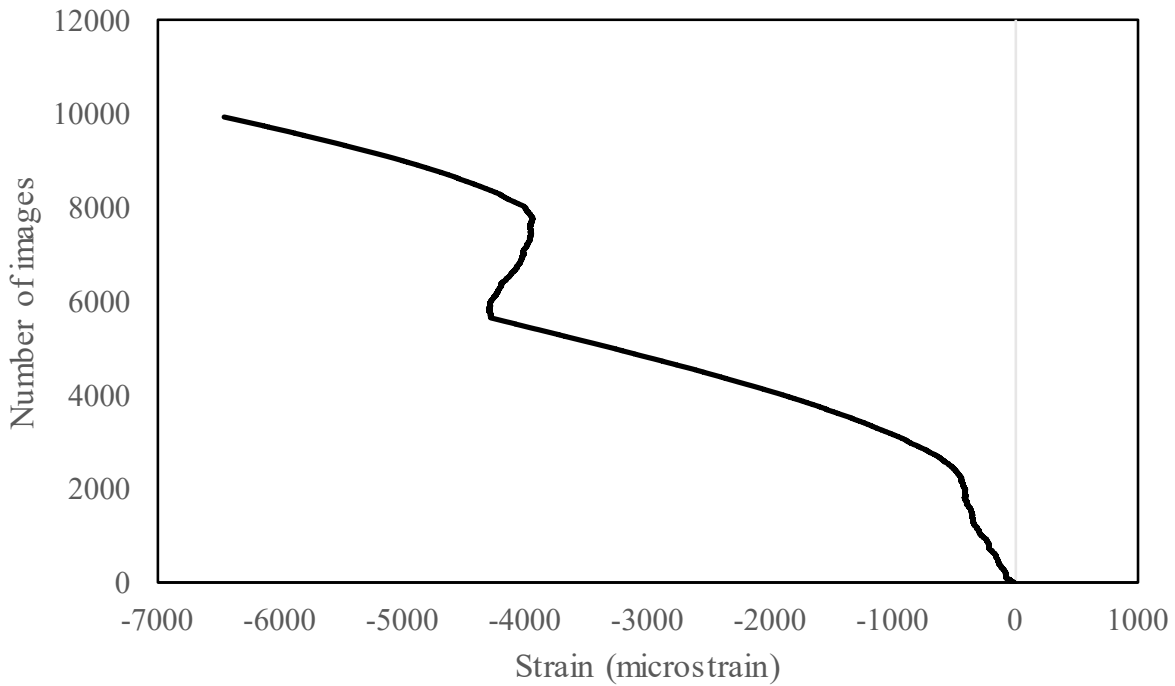


**Figure 2.85** Strain profile calculated from DIC system applied on the CLT girder with adhesive and fasteners

### ***Data from Solar Panels***

As aforementioned, the two solar panels, solar panels 1 and 2, were attached to the east side of the CLT girder to evaluate the efficiency of energy harvesting during the ultimate load test. Voltages from the solar panels were recorded manually for all test runs (170 runs in total). Figure 2.86 displays a relationship between voltages from each panel and the mid-span displacements recorded from the actuator. In this figure, the voltages in both panels are found to be declined with an increment in the mid-span displacement of the girder. This tendency was due to the downward movement of both panels from the light source as the deflection of the girder loaded with the actuator increased. The amounts of voltage created between the panels 1 and 2 are observed to be slightly different. Specifically, the panel 1 exhibits the significant increase in the voltage at 45.34 mm deflection as a result of its upward movement after the flexural cracking, whereas the voltage of the solar panel 2 did not appear to be significant changed at that deflection. Note that both panels were not damaged during this test. Along with the voltage-displacement relationship, it can be interpreted that the efficiency of energy harvesting relied on the location of solar panels from the applied load under the same condition of the light source.

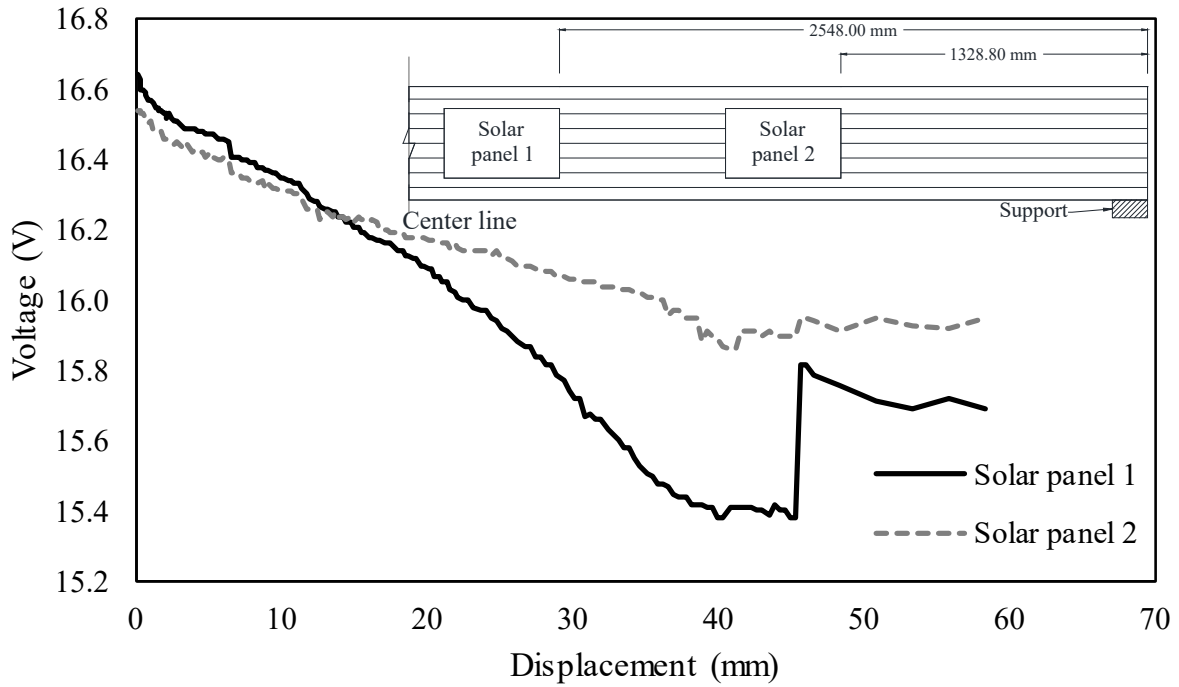


**Figure 2.86** Relationship between voltage and displacement of CLT girder with adhesive and fasteners

### 2.4.3 Performance on CLT Bridge System

This section involves summarizing instrumentation for ultimate strength testing of the CLT bridge system, testing procedure, and results and discussion.

#### 2.4.3.1 Instrumentation

The full-scale laboratory testing of CLT bridge system fabricated with one CLT deck, two CLT girders, and two CLT diaphragms is shown in Figure 2.87.

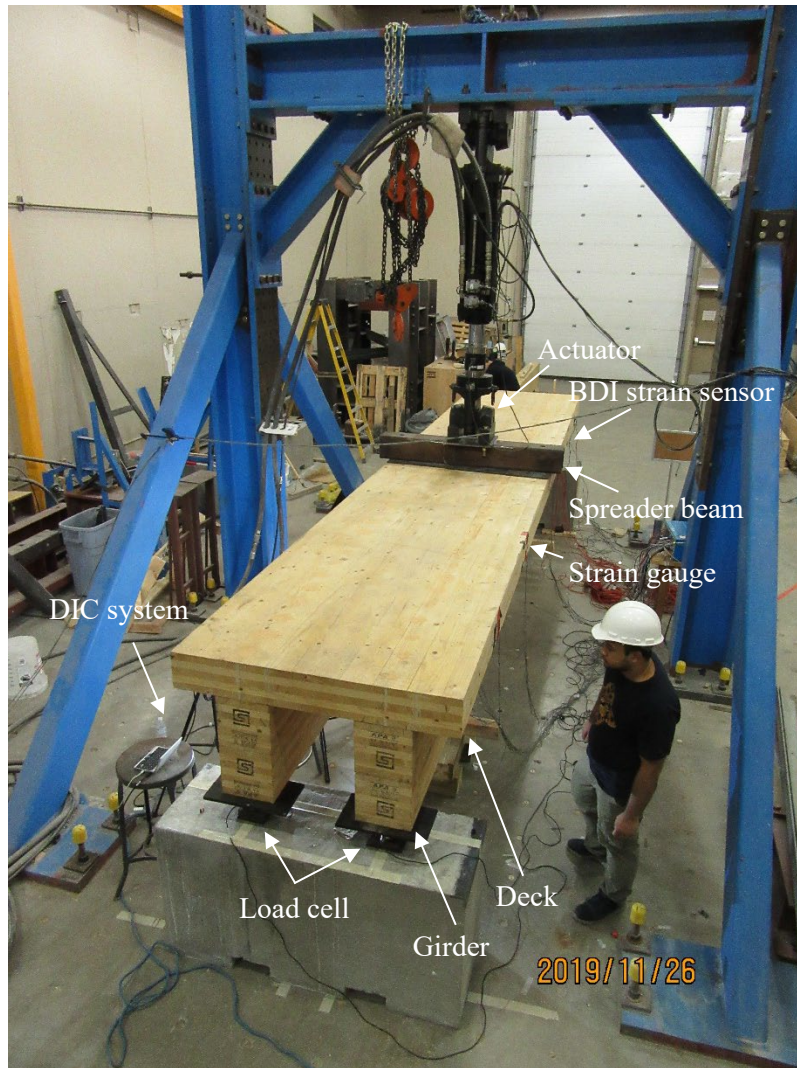


**Figure 2.87** Testing setup for CLT bridge system

The CLT deck having 5 lams has dimensions of 6.40 m long, 0.17 m deep, and 1.22 m wide, while the CLT girder having 14 lams has dimensions of 6.40 m length, 0.48 m depth, and 0.24 m width. The CLT diaphragm made with 7 lams has dimensions of 0.36 m length, 0.23 m depth, and 0.12 m width. As shown in Figure 2.88a, the 14 lams in the CLT girder were designated as GL01 to GL14 from the bottom lam, while the 5 lams in the deck were designated as DL01 to DL05 from the bottom lam. GL indicates “Girder Lam” and DL is defined as “Deck Lam”. To measure testing data such as strain and imagery, both the contact and non-contact sensors used for the previous CLT girder testings were installed on the CLT bridge system as well. The data acquisition system (see Figure 2.88b) was utilized to record the data from the contact sensors during the test of the CLT bridge system. The actuator and data acquisition system connected with the contact sensors were controlled through the computers in the control room as shown in Figure 2.88c. Imagery from the non-contact sensors such as DIC system (see Figure 2.88d) were collected during the test.

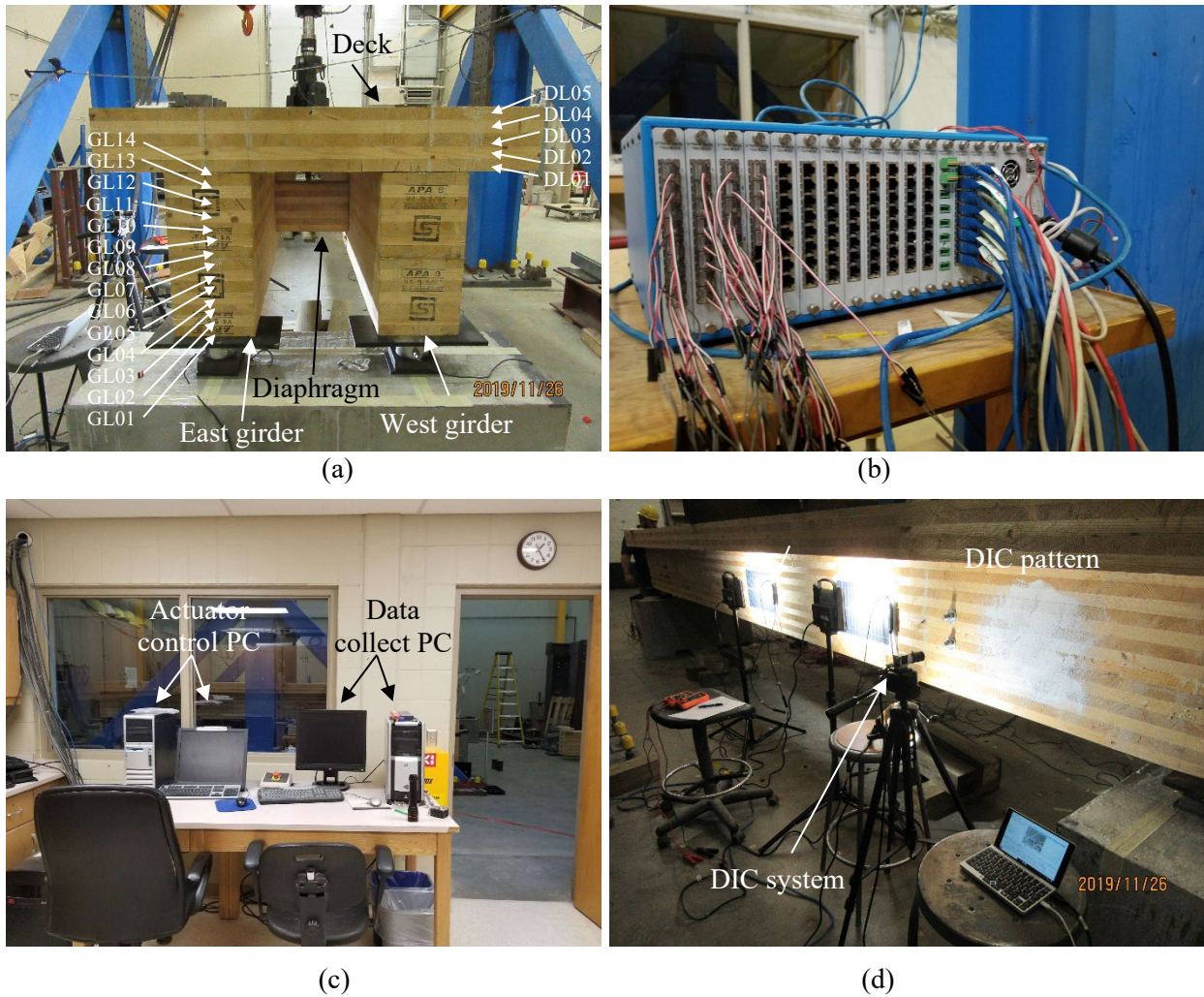


**Figure 2.88** Testing setup for CLT bridge system: (a) bridge lam number designation; (b) data acquisition system; (c) control room; and (d) DIC system

The general instrumentation is shown in Figure 2.89. Figure 2.89a shows the plan view of this testing setup. Figure 2.89b displays the location of the strain gauges and BDI strain sensors installed on the west side of the bridge. DIC system and solar panels mounted on the east side of the bridge are shown in Figure 2.89c. In this figure, the bridge was inspected with UAV on the southeast side. Figure 2.89d shows the schematic of LVDTs, the string pot installed underneath the deck, and load cells installed underneath the girder.

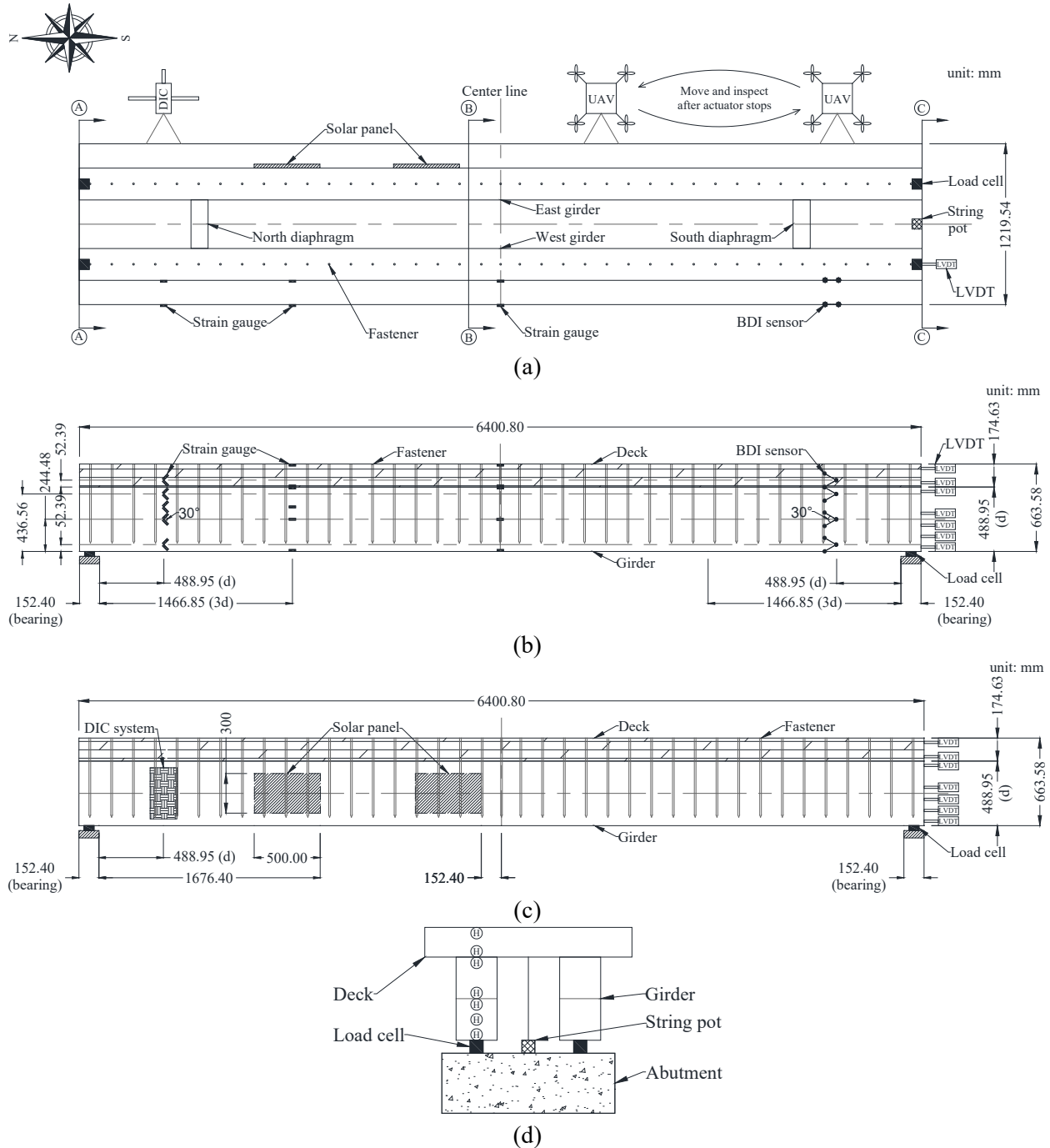


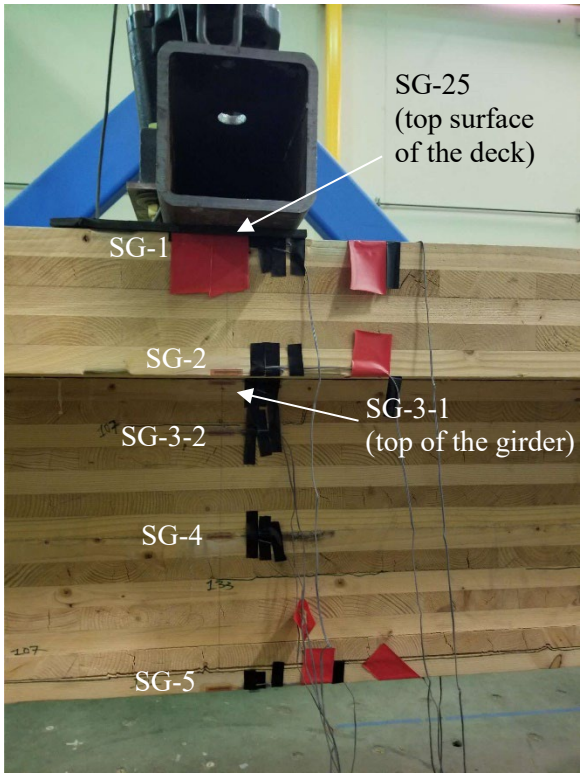
**Figure 2.89** Instrumentation plan for bridge testing: (a) plan view; (b) elevation view (west); (c) elevation view (east); and (d) instrumentation at the south edge of the bridge

For the installation of contact sensors, 29 strain gauges and 8 BDI strain sensors were installed on the bridge (see Figures 2.89a and 2.89b). The 10 strain gauges were installed at a distance of  $d$ , and the 6 strain gauges were installed at a distance of  $3d$  from the north support on the west side of the bridge system. The 9 strain gauges were attached to the mid-span of the bridge, where  $d$  indicates the design depth of the girder. The 4 strain gauges were installed on the top and bottom of each diaphragm.

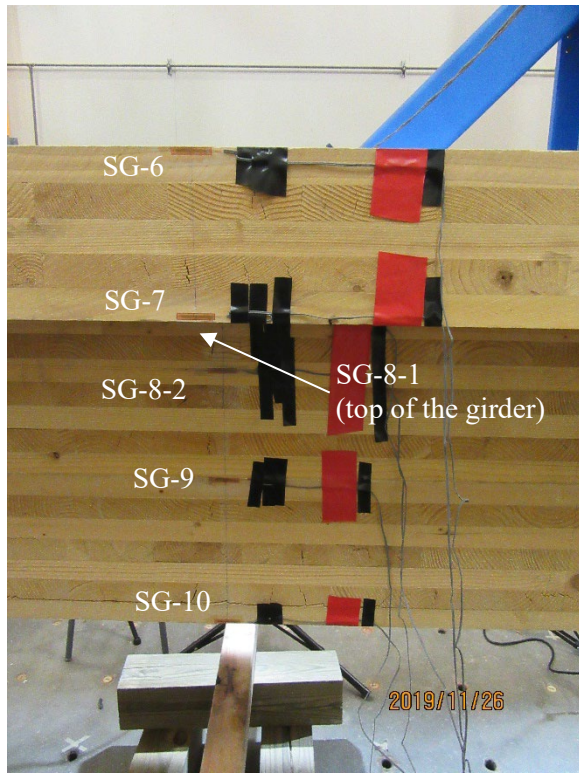
Similarly, 8 BDI strain sensors were only mounted at a distance of  $d$  from the support at the south end of the bridge due to the limited capability of the data acquisition system. As delineated before, the maximum shear is expected at a distance of  $d$  from the support (AASHTO 2012), where the strain gauges and BDI strain sensors were installed to analyze the shear strain at those locations. The strain gauges were also installed at a distance  $3d$  from the support of the girder where the critical shear may occur (AASHTO 2012).

The string pot was installed in the center underneath the deck at the south support of the bridge to collect displacement. 7 LVDTs were instrumented at the south edge of the bridge to measure slippage between CLT lams. In detail, two LVDTs installed on the lower side of the girder (GL01 and GL02) recorded local slip between lams. The bonding performance of the girder was evaluated by examining the slip between two 7-ply CLT beams recorded from two LVDTs located in the middle of girder (GL07 and GL08). To evaluate the bonding performance between the girder and deck, two LVDTs recorded slip between deck and girder installed at the bottom of the deck (DL01) and the top of the girder (GL14). One LVDT was further attached to the upper side of the deck (DL04) to check the slippage between the deck and the girder.

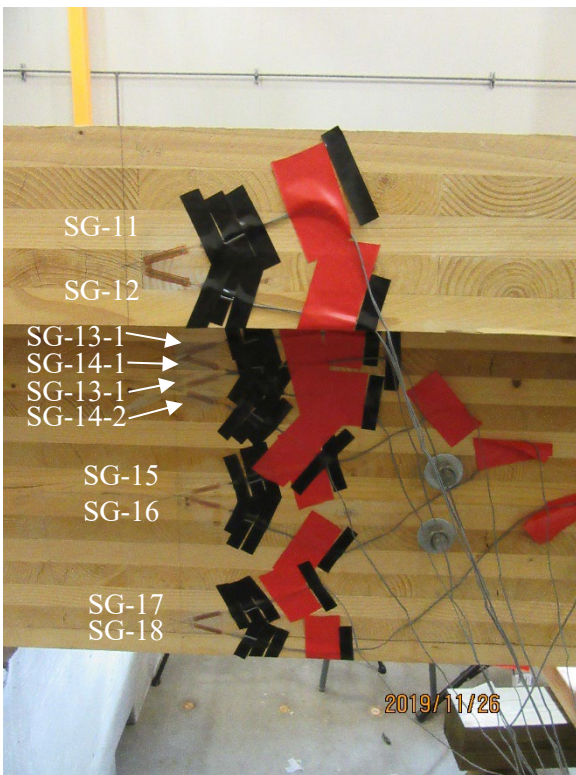
Figure 2.90 shows the location of all the contact sensors instrumented in the bridge. Strain gauges SG-1 through SG-5 and SG-25 were mounted in mid-span (see Figure 2.90a), SG-6 through SG-10 were installed at  $3d$  from the north support (see Figure 2.90b), and SG-11 through SG-18 were installed at  $d$  from the north support (see Figure 2.90c). To assess the load distribution, SG-19 and SG-20 were installed in the mid-span underneath the west and east girder, respectively (see Figures 2.90d and 2.90e). SG-21 through SG-24 were attached on the top and bottom of the diaphragms installed at north and south side of the bridge as shown in Figures 2.90f and 2.90g. BDI strain sensors BDI-1 through BDI-8 were mounted at  $d$  from the south support (see Figure 2.90h). 7 LVDTs, one string pot, and two load cells were installed on the south edge of the bridge as displayed in Figure 90i. Note, a total of four load cells recorded reaction force underneath each girder at the north and south edge of the bridge. The 7 LVDTs were attached on the south face of the bridge as seen in Figure 2.90j. As described earlier, two strain gauges were mounted at an angle of 30 degree between gauges to accurately measure shear strain as shown in Figures 2.90c and 2.90h, respectively. According to the strain gauge installation manual (micro-measurement, 2010), the shear strain is calculated from Equation 44.



(a)



(b)



(c)



(d)



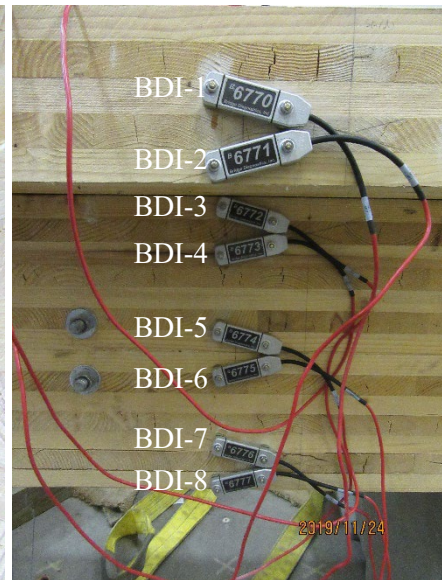
(e)



(f)



(g)



(h)



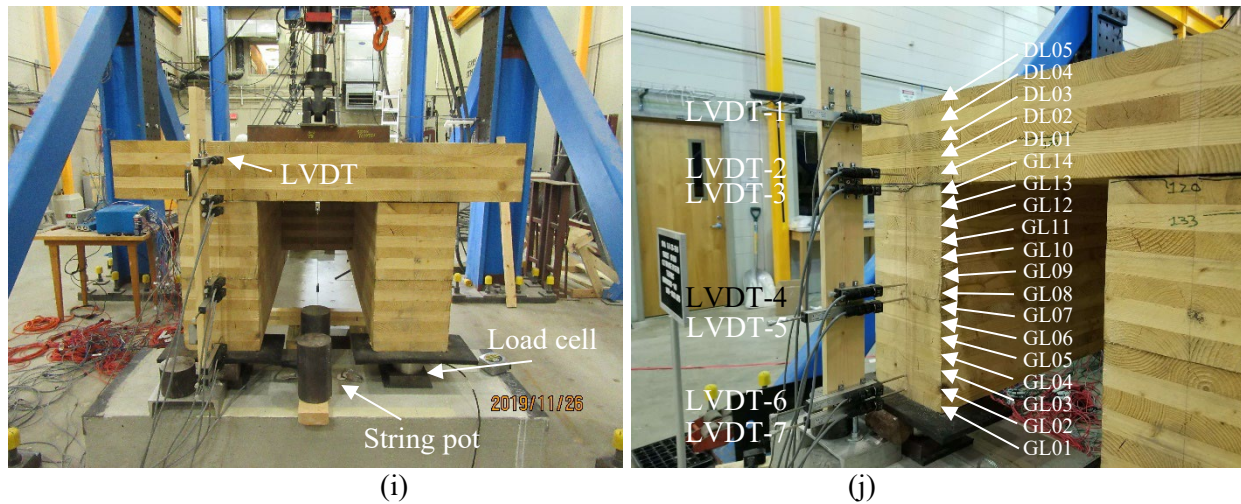
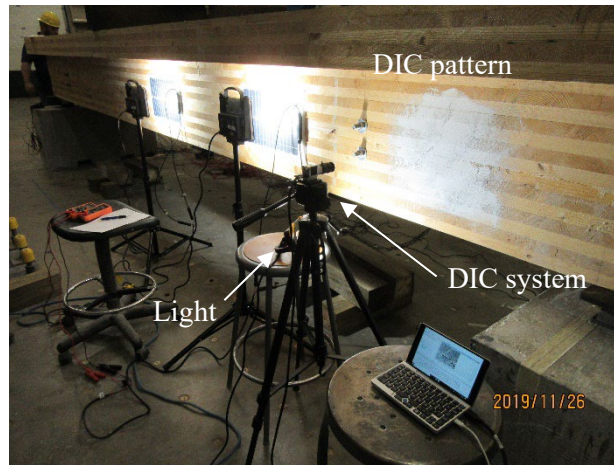


**Figure 2.90** Contact sensor installation for CLT bridge system: (a) strain gauges at mid-span; (b) strain gauges at distance  $3d$  from north support; (c) strain gauges at distance  $d$  from north support; (d) strain gauge underneath west girder; (e) strain gauge underneath east girder; (f) strain gauges on north diaphragm; (g) strain gauges on south diaphragm; (h) BDI strain sensors at distance  $d$  from south support; (i) LVDTs, string pot, and load cells at south edge; and (j) LVDTs at south edge

For the non-contact sensor installation, UAV Phantom 4 equipped with a camera (Appendix G) and DIC camera (Appendix I and J) were applied to the east side of the bridge. The camera mounted on UAV collected images on the south east surface of the bridge during inspection, while the DIC system was installed on the north east side of the bridge at  $d$  from the north support to record images for the calculation of strain (see Figure 2.91a). Note that the images from UAV were used to identify damage and estimate deflection at the mid-span of the bridge and the DIC image-based strain values were compared with the strains recorded from the contact sensors installed on the north-west side of the bridge at the same distance from the north support. The installation of the non-contact sensors is shown in Figure 2.91a for DIC system and Figure 2.91b for UAV.

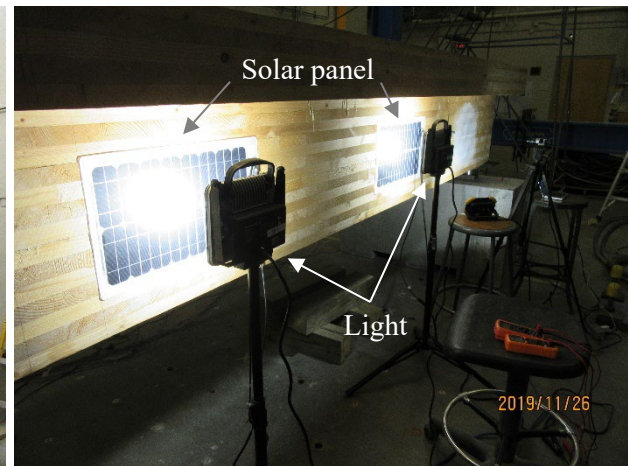
Additionally, two solar panels were installed on the east side of the girder to examine the correlation between solar energy harvesting and bridge behavior resulting from the testing. In Figure 2.91c, one solar panel designated “solar panel 1” was glued 0.15 m away from the center of the girder to collect the solar energy harvesting under critical location, while another solar panel named “solar panel 2” was mounted 1.83 m away from the north edge of the bridge to compare energy harvesting. To collect an amount of solar energy harvesting during the testing, a light was installed at 0.15 m distance from each solar panel, where each was capable of harvesting the maximum voltage 16.41 V.



(a)



(b)



(c)

**Figure 2.91** Non-contact sensor and solar panel for CLT bridge system: (a) DIC system; (b) UAV-enabled inspection; and (c) solar panel.

### 2.4.3.2 Testing Procedure

As seen in Figure 2.92, a testing procedure that can be broken into three steps: 1) loading, 2) measurement, and 3) inspection. The first step was to load the bridge until failure using the actuator with a capacity of 500 kN with displacement control. The second step was collecting data (encompassing load, deflection, strain, image, and voltage) for each test run from all the contact (including strain gauges, BDI sensors, and LVDTs) and non-contact sensors (including DIC system and UAV camera. The contact sensors were linked to the 128-channel data acquisition system, where the system can record 10 sets of data per second for each channel. The non-contact sensors were applied to record images at each inspection phase. For this step, voltage and current quantities from the solar panels were also measured from a multimeter at each test run. The bridge was inspected at regular intervals of loading which is the third step of the test. Visual inspections were conducted on all the sides of the bridge with the UAV and digital cameras when there was necessity to identify damage and/or to capture associated images at a certain test run. During this test, a total of 140 test runs and 7 inspections including the initial inspection were completed.

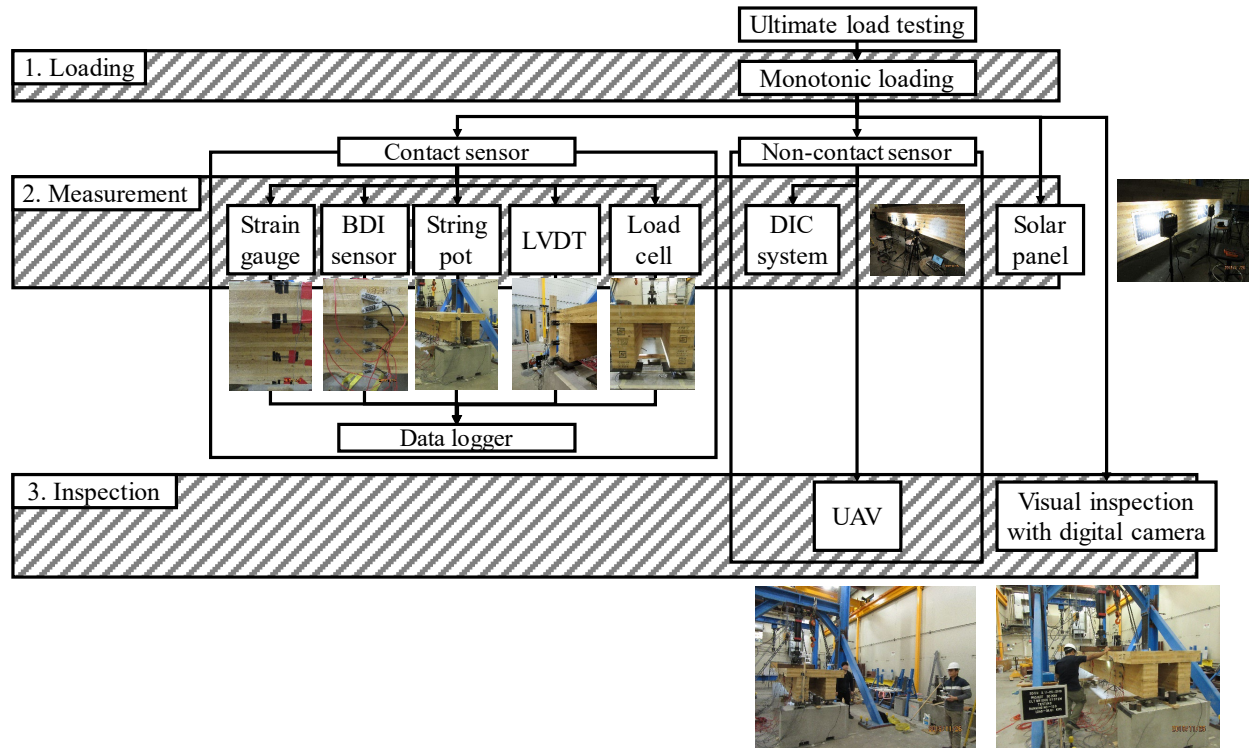


**Figure 2.92** Testing and data collection procedure of CLT bridge system

### 2.4.3.3 Results and Discussion

This section presents results from the ultimate strength testing for the CLT bridge system. All the data, including strain, slippage, deflection, and voltage along with imagery, obtained from the contact and non-contact sensors have been analyzed to evaluate structural performance of the bridge system.

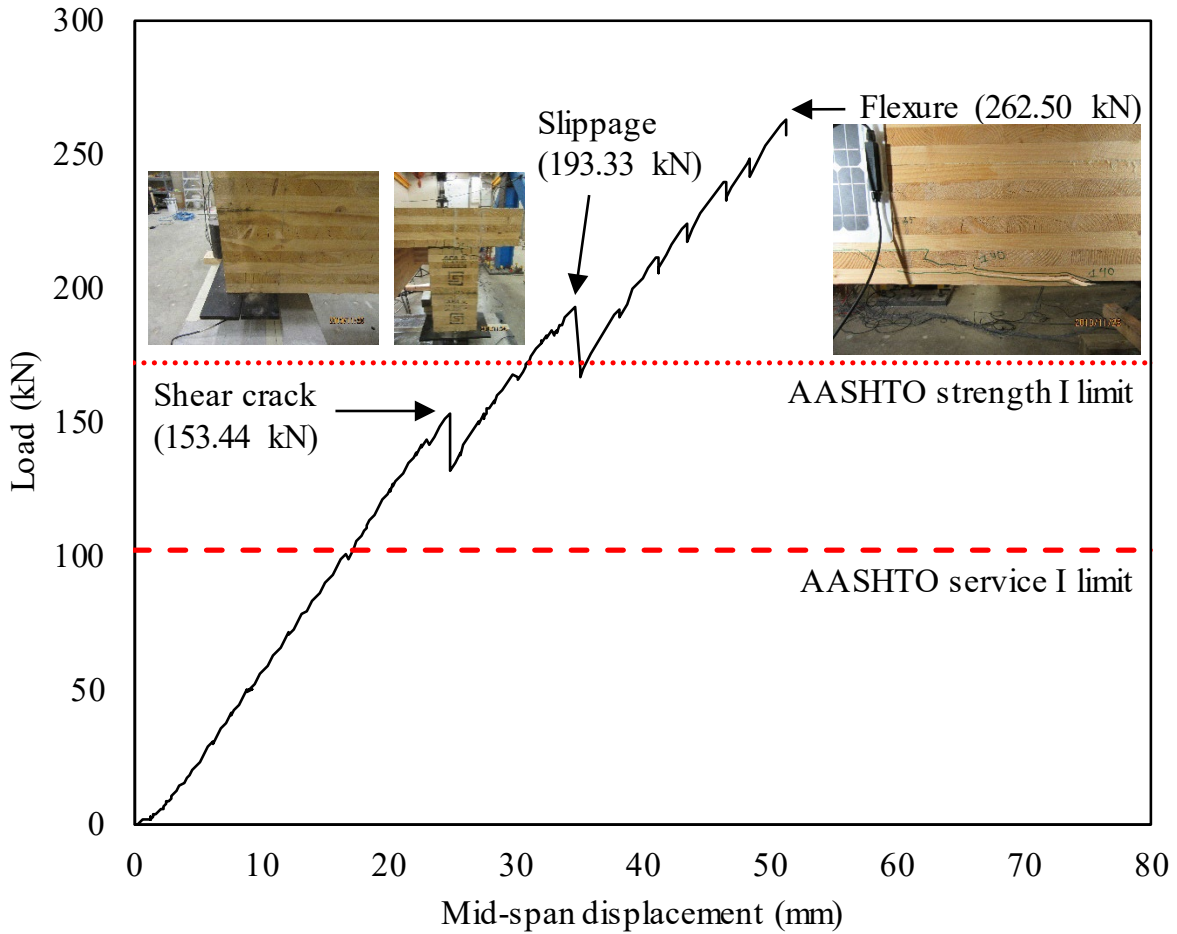
#### *Data from Contact Sensors*

A load-displacement curve is shown in Figure 2.93, where three failure stages, including the first failure: shear crack (153.44 kN) at 24.77 mm, the second failure: slippage failure (193.33 kN) at 34.67mm, and the third failure: flexural failure (262.50 kN) at 51.21 mm, were observed. As illustrated in Figure 2.94a, the first failure due to shear crack was observed at the south edge of the east girder. The second failure was spotted due to the slippage between the top of the girder and bottom of the deck as shown in Figure 2.94b. The third failure due to flexure was observed at the bottom of the east girder at an approximate distance of 2.5 m from the north edge as shown in Figure 2.94c. Based on the results, the ultimate strength of the bridge system was found to be 262.50 kN at the flexural failure. The strength of the tested CLT bridge is 34.65% higher than the AASHTO strength I limit strength and 61.14% higher than the AASHTO service I limit strength. The AASHTO limit strengths are also presented in Figure 2.93. Note, the AASHTO strength I limit strength and service I limit strength were calculated using Equations 49 and 50 (see the detailed calculation in Appendix L).

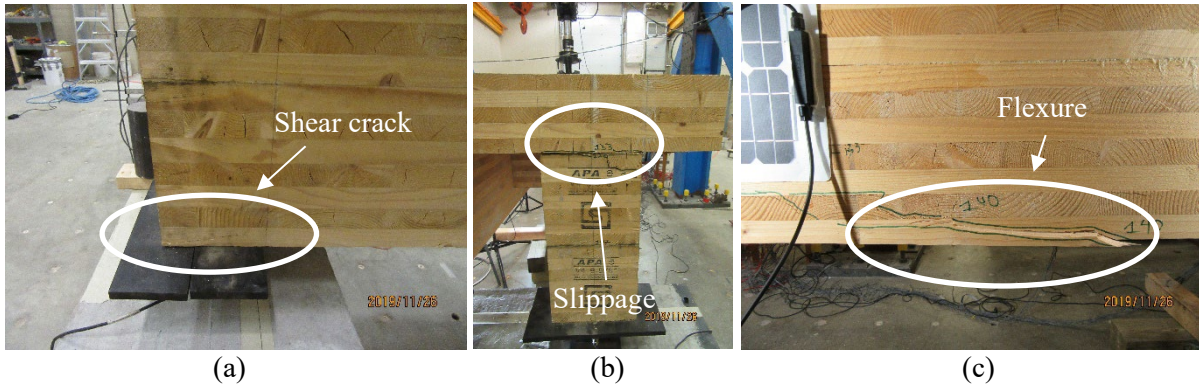
$$\text{AASHTO Strength I limit} = 1.25 DC + 1.75 LL \quad (49)$$

$$\text{AASHTO Service I limit} = 1.0 DC + 1.0 LL + 0.3 WS \quad (50)$$

where DC = component self-weight  
 LL = vehicle live load  
 WS = wind load on structure

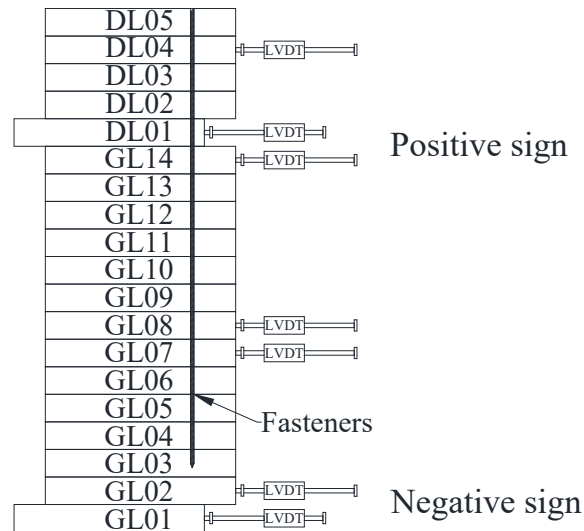


**Figure 2.93** Load-displacement curve for tested CLT bridge system



**Figure 2.94** Representative failure modes: (a) shear crack at south edge of the east girder, (b) slippage at south edge of the west girder, and (c) flexure failure on the east girder.

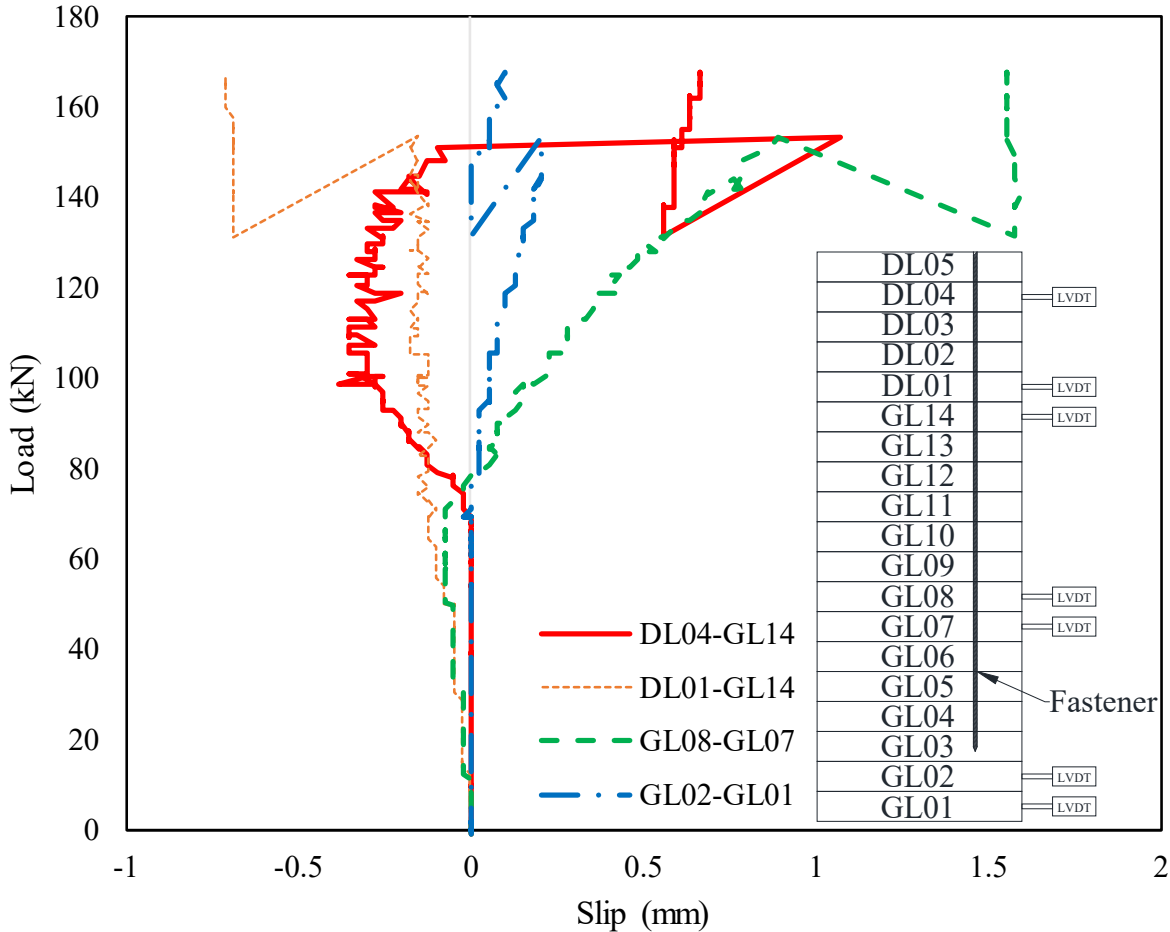
As mentioned previously, 7 LVDTs were installed at GL01, GL02, GL07, GL08, GL14, DL01, and DL04 (refer to schematic in Figure 2.95) to collect lateral displacements of 7 lams. One LVDT was installed at the top of the deck (DL04), whereas three sets of LVDTs were installed at the bottom of the deck-top of the girder (DL01 and GL14), middle of the girder (GL08 and GL07), and the lowest two lams (GL02 and GL01). To observe the behavior of deck and girder (deck top), lateral displacements of DL04 and GL14 and DL01 and GL14 were compared, while the other two sets of LVDTs recorded slippage between girder lams as shown in Figure 2.96. In this figure, slippage values defined as the difference in displacement of two lams were expressed in terms of positive and negative signs. If the displacement in the upper lam is larger than the displacement in the lower lam, the value is considered a positive slippage, while a negative slippage is deemed when the lower lam's displacement is larger than the upper one.



**Figure 2.95** Slippage sign convention

In Figure 2.96, the LVDT set installed at the deck bottom and girder top (DL01 and GL14) shows negative slippage, whereas the LVDT sets mounted on the girder middle (GL08 and GL07) and girder bottom (GL02 and GL01) exhibit mostly positive slippage during the testing. However, the LVDT set designated DL04 and GL14 changed the direction of slippage from negative to positive at 153.44 kN due to the shear cracking as shown in Figure 2.96. Note, the LVDTs were removed right after the first failure mainly caused by the shear cracking to avoid any damage to the instruments. The absolute maximum

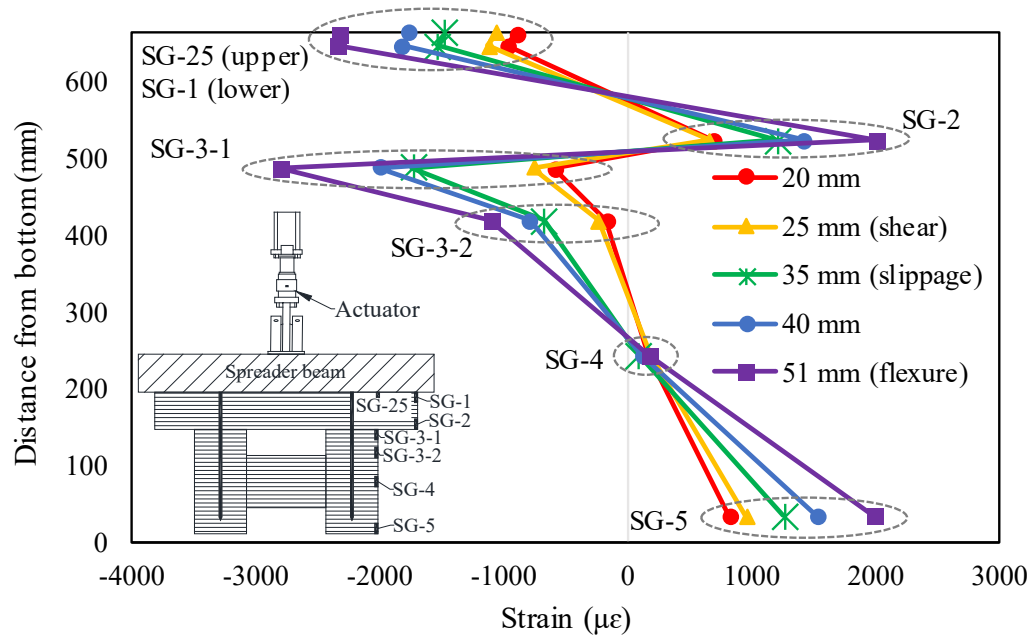
slippages recorded between DL04 and GL14, DL01 and GL14, GL07 and GL08, and GL02 and GL01 were 1.07 mm, 0.71 mm, 1.60 mm, and 0.20 mm, respectively. It turns out that the largest maximum slippage occurred between GL07 and GL08 based on all the slip results measured until shortly after the shear cracking took place.



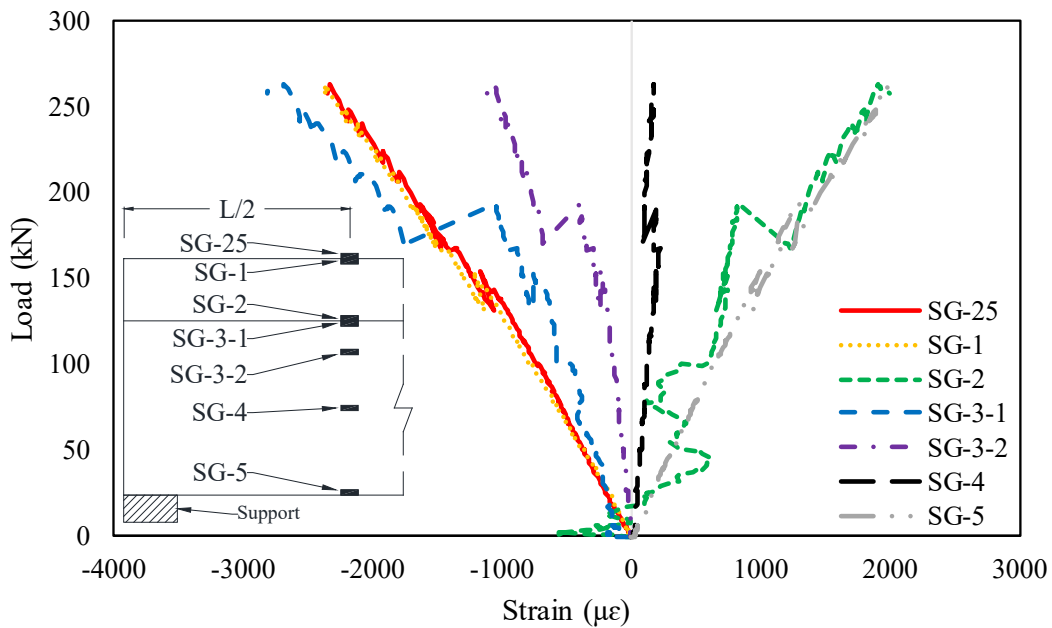
**Figure 2.96.** Slip between CLT lam obtained by LVDTs

Figure 2.97a shows the strain profile along the distance from the bottom of the girder to evaluate the neutral axis of the bridge at mid-span of the bridge. As stated before, 7 strain gauges were installed at the top surface of the deck (SG-25), at the top of the deck side (SG-1), at the bottom side of the deck (SG-2), at the top of the girder (SG-3-1), at a theoretically calculated neutral axis (SG-3-2), at the center of the girder (SG-4), and at the bottom of the girder (SG-5). SG-25, SG-3-1, SG-3-2, SG-4, and SG-5 were installed in the same vertical alignment, but any strain gauge was not able to be installed at the bottom surface of the deck. When determining the neutral axes, data from SG-2 representing the bottom side of the deck was used instead. In Figure 2.97a, the locations of the neutral axes corresponding to each of the critical deflections of 20 mm, 25 mm (shear failure), 35 mm (slippage failure), 40 mm, and 51 mm (flexure failure) are determined. It appears that there exist two neutral axes for the CLT deck and the CLT girder, which means the tested bridge behaves as a non-composite section. In detail, the average neutral axis of the CLT deck at the deflections of 20 mm through 51 mm was located at 86.93mm from the bottom of the deck, while that of the CLT girder was positioned at 288.54 mm from the bottom of the girder.

In Figure 2.97b, SG-1 and SG-25 show similar strain quantities during the testing as expected. The strain gauges SG-2, SG-3-1, SG-4, and SG-3-2 manifest a significant change in the strain at 193.33 kN due to slippage failure. Negative strain in compression is observed in SG-25, SG-1, SG-3-1, and SG-3-2, whereas positive strain in tension is observed in SG-4 and SG-5. However, negative strain in compression is initially found in SG-2 until 16.72 kN after which the direction of the strain changes to positive in tension. At the early stage, the behavior of the CLT bridge at the mid-span was found to be composite, which later changed to non-composite behavior after 16.72 kN.



(a)

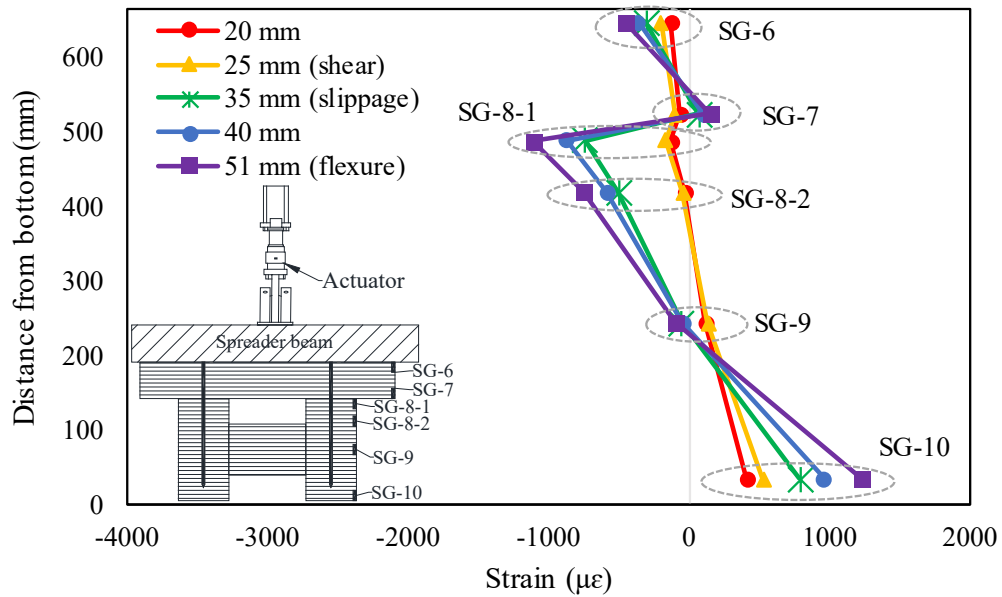


(b)

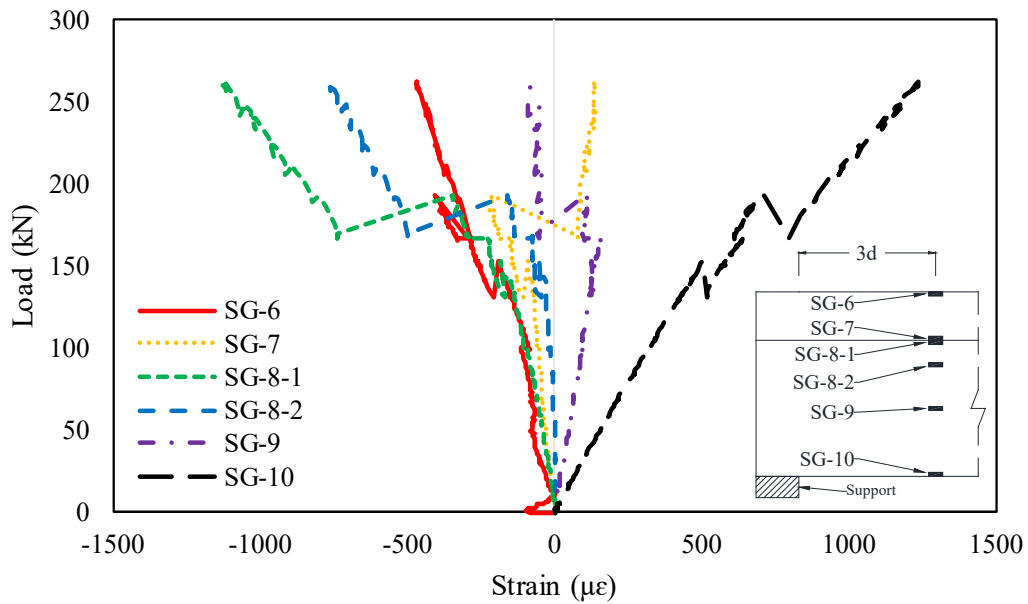
**Figure 2.97** Strain gauges installed on mid-span of bridge: (a) strain profile and (b) load-strain curves

Figure 2.98a shows the strain profile along the distance from the bottom of the girder to evaluate the neutral axis of the bridge at  $3d$  from the north support. Again, the strain gauges were installed at the top of the deck (SG-6), bottom of the deck (SG-7), top of the girder (SG-8-1), at the expected neutral axis (SG-8-2), in the middle of the girder (SG-9), and at the bottom of the girder (SG-10). In Figure 2.98a, the locations of the neutral axes corresponding to each of the critical deflection of 20 mm, 25 mm (shear failure), 35 mm (slippage failure), 40 mm, and 51 mm (flexure failure) are determined. The average neutral axis at the deflections of 20 mm through 25 mm was located at 379.72 mm from the bottom of the girder, indicating that the tested bridge acts as a composite section. After the slippage failure, however, it is obvious that there are two neutral axes for the deck and the girder, where the tested bridge shows non-composite behavior. The average neutral axes at the deflections of 35 mm through 51 mm were located at 63.46 mm from the bottom of the deck and 231.34 mm from the bottom of the girder. It has been demonstrated that the slippage failure has significantly affected the neutral axis of the CLT bridge at  $3d$  from the north support. In Figure 2.98b, a significant change in the strain is observed in all strain gauges due to the slippage failure after the load reached 193.33 kN. Specifically, the strain recorded from SG-7 changed from negative to positive at 193.33 kN due to the slippage failure.





(a)



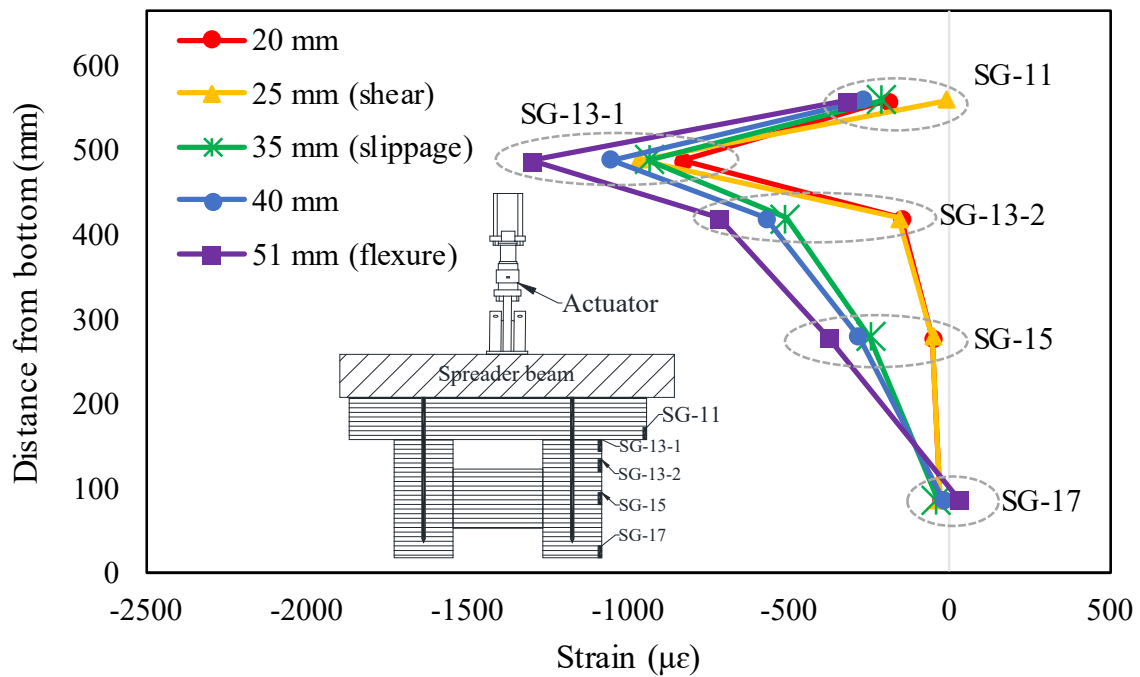
(b)

**Figure 2.98** Strain gauges installed on  $3d$  from the north support: (a) strain profile and (b) load-strain curves

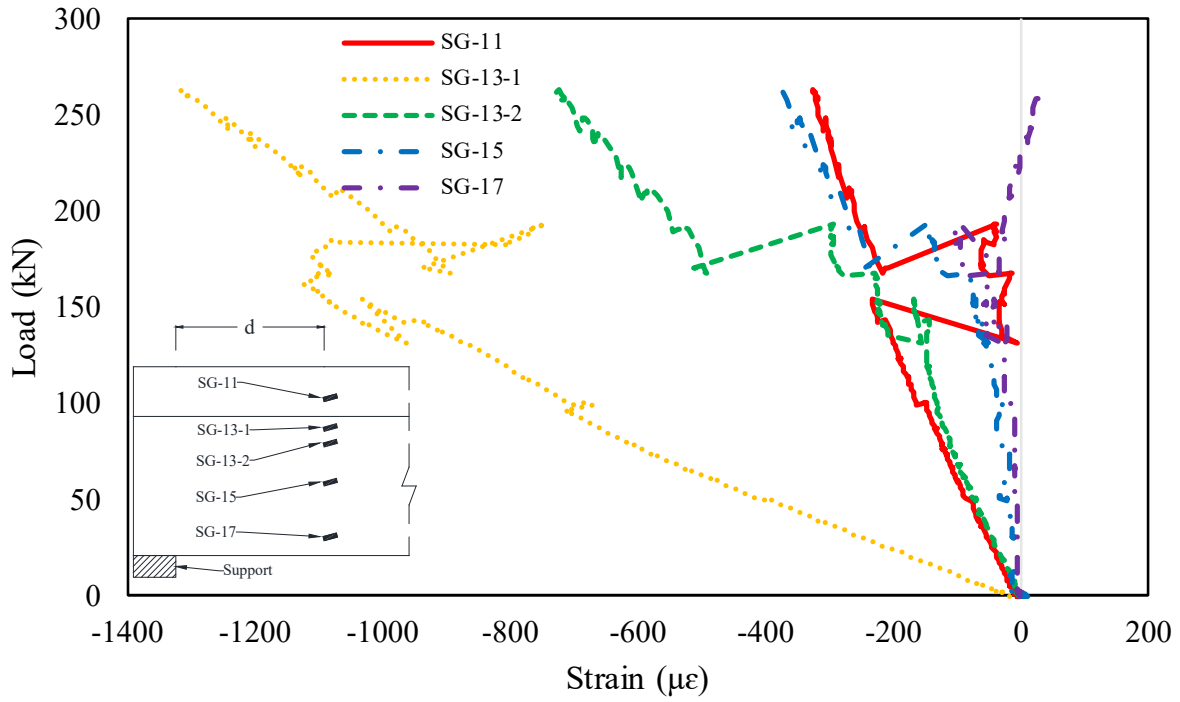
As depicted in Figure 2.99, strain profiles were created from data recorded from the strain gauges installed at  $d$  from the north support of the girder. It should be reminded that these gauges were installed at the bottom of the deck (SG-11 and SG-12), top of the girder (SG-13-1 and SG-14-1), theoretically calculated neutral axis (SG-13-2 and SG-14-2), middle of the girder (SG-15 and SG-16), and bottom of the girder (SG-17 and SG-18). SG-11, SG-13-1, SG-13-2, SG-15, and SG-17 in Figures 2.99a and 2.99b

indicate upper gauges installed at an up angle of 15 degree with respect to a reference line, whereas SG-12, SG-14-1, SG-14-2, SG-16, and SG-18 in Figures 2.99c and 2.99d indicate lower gauges mounted on a down angle of 15 degree from the reference line.

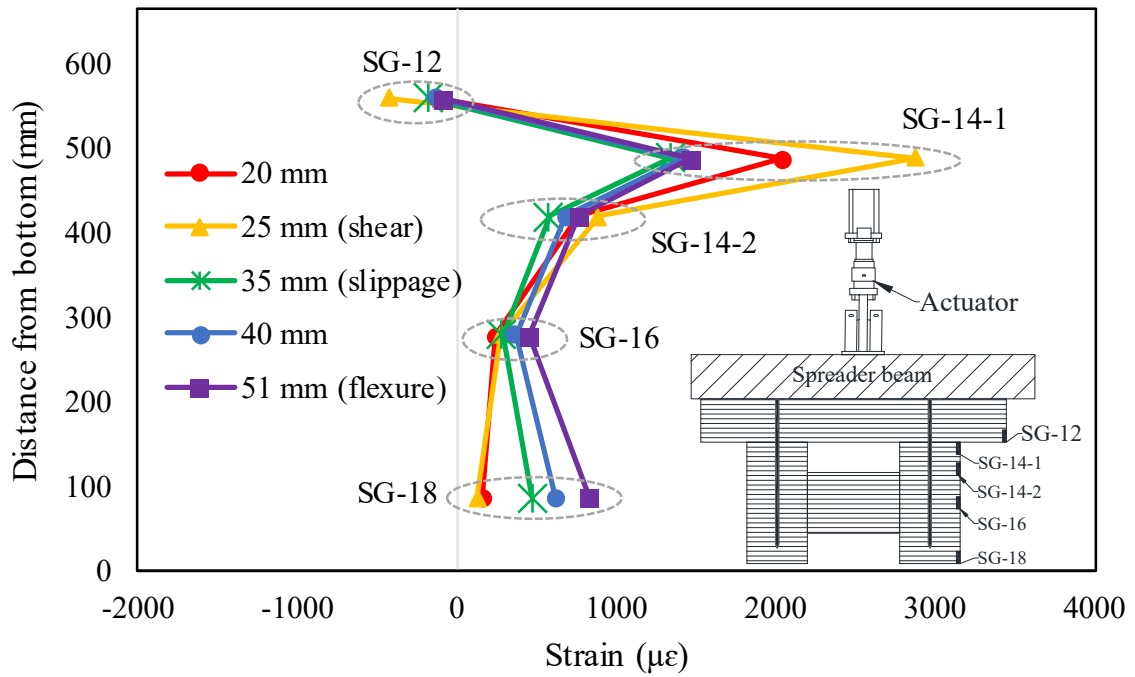
In Figure 2.99a, the neutral axis at the deflections of 20 mm through 40 mm was out of boundary of the bridge depth, whereas the neutral axis at 51 mm (flexural failure) was located at 100.25 mm from the bottom of the girder. In Figure 2.99b, negative strain in compression is observed in all strain gauges before 231.92 kN load, whereas the strain from SG-17 changes from negative in compression to positive in tension after 231.92 kN. The strain recorded from SG-11 changed significantly at 153.44 kN due to the shear cracking and 193.33 kN due to the slippage failure. As shown in Figure 2.99c, the average neutral axis to all the deflections is 28.78 mm from the bottom of the deck. No significant change in the neutral axes was found during the testing. In Figure 2.99d, all the strain gauges, SG-14-1 in particular, show a significant change in strain at 193.33 kN, whereas the strain obtained from SG-12 changes abruptly at 153.44 kN due to the shear cracking. Interestingly, SG-12 show negative strain in compression for the entire testing period.



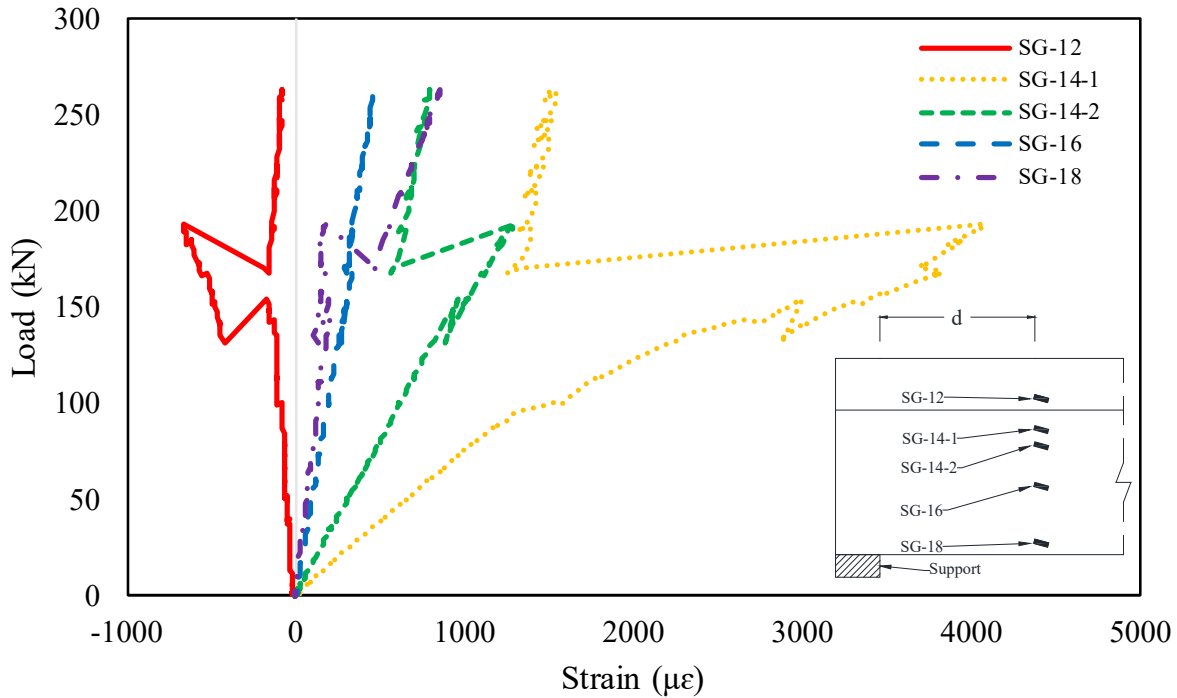
(a)



(b)



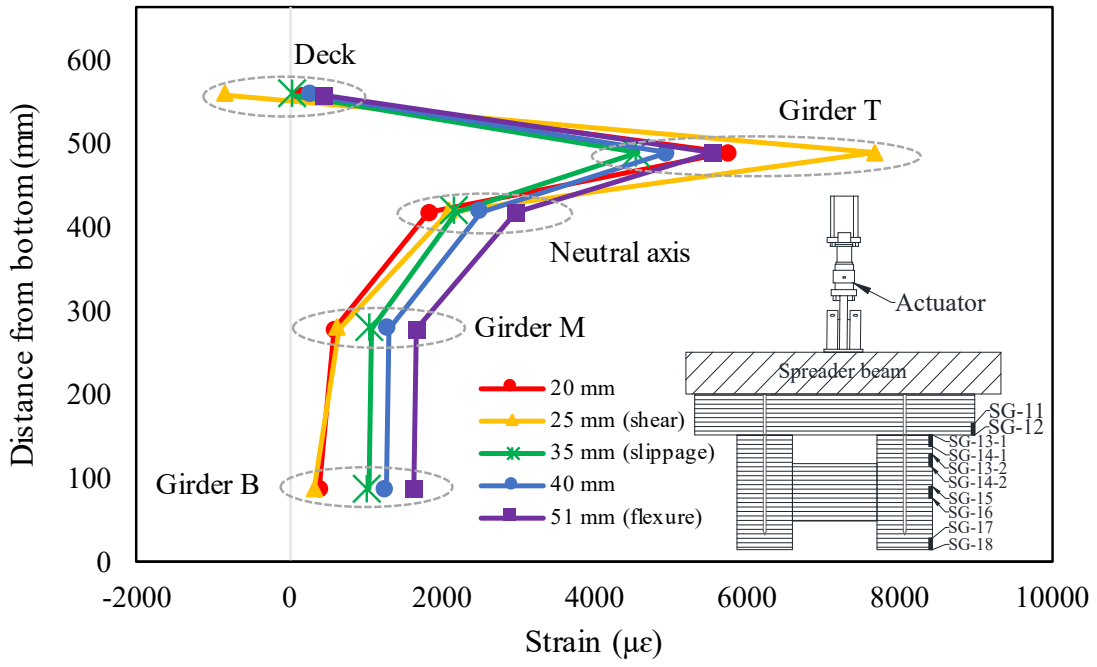
(c)



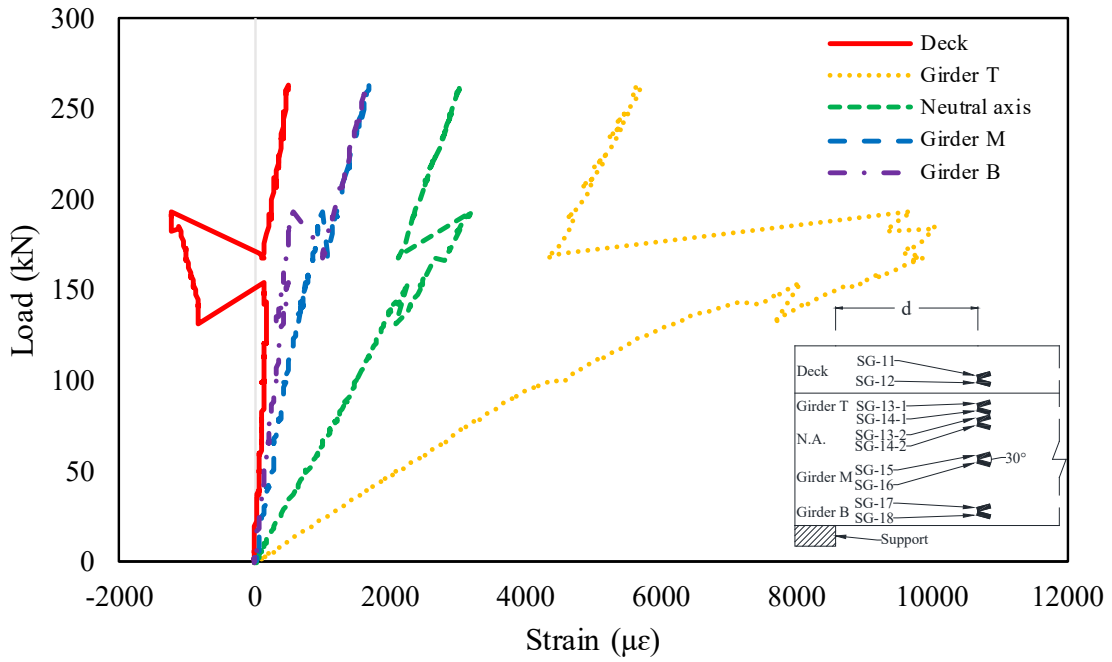
(d)

**Figure 2.99** Strain gauges installed on  $d$  from the north support: (a) strain profile (upper); (b) load-strain curves (upper); (c) strain profile (lower); and (d) load-strain curves (lower)

Figure 2.100a shows the profile of the shear strain along the distance from the bottom of the girder to evaluate the neutral axis of the bridge at  $d$  from the north support. As described formerly, 10 strain gauges collected shear strain data on the west side of the bridge at  $d$  from the north support. The strain gauges were attached on the lower side of the deck (Deck, SG-11 and SG-12), at the top of the girder (Girder T, SG-13-1 and SG-14-1), at theoretically predicted neutral axis (Neutral Axis, SG-13-1 and SG-14-1), at the center of the girder (Girder M, SG-15 and SG-16), and at the bottom of the girder (Girder B, SG-17 and SG-18). The shear strain calculated using the strain values gained from each pair of two strain gauges installed at an angle of 30 degree (e.g., SG-11 and SG-12) through Equation 44 is plotted in Figure 100a for the strain profile and Figure 2.100b for the load-strain curve. At the deflections of 20mm, 35 mm, 40mm, and 51 mm, any neutral axes are not discovered within the depth of the bridge as shown in Figure 2.100a. In this figure, however, the neutral axis at the deflection of 25 mm is located at 45.27 mm from the bottom of the deck. As depicted in Figure 2.100b, the maximum shear strain appears at the top of the west girder (Girder T). This trend is not consistent with the fact that the maximum shear strain occurs at the expected neutral axis of ordinary bridge systems that do not tend to have any slippage failure.



(a)

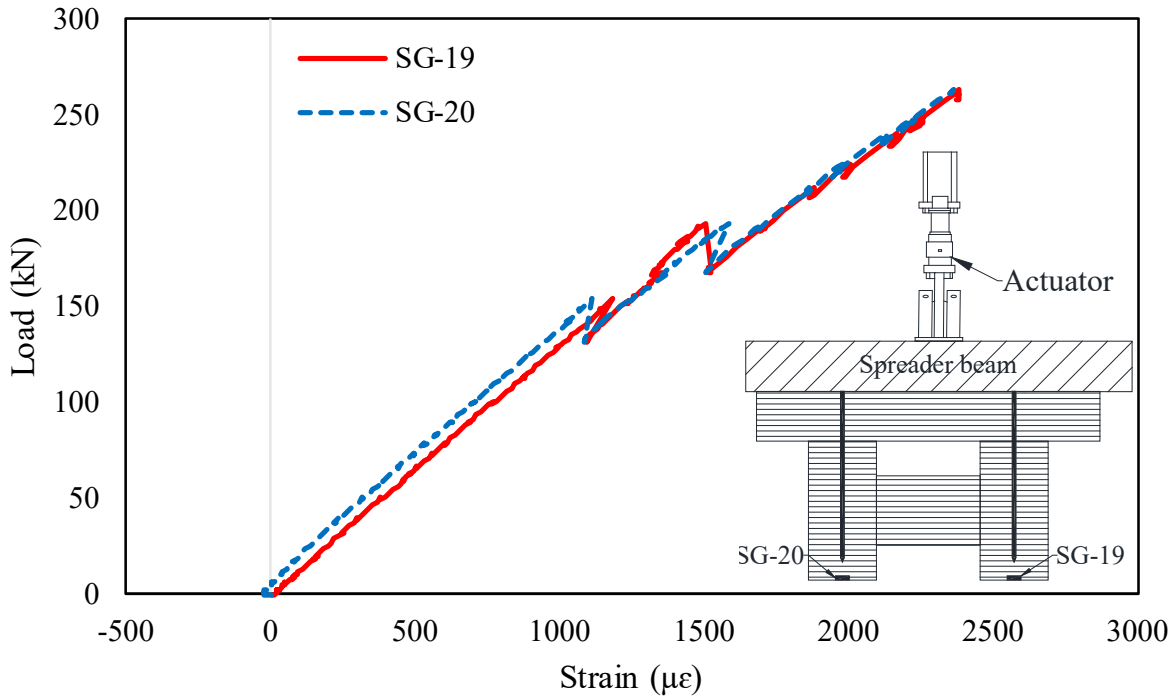


(b)

Note: Girder T, Girder M, Girder B, and N.A. indicate girder top, girder middle, girder bottom, and neutral axis, respectively.

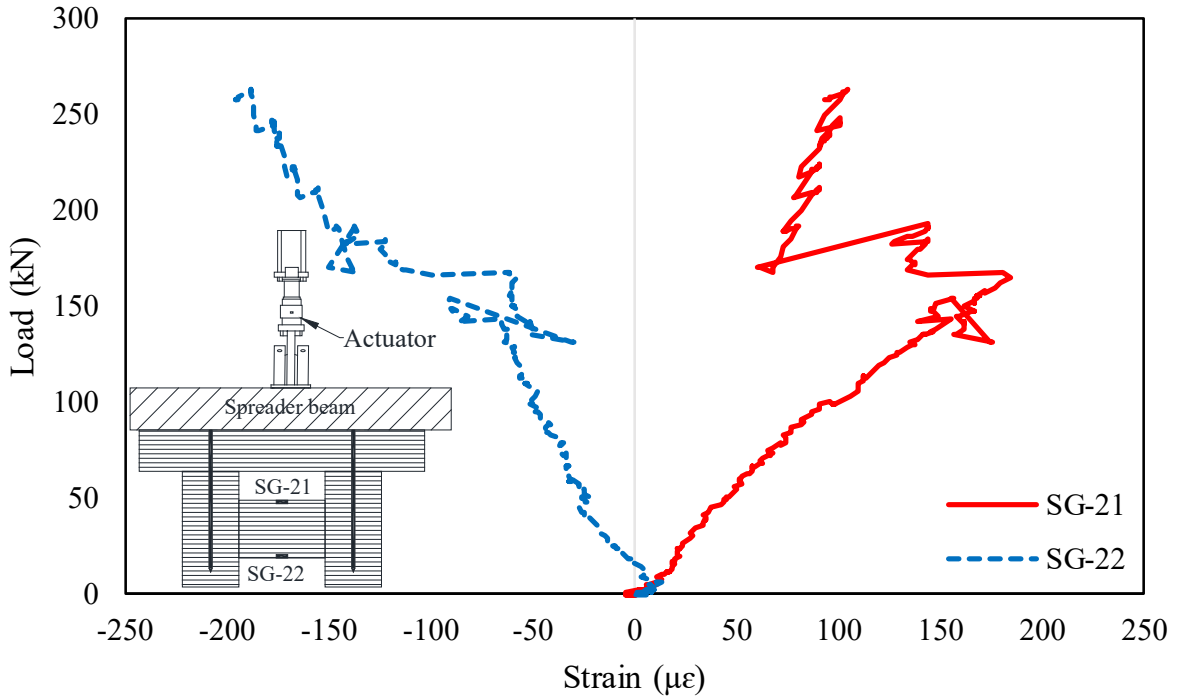
Figure 2.100 Shear strain on  $d$  from the north support: (a) strain profile and (b) load-strain curves

Figure 2.101 shows load-strain curves for both CLT girders. It should be reminded that the strain gauges were installed underneath the west girder (SG-19) and the east girder (SG-20) at the mid-span. Positive strain in tension was observed at the location of both SG-19 and SG-20 as anticipated. A significant change in the strain was observed in all strain gauge locations due to shear crack at 153.44 kN and slippage failure at 193.33 kN. In this figure, the strain obtained from SG-19 and SG-20 followed the similar trend during the testing, which means each girder shares the applied load almost equally.

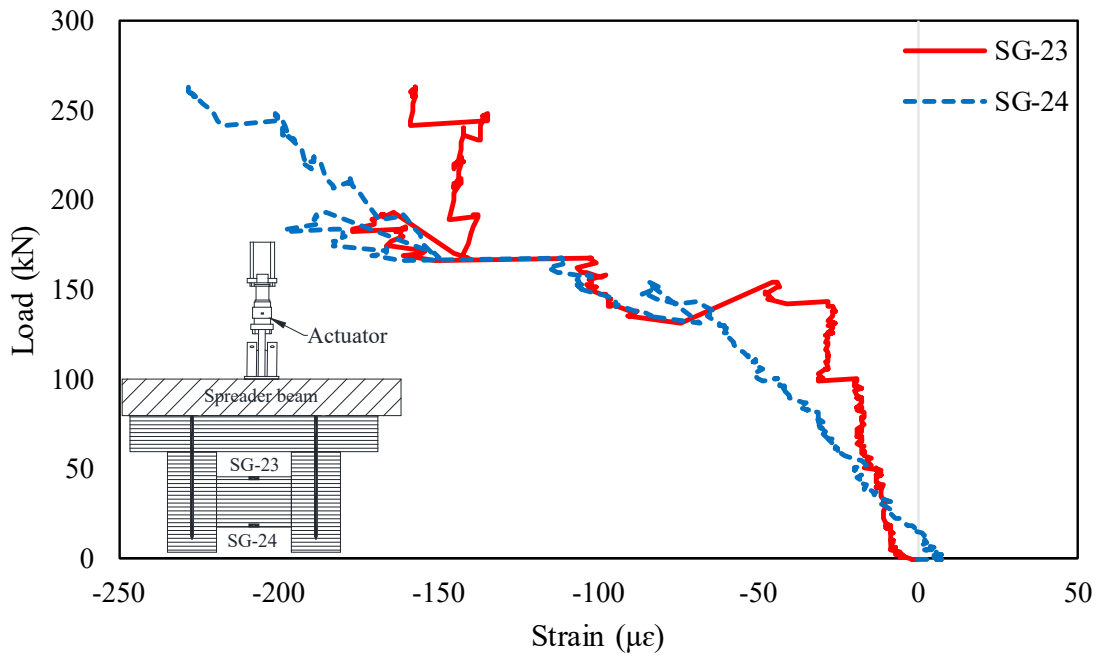


**Figure 2.101** Strain gauges installed underneath the girders at mid-span

Figure 2.102 shows load-strain curves for the north and south diaphragms, where each diaphragm was installed between the girders. The strain gauges SG-21 and SG-22 were attached to the top and bottom of the north diaphragm, and the strain gauges SG-23 and SG-24 were mounted on the top and bottom on the south diaphragm. As depicted in Figure 2.102a, positive strain in tension and negative strain in compression can be observed for SG-21 and SG-22, respectively. As shown in Figure 2.102b, both SG-23 and SG-24 gauges show negative strain in compression. Noticeably, the strain behavior for the south diaphragm is different from that for the north diaphragm as a result of the initial shear cracking at the east girder at the south support.



(a)



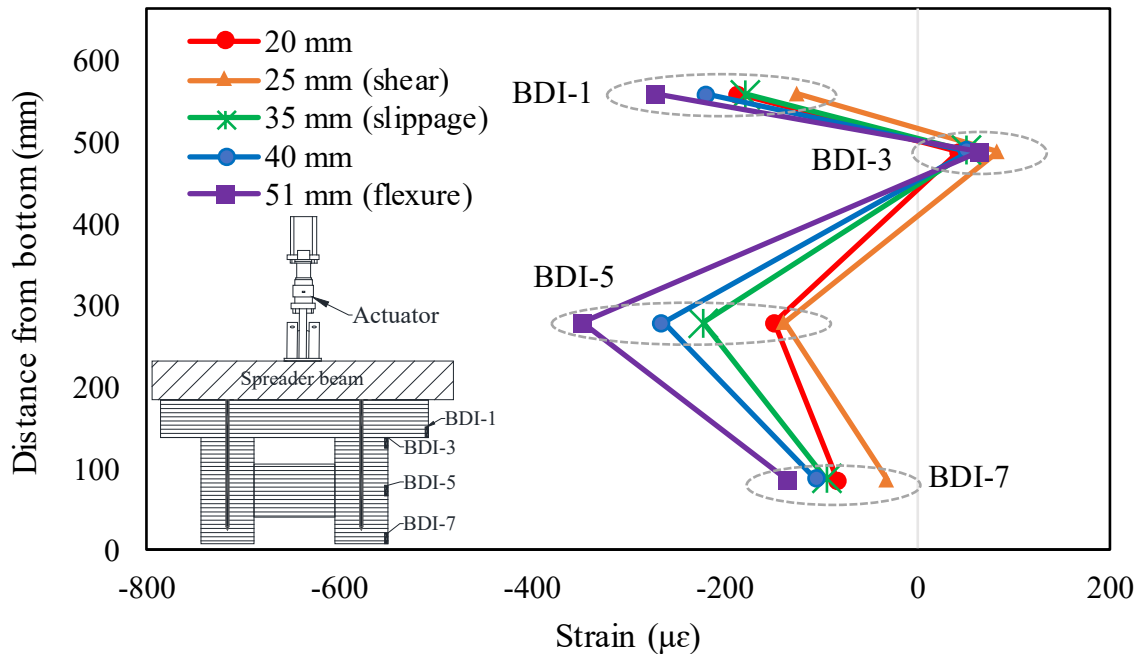
(b)

**Figure 2.102** Strain gauges installed on the diaphragms: (a) north diaphragm and (b) south diaphragm

Figures 2.103 and 2.104 display the strain profiles and load-strain curves recorded from the BDI strain sensors at  $d$  from the south support of the bridge. Again, the 8 strain sensors were installed at the bottom of the deck (BDI-1 and BDI-2), at the top of the girder (BDI-3 and BDI-4), in the middle of the girder

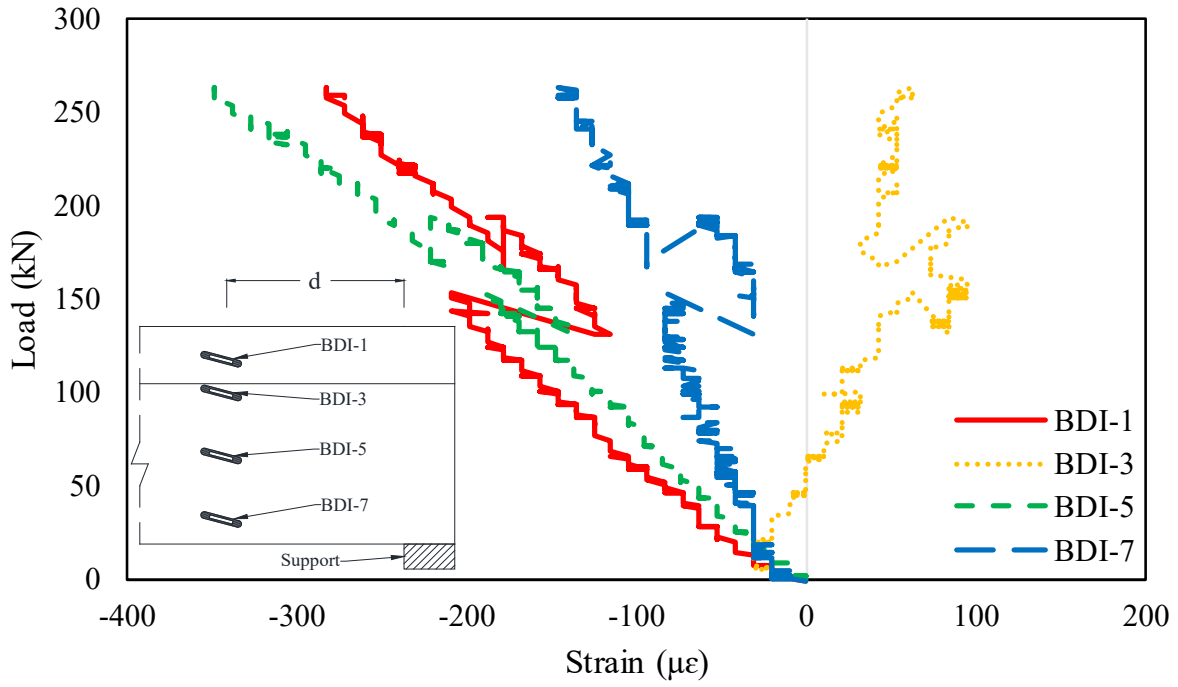
(BDI-5 and BDI-6), and at the bottom of the girder (BDI-7 and BDI-8). BDI-1, BDI-3, BDI-5, and BDI-7 in Figures 2.103a and 2.103b mean upper gauges installed at an up angle of 15 degree with respect to a reference line, whereas BDI-2, BDI-4, BDI-6, and BDI-8 in Figures 2.103c and 2.103d stand for lower gauges mounted at an down angle of 15 degree from the reference line.

In Figure 2.103a, the neutral axes corresponding to critical deflections of 20 mm, 25 mm (shear failure), 35 mm (slippage failure), 40 mm, and 51 mm (flexure failure) are evaluated. The average neutral axes were positioned at 16.64 mm from the bottom of the deck and 442.43 mm from the bottom of the girder at the deflections of 20 mm through 51 mm, indicating that the tested bridge exhibits a non-composite behavior. In Figure 2.103b, negative strain in compression is observed at BDI-1, BDI-5, and BDI-7, whereas positive strain in tension is noticed at BDI-3 after 46.30 kN. As illustrated in Figure 2.103c, the average neutral axis is positioned at 54.87 mm from the bottom of the deck at the deflections of 20 mm through 51 mm, but the neutral axes of the girder are out of the girder depth. It is apparent that no significant change in the position of neutral axes for both deck and girder occurs during the testing. As shown in Figure 2.103d, BDI-4, BDI-6, and BDI-8 are found to be in tension with positive strain, whereas negative strain in compression is observed at the location of BDI-2. Figures 2.103b and 2.103d displayed an abrupt change in strain after the slippage failure at 193.33 kN.

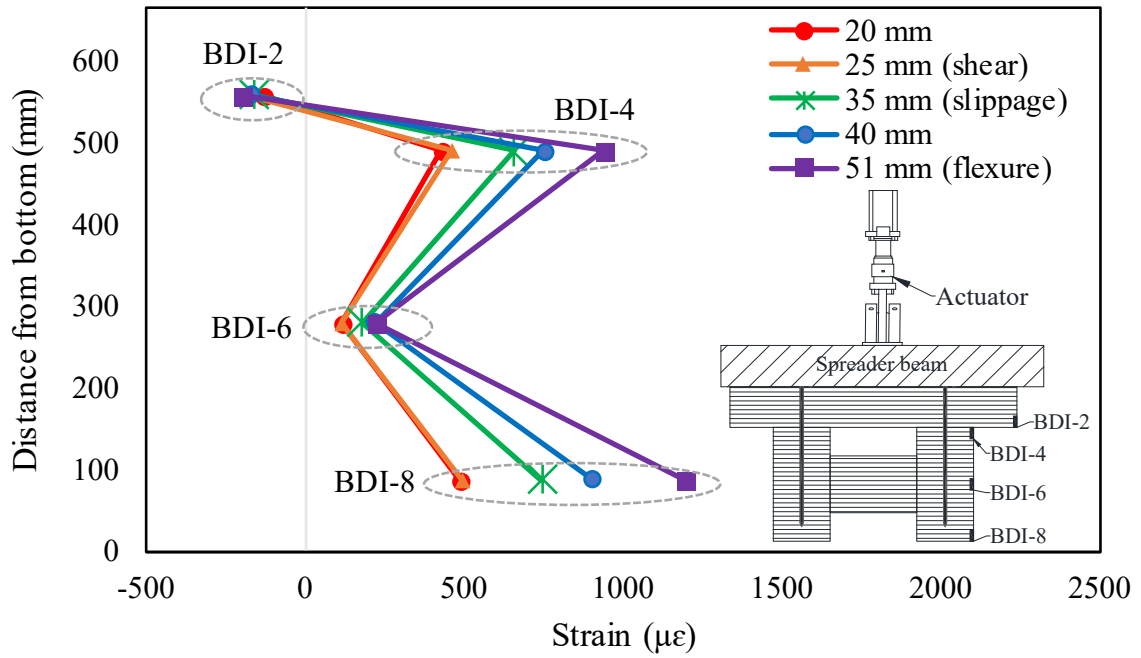


(a)

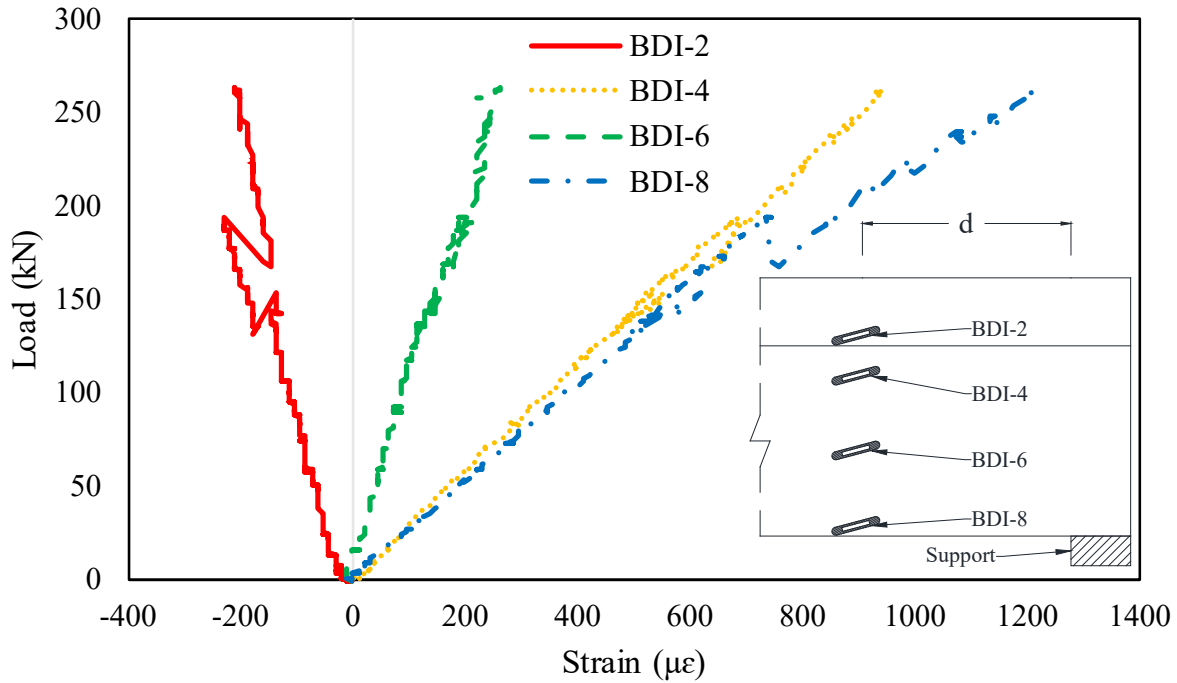




(b)



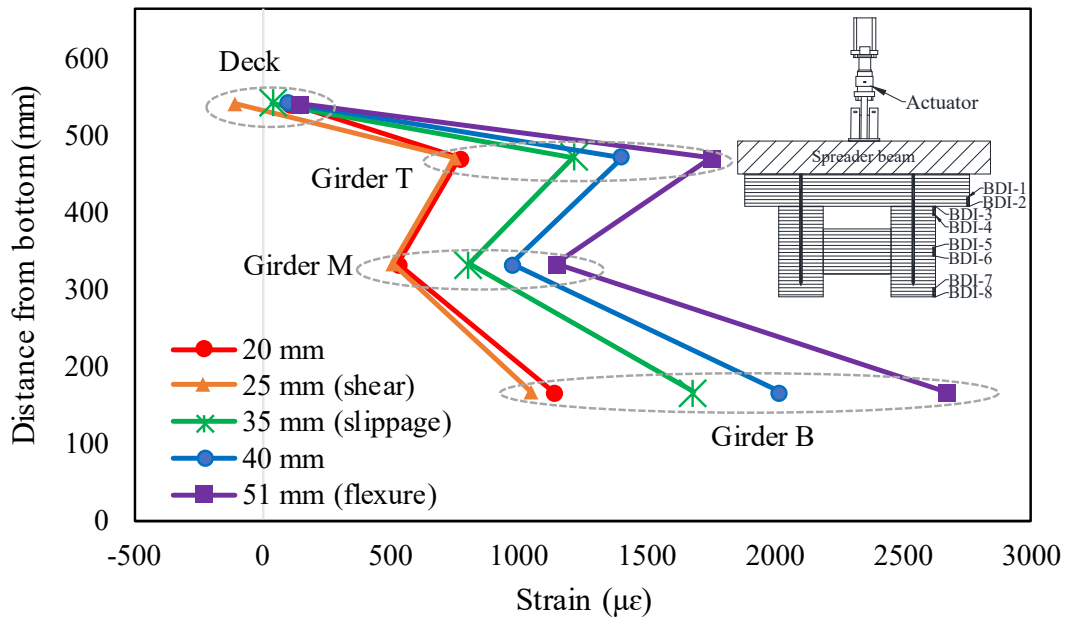
(c)



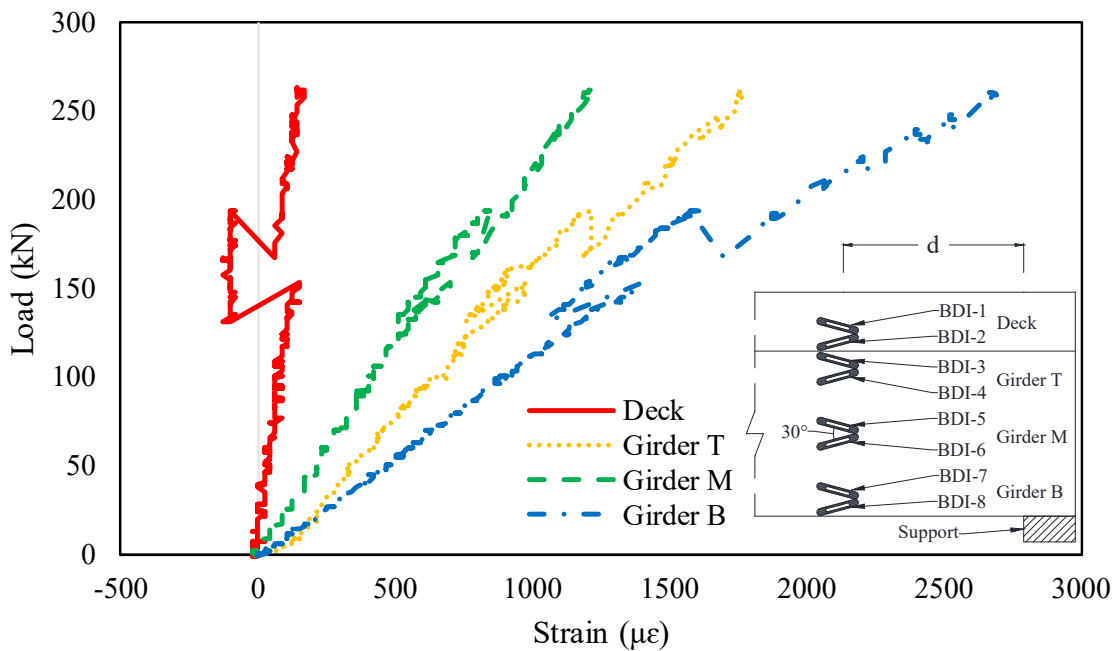
(d)

**Figure 2.103** BDI strain sensors installed on  $d$  from the south support: (a) strain profile (upper); (b) load-strain curves (upper); (c) strain profile (lower); and (d) load-strain curves (lower)

Figure 2.104 shows the shear strain calculated from Equation 44 using each pair of two strain values presented in Figures 103c through 103d. As described above, BDI strain sensors were mounted on the lower side of the deck (Deck, BDI-1 and BDI-2), at the top of the girder (Girder T, BDI-3 and BDI-4), at the middle of the girder (Girder M, BDI-5 and BDI-6), and at the bottom of the girder (Girder B, BDI-7 and BDI-8). As shown in Figure 2.104a, the neutral axis was positioned at 43.76 mm from the deck for 25 mm deflection, whereas no neutral axis was discovered at the remaining deflections of 20 mm, 35 mm, 40 mm, and 51 mm. The maximum shear strain is found to be at the bottom of the girder (Girder B) during testing as shown in Figure 2.104b. This trend is not in line with the fact that maximum shear strain occurs at the neutral axis of composite bridge.



(a)



(b)

Note: Girder T, Girder M, and Girder B specify girder top, girder middle, and girder bottom, respectively.

**Figure 2.104** BDI strain sensors installed on  $d$  from the south support: (a) strain profile and (b) load-strain curves

### Data from Non-contact Sensors

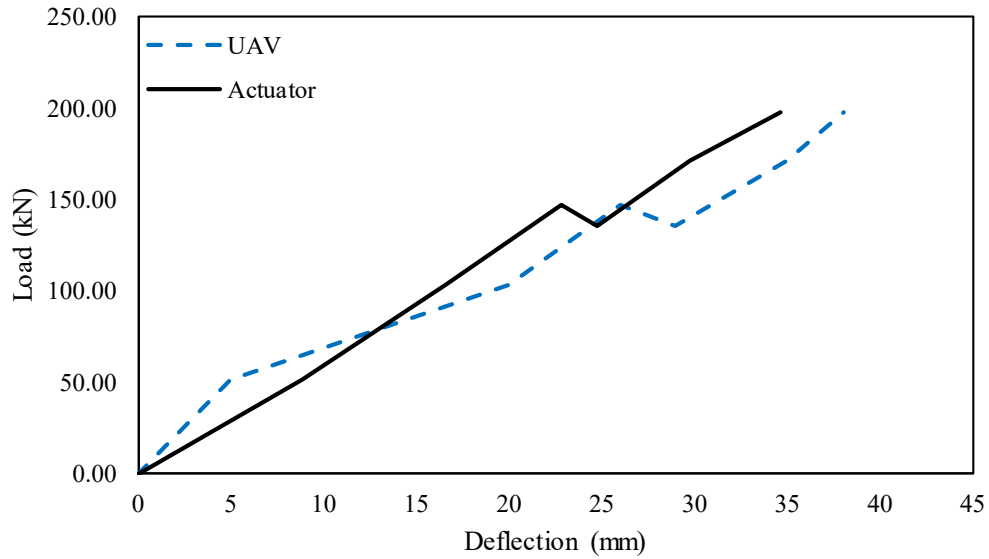
During the testing, the CLT bridge system was inspected at certain intervals with the aforementioned non-contact sensors as shown in Figure 2.105. The UAV (see Figure 2.105a) and DIC system (see Figure 2.105b) in conjunction with the digital camera were used for the inspections. We performed 7 inspections (in total) on the tested CLT bridge. Multiple images were collected from the gimbal camera attached on UAV Phantom 4 to determine the deflection and quantify damage through image processing of the collected images. As used in the previous two CLT girder testings, ImageJ coupled with the same algorithm was applied to this testing to measure the deflection and detect damage on the CLT bridge.



**Figure 2.105** Non-contact sensor operation: (a) UAV and (c) DIC system

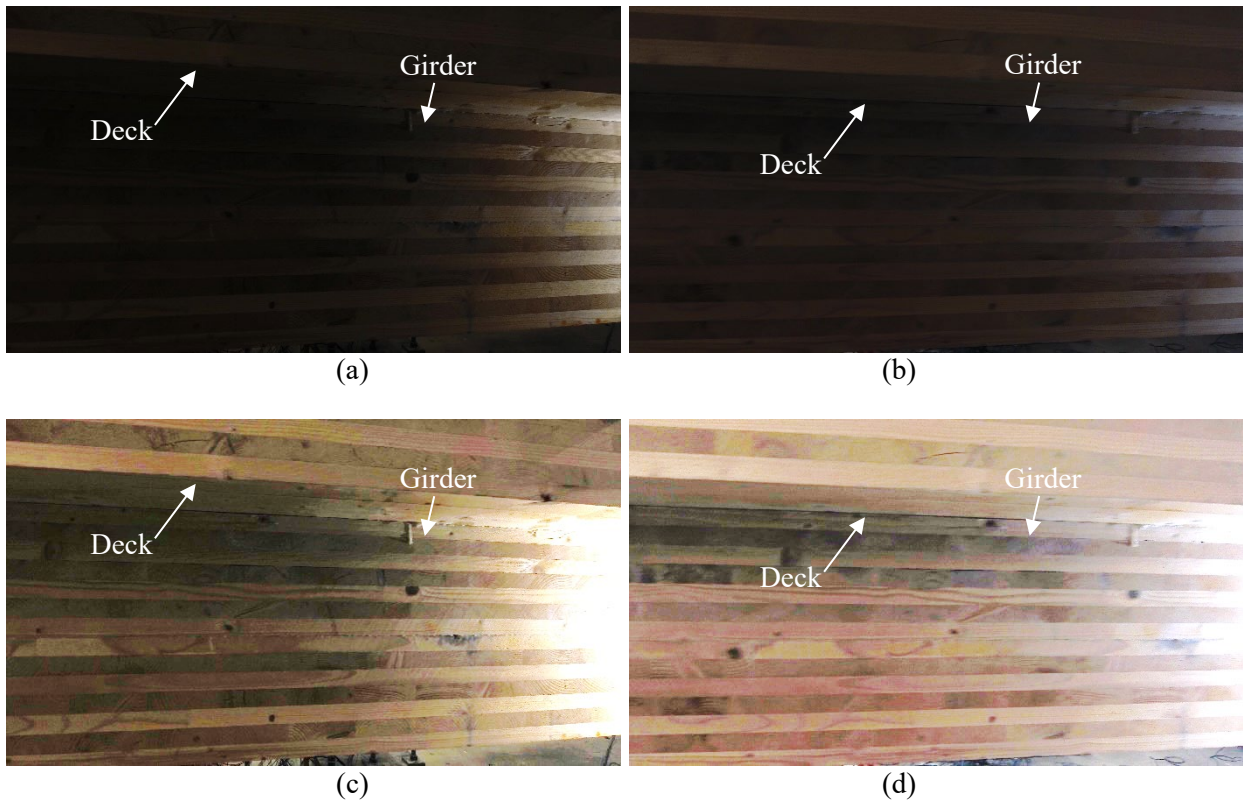
Deflection in the bridge system was analyzed using ImageJ software to measure deflection and the size of the damage. Pixel-based relative length can be measured with ImageJ. A graphical comparison of the deflections at mid-span recorded from the UAV and actuator is shown in Figure 2.106. The average difference between the deflection measured from inspection images captured from UAV and actuator's deflection was found to be 5.57 mm as displayed in Figure 2.106. Deflections measured from the UAV were found to be in acceptable range. Note, lam thickness (34.93 mm) was taken as a reference length to calculate the deflection for image analysis.

A comparison of the mid-span deflections measured from the UAV and actuator is shown in Figure 2.106. The average difference between the UAV and actuator deflections was found to be 5.57 mm, and corresponding average percentage error was 17.59%. The results demonstrated the effectiveness of the image analysis incorporating the UAV-enabled inspection images to estimate the mid-span deflection of the CLT bridge system with reasonable level of accuracy.



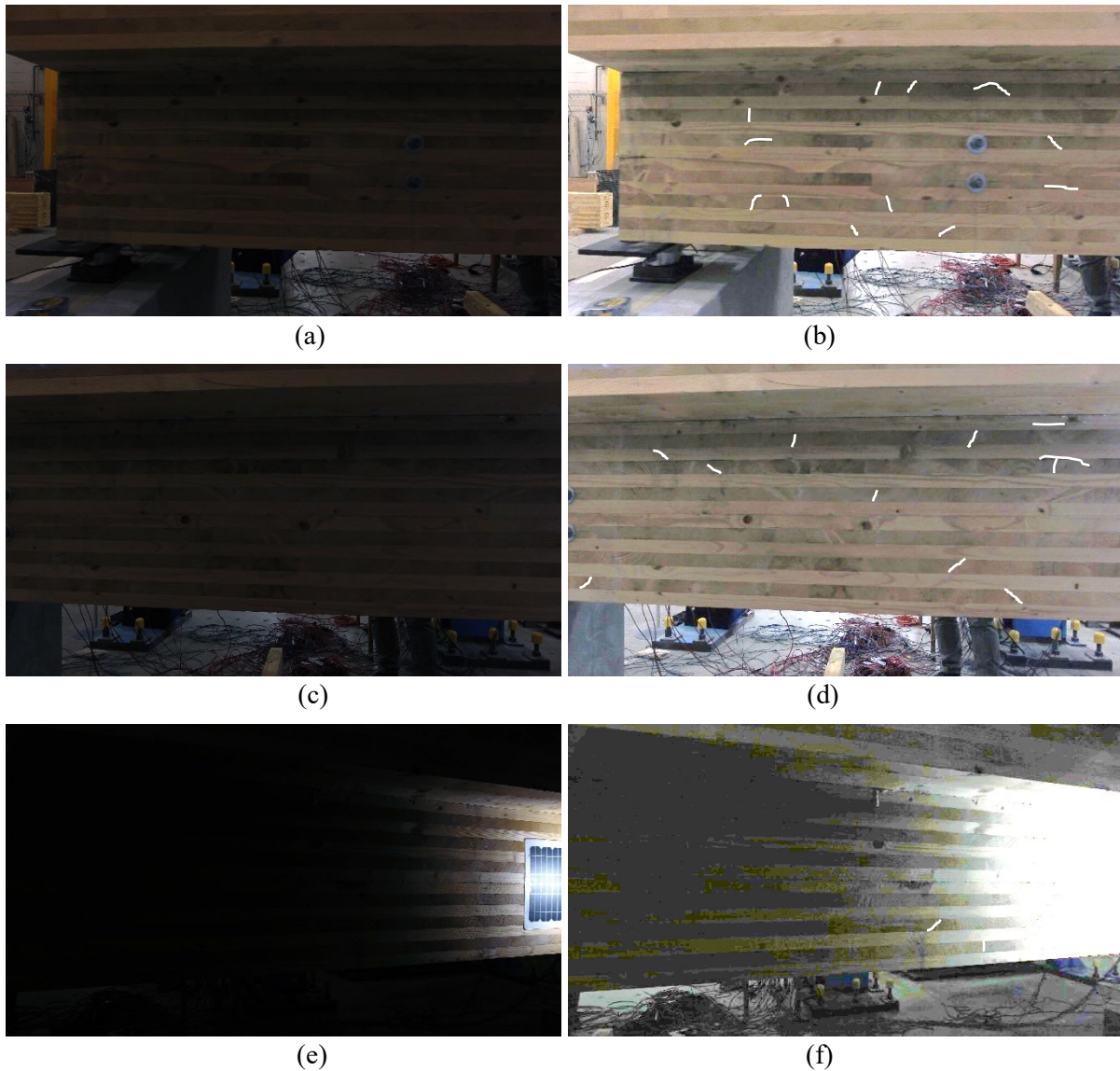
**Figure 2.106** Deflection comparison using UAV and actuator

Figure 2.107 depicts the UAV inspection images utilized for the deflection measurement. Figures 2.107a and 2.107b show raw inspection images taken by the UAV at 0 mm and 51.21 mm deflections. These images have low brightness. With these images, we were not able to identify the position of the actuator and determine the mid-span deflections. For a better deflection measurement, Figure 2.107a was adjusted with 70% brightness and 20% contrast (see Figure 2.107c) and Figure 2.107b was amended with 70% brightness and 30% contrast (see Figures 2.107d). With the adjusted images, the mid-span deflections were efficiently calculated through the image analysis.



**Figure 2.107** Inspection images captured depending on displacement of actuator: (a) 0 mm; (b) 51.21 mm; (c) Figure 2.107a adjusted with brightness 70% and contrast 20%; and (d) Figure 2.107b adjusted with brightness 70% and contrast 30%

With inspection images taken with the UAV, all visible damages on the south east section of the tested CLT bridge system are observed as shown in Figure 2.108. Due to the low brightness of original UAV images (Figure 2.108a, Figure 2.108c, and Figure 2.108e), the brightness and contrast of the images were adjusted as displayed in Figure 2.108b, 2.108d, and 2.108f. Figure 2.108a and 2.108c were adjusted with the brightness of 70% and contrast of -10% as displayed in Figure 2.108b and 108d, respectively. Figure 2.108e was amended with the increase by 90% brightness and the decrease by -20% contrast as depicted in Figure 2.108f. Note, a damage map was not created due to no inspection data from the manipulator, where it could not be operated for the limited space.



**Figure 2.108** South east sections of the east girder of the CLT bridge system before the testing captured by UAV: (a) Sections 1 through 4; (b) Figure 108a adjusted with brightness 70% and contrast -10%; (c) Sections 2 through 6; (d) Figure 108c adjusted with brightness 70% and contrast -10%; (e) Sections 4 through 8; and (f) Figure 108e adjusted with brightness 90% and contrast -20%

The DIC system was coded to take two images per second without considering the displacement controlled by the actuator during the testing. A curve of strain and number of images taken through the DIC system is displayed in Figure 2.109. In this figure, significant changes in the strain are observed at the 2281<sup>st</sup> and 5871<sup>st</sup> image. The shear cracking of the CLT bridge system was found to be the cause of the significant change in the strain at the 2281<sup>st</sup> image. Another substantial change of the strain at the 5871<sup>st</sup> image was attributed to the slippage damage of the CLT bridge. As mentioned before, the DIC strain profile could not be plotted against the actuator load; thereby, it cannot be compared with the strain profile obtained from the contact sensors (i.e., SG-15 and SG-16).

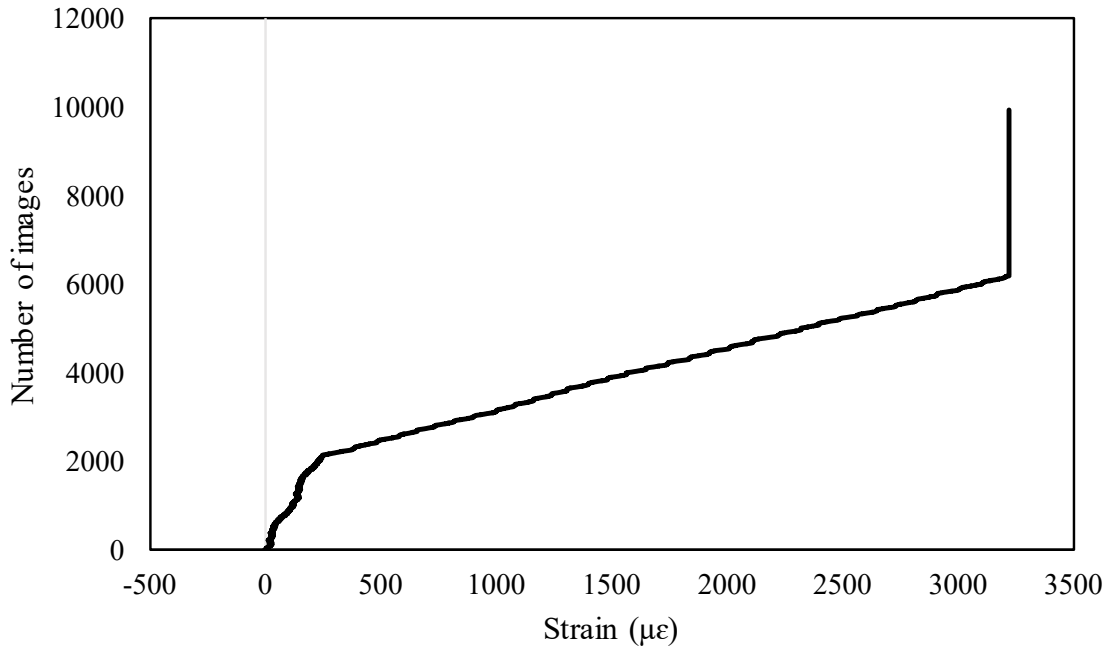


**Figure 2.109** Strain profile calculated from DIC system applied on the CLT bridge system

#### ***Data from Solar Panels***

During the CLT bridge load test, the two solar panels, solar panels 1 and 2, were set up on the east side of the east girder of the CLT bridge system to assess the efficiency of energy harvesting. Voltages from both solar panels were recorded by hand for every test run. Note that the total number of test runs was 140. Figure 2.110 depicts a graphical relationship between the voltages acquired from each of the solar panels and the mid-span displacements measured from the actuator. It is apparent that the voltages in both solar panels decrease with an increase in the mid-span displacement of the CLT bridge system. This was because both solar panels were moved downward from the light source due to an increase in the bridge deflection with the increased load. The amounts of voltage harvested from both solar panels are found to be fairly different. The voltages of the solar panel 1 and 2 appear to be increased slightly at 24.77 mm due to upward movement of both panels after the shear cracking at the south edge of the east girder. Note, there was not any damage on both solar panels during the testing. The results indicated that the efficiency of energy harvesting was mainly related to the location of solar panels from the applied load under the equal condition of the light source.



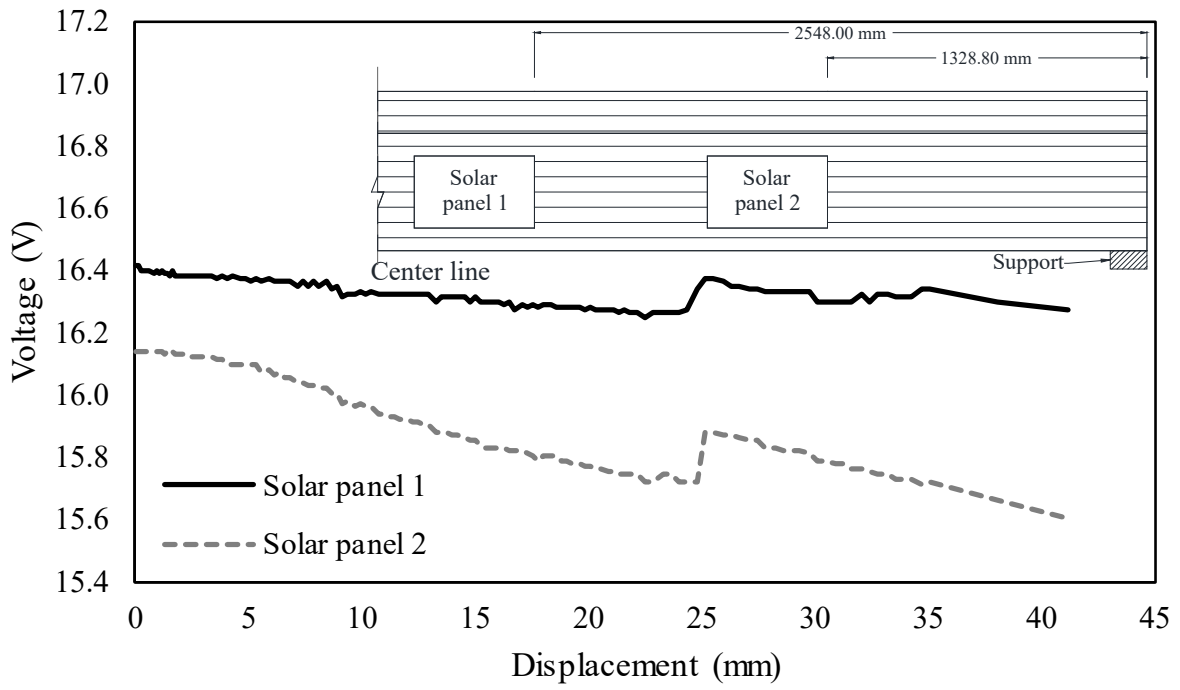


**Figure 2.110** Relationship between voltage and displacement of CLT bridge system

## 2.5 Summary and Conclusions

The main goal of this project was to develop a sustainable and resilient bridge system using CLT products. To achieve this goal, the four objectives, encompassing 1) CLT bridge conceptualization, 2) CLT bridge design, 3) CLT bridge production, and 4) ultimate load testing, were successfully completed. This section involves presenting a summary and key findings resulting from the tasks to accommodate each objective as indicated herein:

### 2.5.1 CLT Bridge Conceptualization

The extensive literature review was accomplished by studying the existing applications of CLT in bridges and other structures. The literature review indicated that there have existed into three main types, including CLT girder bridge, CLT deck bridge, and covered CLT bridge, but most of the CLT bridges have been constructed outside the US and CLT has been used as the bridge decking. Based upon the literature review findings, three different CLT bridge options, which include simple CLT girder bridge, CLT arch bridge, and double T-shaped CLT girder, were conceptualized. Among three options, the simple CLT girder bridge was found to be the most feasible bridge system for this project due to practical maintenance and easy-approaching inspection. Additionally, the literature review performed for the CLT load testing found that the full-scale CLT bridge system fabricated with all CLT components have not been tested to date.

### 2.5.2 CLT Bridge Design

Several timber bridge design codes (e.g., AASHTO Standard bridge design specifications (AASHTO 2002) and CLT building design standards (e.g., Standard for Performance-Rated Cross-Laminated Timber (ANSI/APA 2018) were used. With the codes and standards, the simple CLT girder bridge selected for this project was designed using the properties of CLT materials provided by the local CLT producer, Smartlam. The designed CLT girder bridge with a span length of 6.4 m had the two 14-ply CLT girders (0.24 m wide x 0.48 m deep) with 0.61 m girder spacing center-to-center, the 5-ply CLT decking (0.17 m thick and 1.22 m wide) with an overhang length of 0.30 m along with the two 7-ply CLT diaphragms (0.37 m long x 0.13 wide x 0.24 m deep).

### 2.5.3 CLT Bridge Production

All bridge CLT components necessary for the fabrication of the entire CLT bridge system that was designed were manufactured by the local CLT producer. The manufactured CLT components included eight 7-ply CLT beams, one 5-ply CLT panel, and two 7-ply CLT diaphragms, and they were delivered to the SDSU Structural Laboratory. To fabricate 14-ply CLT girders required to support the 5-ply CLT deck and other external loads such as HS20-44 truck loadings, two clamping methods using adhesive or adhesive and fasteners were proposed and used. The CLT bridge system was fabricated at the SDSU Structural Laboratory using the 5-ply CLT decking, the two 14-ply CLT girders, and the 7-ply CLT diaphragms. The CLT decking was linked to the CLT girders by means of adhesive and fasteners, and each of the CLT diaphragms was connected between the girders at the end supports using rods and nuts.

### 2.5.4 Ultimate Load Testing

The ultimate load testings were performed for the CLT girder bonded with adhesive; the CLT girder bonded with adhesive and fasteners; and the CLT bridge system. For each testing, experimental data, including strain, deflection, and slippage along with images, were obtained through both contact and non-contact sensors. The contact sensors comprised the strain gauges, BDI strain sensors, string pot, and LVDTs, while the noncontact sensors contained the UAV with the gimbal camera, the manipulator with

the smart phone camera, and the digital camera, and DIC camera. Each of the testings followed the proposed three-step procedure, which included monotonic loading, measurement using the contact sensors, and inspection through the non-contact sensors. The detailed findings from each testing are in the following subsection.

#### 2.5.4.1 CLT Girder with Adhesive

The testing results for the adhesively bonded CLT girder indicated that:

- Two different failures, slippage failure at 49.53 mm resulting from 62.74 kN load and flexural failure at 73.66 mm corresponding to 52.32 kN load, were observed. The slippage failure was spotted with the slippage between the top and bottom 7-ply CLT beams, while the flexural failure was observed at the bottom of the 14-ply CLT girder at the mid-span. It was found that the ultimate strength of the girder (62.74kN) was 43.74% higher than the AASHTO strength I limit strength and 65.73% higher than the AASHTO service I limit strength, respectively.
- The maximum slippages at the top, middle, and bottom of the girder were found to be 0.48 mm, 0.56 mm, and 0.41 mm, respectively before the slippage failure. Before the slippage failure, the slippage between the two 7-ply beams (GL07 and GL08) exhibited the maximum value.
- At the mid-span of the girder, SG-1 and SG-2 showed a significant change in the strain at 62.74 kN due to the slippage failure, whereas SG-3 exhibited the change in the strain at 51.02 kN corresponding to 36.93 mm deflection. Based on these observations, loss of section properties of the girder at the bottom was found to be initiated at 36.93mm deflection, and significant loss in the section properties were found after the slippage failure as well.
- Negative strain in compression was observed at SG-4 and SG-5 at a distance of  $3d$  from the north support, whereas positive strain in tension was found at SG-6. A significant change in the strain was observed in all strain gauge locations due to the slippage failure at 74 kN.
- The maximum shear strain was found at the top of the girder at  $d$  from the north support due to the slippage failure between GL07 and GL08, while the maximum shear strain was found at the middle of the girder at  $d$  from the south support before the slippage failure. This follows the general strain trend, where maximum shear strain occurs at the center of conventional girders such as concrete and steel girders.
- At  $3d$  from the south support, the average neutral axis for the deflections of 60 mm and 74 mm representing the post slippage failure was located at 3.13 mm from the bottom of the girder. The significant change in the strain values was found in all BDI strain sensors after the slippage failure at 62.74 kN.
- The deflections obtained from the manipulator and UAV were in agreement with those recorded from the actuator. The average difference between the deflections measured from the manipulator and UAV and the directly measured deflections through the actuator over the testing was found to be 2.09 mm and 2.01 mm, respectively, and corresponding average percentage errors were 17.49% and 16.72%.
- The comprehensive damage map created using the inspection images from the manipulator was used to visually identify propagated damage, cracks 1 and 2 on the south east side of the girder. These cracks in terms of length and thickness were, in an efficient manner, quantified using the image analysis of the inspection images from the manipulator and UAV. DIC image data was successfully used to diagnose the significant change of the strain due to the slippage failure on the girder, although the DIC data was not exploited to compare with the strain data.

- The analysis of solar panel data revealed that the efficiency of energy harvesting during the girder testing was dependent on the location of solar panels from the applied load under the same condition of the light source.

#### 2.5.4.2 CLT Girder with Adhesive and Fasteners

Based upon the testing results, the following conclusions were made:

- Two different failures, significant flexural cracking at 45.34 mm resulting from 74.77 kN and complete flexural failure at 58.45 mm corresponding to 79.89 kN, were observed. The flexural cracking was spotted at the bottom of the girder at mid-span and the significant propagation of the flexural cracking was observed from the bottom lam through the bottom surface at the mid-span. The ultimate strength of the girder (79.89 kN) was 55.81% higher than the AASHTO strength I limit strength and 73.09% higher than the AASHTO service I limit strength, independently.
- The maximum slippages at the top, middle, and bottom of the girder before the flexural cracking were found to be 0.84 mm, 0.43 mm, and 0.41 mm, respectively. The maximum slippage at the top of the girder was due to the lower bonding strength between the unscrewed top two lams (GL13 and GL14) when compared with the screwed lams before the flexure cracking.
- At the mid-span of the girder, the neutral axes were near the center of the girder depth before the flexural failure, however, the neutral axis shifted down to the bottom of the girder at 58 mm deflection after the flexural failure.
- At  $3d$  from the north support, all the neutral axes were located near the center of the girder depth, which indicated no significant movement of neutral axis in the girder during the testing.
- At  $d$  from the north support, the neutral axes were not found within the girder depth at the deflections of 20 mm, 40 mm, and 58 mm. The maximum shear strain was found at the bottom of the girder. At  $d$  from the south support, the neutral axes were not positioned within the girder depth at the deflections of 20 mm through 58 mm. The maximum shear strain was found to be at the center of the girder before the flexural cracking and failure.
- At  $3d$  from the south support, the average neutral axis at the deflections of 20 mm and 58 mm was located at 218.16 mm from the bottom of the girder. The substantial change in the strain value was found in all BDI strain sensors after the flexural cracking and failure.
- The deflections estimated from the image analysis coupled with the inspection images from the manipulator and UAV were in line with those from the actuator. The results indicated that the image analysis incorporating the manipulator- and UAV-based inspection images was able to calculate the mid-span deflections with the level of accuracy with the average percentage errors of 18.46% and 18.66%.
- The detailed inspection damage map with an aid from the manipulator demonstrated its efficiency to detect the extended cracks on the south east side of the girder. The use of DIC image data was capable of detecting the significant change of the strain as a result of the flexural cracking on the girder. However, the DIC data could not be compared with the strain data.
- The efficiency of energy harvesting from the solar panels on the girder testing relied on the location of solar panels from the applied load under the equal condition of the light source. This was aligned with the findings from the adhesive CLT girder testing.

### 2.5.4.3 CLT Bridge System

The following conclusions were derived from the bridge testing:

- It was found that three different failures, shear crack (153.44 kN) at 24.77 mm, slippage failure (193.33 kN) at 34.67mm, and flexural failure (262.50 kN) at 51.21 mm, occurred during the testing. The first failure due to the shear crack was observed at the south edge of the east girder and the second failure was spotted due to the slippage between the top of the girder and the bottom of the deck. The last failure due to the flexure was revealed at the bottom of the east girder.
- The ultimate strength of the tested bridge (262.50 kN) was 34.65% higher than the AASHTO strength I limit strength and 61.14% higher than the AASHTO service I limit strength, correspondingly.
- It turned out that the largest maximum slippage occurred between GL07 and GL08 based on all the slip results measured until shortly after the shear cracking took place.
- At the early stage of the testing, the behavior of the bridge in the mid-span was found to be composite, which later changed to non-composite behavior after 16.72 kN.
- At  $3d$  from the north support, the significant change in the strain was observed in all strain gauge locations due to the slippage failure after the load reached 193.33 kN.
- At  $d$  from the north support, the neutral axis at the deflection of 25 mm was located at 45.27 mm from the bottom of the deck. The maximum shear strain was discovered at the top of the west girder on the strain gauge set “Girder T”.
- At  $d$  from the south support, the neutral axis was positioned at 43.76 mm from the deck for the 25 mm deflection. The maximum shear strain was observed at the bottom of the girder during testing.
- The comparison in deflection between the UAV and the actuator demonstrated the effectiveness of the image analysis incorporating the UAV-enabled inspection images to determine the mid-span deflection of the bridge system with the average percentage error of 17.59%.
- The use of DIC image data was efficient to examine the significant change of the strain caused by the shear and slippage damage.
- The voltage-and-displacement relationship demonstrated that the efficiency of energy harvesting was principally in proportion to the movement of solar panels due to the deflection of the bridge system under the equal condition of the light source. This was in agreement with the discoveries from the testings of the adhesive girder and the girder with adhesive and fasteners.

### 3. REFERENCES

- Abrahamsen, R. B., and Nyløkken, T. E. (2010). "HUNDORP BRIDGE: Bridge deck rehabilitation using cross-laminated timber." *Sweco*, 25.
- Aicher, S., and Dill-Langer, G. (2000). "Basic considerations to rolling shear modulus in wooden boards." *Otto-Graf-Journal*, 11, 157.
- AITC (American Institute of Timber Construction). (1987). Design standard specifications for structural glued laminated timber of softwood species. American Institute of Timber Construction, Englewood, CO, 28.
- American Association of State Highway and Transportation Officials (AASHTO). (2002). Standard Specifications for Highway Bridges. American Association of State Highway and Transportation Officials, Inc., Washington, DC.
- American Association of State Highway and Transportation Officials (AASHTO). (2012). AASHTO LRFD Bridge Design Specifications. American Association of State Highway and Transportation Officials, Inc., Washington, DC.
- ANSI (American National Standards Institute)/APA (American Plywood Association). (2018). Standard for Performance-Rated Cross-Laminated Timber. ANSI/APA PRG 320-2018, American National Standards Institute, Tacoman, WA.
- APA (American Plywood Association). (2016). North American CLT vs. Imported Product: Stringent Standard Assures Consistent Value and Performance. APA, Tacoma, WA, 3.
- ASCE (American Society of Civil Engineers). (2017). "Infrastructure Report Card." <<https://www.infrastructurereportcard.org/cat-item/bridges/>> (Mar. 22, 2018).
- Athena Sustainable Materials Institute. (2017). Design Building University of Massachusetts, Amherst: An Environmental Building Declaration According to EN 15978 Standard. Amherst Technical Report, Athena Sustainable Materials Institute, 53.
- Avent, A. (1985). "Decay, Weathering and Epoxy Repair of Timber." *Journal of Structural Engineering*, 111(2), 328–342.
- AWC (American Wood Council). (2015). National Design Specification (NDS) for Wood Construction. ANSI/AWC NDS-2015, American Wood Council, Leesburg, VA.
- Bauordnungsrecht. (2016). Baurecht: Bauordnungsrecht Einschliesslich Offentliches Baunachbarschutzrecht (Recht Und Verwaltung). Kohlhammer, Stuttgart, Germany.
- Behrens, H., and Benner, P. (2015). A New Bridge Proposal-Road Bridge with a Cross-Laminated Timber Slab. Lunds Universitet, Sweden.
- Breyer, D. E., Fridley, K. J., Cobeen, K. E., and Pollock, D. G. (2007). Design of Wood Structures—ASD/LRFD. McGraw-Hill, New York.
- Buck, D., Wang, X. (Alice), Hagman, O., and Gustafsson, A. (2016). "Bending Properties of Cross Laminated Timber (CLT) with a 45° Alternating Layer Configuration." *BioResources*, 11(2), 4633–4644.
- CBI Ministry of Foreign Affairs. (2017). "Exporting cross laminated timber (CLT) to Western Europe." [www.cbi.eu](http://www.cbi.eu), <<https://www.cbi.eu/market-information/timber-products/cross-laminated-timber/europe/>> (Jul. 22, 2018).

- Cecobois. (2018). "Maicasagi Bridge." Cecobois, <<https://www.cecobois.com/en/projects/maicasagi-bridge>> (Jul. 22, 2018).
- Chen, Y., and Lam, F. (2013). "Bending Performance of Box-Based Cross-Laminated Timber Systems." *Journal of Structural Engineering*, 139(12), 04013006.
- Detail. (2012). "Vorgefertigtes Bauen mit Holz." Detail.de, <<https://www.detail.de/artikel/vorgefertigtes-bauen-mit-holz-8765/>> (Aug. 30, 2018).
- Egorov, V., Poirier, L.-P., and Lévesque, M. (2018). "Conception et construction d'un pont à Chibougamau." Maicasagi Bridge, <<https://www.nordic.ca/en/projects/structures/maicasagi-bridge>>.
- EN 1995-2 (CEN, European Committee for Standardisation). (2004). Eurocode 5: Design of timber structures - Part 2: Bridges. Brussels, 29.
- ESR-3179. (2018). SWG ASSY 3.0 WOOD SCREWS. International Code Council, 8.
- Forest Products Laboratory. (2010). Wood handbook—Wood as an engineering material. Department of Agriculture, Forest Service, Forest Products Laboratory, Madison, WI: U.S., 508.
- Fumoto, H. (2014). "Japan's First CLT Building Completed." <http://canadawood.org>, <<http://canadawood.org/blog/japans-first-clt-building-completed/>> (Aug. 21, 2018).
- Gu, H., and Bergman, R. (2018). Life Cycle Assessment and Environmental Building Declaration for the Design Building at the University of Massachusetts. United States Department of Agriculture, 73.
- He, M., Sun, X., and Li, Z. (2018). "Bending and compressive properties of cross-laminated timber (CLT) panels made from Canadian hemlock." *Construction and Building Materials*, 185, 175–183.
- Hearn, E. J. (1997). "CHAPTER 7 - SHEAR STRESS DISTRIBUTION." *Mechanics of Materials 1* (Third Edition), E. J. Hearn, ed., Butterworth-Heinemann, Oxford, 154–175.
- Karacabeyli, E., and Douglas, B. (2013). CLT Handbook: cross-laminated timber. Special Publication SP-529E, FPInnovations, U.S. Department of Agriculture, Forest Service, Forest Products Laboratory, Binational Softwood Lumber Council (BSLC), Pointe-Claire, QC.
- Lefebvre, D., and Richard, G. (2014). "Design and construction of a 160-Metre-Long Wood Bridge in Mistissini, Québec." 20, 1–15.
- Li, M., Lam, F., and Li, Y. (2014). "Evaluating rolling shear strength properties of cross laminated timber by torsional shear tests and bending tests." WCTE 2014, World Conference on Timber Engineering, Quebec City, Canada, 280.
- Masoudnia, R., Hashemi, A., and Quenneville, P. (2018). "Predicting the Effective Flange Width of a CLT Slab in Timber Composite Beams." *Journal of Structural Engineering*, 144(7), 04018084.
- micro-measurement. (2010). Strain Gages and Instruments. Tech Note, micro-measurement, 6.
- Nie, X. (2015). "Failure mechanism of rolling shear failure in cross-laminated timber." University of British Columbia.
- Poulin, M., Viau, C., Lacroix, D. N., and Doudak, G. (2018). "Experimental and Analytical Investigation of Cross-Laminated Timber Panels Subjected to Out-of-Plane Blast Loads." *Journal of Structural Engineering*, 144(2), 04017197.

- Ritter, M. A. (1990). *Timber Bridges: Design, Construction, Inspection, and Maintenance*. U.S. Department of Agriculture, Forest Service, Washington, DC, 944.
- Salokangas, L., and Garnier, R. (2013). “Applicability of Cross Laminated Timber in Bridges.” *International Conference on Timber Bridges*, Las Vegas, 11.
- Sasaki, T., Ariyama, Y., Araki, S., Toyoda, J., Yamauchi, H., and Hayashi, T. (2017). “Development of Waterproofing Treatment for Cross Laminated Timber Slabs.” *Paper Reports on Use of Wood for Civil Engineering* 16, 39–44.
- Schrödter, H., and Breuer, R. (1998). *Baugesetzbuch:[BauGB; in der Fassung des Gesetzes zur Änderung des Baugesetzbuchs und zur Neuregelung des Rechts der Raumordnung (Bau- und Raumordnungsgesetz 1998-BauROG) vom 18. August 1997; berichtigt durch Bekanntmachung vom 16. Januar 1998]; Kommentar*. Vahlen.
- Serrano, E. (2009). “Limnologen–Experiences from an 8-storey timber building.” *Internationales Holzbau-Forum 09*, Vaxjo, Sweden, 1–12.
- Smartlam. (2018a). *SmartLam Cross-Laminated Timber*. Production report, APA, 5.
- Smartlam. (2018b). *Cross-Laminated Timber 2018 Specification Guide*. SMARTLAM, Columbia Falls, MT, 73.
- Wacker, J. P., and Smith, M. H. (2001). *Standard Plans for Timber Bridge Superstructures*. General Technical Report (GTR), Gen. Tech. Rep., U.S. Department of Agriculture, Forest Service, Forest Products Laboratory, Madison, WI, 53.
- Waugh Thistleton Architects. (2018). “Murray Grove.” <http://waughthistleton.com>, <<http://waughthistleton.com/murray-grove/>> (Aug. 30, 2018).
- Wood for Good. (2018). “Bridport House.” [woodforgood.com](http://woodforgood.com), <<https://woodforgood.com/case-studies/bridport-house/>> (Aug. 30, 2018).
- Zumbrunnen, P. (2013). “Multi-Story residential CLT Buildings – the UK’s experience and future potential.” *Internationales Forum-Holzbau 2013*, Auckland, New Zealand, 1–12.



## APPENDIX A. CLT PROPERTIES

**SmartLam Cross-Laminated Timber**  
**SmartLam, LLC**

**PR-L319**

Revised August 15, 2018

Products: SmartLam Cross-Laminated Timber  
SmartLam, LLC

1863 13<sup>th</sup> Street West  
Columbia Falls, MT 59912  
(406) 862-0098

[www.smartlam.com](http://www.smartlam.com)

1. Basis of the product report:
  - 2018 and 2015 International Building Code (IBC): Section 2303.1.4 Structural Glued Cross-Laminated Timber
  - 2012 IBC: Section 104.11 Alternative materials
  - 2018 and 2015 International Residential Code (IRC): Sections R502.1.6, R602.1.6, and R802.1.6 Cross-Laminated Timber
  - 2012 IRC: Section R104.11 Alternative materials
  - ANSI/APA PRG 320-2017, PRG 320-2012, and PRG 320-2011 Performance Rated Cross-Laminated Timber, recognized in the 2018 IBC and IRC, 2015 IRC, and 2015 IBC, respectively
  - APA Reports T2016P-34, T2016P-36, and T2017P-16A, and other qualification data
2. Product description:

SmartLam cross-laminated timber (CLT) is manufactured with Spruce-pine-fir south (SPF-S) or Hem-fir lumber in accordance with a custom layup combination approved by APA through product qualification and/or mathematical models using principles of engineering mechanics. Allowable design properties for lumber laminations used in SmartLam CLT are provided in Table 1. SmartLam CLT can be used in floor, roof, and wall applications, and is manufactured with nominal widths of 12 to 120 inches, thicknesses of 4 1/8 to 12 3/8 inches, and lengths up to 40 feet.
3. Design properties:

SmartLam CLT shall be designed with the design capacities provided in Tables 2 and 3. Note that the unbalanced layups listed in Table 3 can be only used in simple span applications and the compression side must be stamped with the word "TOP", which shall be installed on the compression (top) side of the simple span. The design adjustment factors, such as load duration, creep, moisture, and temperature factors, etc., shall be based on the 2015 National Design Specification for Wood Construction (NDS) and approved by the engineer of record. The lateral resistance of SmartLam CLT, when used as shearwalls or diaphragms, depends on the panel-to-panel connection and anchorage designs, and shall be consulted with the CLT manufacturer and approved by the engineer of record.
4. Product installation:

SmartLam CLT shall be installed in accordance with the recommendations provided by the manufacturer ([www.smartlam.com](http://www.smartlam.com)) and the engineering drawing approved by the engineer of record. Permissible details shall be in accordance with the engineering drawing.
5. Fire-rated assemblies:

Procedures specified in Chapter 16 of the 2015 NDS shall be permitted for use in designing SmartLam CLT for a fire exposure up to 2 hours.

6. Limitations:
  - a) SmartLam CLT shall be designed in accordance with principles of mechanics using the design properties specified in this report or provided by the manufacturer.
  - b) SmartLam CLT products shall be limited to dry service conditions where the average equilibrium moisture content of solid-sawn lumber is less than 16 percent.
  - c) Design properties for SmartLam CLT, when used as beams or lintels with loads applied parallel to the face-bond gluelines, are beyond the scope of this report.
  - d) Unblanced SmartLam CLT layups shall be limited to simple span applications and shall be installed with the "TOP" mark on the compression (top) side of the simple span.
  - e) SmartLam CLT shall be manufactured in accordance with the custom layup combination specified in this report and documented in the SmartLam in-plant manufacturing standard approved by APA.
  - f) SmartLam CLT is produced at the SmartLam, LLC, Columbia Falls, Montana facilities under a quality assurance program audited by APA.
  - g) This report is subject to re-examination in one year.
7. Identification:

SmartLam CLT described in this report is identified by a label bearing the manufacturer's name (SmartLam) and/or trademark, the APA assigned plant number (1119), the product standard (ANSI/APA PRG 320), the APA logo, the CLT grade (SL-V4), the report number PR-L319, and a means of identifying the date of manufacture.

Table 1. ASD Reference Design Values<sup>(a)</sup> for Lumber Laminations Used in SmartLam CLT (for Use in the U.S.)

CLT Grade	Laminations Used in Major Strength Direction						Laminations Used in Minor Strength Direction					
	F <sub>b</sub> (psi)	E (10 <sup>6</sup> psi)	F <sub>t</sub> (psi)	F <sub>c</sub> (psi)	F <sub>v</sub> (psi)	F <sub>s</sub> (psi)	F <sub>b</sub> (psi)	E (10 <sup>6</sup> psi)	F <sub>t</sub> (psi)	F <sub>c</sub> (psi)	F <sub>v</sub> (psi)	F <sub>s</sub> (psi)
SL-V4	775	1.1	350	1,000	135	45	775	1.1	350	1,000	135	45

For SI: 1 psi = 0.006895 MPa

<sup>(a)</sup> Tabulated values are allowable design values and not permitted to be increased for the lumber flat use or size factor in accordance with the NDS. The design values shall be used in conjunction with the section properties provided by the CLT manufacturer based on the actual layup used in manufacturing the CLT panel (see Tables 2 and 3).

Table 2. ASD Reference Design Values<sup>(a)</sup> for SmartLam **Balanced** CLT Listed in Table 1 (for Use in the U.S.)

CLT Layup <sup>(b)</sup>	Layup ID <sup>(c)</sup>	Thick-ness, t <sub>p</sub> (in.)	Lamination Thickness (in.) in CLT Layup										Major Strength Direction				Minor Strength Direction				
			=	⊥	=	⊥	=	⊥	=	⊥	=	⊥	(F <sub>c</sub> S) <sub>eff,1.0</sub> (lb-ft/ft)	(EI) <sub>eff,1.0</sub> (10 <sup>6</sup> lb-ft-in. <sup>2</sup> /ft)	(GA) <sub>eff,1.0</sub> (10 <sup>6</sup> lb/ft)	V <sub>s,0</sub> (lb/ft)	(F <sub>c</sub> S) <sub>eff,1.90</sub> (lb-ft/ft)	(EI) <sub>eff,1.90</sub> (10 <sup>6</sup> lb-ft-in. <sup>2</sup> /ft)	(GA) <sub>eff,1.90</sub> (10 <sup>6</sup> lb/ft)	V <sub>s,90</sub> (lb/ft)	
SL-V4 <sup>(d)</sup>	3-alt	4 1/8	1 3/8	1 3/8	1 3/8									1,800	74	0.41	1,490	245	2.9	0.41	495
	4-maxx	5 1/2	1 3/8	1 3/8	1 3/8 x 2	1 3/8								2,925	161	0.49	1,980	975	23	0.85	990
	5-alt	6 7/8	1 3/8	1 3/8	1 3/8	1 3/8	1 3/8							4,150	286	0.83	2,480	2,120	74	0.83	1,490
	5-maxx	6 7/8	1 3/8 x 2	1 3/8	1 3/8 x 2	1 3/8								5,150	355	0.85	2,480	245	2.9	0.49	495
	6-maxx	8 1/4	1 3/8 x 2	1 3/8 x 2	1 3/8 x 2	1 3/8								7,200	596	0.83	2,975	975	23	0.83	990
	7-alt	9 5/8	1 3/8	1 3/8	1 3/8	1 3/8	1 3/8	1 3/8	1 3/8	1 3/8				7,325	707	1.2	3,475	4,875	286	1.2	2,480
	7-maxx	9 5/8	1 3/8 x 2	1 3/8	1 3/8	1 3/8	1 3/8	1 3/8 x 2						9,425	909	1.2	3,475	2,120	74	0.89	1,490
	8-maxx	11	1 3/8 x 2	1 3/8	1 3/8 x 2	1 3/8	1 3/8	1 3/8 x 2						11,875	1,309	1.7	3,950	3,425	161	0.97	1,980
	9-alt	12 3/8	1 3/8	1 3/8	1 3/8	1 3/8	1 3/8	1 3/8	1 3/8	1 3/8	1 3/8	1 3/8		11,375	1,410	1.7	4,450	8,625	707	1.7	3,475
	9-maxx	12 3/8	1 3/8 x 2	1 3/8	1 3/8	1 3/8	1 3/8	1 3/8	1 3/8	1 3/8 x 2				14,600	1,811	1.6	4,450	4,875	286	1.3	2,480

For SI: 1 in. = 25.4 mm; 1 ft = 304.8 mm; 1 lbf = 4.448N

<sup>(a)</sup> Tabulated values are allowable design values and not permitted to be increased for the lumber flat use or size factor in accordance with the NDS.

<sup>(b)</sup> The CLT layups are developed based on ANSI/APA PRG 320, as permitted by the standard.

<sup>(c)</sup> The layup designation refers to the number of layers and the layup series (alt or maxx).

<sup>(d)</sup> The SL-V4 grade uses all visually graded No. 2 SPF-S or Hem-fir lumber in both major and minor strength directions.

Table 3. ASD Reference Design Values<sup>(a)</sup> for SmartLam **Unbalanced** CLT<sup>(b)</sup> Listed in Table 1 (for Use in the U.S.)

CLT Layout <sup>(c)</sup>	Layout ID <sup>(d)</sup>	Thick-ness, $t_p$ (in.)	Lamination Thickness (in.) in CLT Layout									Major Strength Direction				Minor Strength Direction			
			=	⊥	=	⊥	=	⊥	=	⊥	=	⊥	$(F_c S)_0$ (lb <sub>f</sub> -ft/ft)	$(E I)_{eff,1.0}$ (10 <sup>6</sup> lb <sub>f</sub> -in. <sup>2</sup> /ft)	$(GA)_{eff,1.0}$ (10 <sup>6</sup> lb <sub>f</sub> /ft)	$V_{s,0}$ (lb <sub>f</sub> /ft)	$(F_c S)_{eff,1.90}$ (lb <sub>f</sub> -ft/ft)	$(E I)_{eff,1.90}$ (10 <sup>6</sup> lb <sub>f</sub> -in. <sup>2</sup> /ft)	$(GA)_{eff,1.90}$ (10 <sup>6</sup> lb <sub>f</sub> /ft)
SL-V4 <sup>(e)</sup>	4-alt	5 1/2	1 3/8	1 3/8	1 3/8	1 3/8						1,800	74	0.41	1,490	245	2.9	0.41	495
	6-alt	8 1/4	1 3/8	1 3/8	1 3/8	1 3/8	1 3/8	1 3/8				4,150	286	0.83	2,480	2,120	74	0.83	1,490
	8-alt	11	1 3/8	1 3/8	1 3/8	1 3/8	1 3/8	1 3/8	1 3/8	1 3/8		7,325	707	1.2	3,475	4,875	286	1.2	2,480

For SI: 1 in. = 25.4 mm; 1 ft = 304.8 mm; 1 lbf = 4.448N

- (a) Tabulated values are allowable design values and not permitted to be increased for the lumber flat use or size factor in accordance with the NDS. Tabulated values ignore the contribution of the outermost compression layer.
- (b) Unbalanced CLT layouts can be only used in simple span applications. The compression side must be stamped with the word "TOP", which shall be installed on the compression (top) side of the simple span.
- (c) The CLT layouts are developed based on ANSI/APA PRG 320, as permitted by the standard.
- (d) The layout designation refers to the number of layers and the layout series (alt).
- (e) The SL-V4 grade uses all visually graded No. 2 SPF-S or Hem-fir lumber in both major and minor strength directions.

APA – *The Engineered Wood Association* is an approved national standards developer accredited by American National Standards Institute (ANSI). APA publishes ANSI standards and Voluntary Product Standards for wood structural panels and engineered wood products. APA is an accredited certification body under ISO/IEC 17065 by Standards Council of Canada (SCC), an accredited inspection agency under ISO/IEC 17020 by International Code Council (ICC) International Accreditation Service (IAS), and an accredited testing organization under ISO/IEC 17025 by IAS. APA is also an approved Product Certification Agency, Testing Laboratory, Quality Assurance Entity, and Validation Entity by the State of Florida, and an approved testing laboratory by City of Los Angeles.

**APA – THE ENGINEERED WOOD ASSOCIATION  
HEADQUARTERS**

7011 So. 19<sup>th</sup> St. • Tacoma, Washington 98466  
Phone: (253) 565-6600 • Fax: (253) 565-7265 • Internet Address: [www.apawood.org](http://www.apawood.org)

**PRODUCT SUPPORT HELP DESK**  
(253) 620-7400 • E-mail Address: [help@apawood.org](mailto:help@apawood.org)

**DISCLAIMER**

APA Product Report® is a trademark of APA – *The Engineered Wood Association*, Tacoma, Washington. The information contained herein is based on the product evaluation in accordance with the references noted in this report. Neither APA, nor its members make any warranty, expressed or implied, or assume any legal liability or responsibility for the use, application of, and/or reference to opinions, findings, conclusions, or recommendations included in this report. Consult your local jurisdiction or design professional to assure compliance with code, construction, and performance requirements. Because APA has no control over quality of workmanship or the conditions under which engineered wood products are used, it cannot accept responsibility for product performance or designs as actually constructed.

## APPENDIX B. CLT QUOTATION



SMARTLAM, LLC  
 PO BOX 2070, Columbia Falls, MT. 59912  
 Phone: 406.892.2241  
 sales@smartlam.com  
 www.SmartLam.com

**BID SUMMARY**

**SDSU Bridge**

Plan Description: email  
 Customer: South Dakota State University  
 Primary Contact: Junwon Seo  
 Project Street Address: 0  
 Project City & State: Brookings, SD  
 Project Postal/ZIP Code: 0

Plan Set Date: March 4th  
 Date: 3/5/2019  
 Phone: 605.688.5226  
 Email: junwon.seo@sdstate.edu  
 Completed By: Nick Desimone  
 Quote Number: 190205ND  
 Addendum: 0  
 Valid Until: 3/26/2019

**Cross Laminated Timber Scope**

CLT SPECIFICATIONS	QTY	SQUARE FT	CUBIC FT.	WEIGHT	SUBTOTAL
Deck : 5 ALT SL-V4	1	80	46	1763	\$1,697.00
Girders & Diaphragms: 7 ALT SL-V4	10	134	107	4139	\$6,449.50
Shipping Estimate:					\$3,135.00
<b>TOTALS:</b>	<b>11</b>	<b>214</b>	<b>153</b>	<b>5,902</b>	<b>\$11,281.50</b>

**CROSS LAMINATED TIMBER NARRATIVE**

Includes CLT package consisting of SL-V4 CLT panels manufactured using Spruce, Pine & Fir - South 2x6 or 2x8 timber members laminated together using PURBOND Polyurethane adhesive. CNC fabrication included.  
 Each panel will have an Architectural Finish and will be sanded on 1 side only.  
 Shop Sealer will be applied to all faces of each panel.  
 Shop drawings and Engineering Support Included.  
 Excluded from this quote are the items: Taxes, Customs, Brokerage & Duty.  
 Installation services to be provided by others, not included within this quote.  
 FSC Certification, Chain of Custody/LEED Documentation is NOT included with this quote. Additional fee for this service.

**SHIPPING TERMS & CONDITIONS**

*(INCLUDED IN TOTAL ABOVE)*

SmartLam LLC makes every effort to provide accurate shipping dates & estimates. However all shipping dates & amounts supplied in this quote are estimates only. The customer will be responsible for any additional shipping fees above the estimated amount.

<b>Total Trucks:</b> 1	<b>Shipment Type:</b> Legal Load	<b>Shipping Estimate:</b> \$3,135.00
------------------------	----------------------------------	--------------------------------------

**SMARTLAM PAYMENT TERMS**

All orders require a 50% deposit upon execution of purchase order to secure of raw materials.  
**\*\* Quotes are good for 30 days and may vary due to the fluctuating price of our raw materials. \*\***

I AGREE TO THE WARRANTY, TERMS AND CONDITIONS OUTLINED ON BACK OF SHEET.

**PURCHASER**  
 PRINTED NAME: \_\_\_\_\_  
 AUTHORIZED SIGNATURE: \_\_\_\_\_  
 DATE: \_\_\_\_\_  
 PO Number: \_\_\_\_\_  
 Billing Address: \_\_\_\_\_  
 \_\_\_\_\_  
 \_\_\_\_\_

**SMARTLAM**  
 PRINTED NAME: \_\_\_\_\_  
 AUTHORIZED SIGNATURE: \_\_\_\_\_  
 DATE: \_\_\_\_\_





## **APPENDIX C. POLYURETHANE ADHESIVE SPECIFICATION**



## TITEBOND POLYURETHANE GLUE

Titebond Polyurethane Glue is a breakthrough in adhesive technology. It is the only polyurethane glue to combine a long 30-minute working time with a short 45-minute clamp time\*. It is a versatile, professional-strength glue specifically formulated for multi-purpose applications. In addition to its superior wood-to-wood performance, Titebond Polyurethane Glue is ideal for metals, ceramics, most plastics, HPL, Corian®, stone and other porous/non-porous materials. It is ready-to-use, offers excellent sandability and is unaffected by finishes.



### Features & Benefits

- 100% waterproof (Passes ANSI Type I & II water-resistance testing)
- Bonds virtually everything
- Epoxy-like strength - No mixing
- Short clamp & fast cure
- Excellent sandability
- 100% solids
- Solvent free

### SPECIFICATIONS

CONFORMS TO ASTM D-4236

## Application Guidelines

---

**Application Temperature:** Above 50°F

**Assembly Time After Glue Application:** 25-30 minutes (70°F./50%RH)

**Minimum Required Spread :** Approximately 6 mils or 250 square feet per gallon

**Required Clamping Pressure:** Enough to bring joints tightly together (generally, 30-80 psi for HPL, 100-150 psi for softwoods, 125-175 psi for medium woods and 175-250 psi for hardwoods).

**Method of Application:** Easily spread with a roller spreader or brush, or may be transferred to plastic bottles for finer gluing applications.

**Cleanup:** Mineral spirits while glue is wet. Scrape or sand off dried excess.

## Bond Strength ASTM D-905 (On Hard Maple)

---

Temperature	Strength	Wood Failure
Room Temperature	3,500+ psi	60%
150°F. Overnight	3,000 psi	50%

## Physical Properties

---

**Type:** Polyurethane

**Calculated VOC:** 0 g/L

**State:** Liquid

**Weight Per Gallon:** 9.55 lbs.

**Color:** Brown

**Flashpoint:** > 200°F

**Dried Film:** Yellow

**Freeze/thaw Stability:** Stable

**Solids:** 100%

**Viscosity:** 8,500 cps

**Storage Life:** 12 months in tightly closed containers at 75°F

## Limitations

---

Titebond Polyurethane Glue is not for structural applications or for use below the waterline. For ease of application, the glue, temperature and materials to be bonded should be above 50°F. Lower temperatures will cause the glue to thicken.

## Product SKUs

Part Number	UPC	Case UPC	Size	Weight	Units Per Package	Packages Per Pallet
2300	037083023008	10037083023005	12 Oz. Bottle	6.05	6	212
2302	037083023022	10037083023029	4 Oz. Bottle	4.29	12	245
2303	037083023039	10037083023036	8 Oz. Bottle	8.22	12	165
2308			52 Gallon Drum	530.72	1	4

## Caution Statement

**WARNING: EYE AND SKIN IRRITANT. POTENTIAL SKIN AND RESPIRATORY SENSITIZER.**

Contains isocyanate containing polymers. Contact causes eye irritation. Prolonged or repeated skin exposure may cause irritation and sensitization or allergic reaction. Contact may stain skin. Do not allow eye contact. Avoid prolonged or repeated contact with skin. In case of eye contact, flush immediately with plenty of water for at least 15 minutes and seek medical attention. For skin, wash thoroughly with soap and water. For additional information, refer to Safety Data Sheet. **KEEP OUT OF THE REACH OF CHILDREN.**

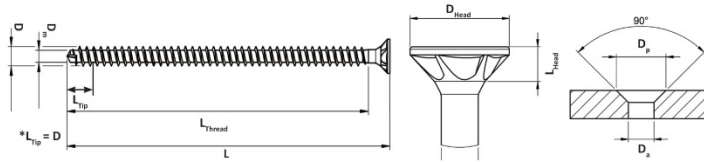
**Important Notice:** Our recommendations, if any, for the use of this product are based on tests believed to be reliable. Since the use of this product is beyond the control of the manufacturer, no guarantee or warranty, expressed or implied, is made as to such use or effects incidental to such use, handling or possession or the results to be obtained, whether in accordance with the directions or claimed so to be. The manufacturer expressly disclaims responsibility therefore. Furthermore, nothing contained herein shall be construed as a recommendation to use any product in conflict with existing laws and/or patents covering any material or use.

2020 Bruck Street, Columbus, Ohio 43207  
CUSTOMER SERVICE 1-800-669-4583  
TECH SERVICE 1-800-347-4583  
www.titebond.com

**APPENDIX D. FASTENER SPECIFICATION**

# ASSY VG CSK

## Specifications



Item #	Box size	D	L		L <sub>thread</sub>		D <sub>head</sub>	D <sub>m</sub>	D <sub>a</sub>	D <sub>p</sub>	L <sub>head</sub>	Bit
	pieces		in.	[mm]	in.	[mm]						
140080080000102	75	5/16" [8]	3 1/8"	[80]	2 1/2"	[61]	0.591" [15]	0.196" [5]	0.354" [9]	0.748" [19]	0.181" [4.6]	AW 40
140080120000102	75		4 3/4"	[120]	4"	[103]						
140080140000102	75		5 1/2"	[140]	4 7/8"	[123]						
140080160000102	75		6 1/4"	[160]	5 5/8"	[143]						
140080180000102	75		7 1/8"	[180]	6 3/8"	[163]						
140080200000102	75		7 7/8"	[200]	7 1/4"	[183]						
140080220000102	75		8 5/8"	[220]	8"	[203]						
140080240000102	75		9 1/2"	[240]	8 3/4"	[223]						
140080260000102	75		10 1/4"	[260]	9 5/8"	[243]						
140080280000102	75		11"	[280]	10 3/8"	[263]						
140080300000102	75		11 7/8"	[300]	11 1/8"	[283]						

Item #	Box size	D	L		L <sub>thread</sub>		D <sub>head</sub>	D <sub>m</sub>	D <sub>a</sub>	D <sub>p</sub>	L <sub>head</sub>	Bit
	pieces		in.	[mm]	in.	[mm]						
140100100000102	50	3/8" [10]	4"	[100]	3"	[77]	0.728" [18.5]	0.244" [6.2]	0.433" [11]	0.944" [24]	0.255" [6.5]	AW 50
140100140000102	50		5 1/2"	[140]	4 7/8"	[125]						
140100160000102	50		6 1/4"	[160]	5 3/4"	[145]						
140100180000102	50		7 1/8"	[180]	6 1/2"	[165]						
140100200000102	50		7 7/8"	[200]	7 1/4"	[185]						
140100220000102	50		8 5/8"	[220]	8 1/8"	[205]						
140100240000102	50		9 1/2"	[240]	8 7/8"	[225]						
140100260000102	50		10 1/4"	[260]	9 5/8"	[245]						
140100280000102	50		11"	[280]	10 3/8"	[265]						
140100300000102	50		11 7/8"	[300]	11 1/4"	[285]						
140100320000102	50		12 5/8"	[320]	12"	[305]						
140100340000102	50		13 3/8"	[340]	12 3/4"	[325]						
140100360000102	50		14 1/4"	[360]	13 5/8"	[345]						
140100380000102	50		15"	[380]	14 3/8"	[365]						
140100400000102	50		15 3/4"	[400]	15 1/8"	[385]						
140100430000102	25		16 7/8"	[430]	16 3/8"	[415]						
140100460000102	25		19"	[480]	18 1/4"	[465]						
140100530000102	25		20 7/8"	[530]	20 1/8"	[512]						
140100580000102	25		22 7/8"	[580]	22 1/8"	[562]						
140100650000102	25		25 5/8"	[650]	24 7/8"	[632]						
140100700000102	25	27 5/8"	[700]	26 7/8"	[682]							
140100750000102	25	29 1/2"	[750]	28 7/8"	[732]							
140100800000102	25	31 1/2"	[800]	30 3/4"	[782]							

Item #	Box size	D	L		L <sub>thread</sub>		D <sub>head</sub>	D <sub>m</sub>	D <sub>a</sub>	D <sub>p</sub>	L <sub>head</sub>	Bit
	pieces		in.	[mm]	in.	[mm]						
140120120000102	50	1/2" [12]	4 3/4"	[120]	4 1/8"	[105]	0.885" [22.5]	0.280" [7.1]	0.512" [13]	1.024" [26]	0.264" [6.7]	AW 50
140120140000102	50		5 1/2"	[140]	4 7/8"	[125]						
140120160000102	50		6 1/4"	[160]	5 3/4"	[145]						
140120180000102	50		7 1/8"	[180]	6 1/2"	[165]						
140120200000102	50		7 7/8"	[200]	7 1/4"	[185]						
140120220000102	50		8 5/8"	[220]	8 1/8"	[205]						
140120240000102	50		9 1/2"	[240]	8 7/8"	[225]						
140120260000102	50		10 1/4"	[260]	9 5/8"	[245]						
140120280000102	50		11"	[280]	10 3/8"	[265]						
140120300000102	50		11 7/8"	[300]	11 1/4"	[285]						
140120360000102	50		15"	[380]	14 3/8"	[365]						
140120480000102	25		19"	[480]	18 1/4"	[465]						
140120600000102	25	23 5/8"	[600]	23"	[585]							



*Most Widely Accepted and Trusted*

# ICC-ES Evaluation Report

ICC-ES | (800) 423-6587 | (562) 699-0543 | www.icc-es.org

## ESR-3178

Reissued 10/2018

This report is subject to renewal 10/2020.

**DIVISION: 06 00 00—WOOD, PLASTICS AND COMPOSITES**  
**SECTION: 06 05 23—WOOD, PLASTIC, AND COMPOSITE FASTENINGS**

**REPORT HOLDER:**

**SCHRAUBENWERK GAISBACH GMBH (SWG)**

**EVALUATION SUBJECT:**

**SWG ASSY VG PLUS WOOD-DRILLING SCREWS**



*“2014 Recipient of Prestigious Western States Seismic Policy Council (WSSPC) Award in Excellence”*



*ICC-ES Evaluation Reports are not to be construed as representing aesthetics or any other attributes not specifically addressed, nor are they to be construed as an endorsement of the subject of the report or a recommendation for its use. There is no warranty by ICC Evaluation Service, LLC, express or implied, as to any finding or other matter in this report, or as to any product covered by the report.*



Copyright © 2018 ICC Evaluation Service, LLC. All rights reserved.

## ICC-ES Evaluation Report

**ESR-3178**

Reissued October 2018

This report is subject to renewal October 2020.

[www.icc-es.org](http://www.icc-es.org) | (800) 423-6587 | (562) 699-0543

A Subsidiary of the International Code Council®

**DIVISION: 06 00 00—WOOD, PLASTICS AND COMPOSITES**  
**Section: 06 05 23—Wood, Plastic and Composite Fastenings**

**REPORT HOLDER:**

SCRAUBENWERK GAISBACH GmbH (SWG)

**EVALUATION SUBJECT:**

SWG ASSY VG PLUS WOOD-DRILLING SCREWS

**1.0 EVALUATION SCOPE**

**Compliance with the following codes:**

- 2015, 2012, 2009 and 2006 *International Building Code*® (IBC)
- 2015, 2012, 2009 and 2006 *International Residential Code*® (IRC)

**Properties evaluated:**

Structural

**2.0 USES**

SWG Assy VG Plus screws are alternate dowel-type threaded fasteners used in engineered wood-to-wood and steel-to-wood connections. For structures regulated under the IRC, the screws may be used when an engineered design is submitted in accordance with IRC Section R301.1.3.

**3.0 DESCRIPTION**

**3.1 General:**

SWG Assy VG Plus screws are self-drilling, self-tapping screws having a drill point, and one of three head styles (cylindrical, countersunk, or countersunk with milling pockets), as shown in Figures 1 through 3. The heads have a recess for use with an AW drive, which is a proprietary driving bit available from the report holder. The screws are available with nominal diameters of 1/4, 5/16, 3/8 and 1/2 inch (6, 8, 10 and 12 mm). The screws are fully threaded and are available in varying lengths as shown in Table 1. The specified diameters and other dimensions are provided in Table 1 for each screw. The screws are available in boxes of loose fasteners.

**3.2 Materials:**

**3.2.1 SWG Assy VG Plus Screws:** The screws are manufactured from carbon steel wire complying with the manufacturer's specifications. After the heads are formed

and the threads are rolled, the screws are hardened, in accordance with the manufacturer's specifications. The hardened screws are then galvanized with a minimum zinc coating thickness of 5 µm and coated with a lubricant.

**3.2.2 Wood Members:** Wood members may be sawn lumber; structural glued laminated timber (glulam) or parallel strand lumber (PSL) which is a type of structural composite lumber (SCL). Sawn wood side and main members must have a moisture content less than or equal to 19 percent at the time of screw installation and while in service. Glulam members must have a moisture content of less than 16 percent at the time of screw installation and while in service. For PSL, the moisture content at the time of installation and in service must be in accordance with the applicable ICC-ES evaluation report on the PSL. Sawn lumber must have an assigned specific gravity, as specified in Table 12.3.3A of the 2015 ANSI/AWC *National Design Specification for Wood Construction*® (NDS-15) (Table 11.3.3.A of NDS-12 for the 2012 IBC, Table 11.3.2A of NDS-05 for the 2009 and 2006 IBC) within the ranges given in Tables 2 through 4 in this report. Glulam must have Specific Gravity for Fastener Design, given in Section 5 of the NDS Supplement, within the ranges given in Tables 2 through 4 in this report. Parallel strand lumber (PSL) must have a minimum equivalent specific gravity, given in the applicable ICC-ES evaluation report, of 0.50.

The thickness of the wood main member,  $t_m$ , must be sufficient to ensure that the tip of the screw is embedded in the wood, with a minimum thickness of wood beyond the tip (cover) of 3/8 inch (9.5 mm). Unless noted otherwise, the minimum thickness of both main and side members must also be as follows: 15/16 inch (24 mm) for 1/4-inch-diameter (6 mm) screws; 1 3/16 inches (30 mm) for 5/16-inch-diameter (8 mm) screws; 1 9/16 inches (40 mm) for 3/8-inch-diameter (10 mm) screws; and 3 3/16 inches (80 mm) for 1/2-inch-diameter (12 mm) screws.

**3.2.3 Steel Side Plates:** Steel side plates must comply with the minimum requirements of ASTM A36. Steel plate thickness must be as required by Section 4.1.2. For use with screws installed at an incline, slotted holes must be predrilled to accommodate wedge washers.

**3.2.4 Wedge Washers:** Steel wedge washers are provided by the screw manufacturer for use with screws installed at an incline through steel side plates into wood members. See Figure 6.

**4.0 DESIGN AND INSTALLATION**

**4.1 Design:**

For design information for Assy VG Plus screws used in wood-to-wood connections where the screws are installed



perpendicular to the grain of the wood main member, see Section 4.1.1.

For design information for groups of Assy VG Plus screws used in wood-to-wood and steel-to-wood connections used to transfer lateral load, where the screws are installed at a 45 degree angle to the grain of the wood member(s), see Section 4.1.2.

#### 4.1.1 Connections with Screws Installed Perpendicular to the Grain of the Main Member:

**4.1.1.1 Governing Design Values:** The allowable lateral load for a single-screw connection is the lesser of: (a) the reference lateral design value described in Section 4.1.1.2, adjusted by all applicable adjustment factors, and (b) the allowable screw shear strength given in Table 1. The allowable load for a single-screw connection in which the screw is subject to tension is the least of: (a) the reference withdrawal design value described in Section 4.1.1.3, multiplied by the effective thread penetration in the main member,  $p_{t,m}$ , (length in the main member minus the tip length) and adjusted by all applicable adjustment factors; (b) the greater of the following, adjusted by all applicable adjustment factors: the reference withdrawal design value described in Section 4.1.1.3, multiplied by the effective thread penetration in the side member,  $p_{t,s}$ , (length in the side member minus the unthreaded length) and the reference head pull-through design value described in Section 4.1.1.3; and (c) the allowable screw tension strength given in Table 1.

**4.1.1.2 Reference Lateral Design Values (Z):** Reference lateral design values for select wood-to-wood connection configurations are given in Table 2. For other connection configurations, reference lateral design values for single shear connections with the screws loaded parallel or perpendicular to grain may be determined in accordance with Section 12.3.1 of NDS-15 (Section 11.3.1 of NDS-12 and NDS-05 for the 2012, 2009 and 2006 IBC) using the following parameters and limitations:

1. The applicable specified bending yield strength from Table 1 must be used for design.
2. The wood side member thickness must be a minimum of  $1\frac{3}{4}$  inches (45 mm).
3. The minimum effective screw penetration into the main member, excluding tip length, must be 6D, where D is the nominal diameter of the screw.
4. For sawn lumber, the specific gravity used for design purposes must be the assigned specific gravity in accordance with Table 12.3.3A of NDS-15 (Table 11.3.3A of NDS-12 for the 2012 IBC, Table 11.3.2A of NDS-05 for the 2009 and 2006 IBC).
5. For glulam, the specific gravity used for design purposes must be the applicable Specific Gravity for Fastener Design, given in Section 5 of the NDS Supplement.
6. For PSL, the specific gravity used for design purposes must be the equivalent specific gravity for the PSL given in the applicable ICC-ES evaluation report.

**4.1.1.3 Reference Withdrawal Design Values (W) and Head Pull-through Design Values ( $W_H$ ):** Reference withdrawal design values and reference head pull-through design values for SWG Assy VG Plus screws are given in Tables 3 and 4, respectively. The minimum effective screw penetration into the main member,  $p_t$ , excluding tip length, must be 8D.

**4.1.1.4 Adjustments to Reference Design Values:** Reference design values must be adjusted in accordance

with the requirements for dowel-type fasteners in Section 11.3 of NDS-15 (Section 10.3 of the NDS-12 and NDS-05 for the 2012, 2009 and 2006 IBC). Use is limited to dry in-service conditions, such that the wet service factor,  $C_M$ , is 1.0 in accordance with the NDS. The reference design values must also be adjusted in accordance with the requirements in Section 12.5 of NDS-15 (Section 11.5 of NDS-12 and NDS-05 for the 2012, 2009 and 2006 IBC) applicable to screws.

**4.1.1.5 Connections with Multiple Screws:** Connections containing multiple SWG Assy VG Plus screws must be designed in accordance with Sections 11.2.2 and 12.6 of NDS-15 (Sections 10.2.2 and 11.6 of NDS-12 and NDS-05 for the 2012, 2009 and 2006 IBC).

**4.1.1.6 Combined Loading:** Where SWG Assy VG Plus screws are subjected to combined lateral and withdrawal loads, connections must be designed in accordance with Section 12.4.1 of NDS-15 (Section 11.4.1 of NDS-12 and NDS-05 for the 2012, 2009 and 2006 IBC).

**4.1.1.7 Capacity Requirements for Wood Members:** When designing a connection, the structural members must be checked for load-carrying capacity in accordance with Section 11.1.2 of NDS-15 (Section 10.1.2 of NDS-12 and NDS-05 for the 2012, 2009 and 2006 IBC), and local stresses within the connection must be checked against Appendix E of the NDS to ensure the capacity of the connection and fastener group.

#### 4.1.2 Connections Made with Multiple Inclined Screws:

**4.1.2.1 General:** Connections used to transfer lateral loads between side members and a main member using groups of SWG Assy VG Plus screws installed at a 45-degree angle to the grain of the wood members must be designed in accordance with this section. Specific design procedures for steel-to-wood connections are addressed in Section 4.1.2.3. Specific design procedures for wood-to-wood connections are addressed in Section 4.1.2.4. The expected slip between the side member(s) and the main member at design load is less than  $\frac{1}{16}$  inch (1.6 mm).

**4.1.2.2 Applicable Parameters:** The design methods presented in Section 4.1.2 apply under the following conditions:

1. The connections are two or three member connections with a wood main member and either wood or steel side member(s).
2. Assigned specific gravity for sawn lumber and glulam, and equivalent specific gravity for PSL, must be within the ranges shown in Tables 3 and 4.
3. Screws used with steel side plates and wedge washers must be Assy VG Plus screws with countersunk heads.
4. The screws must be installed at a 45-degree angle to the wood grain, which is parallel to the direction of the force being transferred between the members.
5. The effective screw penetration in both the wood main member,  $p_{t,m}$ , and the wood side member,  $p_{t,s}$ , must be a minimum of 8D, measured along the axis of the screw.
6. A minimum of 2 screws must be used in each connection.
7. Spacing, edge distance and end distance must be as described in Table 5 and Figures 4, 5 or 7, as applicable.

8. Wood side members must be of sufficient thickness to accommodate a minimum thread length of 8D plus the length of the unthreaded portion of the screw, 'a', shown in Table 1.
9. For connections of steel side plates to wood main members, the spacing between the outermost screws perpendicular to grain must not exceed 5 inches (127 mm).
10. Steel side plate thickness must be as shown in the following table, to accommodate the available wedge washers:

NOMINAL SCREW DIAMETER (inch)	MIN. PLATE THICKNESS (inch)	MAX. PLATE THICKNESS (inch)
5/16	3/16	1/2
3/8	1/4	3/4
1/2	1/4	1

For SI: 1 inch = 25.4 mm

**4.1.2.3 Steel-to-Wood Connections:**

**4.1.2.3.1 Two-member Connections:** The allowable lateral load for a two-member connection with a steel side member and a wood main member must be determined as follows:

1. Determine the length of the screw in the side member as follows:

$$l_s = l_w + t_s / \cos 45^\circ$$

Where:

$l_w$  = the length of the screw in the wedge washer. (See Figure 6)

$t_s$  = the thickness of the steel side member.

2. Determine the effective length of the screw in the main member as follows:

$$p_{t,m} = L - l_s - L_t$$

Where:

$L$  = the length of the screw as shown in Table 1 and Figures 1 through 3.

$L_t$  = the tip length of the screw as shown in Table 1 and Figures 1 through 3.

3. Determine the applicable reference withdrawal design value for the screw installed at 45° to the grain of the wood, in pounds-force per inch,  $W_{45}$ , by referring to Table 3. Then determine the allowable withdrawal strength in the main member,  $W'_m$ , as follows:

$$W'_m = W_{45} \cdot p_{t,m} \cdot C'$$

Where:

$C'$  = the product of all applicable adjustment factors determined in accordance with the NDS.  $C_g$  does not apply.

4. If the allowable withdrawal strength in the main member is less than the allowable fastener tension strength,  $T_a$ , shown in Table 1, the allowable lateral strength of the multiple fastener connection,  $P_a$ , must be determined as follows:

$$P_a = 0.9 \cdot n \cdot W'_m \cdot \cos 45^\circ$$

Where:

$n$  = the number of screws acting together in the shear plane.

5. If the allowable withdrawal strength in the main member exceeds the allowable fastener tension strength,  $T_a$ , shown in Table 1, the allowable lateral strength of the multiple fastener connection must be determined as follows:

$$P_a = 0.9 \cdot n \cdot T_a \cdot \cos 45^\circ$$

6. The structural members must be checked for load-carrying capacity along the entire load path in accordance with the code. This verification must include, but not be limited to, verifying the longitudinal shear capacity of the wood member; the cross tension capacity of the wood member; and the fastener group or individual fastener wood tear out capacities.

**4.1.2.3.2 Three-member Connections:** The allowable lateral load for a three-member connection with two steel side members and a wood main member is equal to two times the allowable lateral load for a two-member connection with a steel side member and a wood main member, determined in accordance with Section 4.1.2.3.1.

**4.1.2.4 Wood-to-wood Connections:**

**4.1.2.4.1 Two-member Connections:** The allowable lateral load for a two-member connection with a wood side member and a wood main member must be determined as follows:

1. Determine the effective length of the screw in the side member as follows:

$$p_{t,s} = (t_s / \cos 45^\circ) - a - l_H$$

Where:

$t_s$  = The thickness of the wood side member.

$a$  = The dimension from the top of the screw head to the start of the threads, as shown in Table 1 and Figures 1 through 3.

$l_H$  = for screws countersunk beneath the surface of the wood, the dimension from the surface of the wood to the top of the countersunk head, measured along the axis of screw.

2. Determine the effective length of the screw in the main member as follows:

$$p_{t,m} = L - (p_{t,s} + a) - L_t$$

3. Determine the applicable reference withdrawal design value for the screw installed at 45° to the grain of the wood, in pounds-force per inch,  $W_{45}$ , by referring to Table 3.

4. Determine the allowable withdrawal strength in the side member and the main member, as follows:

$$W'_s = W_{45} \cdot p_{t,s} \cdot C'$$

$$W'_m = W_{45} \cdot p_{t,m} \cdot C'$$

5. If the allowable withdrawal strength in either the side member or the main member (or both) is less than the allowable fastener tension strength shown in Table 1, the allowable lateral strength of the multiple fastener connection must be determined as follows:

$$P_a = 0.9 \cdot n \cdot \min \left[ \frac{W'_s}{W'_m} \right] \cdot \cos 45^\circ$$

6. If both the allowable withdrawal strength in the side member and the allowable withdrawal strength in the main member exceed the allowable fastener tension strength shown,  $T_a$ , in Table 1, the allowable lateral strength of the connection must be determined as follows:

$$P_a = 0.9 \cdot n \cdot T_a \cdot \cos 45^\circ$$

7. The structural members must be checked for load-carrying capacity in accordance with Section 4.1.2.3.1.

**4.1.2.3.1 Three-member Connections:** The allowable lateral load for a three-member connection with two wood side members and a wood main member is equal to two times the allowable lateral load for a two-member connection with a wood side member and a wood main member, determined in accordance with Section 4.1.2.4.1.

**4.2 Installation:**

**4.2.1 General:** SWG Assy VG Plus screws must be installed in accordance with the manufacturer's published installation instructions, the approved plans and this report.

Screws must be driven using the manufacturer-recommended drive bit, with a rotary drill, or a percussion drill set to rotary only mode. After installation, the flat surface of the countersunk heads and the top of the cylindrical heads must be flush with the surface of the side member, for screws installed perpendicular to wood side members. For screws installed at an incline, the head of the screw relative to the surface of the wood or steel side member must be as shown in Figures 4, 5 and 7, as applicable. The screws must not be overdriven and the side member(s) must be in direct contact with the main member, such that no gap exists between the members.

**4.2.2 End Distance, Edge Distance and Spacing:** Minimum wood member end distances, edge distances and spacing of the screws must be sufficient to prevent splitting of the wood, or as required by Table 5, whichever is greater. When the screws are used in PSL, the minimum screw end and edge distances and spacing must be in accordance with Table 5 or in accordance with the ICC-ES evaluation report on the PSL, whichever is more restrictive. Steel plate edge distance must be a minimum of 1.5 times the diameter of the screw and spacing must be a minimum of 3 times the diameter of the screw. For slotted holes, the minimum edge distance must be measured from the end of the slot.

**4.2.3 Pilot Holes:** Typical installation of SWG Assy VG Plus screws does not require predrilling of the wood member. Predrilling to reduce splitting is recommended by the manufacturer for certain situations, including the following conditions:

1. For species which are prone to splitting, including fir, Douglas fir and spruce.
2. For lumber with thickness  $\leq 1\frac{1}{2}$  inches (35 mm).
3. For laterally loaded screws installed in lumber with a thickness  $\leq 7D$  ( $\leq 14D$  for fir, Douglas fir and spruce).
4. For axially loaded screws installed in lumber with a thickness  $\leq 10D$  and/or a width of less than  $8D$  or  $2\frac{3}{8}$  inches (60 mm), whichever is greater.

Contact the manufacturer's technical support for additional guidance. For recommended sizes of predrilled holes, see Table 6.

**4.2.4 Installation of Inclined Screws:** Screws must be installed such that their main axis is oriented at 45 degrees ( $\pm 3^\circ$ ) to the wood grain. A pre-drill jig is provided by the screw manufacturer to facilitate installation through wood side members at this angle. For installation through steel side plates, a wedge shaped washer is provided by the screw manufacturer for use with slotted holes in the steel plate. A pre-drill jig is provided by the screw manufacturer to facilitate installation through steel side plates with slotted holes. Alternatively, the predrilled holes in the steel plate must be at a 45-degree angle to the surface of the plate.

**4.2.5 Three-member Connections:** Opposing screws installed through the side members with their respective

axes perpendicular to one another must be offset from each other a minimum of 1.5D, to allow them to overlap. It is recommended that opposing screws overlap a minimum of 4D measured along the axis of the screws, to minimize cross-grain tension effects.

**4.3 Special Inspection:** Wood-to-wood or steel-to-wood connections with inclined screws must be considered special cases in accordance with 2015 and 2012 IBC Section 1705.1.1 (2009 IBC Section 1704.15, 2006 IBC Section 1704.13).

**5.0 CONDITIONS OF USE**

The SWG Assy VG Plus screws described in this report comply with, or are suitable alternatives to what is specified in, those codes listed in Section 1.0 of this report, subject to the following conditions:

- 5.1 The screws must be installed in accordance with the manufacturer's published installation instructions, the approved plans and this report. In the case of a conflict between this report and the manufacturer's installation instructions, the more restrictive requirements govern.
- 5.2 Calculations and details demonstrating compliance with this report must be submitted to the code official. The calculations and details must be prepared by a registered design professional where required by the statutes of the jurisdiction in which the project is to be constructed.
- 5.3 SWG Assy VG Plus screws must be installed and used in dry in-service conditions where the moisture content of the wood members complies with Section 3.2.2.
- 5.4 Use of the screws in contact with preservative-treated or fire-retardant-treated wood is outside the scope of this report.
- 5.5 Assy VG Plus screws are manufactured under a quality control program with inspections by ICC-ES.

**6.0 EVIDENCE SUBMITTED**

Data in accordance with the ICC-ES Acceptance Criteria for Alternate Dowel-type Threaded Fasteners (AC233), dated April 2015 (editorially revised August 2015), including data in accordance with Annex A to AC233.

**7.0 IDENTIFICATION**

- 7.1 Individual SWG Assy VG Plus screws are identified in the field by their unique configurations. In addition, the countersunk screw heads are marked with the letters "ASSY", as shown in Figures 2 and 3. Packages of screws are identified with the manufacturer's name (SWG); product name (Assy VG Plus); head type and drive size; screw diameter and length (in both inches and millimeters); and the evaluation report number (ESR-3178).

- 7.2 The report holder's contact information is the following:

**SCHRAUBENWERK GAISBACH GmbH (SWG)**  
**AM BAHNHOF 50**  
**D-74638 WALDENBURG**  
**GERMANY**  
**+49 7942 1000**  
[info@swg-produktion.de](mailto:info@swg-produktion.de)  
[www.swg-produktion.de](http://www.swg-produktion.de)

- 7.3 The technical support company contact information is the following:

**MYTICON TIMBER CONNECTORS INC.**  
**(866) 899-4090**  
[info@my-ti-con.com](mailto:info@my-ti-con.com)  
[www.my-ti-con.com](http://www.my-ti-con.com)

TABLE 1—FASTENER SPECIFICATIONS AND STRENGTHS—SWG ASSY VG PLUS SCREWS

NOMINAL DIAMETER, D (inch)	HEAD STYLE	OUTSIDE THREAD DIAMETER (inch)	ROOT DIAMETER (inch)	THREAD PITCH (inch)	HEAD DIAMETER (inch)	DRIVE TYPE AND SIZE	OVERALL LENGTH <sup>1</sup> (inches)	UNTHREADED PORTION, 'a' (inch)	TIP LENGTH, L <sub>t</sub> (inch)	SPECIFIED BENDING YIELD STRENGTH <sup>2</sup> , F <sub>yb</sub> (psi)	ALLOWABLE FASTENER STRENGTH	
											Tension, T <sub>a</sub> (lbf)	Shear, V <sub>a</sub> (lbf)
1/4	Cylindrical	0.236	0.150	0.102	0.317	AW 30	3 1/2 to 4 3/4	0.394	0.236	129,200	1165	590
							5 1/2 to 10 1/4	0.472				
5/16	Cylindrical	0.315	0.197	0.146	0.390	AW 40	3 7/8 to 11	0.551	0.315	132,500	1775	1105
							11 3/4 to 17 3/4	0.590				
							18 7/8 to 23 5/8	0.787				
	Countersunk	0.315	0.197	0.146	0.583	AW 40	3 7/8 to 11	0.551	0.315	132,500	1775	1105
							11 3/4 to 17 3/4	0.590				
							18 7/8 to 23 5/8	0.787				
3/8	Cylindrical	0.394	0.244	0.173	0.528	AW 50	4 3/4 to 17 3/4	0.709	0.394	136,600	2550	1835
							18 7/8 to 31 1/2	0.905				
	Countersunk	0.394	0.244	0.173	0.772	AW 50	4 3/4 to 17 3/4	0.709	0.394	136,600	2550	1835
							18 7/8 to 31 1/2	0.905				
1/2	Cylindrical	0.472	0.280	0.236	0.559	AW50	5 1/2 to 9 1/2	0.827	0.472	166,300	3470	2095
							12 1/4 to 23 5/8	1.024				
	Countersunk	0.472	0.280	0.232	0.868	AW 50	5 1/2 to 9 1/2	0.827	0.472	166,300	3470	2095
							12 1/4 to 23 5/8	1.024				

For SI: 1 inch = 25.4 mm, 1 lbf = 4.4 N, 1 psi = 6.89 kPa.

<sup>1</sup> Overall fastener length is measured from top of head to bottom of tip.

<sup>2</sup> Bending yield strength determined in accordance with ASTM F1575 using the root diameter.

TABLE 2—REFERENCE LATERAL DESIGN VALUES (Z) FOR WOOD-TO-WOOD CONNECTIONS<sup>1,2,3,4,5</sup>

FASTENER DESIGNATION <sup>1</sup>	SIDE MEMBER THICKNESS (inches)	MINIMUM FASTENER PENETRATION INTO MAIN MEMBER (inches)	REFERENCE LATERAL DESIGN VALUE, Z (lbF) FOR SPECIFIC GRAVITIES OF											
			0.33			0.42			0.49			0.55		
			Z <sub>  </sub>	Z <sub>L/  </sub>	Z <sub>⊥</sub>	Z <sub>  </sub>	Z <sub>L/  </sub>	Z <sub>⊥</sub>	Z <sub>  </sub>	Z <sub>L/  </sub>	Z <sub>⊥</sub>	Z <sub>  </sub>	Z <sub>L/  </sub>	Z <sub>⊥</sub>
1/4" x 4"	2	1 3/4	99	99	99	123	123	123	142	142	142	158	158	158
1/4" x 5 1/2"	2 3/4	2 1/2	99	99	99	123	123	123	142	142	142	158	158	158
1/4" x 6 1/4"	3 1/2	2 1/2	99	99	99	123	123	123	142	142	142	158	158	158
1/4" x 7 1/8"	4	2 1/8	99	99	99	123	123	123	142	142	142	158	158	158
1/4" x 7 7/8"	5 1/2	2 1/8	99	99	99	123	123	123	142	142	142	158	158	158
1/4" x 8 5/8"	6	2 1/8	99	99	99	123	123	123	142	142	142	158	158	158
1/4" x 9 1/2"	7	2 1/4	99	99	99	123	123	123	142	142	142	158	158	158
1/4" x 11 3/4"	7 1/2	4	99	99	99	123	123	123	142	142	142	158	158	158
1/4" x 11 3/4"	8	3 1/2	99	99	99	123	123	123	142	142	142	158	158	158
1/4" x 11 3/4"	9	2 1/2	99	99	99	123	123	123	142	142	142	158	158	158
5/16" x 4 3/8"	2	2 1/16	148	118	118	194	155	155	223	179	179	248	199	199
5/16" x 5 1/2"	2 3/4	2 1/16	155	124	124	194	155	155	223	179	179	248	199	199
5/16" x 6 1/8"	3 1/2	2 1/16	155	124	124	194	155	155	223	179	179	248	199	199
5/16" x 7 1/8"	4	2 13/16	155	124	124	194	155	155	223	179	179	248	199	199
5/16" x 7 1/8"	5 1/2	2 1/16	155	124	120	194	155	155	223	179	179	248	199	199
5/16" x 8 5/8"	6	2 5/16	155	124	124	194	155	155	223	179	179	248	199	199
5/16" x 9 1/2"	7	2 1/16	155	124	124	194	155	155	223	179	179	248	199	199
5/16" x 11"	7 1/2	3 3/16	155	124	124	194	155	155	223	179	179	248	199	199
5/16" x 12 5/8"	8	4 3/16	155	124	124	194	155	155	223	179	179	248	199	199
5/16" x 13 3/8"	9	4 1/16	155	124	124	194	155	155	223	179	179	248	199	199
5/16" x 14 3/8"	10	3 13/16	155	124	124	194	155	155	223	179	179	248	199	199
5/16" x 15 3/4"	11	4 1/16	155	124	124	194	155	155	223	179	179	248	199	199
5/16" x 16 3/8"	12	4 1/16	155	124	124	194	155	155	223	179	179	248	199	199
5/16" x 18 1/8"	14	4 3/16	155	124	124	194	155	155	223	179	179	248	199	199
5/16" x 20 7/8"	16	4 9/16	155	124	124	194	155	155	223	179	179	248	199	199
5/16" x 22 1/8"	18	4 1/16	155	124	124	194	155	155	223	179	179	248	199	199
3/8" x 5 1/2"	2	3 1/8	170	136	136	239	191	191	289	231	231	321	257	257
3/8" x 5 1/2"	2 3/4	2 3/8	186	149	149	251	201	201	289	231	231	321	257	257
3/8" x 6 1/4"	2 3/4	3 1/8	201	161	161	251	201	201	289	231	231	321	257	257
3/8" x 7 1/8"	3 1/2	3 1/4	201	161	161	251	201	201	289	231	231	321	257	257
3/8" x 7 1/8"	4	3 1/2	201	161	161	251	201	201	289	231	231	321	257	257
3/8" x 9 1/2"	5 1/2	3 5/8	201	161	161	251	201	201	289	231	231	321	257	257
3/8" x 11 3/4"	6	5 3/8	201	161	161	251	201	201	289	231	231	321	257	257
3/8" x 11 3/4"	7	4 3/8	201	161	161	251	201	201	289	231	231	321	257	257
3/8" x 12 5/8"	7 1/2	4 3/4	201	161	161	251	201	201	289	231	231	321	257	257
3/8" x 13 3/8"	8	5	201	161	161	251	201	201	289	231	231	321	257	257
3/8" x 13 3/8"	8 1/2	5 1/4	201	161	161	251	201	201	289	231	231	321	257	257
3/8" x 14 1/8"	9	5 3/8	201	161	161	251	201	201	289	231	231	321	257	257
3/8" x 14 1/8"	9 1/2	5 1/8	201	161	161	251	201	201	289	231	231	321	257	257
3/8" x 15"	10	4 3/8	201	161	161	251	201	201	289	231	231	321	257	257
3/8" x 15 3/4"	11	4 3/8	201	161	161	251	201	201	289	231	231	321	257	257
3/8" x 16 3/8"	11 1/2	4 1/2	201	161	161	251	201	201	289	231	231	321	257	257
3/8" x 17 1/4"	12	4 7/8	201	161	161	251	201	201	289	231	231	321	257	257
3/8" x 18 1/8"	13	5 1/2	201	161	161	251	201	201	289	231	231	321	257	257
3/8" x 20 7/8"	14	6 1/2	201	161	161	251	201	201	289	231	231	321	257	257
3/8" x 22 1/8"	16	6 1/2	201	161	161	251	201	201	289	231	231	321	257	257
3/8" x 25 1/8"	18	7 1/4	201	161	161	251	201	201	289	231	231	321	257	257
3/8" x 27 1/2"	20	7 1/8	201	161	161	251	201	201	289	231	231	321	257	257
3/8" x 29 1/2"	21	8 1/8	201	161	161	251	201	201	289	231	231	321	257	257
3/8" x 31 1/2"	22	9 1/8	201	161	161	251	201	201	289	231	231	321	257	257

TABLE 2—REFERENCE LATERAL DESIGN VALUES (Z) FOR WOOD-TO-WOOD CONNECTIONS<sup>1,2,3,4,5</sup> (Continued)

FASTENER DESIGNATION <sup>1</sup>	SIDE MEMBER THICKNESS (inches)	FASTENER PENETRATION INTO MAIN MEMBER (inches)	REFERENCE LATERAL DESIGN VALUE, Z (lbf) FOR SPECIFIC GRAVITIES OF											
			0.33			0.42			0.49			0.55		
			Z <sub>  </sub>	Z <sub>⊥/  </sub>	Z <sub>⊥</sub>	Z <sub>  </sub>	Z <sub>⊥/  </sub>	Z <sub>⊥</sub>	Z <sub>  </sub>	Z <sub>⊥/  </sub>	Z <sub>⊥</sub>	Z <sub>  </sub>	Z <sub>⊥/  </sub>	Z <sub>⊥</sub>
1/2" x 7 1/8"	3 1/2	3 1/8	351	246	198	396	287	264	427	316	295	453	340	321
1/2" x 7 7/8"	3 1/2	3 1/8	351	246	220	396	287	264	427	316	295	453	340	321
1/2" x 7 7/8"	4	3 3/8	351	246	221	396	287	264	427	316	295	453	340	321
1/2" x 9 1/2"	5 1/2	3 1/2	351	246	222	396	287	264	427	316	295	453	340	321
1/2" x 10 1/4"	5 1/2	4 1/4	351	246	222	396	287	264	427	316	295	453	340	321
1/2" x 11 3/4"	6	5 1/4	351	246	222	396	287	264	427	316	295	453	340	321
1/2" x 12 5/8"	7	5 1/8	351	246	222	396	287	264	427	316	295	453	340	321
1/2" x 12 5/8"	7 1/2	4 3/8	351	246	222	396	287	264	427	316	295	453	340	321
1/2" x 13 3/8"	8	4 1/8	351	246	222	396	287	264	427	316	295	453	340	321
1/2" x 13 3/8"	8 1/2	4 3/8	351	246	222	396	287	264	427	316	295	453	340	321
1/2" x 15"	8 1/2	6	351	246	222	396	287	264	427	316	295	453	340	321
1/2" x 14 1/8"	9	4 5/8	351	246	222	396	287	264	427	316	295	453	340	321
1/2" x 14 1/8"	9 1/2	4 1/8	351	246	222	396	287	264	427	316	295	453	340	321
1/2" x 15 3/4"	9 1/2	5 3/4	351	246	222	396	287	264	427	316	295	453	340	321
1/2" x 15"	10	4 1/2	351	246	222	396	287	264	427	316	295	453	340	321
1/2" x 15 3/4"	10	5 1/4	351	246	222	396	287	264	427	316	295	453	340	321
1/2" x 15 3/4"	11	4 1/4	351	246	222	396	287	264	427	316	295	453	340	321
1/2" x 16 3/8"	11	5 1/4	351	246	222	396	287	264	427	316	295	453	340	321
1/2" x 16 3/8"	11 1/2	4 3/8	351	246	222	396	287	264	427	316	295	453	340	321
1/2" x 17 1/4"	11 1/2	5 1/4	351	246	222	396	287	264	427	316	295	453	340	321
1/2" x 17 1/4"	12	4 3/4	351	246	222	396	287	264	427	316	295	453	340	321
1/2" x 18 1/8"	13	4 3/8	351	246	222	396	287	264	427	316	295	453	340	321
1/2" x 20 1/8"	14	6 3/8	351	246	222	396	287	264	427	316	295	453	340	321
1/2" x 23 5/8"	16	7 1/8	351	246	222	396	287	264	427	316	295	453	340	321

For SI: 1 inch = 25.4 mm, 1 lbf = 4.4 N.

<sup>1</sup>Fastener length shown is a minimum. Tabulated values may be applied to longer fasteners, with greater penetration into the main member.

<sup>2</sup>Tabulated reference lateral design values, Z, apply to screws driven into the side grain of the main member, such that the screws are oriented perpendicular to the grain and loaded as follows:

Z<sub>||</sub> : Both side and main members loaded parallel to grain.

Z<sub>⊥/||</sub> : Side member loaded perpendicular to grain; main member loaded parallel to grain

Z<sub>⊥</sub> : Both side and main members loaded perpendicular to grain.

<sup>3</sup>Reference lateral design values must be multiplied by all adjustment factors applicable to wood screws, in accordance with the NDS.

<sup>4</sup>SWG Assy VG Plus screws must be installed and used in dry in-service conditions, such that the wet service factor, C<sub>M</sub>, is 1.0 in accordance with the NDS.

<sup>5</sup>The specific gravity used for design purposes must be the assigned specific gravity for sawn lumber per Table 12.3.3.A of NDS-15 (Table 11.3.3A of NDS-12, Table 11.3.2A of NDS-05) or the applicable Specific Gravity for Fastener Design for glulam, given in Section 5 of the NDS Supplement; or the equivalent specific gravity given in the applicable ICC-ES evaluation report on the PSL product.

TABLE 3—REFERENCE WITHDRAWAL DESIGN VALUES ( $W$ )<sup>2,3</sup> (lbf/in)

NOMINAL FASTENER DIAMETER (inch)	FOR SPECIFIC GRAVITIES (SG) AND EQUIVALENT SPECIFIC GRAVITIES (ESG) OF: <sup>4</sup>				
	Sawn Lumber and Glulam				PSL
	SG = 0.55	SG = 0.49	SG = 0.42	SG = 0.35	ESG ≥ 0.50
<b><math>W_{90}</math> - For screws driven into the side grain of the main member, such that the screws are oriented perpendicular to the grain and loaded in direct withdrawal<sup>1</sup>:</b>					
1/4	230	202	169	137	156
5/16	279	248	212	176	179
3/8	317	280	237	188	211
1/2	331	297	251	209	223
<b><math>W_{45}</math> - For screws driven into the side grain of the main member, such that the screws are oriented at 45 degrees to the grain and loaded along the axis of the screw:</b>					
1/4	197	173	145	118	156
5/16	239	212	182	151	179
3/8	272	240	203	163	211
1/2	284	254	215	179	223

For **SI**: 1 inch = 25.4 mm, 1 lbf = 4.4 N.

<sup>1</sup> Values must be multiplied by all adjustment factors applicable to wood screws, in accordance with the NDS.

<sup>2</sup> SWG Assy VG Plus screws must be installed and used in dry in-service conditions, such that the wet service factor,  $C_M$ , is 1.0 in accordance with the NDS.

<sup>3</sup> Reference withdrawal design values are to be multiplied by the length of thread penetration into the main member. Main member penetration must be at least 8 times the nominal diameter. Thread length does not include the length of the tip.

<sup>4</sup> The specific gravity used for design purposes must be the assigned specific gravity for sawn lumber per Table 12.3.3A of NDS-15 (Table 11.3.3A of NDS-12, Table 11.3.2A of NDS-05) or the applicable Specific Gravity for Fastener Design for glulam, given in Section 5 of the NDS Supplement; and the equivalent specific gravity (ESG) must be the equivalent specific gravity given in the applicable ICC-ES evaluation report on the PSL product.

TABLE 4—REFERENCE HEAD PULL-THROUGH DESIGN VALUES ( $W_{th}$ )<sup>1,2,3</sup> (lbf)

NOMINAL FASTENER DIAMETER (inch)	HEAD TYPE	MINIMUM SIDE MEMBER THICKNESS, $t_s$ (inches)	FOR SPECIFIC GRAVITIES (SG) AND EQUIVALENT SPECIFIC GRAVITIES (ESG) OF: <sup>4</sup>				
			Sawn Lumber				PSL
			SG = 0.55	SG = 0.49	SG = 0.42	SG = 0.35	ESG ≥ 0.50
$\frac{5}{16}$	Countersunk, Countersunk Milling Pocket	$1\frac{3}{8}$	414	350	281	216	398
$\frac{3}{8}$	Countersunk, Countersunk Milling Pocket		474	408	334	266	491
$\frac{1}{2}$	Countersunk, Countersunk Milling Pocket		474	408	334	266	491

For SI: 1 inch = 25.4 mm, 1 lbf = 4.4 N.

<sup>1</sup>Tabulated head pull-through design values,  $W_{th}$ , must be multiplied by all adjustment factors applicable to wood screw withdrawal, in accordance with the NDS.

<sup>2</sup>Design values apply to connections with minimum side member thicknesses,  $t_s$ , as given above.

<sup>3</sup>SWG Assy VG Plus screws must be installed and used in dry in-service conditions, such that the wet service factor,  $C_M$ , is 1.0 in accordance with the NDS.

<sup>4</sup>The specific gravity (SG) used for design purposes must be the assigned specific gravity for sawn lumber per NDS Table 11.3.3A (Table 11.3.2A of the 2005 NDS) or the applicable Specific Gravity for Fastener Design for glulam, given in Section 5 of the NDS Supplement; and the equivalent specific gravity (ESG) must be the equivalent specific gravity given in the applicable ICC-ES evaluation report on PSL product.

TABLE 5—CONNECTION GEOMETRY REQUIREMENTS<sup>1</sup>

CONDITION	MINIMUM DIMENSION (in terms of nominal screw diameter, D)	
	LATERALLY LOADED SCREWS	AXIALLY LOADED SCREWS
<b>Screws Installed Perpendicular to the Surface of the Wood Member</b>		
End distance	7D (10.5D in D-Fir)	5D (7.5D in D-Fir)
Edge distance	Lateral Loading parallel to grain	3D
	Lateral Loading perpendicular to grain	7D
	Axial Load on fastener	-
Spacing between fasteners in a row	7D (10.5D in D-Fir)	5D (7.5D in D-Fir)
Spacing between rows <sup>2</sup>	Loading parallel to grain	4D
	Loading perpendicular to grain	5D
	Axial Load on fastener	-
<b>Screws Installed at an Incline<sup>3</sup></b>		
End distance, $a_{AXIAL}$	5D (7.5D in D-Fir) <sup>4</sup>	
Edge distance, $e_{AXIAL}$	3D	
Spacing between fasteners in a row, $S_{P, AXIAL}$	5D (7.5D in D-Fir)	
Spacing between rows of fasteners, $S_{O, AXIAL}$	2.5D	

<sup>1</sup>End distances, edge distances and screw spacing must be sufficient to prevent splitting of the wood, or as required by this table, whichever is the more restrictive.

<sup>2</sup>Within a row, fasteners may be staggered up to 2D to further reduce the potential for splitting.

<sup>3</sup>See Figures 4 and 5.

<sup>4</sup>End distance must also be sufficient to ensure that the screw is fully embedded in the wood member.



TABLE 7—RECOMMENDED DIAMETER OF PREDRILLED HOLES<sup>1</sup> (inch)

NOMINAL FASTENER DIAMETER (inch)	APPLICABLE LOAD CONDITION AND SPECIFIC GRAVITY		
	Screws Subject to Lateral Load		Screws Loaded Axially
	SG ≤ 0.5	SG > 0.5 and PSL	0.35 ≤ SG ≤ 0.55 and PSL
1/4	5/32	5/32	5/32
5/16	13/64	7/32	13/64
3/8	15/64	1/4	15/64
1/2	17/64	5/16	17/64

For SI: 1 inch = 25.4 mm.

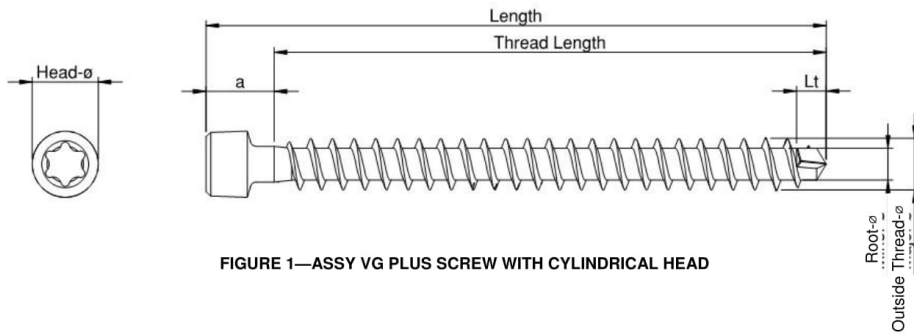


FIGURE 1—ASSY VG PLUS SCREW WITH CYLINDRICAL HEAD

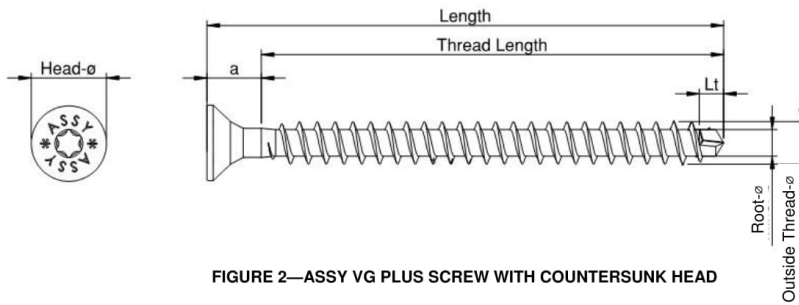


FIGURE 2—ASSY VG PLUS SCREW WITH COUNTERSUNK HEAD

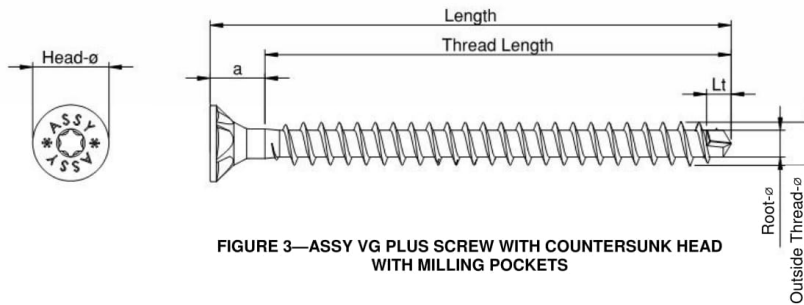
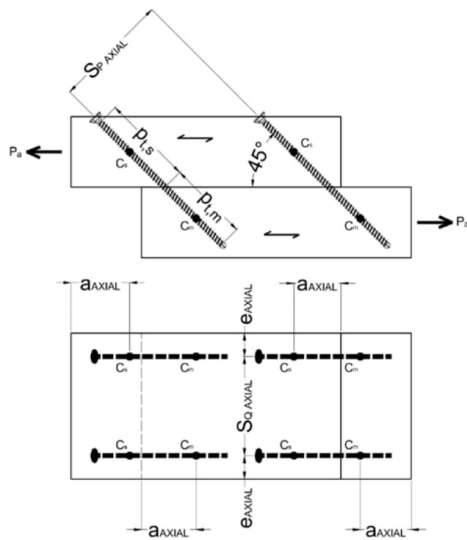


FIGURE 3—ASSY VG PLUS SCREW WITH COUNTERSUNK HEAD WITH MILLING POCKETS



Note:  $C_m$  = Center of gravity of the threaded portion of the screw in the main member;  $C_s$  = Center of gravity of the threaded portion of the screw in the side member.

FIGURE 4—CONNECTION GEOMETRY FOR INCLINED SCREWS IN TWO-MEMBER WOOD-TO-WOOD CONNECTION

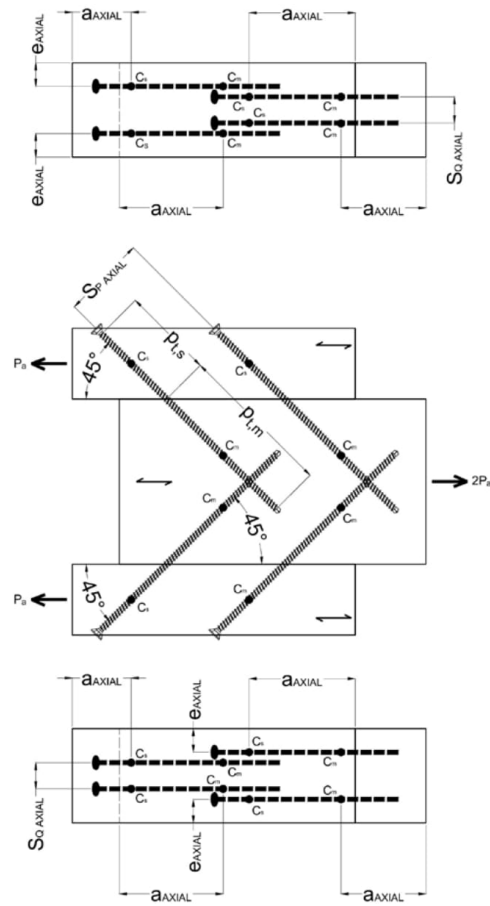


FIGURE 5—CONNECTION GEOMETRY FOR INCLINED SCREWS IN THREE-MEMBER WOOD-TO-WOOD CONNECTION

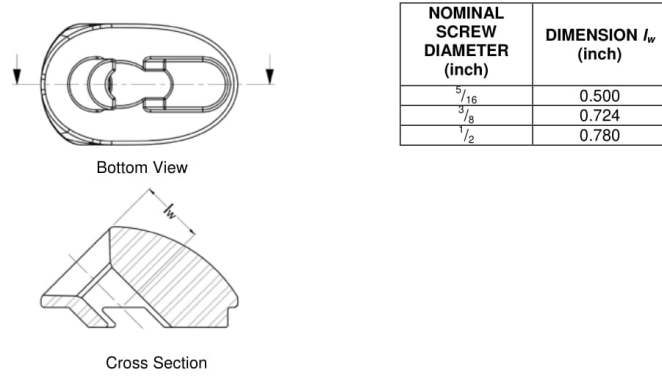
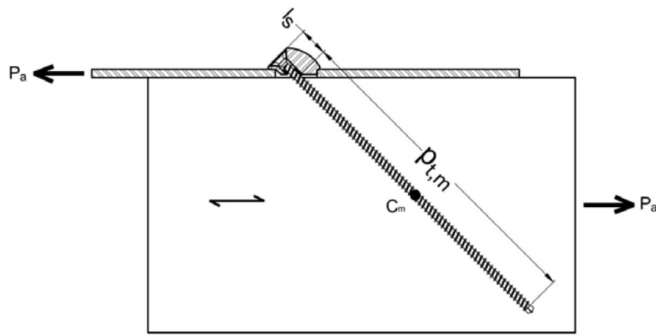


FIGURE 6—STEEL WEDGE WASHER



Note: Minimum dimensions for end distance, edge distance and spacing of the screws in the wood member are as shown in Figure 4.

FIGURE 7—CONNECTION GEOMETRY FOR INCLINED SCREWS  
STEEL-TO-WOOD CONNECTION

## **APPENDIX E. EPOXY GLUE SPECIFICATION**

## Safety Data Sheet

According to OSHA Hazard Communication Standard, 29 CFR 1910.1200

Initial preparation date: 07.25.2018

Page 1 of 9

### Clear Epoxy Resin - Part A

#### SECTION 1: Identification

##### Product identifier

**Product name:** Clear Epoxy Resin - Part A

**Product code:** 50101, 50112, 50114, 50114H, 50132, 50240, 50240H



##### Recommended use of the product and restriction on use

**Relevant identified uses:** Adhesive Part A

**Uses advised against:** Not determined or not applicable.

**Reasons why uses advised against:** Not determined or not applicable.

##### Manufacturer or supplier details

###### Manufacturer:

###### United States

J-B Weld Company, LLC  
400 CMH Road  
Sulphur Springs, TX 75482  
903-885-7696  
info@jbweld.com

##### Emergency telephone number:

###### United States

CHEMTREC

Transportation Emergencies (24 hour): 800-424-9300 or  
703-527-3887

Poison Control Centers (24 hour): medical emergencies 800-222-1222

#### SECTION 2: Hazard(s) identification

##### GHS classification:

Skin irritation, category 2  
Eye irritation, category 2A  
Skin sensitization, category 1

##### Label elements

###### Hazard pictograms:



**Signal word:** Warning

###### Hazard statements:

H315 Causes skin irritation.  
H319 Causes serious eye irritation.  
H317 May cause an allergic skin reaction.

###### Precautionary statements:

P264 Wash skin and eyes thoroughly after handling.  
P280 Wear protective gloves/protective clothing/eye protection/face protection.  
P261 Avoid breathing dust/fume/gas/mist/vapors/spray.  
P272 Contaminated work clothing should not be allowed out of the workplace.  
P321 Specific treatment (see supplemental first aid instructions on this label).  
P362 Take off contaminated clothing and wash before reuse  
P302+P352 IF ON SKIN: Wash with plenty of soap and water.

## Safety Data Sheet

According to OSHA Hazard Communication Standard, 29 CFR 1910.1200

Initial preparation date: 07.25.2018

Page 2 of 9

### Clear Epoxy Resin - Part A

P332+P313 If skin irritation occurs: Get medical advice/attention  
P305+P351+P338 IF IN EYES: Rinse cautiously with water for several minutes. Remove contact lenses, if present and easy to do. Continue rinsing.  
P337+P313 If eye irritation persists get medical advice/attention  
P363 Wash contaminated clothing before reuse  
P333+P313 If skin irritation or a rash occurs: Get medical advice/attention  
P501 Dispose of contents/container in accordance with local regulations.

**Hazards not otherwise classified:** None

### SECTION 3: Composition/information on ingredients

Identification	Name	Weight %
CAS number: 3101-60-8	P-tert-butylphenyl 1-(2,3-epoxy)propyl ether	<5
CAS number: 25068-38-6	Epoxy Resin	<98

#### Additional Information:

The specific chemical identity and/or exact percentage (concentration) of composition has been withheld as a trade secret in accordance with paragraph (i) of the OSHA Hazard Communication Standard (29 CFR §1910.1200).

### SECTION 4: First aid measures

#### Description of first aid measures

##### General notes:

Not determined or not applicable.

##### After inhalation:

Loosen clothing as necessary and position individual in a comfortable position  
Maintain an unobstructed airway  
Get medical advice/attention if you feel unwell

##### After skin contact:

Rinse affected area with soap and water  
If symptoms develop or persist, seek medical attention  
Take off all contaminated clothing  
Gently blot or brush away excess product  
Wash with plenty of lukewarm, gently flowing water  
Get medical advice if skin irritation occurs or you feel unwell

##### After eye contact:

Rinse/flush exposed eye(s) gently using water for 15-20 minutes  
If symptoms develop or persist, seek medical attention  
Rinse eyes cautiously with lukewarm, gently flowing water for several minutes, while holding the eyelids open  
Remove contact lenses, if present and easy to do so  
Continue rinsing for 15-20 minutes  
Get medical advice if eye irritation persists

##### After swallowing:

Rinse mouth thoroughly  
Seek medical attention if irritation, discomfort, or vomiting persists

#### Most important symptoms and effects, both acute and delayed

##### Acute symptoms and effects:

## Safety Data Sheet

According to OSHA Hazard Communication Standard, 29 CFR 1910.1200

Initial preparation date: 07.25.2018

Page 3 of 9

### Clear Epoxy Resin - Part A

Not determined or not applicable.

**Delayed symptoms and effects:**

Not determined or not applicable.

**Immediate medical attention and special treatment**

**Specific treatment:**

Not determined or not applicable.

**Notes for the doctor:**

Not determined or not applicable.

### SECTION 5: Firefighting measures

**Extinguishing media**

**Suitable extinguishing media:**

Use appropriate fire suppression agents for adjacent combustible materials or sources of ignition

**Unsuitable extinguishing media:**

Not determined or not applicable.

**Specific hazards during fire-fighting:**

Thermal decomposition can lead to release of irritating gases and vapors

**Special protective equipment for firefighters:**

Use typical firefighting equipment, self-contained breathing apparatus, special tightly sealed suit

**Special precautions:**

Not determined or not applicable.

### SECTION 6: Accidental release measures

**Personal precautions, protective equipment and emergency procedures:**

Ensure adequate ventilation

Ensure air handling systems are operational

Wear protective eye wear, gloves and clothing

**Environmental precautions:**

Should not be released into the environment

Prevent from reaching drains, sewer or waterway

**Methods and material for containment and cleaning up:**

Wear protective eye wear, gloves and clothing

Absorb with non-combustible liquid-binding material (sand, diatomaceous earth (clay), acid binders, universal binders)

Dispose of contents / container in accordance with local regulations

**Reference to other sections:**

Not determined or not applicable.

### SECTION 7: Handling and storage

**Precautions for safe handling:**

Use only with adequate ventilation.

Avoid breathing mist or vapor.

Do not eat, drink, smoke or use personal products when handling chemical substances.

**Conditions for safe storage, including any incompatibilities:**

Keep container tightly sealed.

Protect from freezing and physical damage.

Store in a cool, well-ventilated area.

## Safety Data Sheet

According to OSHA Hazard Communication Standard, 29 CFR 1910.1200

Initial preparation date: 07.25.2018

Page 4 of 9

### Clear Epoxy Resin - Part A

#### SECTION 8: Exposure controls/personal protection

Only those substances with limit values have been included below.

**Occupational Exposure limit values:**

No occupational exposure limits noted for the ingredient(s).

**Biological limit values:**

No biological exposure limits noted for the ingredient(s).

**Information on monitoring procedures:**

Monitoring of the concentration of substances in the breathing zone of workers or in the general workplace may be required to confirm compliance with an OEL and adequacy of exposure controls.

Biological monitoring may also be appropriate for some substances.

**Appropriate engineering controls:**

Emergency eye wash fountains and safety showers should be available in the immediate vicinity of use or handling.

Provide exhaust ventilation or other engineering controls to keep the airborne concentrations of vapor and mists below the applicable workplace exposure limits (Occupational Exposure Limits-OELs) indicated above.

**Personal protection equipment**

**Eye and face protection:**

Safety goggles or glasses, or appropriate eye protection.

**Skin and body protection:**

Select glove material impermeable and resistant to the substance.

Wear appropriate clothing to prevent any possibility of skin contact.

**Respiratory protection:**

If engineering controls do not maintain airborne concentrations below recommended exposure limits (where applicable) or to an acceptable level (in countries where exposure limits have not been established), an approved respirator must be worn.

**General hygienic measures:**

Avoid contact with skin, eyes and clothing.

Wash hands before breaks and at the end of work.

Wash contaminated clothing before reuse.

#### SECTION 9: Physical and chemical properties

##### Information on basic physical and chemical properties

Appearance	Clear liquid
Odor	Not available
Odor threshold	Not available
pH	Not available
Melting point/freezing point	Not available
Initial boiling point/range	Not available
Flash point (closed cup)	135°C (275°F)
Evaporation rate	Not available
Flammability (solid, gas)	Not available
Upper flammability/explosive limit	Not available
Lower flammability/explosive limit	Not available
Vapor pressure	Not available
Vapor density	Not available
Density	1.15 g/cm <sup>3</sup>



## Safety Data Sheet

According to OSHA Hazard Communication Standard, 29 CFR 1910.1200

Initial preparation date: 07.25.2018

Page 5 of 9

### Clear Epoxy Resin - Part A

Relative density	Not available
Solubilities	Not determined or not available.
Partition coefficient (n-octanol/water)	Not available
Auto/Self-ignition temperature	Not available
Decomposition temperature	Not available
Dynamic viscosity	Not available
Kinematic viscosity	Not available
Explosive properties	Not available
Oxidizing properties	Not available

#### Other information

#### SECTION 10: Stability and reactivity

**Reactivity:**

Does not react under normal conditions of use and storage.

**Chemical stability:**

Stable under normal conditions of use and storage.

**Possibility of hazardous reactions:**

None under normal conditions of use and storage.

**Conditions to avoid:**

None known.

**Incompatible materials:**

None known.

**Hazardous decomposition products:**

None known.

#### SECTION 11: Toxicological information

**Acute toxicity**

**Assessment:** Based on available data, the classification criteria are not met.

**Product data:** No data available.

**Substance data:** No data available.

**Skin corrosion/irritation****Assessment:**

Causes skin irritation

**Product data:**

No data available.

**Substance data:**

Name	Result
Epoxy Resin	Causes skin irritation.
P-tert-butylphenyl 1-(2,3-epoxy)propyl ether	Causes skin irritation

**Serious eye damage/irritation****Assessment:**

Causes serious eye irritation

**Product data:**

No data available.

**Substance data:**

## Safety Data Sheet

According to OSHA Hazard Communication Standard, 29 CFR 1910.1200

Initial preparation date: 07.25.2018

Page 6 of 9

### Clear Epoxy Resin - Part A

Name	Result
Epoxy Resin	Causes serious eye irritation.
P-tert-butylphenyl 1-(2,3-epoxy)propyl ether	Causes serious eye damage

#### Respiratory or skin sensitization

**Assessment:**

May cause an allergic skin reaction

**Product data:**

No data available.

**Substance data:**

Name	Result
Epoxy Resin	May cause an allergic skin reaction.
P-tert-butylphenyl 1-(2,3-epoxy)propyl ether	Result : May cause sensitisation by skin contact.

#### Carcinogenicity

**Assessment:** Based on available data, the classification criteria are not met.

**Product data:** No data available.

**Substance data:** No data available.

**International Agency for Research on Cancer (IARC):** None of the ingredients are listed.

**National Toxicology Program (NTP):** None of the ingredients are listed.

#### Germ cell mutagenicity

**Assessment:** Based on available data, the classification criteria are not met.

**Product data:**

No data available.

**Substance data:** No data available.

#### Reproductive toxicity

**Assessment:** Based on available data, the classification criteria are not met.

**Product data:**

No data available.

**Substance data:** No data available.

#### Specific target organ toxicity (single exposure)

**Assessment:** Based on available data, the classification criteria are not met.

**Product data:**

No data available.

**Substance data:** No data available.

#### Specific target organ toxicity (repeated exposure)

**Assessment:** Based on available data, the classification criteria are not met.

**Product data:**

No data available.

**Substance data:** No data available.

#### Aspiration toxicity

**Assessment:** Based on available data, the classification criteria are not met.

**Product data:**

No data available.

**Substance data:** No data available.

#### Information on likely routes of exposure:

No data available.

#### Symptoms related to the physical, chemical and toxicological characteristics:

## Safety Data Sheet

According to OSHA Hazard Communication Standard, 29 CFR 1910.1200

Initial preparation date: 07.25.2018

Page 7 of 9

### Clear Epoxy Resin - Part A

No data available.

**Other information:**

No data available.

### SECTION 12: Ecological information

**Acute (short-term) toxicity**

**Assessment:** Based on available data, the classification criteria are not met.

**Product data:** No data available.

**Substance data:**

Name	Result
Epoxy Resin	EC50 - Scenedesmus capricornutum - 9 mg/L - 48 h

**Chronic (long-term) toxicity**

**Assessment:** Based on available data, the classification criteria are not met.

**Product data:** No data available.

**Substance data:** No data available.

**Persistence and degradability**

**Product data:** No data available.

**Substance data:** No data available.

**Bioaccumulative potential**

**Product data:** No data available.

**Substance data:** No data available.

**Mobility in soil**

**Product data:** No data available.

**Substance data:** No data available.

**Other adverse effects:** No data available.

### SECTION 13: Disposal considerations

**Disposal methods:**

It is the responsibility of the waste generator to properly characterize all waste materials according to applicable regulatory entities

### SECTION 14: Transport information

#### United States Transportation of dangerous goods (49 CFR DOT)

UN number	Not Regulated
UN proper shipping name	Not Regulated
UN transport hazard class(es)	None
Packing group	None
Environmental hazards	None
Special precautions for user	None

#### International Maritime Dangerous Goods (IMDG)

UN number	UN 3082
UN proper shipping name	Environmentally hazardous substance, liquid, N.O.S. (Phenol, 4,4'-(1-methylethylidene)bis-, polymer with 2-(chloromethyl)oxiran, P-tert-butylphenyl 1-(2,3-epoxy)propyl ether)


### Safety Data Sheet

According to OSHA Hazard Communication Standard, 29 CFR 1910.1200


Initial preparation date: 07.25.2018

Page 8 of 9

#### Clear Epoxy Resin - Part A

UN transport hazard class(es)	9	
Packing group	III	
Environmental hazards	Marine Pollutant	
Special precautions for user	None	
EmS number	F-A, S-F	
Stowage category	A	
Excepted quantities	E1	
Limited quantity	5L	

#### International Air Transport Association Dangerous Goods Regulations (IATA-DGR)

UN number	UN 3082	
UN proper shipping name	Environmentally hazardous substance, liquid, N.O.S. (Phenol, 4,4'-(1-methylethylidene)bis-, polymer with 2-(chloromethyl)oxiran, P-tert-butylphenyl 1-(2,3-epoxy)propyl ether)	
UN transport hazard class(es)	9	
Packing group	III	
Environmental hazards	Marine Pollutant	
Special precautions for user	None	
ERG code	9L	
Excepted quantities	E1	
Passenger and cargo	450L	
Cargo aircraft only	450L	
Limited quantity	30 Kg G	

#### Transport in bulk according to Annex II of MARPOL73/78 and the IBC Code

Bulk Name	None
Ship type	None
Pollution category	None

#### SECTION 15: Regulatory information

##### United States regulations

##### Inventory listing (TSCA):

25068-38-6	Epoxy Resin	Listed
3101-60-8	P-tert-butylphenyl 1-(2,3-epoxy)propyl ether	Listed

**Significant New Use Rule (TSCA Section 5):** Not determined.

**Export notification under TSCA Section 12(b):** Not determined.

**SARA Section 302 extremely hazardous substances:** Not determined.

##### SARA Section 313 toxic chemicals:

25068-38-6	Epoxy Resin	Not Listed
3101-60-8	P-tert-butylphenyl 1-(2,3-epoxy)propyl ether	Not Listed

## Safety Data Sheet

According to OSHA Hazard Communication Standard, 29 CFR 1910.1200

Initial preparation date: 07.25.2018

Page 9 of 9

### Clear Epoxy Resin - Part A

**CERCLA:** Not determined.

**RCRA:** Not determined.

**Section 112(r) of the Clean Air Act (CAA):** Not determined.

#### Massachusetts Right to Know:

25068-38-6	Epoxy Resin	Not Listed
3101-60-8	P-tert-butylphenyl 1-(2,3-epoxy)propyl ether	Not Listed

#### New Jersey Right to Know:

25068-38-6	Epoxy Resin	Not Listed
3101-60-8	P-tert-butylphenyl 1-(2,3-epoxy)propyl ether	Not Listed

#### New York Right to Know:

25068-38-6	Epoxy Resin	Not Listed
3101-60-8	P-tert-butylphenyl 1-(2,3-epoxy)propyl ether	Not Listed

#### Pennsylvania Right to Know:

25068-38-6	Epoxy Resin	Not Listed
3101-60-8	P-tert-butylphenyl 1-(2,3-epoxy)propyl ether	Not Listed

**California Proposition 65:** None of the ingredients are listed.

### SECTION 16: Other information

**Abbreviations and Acronyms:** None

#### Disclaimer:

This product has been classified in accordance with OSHA HCS 2012 guidelines. The information provided in this SDS is correct, to the best of our knowledge, based on information available. The information given is designed only as a guidance for safe handling, use, storage, transportation and disposal and is not to be considered a warranty or quality specification. The information relates only to the specific material designated and may not be valid for such material used in combination with any other materials, unless specified in the text. The responsibility to provide a safe workplace remains with the user.

**NFPA:** 2-0-0

**HMIS:** 2-0-0

Initial preparation date: 07.25.2018

End of Safety Data Sheet

## Safety Data Sheet

According to OSHA Hazard Communication Standard, 29 CFR 1910.1200

Initial preparation date: 07.25.2018

Page 1 of 12

### Clear Epoxy Hardener - Part B

#### SECTION 1: Identification

##### Product identifier

**Product name:** Clear Epoxy Hardener - Part B

**Product code:** 50112, 50112H, 50114, 50114H, 50132, 50240, 50240H



##### Recommended use of the product and restriction on use

**Relevant identified uses:** Adhesive Part B

**Uses advised against:** Not determined or not applicable.

**Reasons why uses advised against:** Not determined or not applicable.

##### Manufacturer or supplier details

###### Manufacturer:

###### United States

J-B Weld Company, LLC  
400 CMH Road  
Sulphur Springs, TX 75482  
903-885-7696  
info@jbweld.com

##### Emergency telephone number:

###### United States

CHEMTREC

Transportation Emergencies (24 hour): 800-424-9300 or  
703-527-3887

Poison Control Centers (24 hour): medical emergencies 800-222-1222

#### SECTION 2: Hazard(s) identification

##### GHS classification:

Flammable liquids, category 4

Skin corrosion, category 1B

Skin sensitization, category 1

Eye irritation, category 2A

##### Label elements

##### Hazard pictograms:



##### Signal word: Danger

##### Hazard statements:

H227 Combustible liquid.

H314 Causes severe skin burns and eye damage.

H317 May cause an allergic skin reaction.

H319 Causes serious eye irritation.

##### Precautionary statements:

P210 Keep away from heat/sparks/open flames/hot surfaces. No smoking.

P280 Wear protective gloves/protective clothing/eye protection/face protection.

P260 Do not breathe dust/fume/gas/mist/vapors/spray.

P264 Wash skin and eyes thoroughly after handling.

P261 Avoid breathing dust/fume/gas/mist/vapors/spray.

## Safety Data Sheet

According to OSHA Hazard Communication Standard, 29 CFR 1910.1200

Initial preparation date: 07.25.2018

Page 2 of 12

### Clear Epoxy Hardener - Part B

P272 Contaminated work clothing should not be allowed out of the workplace.  
P370+P378 In case of fire: Use agents recommended in section 5 for extinction.  
P310 Immediately call a POISON CENTER or doctor/physician.  
P321 Specific treatment (see supplemental first aid instructions on this label).  
P363 Wash contaminated clothing before reuse  
P301+P330+P331 IF SWALLOWED: Rinse mouth. Do NOT induce vomiting.  
P303+P361+P353 IF ON SKIN (or hair): Remove/Take off immediately all contaminated clothing. Rinse skin with water/shower.  
P305+P351+P338 IF IN EYES: Rinse cautiously with water for several minutes. Remove contact lenses, if present and easy to do. Continue rinsing.  
P302+P352 IF ON SKIN: Wash with plenty of soap and water.  
P333+P313 If skin irritation or a rash occurs: Get medical advice/attention  
P337+P313 If eye irritation persists get medical advice/attention  
P403+P235 Store in a well ventilated place. Keep cool.  
P405 Store locked up.  
P501 Dispose of contents/container in accordance with local regulations.

**Hazards not otherwise classified:** None

### SECTION 3: Composition/information on ingredients

Identification	Name	Weight %
CAS number: 112-24-3	Amine	<5
CAS number: 100-51-6	Liquid additive	<2
CAS number: 72244-98-5	Curing Agent	<90
CAS number: 140-31-8	Amine	<5
CAS number: 25620-58-0	Amine	<5
CAS number: 39423-51-3	Amine	<5
CAS number: 3033-62-3	Amine	<1
CAS number: 919-30-2	Liquid additive	<2

#### Additional Information:

The specific chemical identity and/or exact percentage (concentration) of composition has been withheld as a trade secret in accordance with paragraph (i) of the OSHA Hazard Communication Standard (29 CFR §1910.1200).

### SECTION 4: First aid measures

#### Description of first aid measures

##### General notes:

Not determined or not applicable.

##### After inhalation:

## Safety Data Sheet

According to OSHA Hazard Communication Standard, 29 CFR 1910.1200

Initial preparation date: 07.25.2018

Page 3 of 12

### Clear Epoxy Hardener - Part B

Loosen clothing as necessary and position individual in a comfortable position  
Maintain an unobstructed airway  
Get medical advice/attention if you feel unwell  
Take precautions to ensure your own safety  
Remove source of exposure or move person to fresh air and keep comfortable for breathing  
Immediately call a POISON CONTROL CENTER or seek medical attention  
If breathing has stopped, trained personnel should begin rescue breathing  
Avoid mouth-to-mouth contact by using a barrier device  
If the heart has stopped, immediately start cardiopulmonary resuscitation (CPR)

#### After skin contact:

Rinse affected area with soap and water  
If symptoms develop or persist, seek medical attention  
Avoid direct contact and wear chemical protective clothing, if necessary  
Immediately take off all contaminated clothing  
Gently blot or brush away excess product  
Rinse skin with lukewarm, gently flowing water until medical aid is available  
Immediately call a POISON CONTROL CENTER or seek medical attention  
Wash contaminated clothing before re-use or discard

#### After eye contact:

Rinse/flush exposed eye(s) gently using water for 15-20 minutes  
If symptoms develop or persist, seek medical attention  
Avoid direct contact and wear chemical protective gloves, if necessary  
Rinse eyes cautiously with lukewarm, gently flowing water for several minutes, while holding the eyelids open  
Remove contact lenses, if present and easy to do so  
Continue rinsing until medical aid is available  
Immediately call a POISON CONTROL CENTER or seek medical attention

#### After swallowing:

Rinse mouth thoroughly  
Seek medical attention if irritation, discomfort, or vomiting persists  
Immediately call a POISON CONTROL CENTER or seek medical attention  
Do not induce vomiting and rinse mouth  
If vomiting occurs naturally, lie on your side, in the recovery position  
If breathing has stopped, trained personnel should begin rescue breathing  
Avoid mouth-to-mouth contact by using a barrier device  
If the heart has stopped, immediately start cardiopulmonary resuscitation (CPR)

#### Most important symptoms and effects, both acute and delayed

##### Acute symptoms and effects:

Not determined or not applicable.

##### Delayed symptoms and effects:

Not determined or not applicable.

#### Immediate medical attention and special treatment

##### Specific treatment:

Not determined or not applicable.

##### Notes for the doctor:

Not determined or not applicable.

### SECTION 5: Firefighting measures

#### Extinguishing media

Suitable extinguishing media:



## Safety Data Sheet

According to OSHA Hazard Communication Standard, 29 CFR 1910.1200

Initial preparation date: 07.25.2018

Page 4 of 12

### Clear Epoxy Hardener - Part B

Use Water (fog only), dry chemical, chemical foam, carbon dioxide, or alcohol-resistant foam

**Unsuitable extinguishing media:**

Not determined or not applicable.

**Specific hazards during fire-fighting:**

Thermal decomposition can lead to release of irritating gases and vapors

**Special protective equipment for firefighters:**

Use typical firefighting equipment, self-contained breathing apparatus, special tightly sealed suit

**Special precautions:**

Shut off sources of ignition

Carbon monoxide and carbon dioxide may form upon combustion

Heating causes a rise in pressure, risk of bursting and combustion

### SECTION 6: Accidental release measures

**Personal precautions, protective equipment and emergency procedures:**

Ensure adequate ventilation

Ensure air handling systems are operational

Wear protective eye wear, gloves and clothing

**Environmental precautions:**

Should not be released into the environment

Prevent from reaching drains, sewer or waterway

**Methods and material for containment and cleaning up:**

Wear protective eye wear, gloves and clothing

Use spark-proof tools and explosion-proof equipment

Absorb with non-combustible liquid-binding material (sand, diatomaceous earth (clay), acid binders, universal binders)

Dispose of contents / container in accordance with local regulations

**Reference to other sections:**

Not determined or not applicable.

### SECTION 7: Handling and storage

**Precautions for safe handling:**

Use only with adequate ventilation.

Avoid breathing mist or vapor.

Do not eat, drink, smoke or use personal products when handling chemical substances.

Take precautionary measures against electrostatic discharges.

Use only non-sparking tools.

**Conditions for safe storage, including any incompatibilities:**

Keep container tightly sealed.

Protect from freezing and physical damage.

Store in a cool, well-ventilated area.

Store away from all ignition sources (open flames, hot surfaces, direct sunlight, spark sources).

### SECTION 8: Exposure controls/personal protection

Only those substances with limit values have been included below.

**Occupational Exposure limit values:**

Country (Legal Basis)	Substance	Identifier	Permissible concentration
WEEL	Liquid additive	100-51-6	WEEL TWA 10.0 ppm
	Amine	112-24-3	WEEL TWA 1.0 ppm

## Safety Data Sheet

According to OSHA Hazard Communication Standard, 29 CFR 1910.1200

Initial preparation date: 07.25.2018

Page 5 of 12

### Clear Epoxy Hardener - Part B

Country (Legal Basis)	Substance	Identifier	Permissible concentration
ACGIH	Amine	3033-62-3	ACGIH TLV TWA 0.05 ppm
	Amine	3033-62-3	ACGIH TLV STEL 0.15 ppm

**Biological limit values:**

No biological exposure limits noted for the ingredient(s).

**Information on monitoring procedures:**

Monitoring of the concentration of substances in the breathing zone of workers or in the general workplace may be required to confirm compliance with an OEL and adequacy of exposure controls. Biological monitoring may also be appropriate for some substances.

**Appropriate engineering controls:**

Emergency eye wash fountains and safety showers should be available in the immediate vicinity of use or handling.

Provide exhaust ventilation or other engineering controls to keep the airborne concentrations of vapor and mists below the applicable workplace exposure limits (Occupational Exposure Limits-OELs) indicated above. Use explosion-proof ventilation equipment.

**Personal protection equipment**

**Eye and face protection:**

Safety goggles or glasses, or appropriate eye protection.

**Skin and body protection:**

Select glove material impermeable and resistant to the substance.

Wear appropriate clothing to prevent any possibility of skin contact.

**Respiratory protection:**

If engineering controls do not maintain airborne concentrations below recommended exposure limits (where applicable) or to an acceptable level (in countries where exposure limits have not been established), an approved respirator must be worn.

**General hygienic measures:**

Avoid contact with skin, eyes and clothing.

Wash hands before breaks and at the end of work.

Wash contaminated clothing before reuse.

### SECTION 9: Physical and chemical properties

**Information on basic physical and chemical properties**

Appearance	Clear liquid
Odor	Not available
Odor threshold	Not available
pH	Not available
Melting point/freezing point	Not available
Initial boiling point/range	Not available
Flash point (closed cup)	67°C (153°F)
Evaporation rate	Not available
Flammability (solid, gas)	Not available
Upper flammability/explosive limit	Not available
Lower flammability/explosive limit	Not available
Vapor pressure	Not available
Vapor density	Not available
Density	1.127 g/cm <sup>3</sup>

## Safety Data Sheet

According to OSHA Hazard Communication Standard, 29 CFR 1910.1200

Initial preparation date: 07.25.2018

Page 6 of 12

### Clear Epoxy Hardener - Part B

Relative density	Not available
Solubilities	Not determined or not available.
Partition coefficient (n-octanol/water)	Not available
Auto/Self-ignition temperature	Not available
Decomposition temperature	Not available
Dynamic viscosity	Not available
Kinematic viscosity	Not available
Explosive properties	Not available
Oxidizing properties	Not available

#### Other information

#### SECTION 10: Stability and reactivity

**Reactivity:**

Does not react under normal conditions of use and storage.

**Chemical stability:**

Stable under normal conditions of use and storage.

**Possibility of hazardous reactions:**

None under normal conditions of use and storage.

**Conditions to avoid:**

None known.

**Incompatible materials:**

None known.

**Hazardous decomposition products:**

None known.

#### SECTION 11: Toxicological information

**Acute toxicity**

**Assessment:** Based on available data, the classification criteria are not met.

**Product data:** No data available.

**Substance data:**

Name	Route	Result
Liquid additive	inhalation	LC50 Rat: 4.178 mg/L (4 hr)
	oral	LD50 Rabbit: 1,040 mg/kg
		LD50 Rat: 1780 mg/kg
Amine	oral	LD50 - Chicken - 1,500 mg/kg
		LD50 - Rat - 550 mg/kg
		LD50 - Rat - 571 mg/kg
	dermal	LD50 - Rat - > 1,000 mg/kg
		LD50 - Rabbit - 750 mg/kg
inhalation	LC50 - Rat - 4.0 mg/L - 4 h (aerosol)	

**Skin corrosion/irritation****Assessment:**

Causes severe skin burns and eye damage

**Product data:**

No data available.

## Safety Data Sheet

According to OSHA Hazard Communication Standard, 29 CFR 1910.1200

Initial preparation date: 07.25.2018

Page 7 of 12

### Clear Epoxy Hardener - Part B

#### Substance data:

Name	Result
Amine	Corrosive to the skin.
	Causes skin burns
	Causes severe skin burns and eye damage.
	Corrosive to the skin.
Liquid additive	Causes severe skin burns and eye damage.

#### Serious eye damage/irritation

##### Assessment:

Causes serious eye irritation

##### Product data:

No data available.

##### Substance data:

Name	Result
Amine	Corrosive to the eyes.
	Corrosive effect on the eyes.

#### Respiratory or skin sensitization

##### Assessment:

May cause an allergic skin reaction

##### Product data:

No data available.

##### Substance data:

Name	Result
Curing Agent	May cause an allergic skin reaction.
Amine	Sensitization possible through skin contact.
	Sensitization possible through skin contact.
	May cause an allergic skin reaction.

#### Carcinogenicity

**Assessment:** Based on available data, the classification criteria are not met.

**Product data:** No data available.

**Substance data:** No data available.

**International Agency for Research on Cancer (IARC):** None of the ingredients are listed.

**National Toxicology Program (NTP):** None of the ingredients are listed.

#### Germ cell mutagenicity

**Assessment:** Based on available data, the classification criteria are not met.

##### Product data:

No data available.

**Substance data:** No data available.

#### Reproductive toxicity

**Assessment:** Based on available data, the classification criteria are not met.

##### Product data:

No data available.

**Substance data:** No data available.

#### Specific target organ toxicity (single exposure)

**Assessment:** Based on available data, the classification criteria are not met.

##### Product data:

## Safety Data Sheet

According to OSHA Hazard Communication Standard, 29 CFR 1910.1200

Initial preparation date: 07.25.2018

Page 8 of 12

### Clear Epoxy Hardener - Part B

No data available.

**Substance data:** No data available.

#### Specific target organ toxicity (repeated exposure)

**Assessment:** Based on available data, the classification criteria are not met.

**Product data:**

No data available.

**Substance data:** No data available.

#### Aspiration toxicity

**Assessment:** Based on available data, the classification criteria are not met.

**Product data:**

No data available.

**Substance data:** No data available.

#### Information on likely routes of exposure:

No data available.

#### Symptoms related to the physical, chemical and toxicological characteristics:

No data available.

**Other information:**

No data available.

### SECTION 12: Ecological information

#### Acute (short-term) toxicity

**Assessment:** Based on available data, the classification criteria are not met.

**Product data:** No data available.

**Substance data:**

Name	Result
Amine	LC50 - Daphnia magna (Water flea) - 33.9 mg/L - 48 h
	EC50 - Pseudokirchnerella subcapitata - 4.4 mg/L - 72 h

#### Chronic (long-term) toxicity

**Assessment:** Based on available data, the classification criteria are not met.

**Product data:** No data available.

**Substance data:**

Name	Result
Curing Agent	NOEC - Daphnia magna (Water flea) - 3.5 mg/L - 21 d

#### Persistence and degradability

**Product data:** No data available.

**Substance data:** No data available.

#### Bioaccumulative potential

**Product data:** No data available.

**Substance data:** No data available.

#### Mobility in soil

**Product data:** No data available.

**Substance data:** No data available.

**Other adverse effects:** No data available.

### SECTION 13: Disposal considerations

#### Disposal methods:

It is the responsibility of the waste generator to properly characterize all waste materials according to applicable regulatory entities

## Safety Data Sheet

According to OSHA Hazard Communication Standard, 29 CFR 1910.1200


Initial preparation date: 07.25.2018

Page 9 of 12


### Clear Epoxy Hardener - Part B

#### SECTION 14: Transport information


##### United States Transportation of dangerous goods (49 CFR DOT)

<b>UN number</b>	UN 2735
<b>UN proper shipping name</b>	Amines, Liquid, Corrosive, n.o.s. (Triethylenetetramine, 1-Piperazineethanamine)
<b>UN transport hazard class(es)</b>	8 
<b>Packing group</b>	III
<b>Environmental hazards</b>	None
<b>Special precautions for user</b>	None

##### International Maritime Dangerous Goods (IMDG)

<b>UN number</b>	UN 2735
<b>UN proper shipping name</b>	Amines, Liquid, Corrosive, n.o.s. (Triethylenetetramine, 1-Piperazineethanamine)
<b>UN transport hazard class(es)</b>	8 
<b>Packing group</b>	III
<b>Environmental hazards</b>	None
<b>Special precautions for user</b>	None

##### International Air Transport Association Dangerous Goods Regulations (IATA-DGR)

<b>UN number</b>	UN 2735
<b>UN proper shipping name</b>	Amines, Liquid, Corrosive, n.o.s. (Triethylenetetramine, 1-Piperazineethanamine)
<b>UN transport hazard class(es)</b>	8 
<b>Packing group</b>	III
<b>Environmental hazards</b>	None
<b>Special precautions for user</b>	None

##### Transport in bulk according to Annex II of MARPOL73/78 and the IBC Code

<b>Bulk Name</b>	None
<b>Ship type</b>	None
<b>Pollution category</b>	None

#### SECTION 15: Regulatory information

##### United States regulations

##### Inventory listing (TSCA):

72244-98-5	Curing Agent	Listed
100-51-6	Liquid additive	Listed
140-31-8	Amine	Listed

### Safety Data Sheet

According to OSHA Hazard Communication Standard, 29 CFR 1910.1200

Initial preparation date: 07.25.2018

Page 10 of 12

#### Clear Epoxy Hardener - Part B

25620-58-0	Amine	Listed
112-24-3	Amine	Listed
39423-51-3	Amine	Listed
3033-62-3	Amine	Listed
919-30-2	Liquid additive	Listed

**Significant New Use Rule (TSCA Section 5):** Not determined.

**Export notification under TSCA Section 12(b):** Not determined.

**SARA Section 302 extremely hazardous substances:** Not determined.

**SARA Section 313 toxic chemicals:**

72244-98-5	Curing Agent	Not Listed
100-51-6	Liquid additive	Not Listed
140-31-8	Amine	Not Listed
25620-58-0	Amine	Not Listed
112-24-3	Amine	Not Listed
39423-51-3	Amine	Not Listed
3033-62-3	Amine	Not Listed
919-30-2	Liquid additive	Not Listed

**CERCLA:** Not determined.

**RCRA:** Not determined.

**Section 112(r) of the Clean Air Act (CAA):** Not determined.

**Massachusetts Right to Know:**

72244-98-5	Curing Agent	Not Listed
100-51-6	Liquid additive	Listed
140-31-8	Amine	Listed
25620-58-0	Amine	Not Listed
112-24-3	Amine	Listed
39423-51-3	Amine	Not Listed
3033-62-3	Amine	Not Listed
919-30-2	Liquid additive	Not Listed

**New Jersey Right to Know:**

72244-98-5	Curing Agent	Not Listed
100-51-6	Liquid additive	Not Listed
140-31-8	Amine	Listed

## Safety Data Sheet

According to OSHA Hazard Communication Standard, 29 CFR 1910.1200

Initial preparation date: 07.25.2018

Page 11 of 12

### Clear Epoxy Hardener - Part B

25620-58-0	Amine	Listed
112-24-3	Amine	Listed
39423-51-3	Amine	Not Listed
3033-62-3	Amine	Listed
919-30-2	Liquid additive	Not Listed

#### New York Right to Know:

72244-98-5	Curing Agent	Not Listed
100-51-6	Liquid additive	Not Listed
140-31-8	Amine	Listed
25620-58-0	Amine	Listed
112-24-3	Amine	Listed
39423-51-3	Amine	Not Listed
3033-62-3	Amine	Not Listed
919-30-2	Liquid additive	Not Listed

#### Pennsylvania Right to Know:

72244-98-5	Curing Agent	Not Listed
100-51-6	Liquid additive	Listed
140-31-8	Amine	Listed
25620-58-0	Amine	Not Listed
112-24-3	Amine	Listed
39423-51-3	Amine	Not Listed
3033-62-3	Amine	Not Listed
919-30-2	Liquid additive	Not Listed

**California Proposition 65:** None of the ingredients are listed.

### SECTION 16: Other information

**Abbreviations and Acronyms:** None

**Disclaimer:**

This product has been classified in accordance with OSHA HCS 2012 guidelines. The information provided in this SDS is correct, to the best of our knowledge, based on information available. The information given is designed only as a guidance for safe handling, use, storage, transportation and disposal and is not to be considered a warranty or quality specification. The information relates only to the specific material designated and may not be valid for such material used in combination with any other materials, unless specified in the text. The responsibility to provide a safe workplace remains with the user.

**NFPA:** 3-1-0

**HMIS:** 3-1-0

**Initial preparation date:** 07.25.2018



**Safety Data Sheet**

According to OSHA Hazard Communication Standard, 29 CFR 1910.1200

**Initial preparation date:** 07.25.2018

Page 12 of 12

**Clear Epoxy Hardener - Part B**

**End of Safety Data Sheet**

**APPENDIX F. EPOXY-BASED WOOD FILLER SPECIFICATION**

# SAFETY DATA SHEET

4285-

## Section 1. Identification

**Product name** : MINWAX® Stainable Wood Filler  
**Product code** : 4285-  
**Other means of identification** : Not available.  
**Product type** : Solid.

### Relevant identified uses of the substance or mixture and uses advised against

Paint or paint related material.

**Manufacturer** : MINWAX Company  
10 Mountainview Road  
Upper Saddle River, NJ 07458

**Emergency telephone number of the company** : US/Canada: (216) 566-2917  
Mexico: CHEMTREC México 01-800-681-9531. Available 24 hours and 365 days per year

**Product Information Telephone Number** : US/Canada: (800) 523-9299  
Mexico: 01-800-71-73-123 / (52) 53-33-15-01

**Regulatory Information Telephone Number** : US / Canada: (216) 566-2902  
Mexico: 01-800-71-73-123 / (52) 53-33-15-01

**Transportation Emergency Telephone Number** : US / Canada: (800) 424-9300  
Mexico: SETIQ 01-800-00-214-00 / (52) 55-5559-1588 24 hours / 365 days a year

## Section 2. Hazards identification

**OSHA/HCS status** : While this material is not considered hazardous by the OSHA Hazard Communication Standard (29 CFR 1910.1200), this SDS contains valuable information critical to the safe handling and proper use of the product. This SDS should be retained and available for employees and other users of this product.

**Classification of the substance or mixture** : Not classified.

### GHS label elements

**Signal word** : No signal word.

**Hazard statements** : No known significant effects or critical hazards.

### Precautionary statements

**General** : Read label before use. Keep out of reach of children. If medical advice is needed, have product container or label at hand.

**Prevention** : Not applicable.

**Response** : Not applicable.

**Storage** : Not applicable.

**Disposal** : Not applicable.

**Supplemental label elements** WARNING: This product contains chemicals known to the State of California to cause cancer and birth defects or other reproductive harm.

Please refer to the SDS for additional information. Keep out of reach of children. Do not transfer contents to other containers for storage.

**Hazards not otherwise classified** : None known.

**Date of issue/Date of revision** : 3/25/2019 **Date of previous issue** : 10/17/2018 **Version** : 6.03 1/9  
4285- MINWAX® Stainable Wood Filler **SHW-85-NA-GHS-US**

### Section 3. Composition/information on ingredients

**Substance/mixture** : Mixture  
**Other means of identification** : Not available.

#### CAS number/other identifiers

Ingredient name	% by weight	CAS number

Any concentration shown as a range is to protect confidentiality or is due to batch variation.

**There are no ingredients present which, within the current knowledge of the supplier and in the concentrations applicable, are classified as hazardous to health and hence require reporting in this section.**

**Occupational exposure limits, if available, are listed in Section 8.**

### Section 4. First aid measures

#### Description of necessary first aid measures

- Eye contact** : Immediately flush eyes with plenty of water, occasionally lifting the upper and lower eyelids. Check for and remove any contact lenses. Get medical attention if irritation occurs.
- Inhalation** : Remove victim to fresh air and keep at rest in a position comfortable for breathing. Get medical attention if symptoms occur.
- Skin contact** : Flush contaminated skin with plenty of water. Remove contaminated clothing and shoes. Get medical attention if symptoms occur.
- Ingestion** : Wash out mouth with water. Remove victim to fresh air and keep at rest in a position comfortable for breathing. If material has been swallowed and the exposed person is conscious, give small quantities of water to drink. Do not induce vomiting unless directed to do so by medical personnel. Get medical attention if symptoms occur.

#### Most important symptoms/effects, acute and delayed

##### Potential acute health effects

- Eye contact** : No known significant effects or critical hazards.
- Inhalation** : No known significant effects or critical hazards.
- Skin contact** : No known significant effects or critical hazards.
- Ingestion** : No known significant effects or critical hazards.

##### Over-exposure signs/symptoms

- Eye contact** : No specific data.
- Inhalation** : No specific data.
- Skin contact** : No specific data.
- Ingestion** : No specific data.

#### Indication of immediate medical attention and special treatment needed, if necessary

- Notes to physician** : Treat symptomatically. Contact poison treatment specialist immediately if large quantities have been ingested or inhaled.
- Specific treatments** : No specific treatment.
- Protection of first-aiders** : No action shall be taken involving any personal risk or without suitable training.

See toxicological information (Section 11)

<b>Date of issue/Date of revision</b> : 3/25/2019	<b>Date of previous issue</b> : 10/17/2018	<b>Version</b> : 6.03	2/9
4285-	MINWAX® Stainable Wood Filler	<b>SHW-85-NA-GHS-US</b>	

## Section 5. Fire-fighting measures

### Extinguishing media

- Suitable extinguishing media** : Use an extinguishing agent suitable for the surrounding fire.
- Unsuitable extinguishing media** : None known.

**Specific hazards arising from the chemical** : No specific fire or explosion hazard.

**Hazardous thermal decomposition products** : No specific data.

**Special protective actions for fire-fighters** : Promptly isolate the scene by removing all persons from the vicinity of the incident if there is a fire. No action shall be taken involving any personal risk or without suitable training.

**Special protective equipment for fire-fighters** : Fire-fighters should wear appropriate protective equipment and self-contained breathing apparatus (SCBA) with a full face-piece operated in positive pressure mode.

## Section 6. Accidental release measures

### Personal precautions, protective equipment and emergency procedures

- For non-emergency personnel** : No action shall be taken involving any personal risk or without suitable training. Evacuate surrounding areas. Keep unnecessary and unprotected personnel from entering. Do not touch or walk through spilled material. Put on appropriate personal protective equipment.
- For emergency responders** : If specialized clothing is required to deal with the spillage, take note of any information in Section 8 on suitable and unsuitable materials. See also the information in "For non-emergency personnel".

**Environmental precautions** : Avoid dispersal of spilled material and runoff and contact with soil, waterways, drains and sewers. Inform the relevant authorities if the product has caused environmental pollution (sewers, waterways, soil or air).

### Methods and materials for containment and cleaning up

- Small spill** : Move containers from spill area. Vacuum or sweep up material and place in a designated, labeled waste container. Dispose of via a licensed waste disposal contractor.
- Large spill** : Move containers from spill area. Prevent entry into sewers, water courses, basements or confined areas. Vacuum or sweep up material and place in a designated, labeled waste container. Dispose of via a licensed waste disposal contractor. Note: see Section 1 for emergency contact information and Section 13 for waste disposal.

## Section 7. Handling and storage

### Precautions for safe handling

- Protective measures** : Put on appropriate personal protective equipment (see Section 8).
- Advice on general occupational hygiene** : Eating, drinking and smoking should be prohibited in areas where this material is handled, stored and processed. Workers should wash hands and face before eating, drinking and smoking. Remove contaminated clothing and protective equipment before entering eating areas. See also Section 8 for additional information on hygiene measures.

**Conditions for safe storage, including any incompatibilities** : Store in accordance with local regulations. Store in original container protected from direct sunlight in a dry, cool and well-ventilated area, away from incompatible materials (see Section 10) and food and drink. Keep container tightly closed and sealed until ready for use. Containers that have been opened must be carefully resealed and kept upright to prevent leakage. Do not store in unlabeled containers. Use appropriate containment to avoid environmental contamination. See Section 10 for incompatible materials before handling or use.

**Date of issue/Date of revision** : 3/25/2019 **Date of previous issue** : 10/17/2018 **Version** : 6.03 3/9  
4285- MINWAX® Stainable Wood Filler **SHW-85-NA-GHS-US**

## Section 8. Exposure controls/personal protection

### Control parameters

#### Occupational exposure limits (OSHA United States)

Ingredient name	Exposure limits
None.	

#### Occupational exposure limits (Canada)

Ingredient name	Exposure limits
None.	

#### Occupational exposure limits (Mexico)

Ingredient name	Exposure limits
None.	

- Appropriate engineering controls** : Good general ventilation should be sufficient to control worker exposure to airborne contaminants.
- Environmental exposure controls** : Emissions from ventilation or work process equipment should be checked to ensure they comply with the requirements of environmental protection legislation. In some cases, fume scrubbers, filters or engineering modifications to the process equipment will be necessary to reduce emissions to acceptable levels.

### Individual protection measures

- Hygiene measures** : Wash hands, forearms and face thoroughly after handling chemical products, before eating, smoking and using the lavatory and at the end of the working period. Appropriate techniques should be used to remove potentially contaminated clothing. Wash contaminated clothing before reusing. Ensure that eyewash stations and safety showers are close to the workstation location.
- Eye/face protection** : Safety eyewear complying with an approved standard should be used when a risk assessment indicates this is necessary to avoid exposure to liquid splashes, mists, gases or dusts. If contact is possible, the following protection should be worn, unless the assessment indicates a higher degree of protection: safety glasses with side-shields.
- Skin protection**
- Hand protection** : Chemical-resistant, impervious gloves complying with an approved standard should be worn at all times when handling chemical products if a risk assessment indicates this is necessary.
- Body protection** : Personal protective equipment for the body should be selected based on the task being performed and the risks involved and should be approved by a specialist before handling this product.
- Other skin protection** : Appropriate footwear and any additional skin protection measures should be selected based on the task being performed and the risks involved and should be approved by a specialist before handling this product.
- Respiratory protection** : Based on the hazard and potential for exposure, select a respirator that meets the appropriate standard or certification. Respirators must be used according to a respiratory protection program to ensure proper fitting, training, and other important aspects of use.

## Section 9. Physical and chemical properties

### Appearance

- Physical state** : Solid.
- Color** : Not available.
- Odor** : Not available.
- Odor threshold** : Not available.
- pH** : Not available.

<b>Date of issue/Date of revision</b>	: 3/25/2019	<b>Date of previous issue</b>	: 10/17/2018	<b>Version</b>	: 6.03	4/9
4285-	MINWAX® Stainable Wood Filler					<b>SHW-85-NA-GHS-US</b>

## Section 9. Physical and chemical properties

<b>Melting point/freezing point</b>	: Not available.
<b>Boiling point/boiling range</b>	: 100°C (212°F)
<b>Flash point</b>	: Closed cup: 94°C (201.2°F) [Pensky-Martens Closed Cup]
<b>Evaporation rate</b>	: 0.09 (butyl acetate = 1)
<b>Flammability (solid, gas)</b>	: Not available.
<b>Lower and upper explosive (flammable) limits</b>	: Not available.
<b>Vapor pressure</b>	: 2.3 kPa (17.5 mm Hg) [at 20°C]
<b>Vapor density</b>	: 1 [Air = 1]
<b>Relative density</b>	: 0.74
<b>Solubility</b>	: Not available.
<b>Partition coefficient: n-octanol/water</b>	: Not available.
<b>Auto-ignition temperature</b>	: Not available.
<b>Decomposition temperature</b>	: Not available.
<b>Viscosity</b>	: Kinematic (40°C (104°F)): >0.205 cm <sup>2</sup> /s (>20.5 cSt)
<b>Molecular weight</b>	: Not applicable.
<b>Aerosol product</b>	

## Section 10. Stability and reactivity

<b>Reactivity</b>	: No specific test data related to reactivity available for this product or its ingredients.
<b>Chemical stability</b>	: The product is stable.
<b>Possibility of hazardous reactions</b>	: Under normal conditions of storage and use, hazardous reactions will not occur.
<b>Conditions to avoid</b>	: No specific data.
<b>Incompatible materials</b>	: No specific data.
<b>Hazardous decomposition products</b>	: Under normal conditions of storage and use, hazardous decomposition products should not be produced.

## Section 11. Toxicological information

### Information on toxicological effects

#### Acute toxicity

Not available.

#### Irritation/Corrosion

Not available.

#### Sensitization

Not available.

#### Mutagenicity

Not available.

#### Carcinogenicity

Not available.

#### Reproductive toxicity

Not available.

<b>Date of issue/Date of revision</b>	: 3/25/2019	<b>Date of previous issue</b>	: 10/17/2018	<b>Version</b>	: 6.03	5/9
4285-	MINWAX® Stainable Wood Filler			SHW-85-NA-GHS-US		

## Section 11. Toxicological information

### Teratogenicity

Not available.

### Specific target organ toxicity (single exposure)

Not available.

### Specific target organ toxicity (repeated exposure)

Not available.

### Aspiration hazard

Not available.

**Information on the likely routes of exposure** : Not available.

### Potential acute health effects

**Eye contact** : No known significant effects or critical hazards.  
**Inhalation** : No known significant effects or critical hazards.  
**Skin contact** : No known significant effects or critical hazards.  
**Ingestion** : No known significant effects or critical hazards.

### Symptoms related to the physical, chemical and toxicological characteristics

**Eye contact** : No specific data.  
**Inhalation** : No specific data.  
**Skin contact** : No specific data.  
**Ingestion** : No specific data.

### Delayed and immediate effects and also chronic effects from short and long term exposure

#### Short term exposure

**Potential immediate effects** : Not available.  
**Potential delayed effects** : Not available.

#### Long term exposure

**Potential immediate effects** : Not available.  
**Potential delayed effects** : Not available.

#### Potential chronic health effects

Not available.

**General** : No known significant effects or critical hazards.  
**Carcinogenicity** : No known significant effects or critical hazards.  
**Mutagenicity** : No known significant effects or critical hazards.  
**Teratogenicity** : No known significant effects or critical hazards.  
**Developmental effects** : No known significant effects or critical hazards.  
**Fertility effects** : No known significant effects or critical hazards.

### Numerical measures of toxicity

#### Acute toxicity estimates

Not available.



## Section 12. Ecological information

### Toxicity

Not available.

### Persistence and degradability

Not available.

### Bioaccumulative potential

Not available.

### Mobility in soil

**Soil/water partition coefficient (K<sub>oc</sub>)** : Not available.

**Other adverse effects** : No known significant effects or critical hazards.

## Section 13. Disposal considerations

**Disposal methods** : The generation of waste should be avoided or minimized wherever possible. Disposal of this product, solutions and any by-products should at all times comply with the requirements of environmental protection and waste disposal legislation and any regional local authority requirements. Dispose of surplus and non-recyclable products via a licensed waste disposal contractor. Waste should not be disposed of untreated to the sewer unless fully compliant with the requirements of all authorities with jurisdiction. Waste packaging should be recycled. Incineration or landfill should only be considered when recycling is not feasible. This material and its container must be disposed of in a safe way. Empty containers or liners may retain some product residues. Avoid dispersal of spilled material and runoff and contact with soil, waterways, drains and sewers.

## Section 14. Transport information

	<b>DOT Classification</b>	<b>TDG Classification</b>	<b>Mexico Classification</b>	<b>IATA</b>	<b>IMDG</b>
<b>UN number</b>	Not regulated.	Not regulated.	Not regulated.	Not regulated.	Not regulated.
<b>UN proper shipping name</b>	-	-	-	-	-
<b>Transport hazard class(es)</b>	-	-	-	-	-
<b>Packing group</b>	-	-	-	-	-
<b>Environmental hazards</b>	No.	No.	No.	No.	No.
<b>Additional information</b>	-	-	-	-	-

**Special precautions for user** : Multi-modal shipping descriptions are provided for informational purposes and do not consider container sizes. The presence of a shipping description for a particular mode of transport (sea, air, etc.), does not indicate that the product is packaged suitably for that mode of transport. All packaging must be reviewed for suitability prior to shipment, and compliance with the applicable regulations is the sole responsibility of the person offering the product for transport. People loading and unloading dangerous goods must be trained on all of the risks deriving from the substances and on all actions in case of emergency situations.

**Date of issue/Date of revision** : 3/25/2019 **Date of previous issue** : 10/17/2018 **Version** : 6.03 7/9  
4285- MINWAX® Stainable Wood Filler **SHW-85-NA-GHS-US**

## Section 14. Transport information

**Transport in bulk according to Annex II of MARPOL and the IBC Code** : Not available.

**Proper shipping name** : Not available.  
**Ship type** : Not available.  
**Pollution category** : Not available.

## Section 15. Regulatory information

**SARA 313**

SARA 313 (40 CFR 372.45) supplier notification can be found on the Environmental Data Sheet.

**California Prop. 65**

WARNING: This product contains chemicals known to the State of California to cause cancer and birth defects or other reproductive harm.

**International regulations**

**International lists**

- Australia inventory (AICS)**: Not determined.
- China inventory (IECSC)**: Not determined.
- Japan inventory (ENCS)**: Not determined.
- Japan inventory (ISHL)**: Not determined.
- Korea inventory (KECI)**: Not determined.
- Malaysia Inventory (EHS Register)**: Not determined.
- New Zealand Inventory of Chemicals (NZIoC)**: Not determined.
- Philippines inventory (PICCS)**: Not determined.
- Taiwan Chemical Substances Inventory (TCSI)**: Not determined.
- Thailand inventory**: Not determined.
- Turkey inventory**: Not determined.
- Vietnam inventory**: Not determined.

## Section 16. Other information

**Hazardous Material Information System (U.S.A.)**

Health	*	2
Flammability		1
Physical hazards		0

The customer is responsible for determining the PPE code for this material. For more information on HMIS® Personal Protective Equipment (PPE) codes, consult the HMIS® Implementation Manual.

**Caution:** HMIS® ratings are based on a 0-4 rating scale, with 0 representing minimal hazards or risks, and 4 representing significant hazards or risks. Although HMIS® ratings and the associated label are not required on SDSs or products leaving a facility under 29 CFR 1910.1200, the preparer may choose to provide them. HMIS® ratings are to be used with a fully implemented HMIS® program. HMIS® is a registered trademark and service mark of the American Coatings Association, Inc.

**Procedure used to derive the classification**

Classification	Justification
Not classified.	

**History**

**Date of printing** : 3/25/2019  
**Date of issue/Date of revision** : 3/25/2019  
**Date of previous issue** : 10/17/2018  
**Version** : 6.03

<b>Date of issue/Date of revision</b> : 3/25/2019	<b>Date of previous issue</b> : 10/17/2018	<b>Version</b> : 6.03
4285- MINWAX® Stainable Wood Filler		8/9 SHW-85-NA-GHS-US

## Section 16. Other information

**Key to abbreviations** : ATE = Acute Toxicity Estimate  
BCF = Bioconcentration Factor  
GHS = Globally Harmonized System of Classification and Labelling of Chemicals  
IATA = International Air Transport Association  
IBC = Intermediate Bulk Container  
IMDG = International Maritime Dangerous Goods  
LogPow = logarithm of the octanol/water partition coefficient  
MARPOL = International Convention for the Prevention of Pollution From Ships, 1973 as modified by the Protocol of 1978. ("Marpol" = marine pollution)  
UN = United Nations

✔ Indicates information that has changed from previously issued version.

### Notice to reader

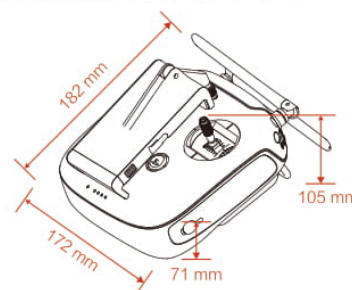
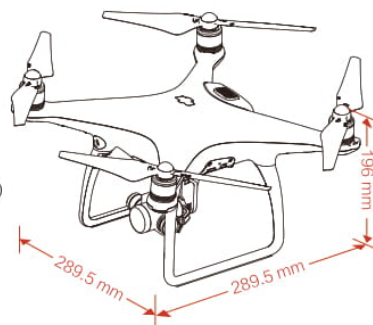
It is recommended that each customer or recipient of this Safety Data Sheet (SDS) study it carefully and consult resources, as necessary or appropriate, to become aware of and understand the data contained in this SDS and any hazards associated with the product. This information is provided in good faith and believed to be accurate as of the effective date herein. However, no warranty, express or implied, is given. The information presented here applies only to the product as shipped. The addition of any material can change the composition, hazards and risks of the product. Products shall not be repackaged, modified, or tinted except as specifically instructed by the manufacturer, including but not limited to the incorporation of products not specified by the manufacturer, or the use or addition of products in proportions not specified by the manufacturer. Regulatory requirements are subject to change and may differ between various locations and jurisdictions. The customer/buyer/user is responsible to ensure that his activities comply with all country, federal, state, provincial or local laws. The conditions for use of the product are not under the control of the manufacturer; the customer/buyer/user is responsible to determine the conditions necessary for the safe use of this product. The customer/buyer/user should not use the product for any purpose other than the purpose shown in the applicable section of this SDS without first referring to the supplier and obtaining written handling instructions. Due to the proliferation of sources for information such as manufacturer-specific SDS, the manufacturer cannot be responsible for SDSs obtained from any other source.

<b>Date of issue/Date of revision</b> : 3/25/2019	<b>Date of previous issue</b> : 10/17/2018	<b>Version</b> : 6.03	9/9
4285- MINWAX® Stainable Wood Filler		<b>SHW-85-NA-GHS-US</b>	

## **APPENDIX G. DJI PHANTOM 4 SPECIFICATION**

## Specifications

<b>• Aircraft</b>	
Weight (Including Battery)	1380 g
Max Ascent Speed	6 m/s ( Sport mode )
Max Descent Speed	4 m/s ( Sport mode )
Max Speed	20 m/s ( Sport mode )
Max Service Ceiling Above Sea Level	19685 feet ( 6000 m ) ( Software altitude limit: 400 feet above takeoff point )
Max Flight Time	Approx. 28 minutes
Operating Temperature Range	32° to 104° F ( 0° to 40° C )
Satellite Systems	GPS / GLONASS
<b>• Gimbal</b>	
Controllable Range	Pitch: -90° to +30°
<b>• Obstacle Sensing System</b>	
Obstacle Sensory Range	2 – 49 feet ( 0.7 – 15 m )
Operating Environment	Surface with clear pattern and adequate lighting ( lux > 15 )
<b>• Vision Positioning System</b>	
Velocity Range	≤10 m/s ( 2 m above ground )
Altitude Range	0 – 33 feet ( 0 – 10 m )
Operating Range	0 – 33 feet ( 0 – 10 m )
Operating Environment	Surfaces with a clear pattern and adequate lighting ( lux > 15 )
<b>• Camera</b>	
Sensor	1/2.3" Effective pixels:12 M
Lens	FOV ( Field Of View ) 94° 20 mm ( 35 mm format equivalent ) f/2.8 focus at ∞
ISO Range	100 – 3200 ( video ) 100 – 1600 ( photo )
Electronic Shutter Speed	8 s to 1/8000 s
Max Image Size	4000x3000
Still Photography Modes	Single shot Burst shooting: 3 / 5 / 7 frames Auto Exposure Bracketting ( AEB ): 3 / 5 bracketed frames at 0.7 EV Bias Time-lapse, HDR
Video Recording Modes	UHD: 4096x2160 (4K) 24 / 25p 3840x2160 (4K) 24 / 25 / 30p 2704x1520 (2.7K) 24 / 25 / 30p FHD: 1920x1080 24 / 25 / 30 / 48 / 50 / 60 / 120p HD: 1280x720 24 / 25 / 30 / 48 / 50 / 60p 60 Mbps
Max Video Bitrate	60 Mbps
Supported File Systems	FAT32 ( ≤ 32 GB ); exFAT ( > 32 GB )
Photo	JPEG, DNG ( RAW )
Video	MP4 / MOV ( MPEG – 4 AVC / H.264 )
Supported SD Cards	Micro SD, Max capacity: 64GB. Class 10 or UHS-1 rating required
Operating Temperature	32° to 104° F ( 0° to 40° C )
<b>• Remote Controller</b>	
Operating Frequency	2.400 GHz to 2.483 GHz
Max Transmission Distance	FCC Compliant: 3.1 mi ( 5 km ); CE Compliant: 2.2 mi ( 3.5 km ) ( Unobstructed, free of interference )
Operating Temperature	32° to 104° F ( 0° to 40° C )
Battery	6000 mAh LiPo 2S
Transmitter Power ( EIRP )	FCC: 23 dBm; CE: 17 dBm
Operating Voltage	7.4V @ 1.2A
<b>• Charger</b>	
Voltage	17.4 V
Rated Power	100 W
<b>• Intelligent Flight Battery ( PH4 - 5350 mAh -15.2 V )</b>	
Capacity	5350 mAh
Voltage	15.2 V
Battery Type	LiPo 4S
Energy	81.3 Wh
Net Weight	462 g
Operating Temperature	14° to 104° F ( -10° to 40° C )
Max Charging Power	100 W



CE 1313 RoHS

This device complies with part 15 of the FCC Rules. Operation is subject to the following two conditions:  
(1) This device may not cause harmful interference, and  
(2) this device must accept any interference received, including interference that may cause undesired operation.

©2016 DJI. All Rights Reserved.  
Designed by DJI. Printed in China.

Download the user manual for more information:  
<http://www.dji.com/product/phantom-4>



※ This Quick Start Guide is subject to change without prior notice.

## **APPENDIX H. IPHONE 6S PLUS'S IMAGE SENSOR SPECIFICATION**

## Camera

## Video Recording

Single 12MP Wide camera

4K video recording at 30 fps

Wide:  $f/2.2$  aperture

1080p HD video recording at 30 fps or 60 fps

—

—

—

Optical image stabilization

Optical image stabilization for video

Digital zoom up to 5x

Digital zoom up to 3x

True Tone flash

—

—

—

Slo-mo video support for 1080p at 120 fps and 720p at 240 fps

—

HDR for photos

Time-lapse video with stabilization

## **APPENDIX I. DIC SENSOR SPECIFICATION**



Basler ace Classic	acA1600-20um/uc	acA1920-25um/uc	acA2000-165um/uc
<b>Model Specifications</b>			
Resolution (HxV pixels)	1626x1236	1920x1080	2048x1088
Sensor	Sony ICX274	ON Semiconductor MT9P031	CMOSIS CMV2000
Sensor Size (optical)	1/1.8"	1/3.7"	2/3"
Sensor Technology	CCD, global shutter	CMOS, rolling shutter	CMOS, global shutter
Pixel Size [ $\mu\text{m}^2$ ]	4.4x4.4	2.2x2.2	5.5x5.5
Frame Rate [fps]	20	26	165
Mono/Color	Mono/Color		
Pixel Format	Mono (8, 12, 12 Packed), Bayer BG (8, 12, 12 Packed), YCbCr422_8, RGB8, BGR8	Mono (8, 12, 12 Packed), Bayer GB (8, 12, 12 Packed), YCbCr422_8	Mono (8, 12, 12 Packed)*, Bayer BG (8, 12, 12 Packed)
Lens Mount	C, CS*	C	C
Digital I/O	1 opto-isolated input + 1 opto-isolated output + 2 Fast-GPIO (configurable as In/Out)		
Power Consumption	3.5 W	2.2 W	3.2 W

\* only available for monochrome model

Basler ace Classic	acA2000-165umNIR	acA2040-90um/uc	acA2040-90umNIR
<b>Model Specifications</b>			
Resolution (HxV pixels)	2048x1088	2048x2048	2048x2048
Sensor	CMOSIS CMV2000 NIR-enhanced	CMOSIS CMV4000	CMOSIS CMV4000 NIR-enhanced
Sensor Size (optical)	2/3"	1"	1"
Sensor Technology	CMOS, global shutter		
Pixel Size [ $\mu\text{m}^2$ ]	5.5x5.5		
Frame Rate [fps]	165	90	90
Mono/Color	Mono NIR-enhanced	Mono/Color	Mono NIR-enhanced
Pixel Format	Mono (8, 12, 12 Packed)	Mono (8, 12, 12 Packed)*, Bayer BG (8, 12, 12 Packed)	Mono (8, 12, 12 Packed)
Lens Mount	C		
Digital I/O	1 opto-isolated input + 1 opto-isolated output + 2 Fast-GPIO (configurable as In/Out)		
Power Consumption	3.2 W		

\* only available for monochrome model

**APPENDIX J. DIC LENS SPECIFICATION**

**computer**

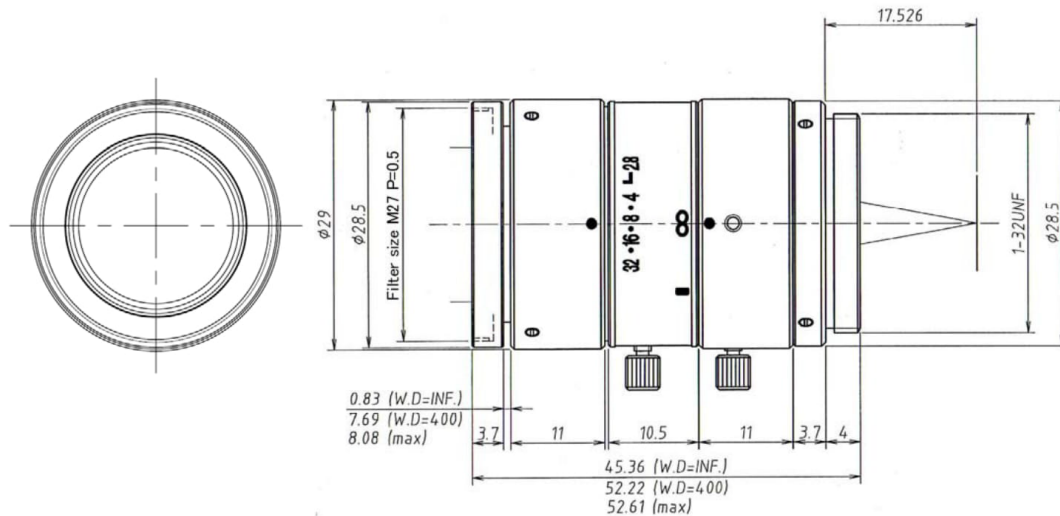
## M5028-MPW2

f=50mm F2.8  
for 2/3 type Cameras, 5 Megapixel  
C-Mount

Model No.		M5028-MPW2		Effective	Front	φ 18.0mm	
Focal Length		50mm		Lens Aperture	Rear	φ 12.0mm	
Max. Aperture Ratio		1:2.8			Distortion	2/3 type	0.027%(y=5.5)
Max. Image Format		8.8mm x 6.6mm(φ 11mm)		1/1.8 type		0.017%(y=4.32)	
Operation Range	Iris	F2.8 - F32.0		1/2 type		0.015%(y=4.0)	
	Focus	0.4m - Inf.		Back Focal Length	27.7mm		
Control	Iris	Manual		Flange Back Length	17.526mm		
	Focus	Manual		Mount	C-マウント		
Object Dimension at M.O.D.	2/3 Type	4.78cm x 6.38cm		Filter Size	M27.0 P=0.5mm		
	1/1.8 Type	3.77cm x 5.00cm		Dimensions	φ 29mm x 45.36mm		
	1/2 Type	3.48cm x 4.64cm		Weight	69.0g		
Angle of View	D	2/3 type	12.5°	1/1.8 tyoe	9.9°	1/2 type	9.1°
	H		10.0°		7.9°		7.3°
	V		7.5°		5.9°		5.5°
Operating Temperature		-10°C - +50°C					

M.O.D. : Minimum Object Distance

### Dimensions



Specification is subject to change without any notice.

2012.04

**APPENDIX K. SOLAR PANEL SPECIFICATION**

## Product description

NUZAMAS Solar panels made with cells Sun Power (SP) range are the most efficient commercially available solar cells worldwide. This range uses standard monocrystalline cells with an efficiency exceeding 22%. These panels are used where maximum output is required for a given space.

At just 1/8th the weight of a standard domestic panel, NUZAMAS Solar flexible panels are the ultimate in lightweight, flexible, monocrystalline solar. The panels are constructed with highly efficient solar cells supported in a unique polymer that allows for flexibility and significant weight reduction. These panels have no aluminium or steel backing like other semi-flexible panels, which means they are extremely lightweight. At just 1.5mm thick and weighing only 0.5KGs, they are the thinnest and lightest panels available in the world. **Please noted:**

Do not wire the flexible solar panel in parallel or in series to avoid overheating Not recommended to glue the panel on top. Leave a space underneath for the back panel to breath

### Features:

Sun Power Cells with 22% efficiency

Widely used in RV /boat /Caravan/Camping

Anti-reflective coating improves light absorption

The best solutions for your outdoor activity power back up

Meeting highest international standards

### Specifications

Mono-Crystalline: 20W

Max Power Voltage: 17V

Max Power Current: 1.0A

Module Efficiency: 22%

Size: 50cm x 30cm

### In the box

1 x 20W NUZAMAS solar Panel

**APPENDIX L. AASHTO STRENGTH I LIMIT STRENGTH AND SERVICE  
I LIMIT STRENGTH CALCULATION**

AASHTO strength I limit strength and the AASHTO service I limit strength can be calculated using Table 3.4.1-1 in the AASHTO LRFD Bridge Design Specifications (AASHTO 2012). Based on the table, the AASHTO strength I limit is the sum of  $1.25 \times DC$ , component self-weight, and  $1.75 \times LL$ , vehicle live load, whereas the AASHTO service I limit is the sum of  $1.00 \times DC$ ,  $1.00 \times LL$ , and  $0.3 \times WS$ , where wind loads on the structure, which means, for this project, the CLT girder or CLT bridge system), as displayed in Equations 51 and 52. To calculate DC, a volume of CLT component and density of CLT component are required. The calculated DC for the CLT girder and bridge system is 3.33 kN and 12.73 kN, respectively, whereas LL for the CLT girder and the CLT bridge system is calculated to be 17.79 kN and 88.96 kN, correspondingly. With these values, the calculated AASHTO strength I limit strength for the girder and the bridge system are found to be 35.30 kN and 17.59 kN.

$$\text{AASHTO Strength I limit} = 1.25 DC + 1.75 LL \quad (51)$$

$$\text{AASHTO Service I limit} = 1.0 DC + 1.0 LL + 0.3 WS \quad (52)$$

where DC = component self-weight

LL = vehicle live load

WS = wind load on structure

For the AASHTO service I limit strength, the wind load is calculated as per Section 3.8.1.2 in AASHTO LRFD Bridge Design Specifications (AASHTO 2012). For the calculation, the CLT bridge system is assumed to be constructed 40 ft from the ground in the open country and  $V_{30}$  is the same with  $V_B$ .  $V_0$  is considered 8.20 mph and  $Z_0$  is taken as 0.23 ft according to Table 3.8.1.1-1 of AASHTO (2012) since this bridge system is located in the open country. From Equation 53,  $V_{DZ}$  is calculated 105.75 mph. To calculate the design wind load ( $P_D$ ), windward load,  $P_B$ , is selected from Table 3.8.1.2.1-1 of the AASHTO (2012) and the selected  $P_B$  is 0.05 ksf for the girder and 0.04 ksf for the deck. With the computed values of  $P_B$ ,  $P_D$  is calculated to be 0.06 ksf for the CLT girder and 0.04 ksf for the CLT deck. To obtain WS,  $P_D$  should be multiplied by an exposed area, which is found to be 8.38 kN and 10.77 kN for the CLT girder and the CLT bridge system, separately. Note, the details of calculation values are provided in the following excel sheet.

$$V_{DZ} = 2.5 V_0 \left( \frac{V_{30}}{V_B} \right) \ln \left( \frac{Z}{Z_0} \right) \quad (53)$$

$$P_D = P_B \left( \frac{V_{DZ}}{V_B} \right)^2 \quad (54)$$

where  $V_{DZ}$  = design wind velocity at design elevation, Z (mph)

$V_{30}$  = wind velocity at 30.0 ft above low ground or above design water level (mph)

$V_B$  = base wind velocity of 100 mph at 30.0 ft height, yielding design pressures specified in Articles 3.8.1.2.1 and 3.8.1.2.2 of AASHTO (2012)

Z = height of structure at which wind loads are being calculated as measured from low ground, or from water level, > 30.0 ft

$V_0$  = friction velocity, a meteorological wind characteristic taken, as specified in Table 3.8.1.1-1 of AASHTO (2012), for various upwind surface characteristics (mph)

$Z_0$  = friction length of upstream fetch, a meteorological wind characteristic taken as specified in Table 3.8.1.1-1 of AASHTO (2012) (ft)

$P_D$  = design wind pressure (ksf)

$P_B$  = base wind pressure specified in Table 3.8.1.2.1-1 of AASHTO (2012) (ksf)

Note: 1mph = 1.6 km/h, 1 ft = 0.3048 m, and 1 ksf = 6.94 kPa

		DC			LL			WS		Total
Strength I	CLT girder	1.25 x	3.33	+	1.75 x	17.79			=	35.30 kN
Service I	CLT girder	1.00 x	3.33	+	1.00 x	17.79	+	0.30 x	8.38	= 23.64 kN
Strength I	CLT bridge	1.25 x	12.73	+	1.75 x	88.96			=	171.59 kN
Service I	CLT bridge	1.00 x	12.73	+	1.00 x	88.96	+	0.30 x	10.77	= 104.92 kN

DC for CLT girder		DC for CLT deck		DC for CLT diaphragm		DC for CLT bridge	
Density	4.41 kN/m <sup>3</sup>	Density	4.41 kN/m <sup>3</sup>	Density	4.41 kN/m <sup>3</sup>		
Width	0.24 m	Width	1.22 m	Width	0.13 m		
Depth	0.49 m	Depth	0.17 m	Depth	0.10 m		
Length	6.40 m	Length	6.40 m	Length	0.37 m		
Volume	0.76 m <sup>3</sup>	Volume	1.36 m <sup>3</sup>	Volume	0.00 m <sup>3</sup>		
Weight	3.33 kN		6.02 kN		0.02 kN		12.73 kN

LL for CLT girder		LL for CLT bridge	
Truck	88.96 kN	Truck	88.96 kN
DF	0.20		
LL	17.79 kN	LL	88.96 kN

WS		CLT girder		CLT deck		CLT bridge	
$V_0$	8.20 mph	Depth	1.60 ft	Depth	0.57 ft		
$V_{30} = V_B$	100.00 mph	Length	21.00 ft	Length	21.00 ft		
Z	40.00 ft	Area	33.69 ft <sup>2</sup>	Area	12.03 ft <sup>2</sup>		
$Z_0$	0.23 ft						
$V_{DZ}$	105.75 mph	$P_B$	0.05 ksf	$P_B$	0.04 ksf		
		$P_D$	0.06 ksf	$P_D$	0.04 ksf		
		WS	1.88 kips	WS	0.54 kips	WS	2.42 kips
			8.38 kN				10.77 kN